

**EVALUATION OF SEISMIC PERFORMANCE
OF CONCRETE FRAME STRUCTURES IN CANADA**

by

PATRICK PAULTRE, ing.

Department of Civil Engineering and Applied Mechanics

McGill University

Montreal, Canada

July 1987

A thesis submitted to the Faculty of Graduate Studies
and Research in partial fulfillment of the requirements
for the degree of Doctor of Philosophy

© Patrick Paultre 1987

to the memory of my father Emile

to my mother Franchette

to my wife Solange

to my daughter Genevieve

ABSTRACT

Three buildings in Montreal and three buildings in Vancouver were designed for different level of "ductility" according to the 1985 National Building Code of Canada and the 1984 Canadian Concrete Code.

Three full scale reinforced concrete specimens representing an exterior beam-column-slab subassemblage of the Montreal structure were tested in order to determine the behaviour of these components. The role of the spandrel beam in limiting the effective slab width and its role in transferring shear to the joint region were investigated.

Analytical procedures were developed in order to predict the responses of main structural components to the combined loading effects of axial load, moment and shear. In addition a hysteretic behavioural model was developed in order to account for strength and stiffness degradation as well as pinching of the hysteretic response.

The analytical procedures were then used to model the responses of the components of these buildings. Non-linear dynamic analyses were carried out on each building for a series of artificially generated accelerograms. The results of the tests as well as the results of the non-linear dynamic analyses enabled an assessment of the performance of different building designs and an assessment of current code requirements.

SOMMAIRE

Trois bâtiments situés à Montréal et trois bâtiments situés à Vancouver ont été dimensionnés avec des facteurs de ductilité différents selon le Code National du Bâtiment édition 1985 et le Code Canadien du Béton édition 1984.

Trois spécimens grandeur réelle représentant un ensemble colonne extérieure, poutre et plancher des bâtiments de Montréal ont été testés dans le but de déterminer leur comportement sous charges renversées. Le rôle de la poutre de rive dans la participation d'une largeur "efficace" de la dalle dans la résistance de la poutre principale a été étudié, de même que la transmission des contraintes de cisaillement de la poutre de rive au joint.

Des méthodes analytiques ont été développées permettant de prédire les déformations des éléments principaux d'une structure sous une combinaison de charge axiale, flexion et cisaillement. De plus un modèle permettant de décrire la réponse d'un élément en béton-armé sous charge cyclique a été développé. Ce modèle tient compte de la perte de rigidité, de la perte de résistance ainsi que du rétrécissement de la courbe de réponse.

Ces méthodes furent utilisées dans la modélisation de la réponse des composantes des bâtiment mentionnés plus haut. Des analyses dynamiques non-linéaires de ces bâtiments ont été effectuées avec comme chargement dynamique un ensemble de tremblements de terre générés artificiellement.

Les résultats des essais ainsi que les résultats des analyses dynamiques non-linéaires ont permis une évaluation de la performance des différents genres de bâtiments et une évaluation des règlements des codes du bâtiment en vigueur.

ACKNOWLEDGEMENTS

The author would like to express his appreciation to Professor Denis Mitchell for his skillful guidance, his encouragement and his understanding throughout the course of this research programme.

The author takes this opportunity to thank Professor René Tinawi of Ecole Polytechnique for his interest in the research programme.

In addition the writer wishes to express his gratitude to Suzanne Rattray for testing specimens K0.7 and K1.3 and to Dan Castele and George Covell for assisting with the construction and testing of specimen OldK1.3.

The experimental research was carried out in the Jamieson Structures Laboratory in the Department of Civil Engineering and Applied Mechanics at McGill University. The author is particularly grateful for the assistance given by B. Cockayne and R. Sheppard.

Thanks are extended to Alain Dandurand for his expert assistance in preparing some of the figures.

The financial assistance provided by the Natural Sciences and Engineering Research Council of Canada and by the Fonds pour la Formation de Chercheurs et l'Aide à la Recherche of the Government of Québec is gratefully acknowledged.

This manuscript was prepared with Donald Knuth's \TeX typesetting program and printed on a HP LaserJet⁺ Printer.

TABLE OF CONTENTS

ABSTRACT	i
SOMMAIRE	ii
ACKNOWLEDGEMENTS	iii
LIST OF FIGURES	vii
LIST OF TABLES	xiii
LIST OF SYMBOLS	xvi
1 INTRODUCTION	1
1.1 PREVIOUS RESEARCH	2
1.1.1 Seismic Risk Analysis and Seismic Zoning	3
1.1.2 Reversed Cyclic Loading Tests	3
1.1.3 Non-linear Dynamic Analysis of Reinforced Concrete Structures	6
1.2 OBJECTIVES	12
2 CANADIAN SEISMICITY AND GENERATION OF ACCELEROGRAMS	14
2.1 SEISMIC RISK ANALYSIS	14
2.1.1 Extreme Value Method - Milne and Davenport	14
2.1.2 Point Source Model - Cornell Method	15
2.2 THE 1985 SEISMIC ZONING MAP OF CANADA	18
2.3 GENERATION OF ACCELEROGRAMS	19
3 MOMENT RESISTING FRAME STRUCTURES DESIGNED FOR MONTREAL AND VANCOUVER	34
3.1 GEOMETRY OF STRUCTURES	34
3.2 DESIGN PARAMETERS	35
3.3 ANALYSIS ASSUMPTIONS AND IDEALIZATION	37
3.4 LOAD COMBINATION AND LOAD EFFECTS	38
3.5 DESIGN SUMMARY AND COMPARISONS	39

4 REVERSED CYCLIC LOADING TESTS OF FULL SCALE CONCRETE FRAME SUB-ASSEMBLAGES	45
4.1 DESIGN OF TEST SPECIMENS	45
4.2 DETAILS OF TEST SPECIMENS	47
4.2.1 Test Set-Up	47
4.2.2 Details of Reinforcement	48
4.2.2.1 Specimen Old K1.3	51
4.2.2.2 Specimen K1.3	51
4.2.2.3 Specimen K0.7	53
4.2.3 Material Properties	56
4.2.3.1 Steel	56
4.2.3.2 Concrete	56
4.2.4 Instrumentation and Experimental Procedure	57
4.3 EXPERIMENTAL RESULTS AND OBSERVATIONS	61
4.3.1 Specimen Old K1.3	61
4.3.2 Specimen K1.3	65
4.3.2 Specimen K0.7	69
4.3 COMPARISONS OF EXPERIMENTAL RESULTS	75
5 PREDICTIONS OF MEMBER BEHAVIOUR AND COMPARISONS WITH TEST RESULTS	81
5.1 PREDICTING FLEXURE AND AXIAL LOAD RESPONSE	81
5.2 PREDICTING MOMENT-AXIAL LOAD-SHEAR RESPONSE	89
5.3 ACCOUNTING FOR BOND-SLIP EFFECTS	98
5.4 RESPONSE OF SUBASSEMBLAGES	103
5.4.1 Role of Spandrel Beam	103
5.4.2 Beam Responses	105
5.4.3 Column and Joint Responses	107
5.4.4 Total Responses	110

6 PREDICTING NON-LINEAR DYNAMIC RESPONSE OF CONCRETE STRUCTURES	115
6.1 NON-LINEAR DYNAMIC ANALYSIS USING DRAIN-2D	115
6.1.1 Equation of Motion	115
6.1.2 Solution Procedure	116
6.1.3 Mass Matrix	119
6.1.4 Tangent Stiffness Matrix	119
6.1.4.1 Dual Component Element - Beam-Column Model . . .	120
6.1.4.2 Single Component Element - Physical hinge beam model .	123
6.1.4.3 $P-\Delta$ Effects - Geometric Stiffness	124
6.1.5 Damping Matrix	124
6.2 REFINED HYSTERETIC MODEL	125
6.3 ESTIMATING DAMAGE	129
6.3.1 Member Damage	129
6.3.2 Structural and Non-Structural Damage	131
7 EVALUATION OF PREDICTED RESPONSES	135
7.1 ROOF DISPLACEMENT TIME HISTORIES	135
7.2 LOCATIONS AND TYPES OF PLASTIC HINGES	136
7.3 ENVELOPES OF LATERAL DISPLACEMENTS	137
7.4 INTERSTOREY DRIFTS AND DAMAGE ESTIMATES	137
7.5 INELASTIC DEFORMATION AND FLEXURAL STRENGTH DEMANDS	140
7.6 LATERAL FORCES AND SHEAR STRENGTH DEMANDS	141
7.7 INFLUENCE OF COLUMN SIZE ON THE RESPONSE	142
8 DESIGN RECOMMENDATIONS AND CONCLUSIONS	178
REFERENCES	183
STATEMENT OF ORIGINALITY	189
APPENDIX A	190

LIST OF FIGURES

1.1	Summary of detailing requirements for beams and columns.	2
1.2	Hysteresis models.	7
1.3	Modified Takeda model, Litton [36]	10
2.1	1970 Seismic Zoning Map of Canada	15
2.2	Methodology for derivation of seismic zoning map.	17
2.3	Zones of earthquake occurrence and magnitudes (M) of earthquakes in Eastern Canada [49]	19
2.4	Zones of earthquake occurrence and magnitudes (M) of earthquakes in Western Canada [49]	19
2.5	1984 Seismic zoning maps of Canada [2]	21
2.6	Representative variation of response spectra for four different locations in Canada	22
2.7	General characteristics of intensity function	24
2.8	Intensity functions assumed for Western and Eastern Canada.	24
2.9	Simulated Ground Motion 1-Montreal Region	26
2.10	Simulated Ground Motion 2-Montreal Region	27
2.11	Simulated Ground Motion 3-Montreal Region	28
2.12	Simulated Ground Motion 1-Vancouver Region.	29
2.13	Simulated Ground Motion 2-Vancouver Region.	30
2.14	Simulated Ground Motion 3-Vancouver Region.	31
2.15	Pseudo-Velocity Response Spectra-Montreal Region.	32
2.16	Pseudo-Velocity Response Spectra-Vancouver Region	33
3.1	Elevation and plan view of prototype structure	36
3.2	Mathematical model for CMPT FRAME-2D program	37
3.3	Mode shapes and natural period of vibration for Montreal buildings . . including modal participation factor (mpf)	40
3.4	Mode shapes and natural period of vibration for Vancouver buildings . including modal participation factor (mpf)	41

3.5	Reinforcement Details for Montreal Buildings	43
3.6	Reinforcement Details for Vancouver Buildings	44
4.1	Specimen location	46
4.2	Test specimen dimensions and test set-up	47
4.3	Photograph of test set up for specimen Old K1.3	49
4.4	Reinforcement details of specimens	50
4.5	Photographs of reinforcing cage for specimen Old K1.3	52
4.6	Photographs of reinforcing cage for specimen K1.3	54
4.7	Photographs of reinforcing cage for specimen K0.7	55
4.8	Specimen instrumentation	58
4.9	Loading and deflection history	60
4.10	Hysteretic load-tip deflection response for Specimen Old K1.3	62
4.11	Specimen Old K1.3 at different load stages	63
4.12	Buckling of longitudinal reinforcement in main beam of Specimen Old K1.3	64
4.13	Strain distribution in slab longitudinal reinforcement for all three specimens	65
4.14	Beam tip deflection components for Specimen Old K1.3	66
4.15	Hysteretic load-tip deflection response for Specimen K1.3	67
4.16	Specimen K1.3 at different load stages	68
4.17	Exterior face of specimen K1.3 at end of test	70
4.18	Beam tip deflection components for specimen K1.3	71
4.19	Hysteretic load-tip deflection response for Specimen K0.7	72
4.20	Specimen K0.7 at different load stages	73
4.21	Exterior face of specimen K0.7 at end of test	74
4.22	Beam tip deflection components for specimen K0.7	75
4.23	Specimen K0.7 close to failure	76
4.24	Comparisons of responses and appearance of specimens near failure	79
4.25	Envelopes of responses	80
5.1	Predicting flexural response	82

5.2	Stress-strain relationship for concrete confined by rectangular hoops, Kent and Park [14]	82
5.3	Idealization for the stress-strain relationship for steel in tension or compression, Park and Paulay [18]	84
5.4	Average stress-strain relationship for cracked concrete in tension, Vecchio and Collins [71]	84
5.5	Accounting for variation of strains across the flange of T section	86
5.6	Influence on moment-curvature response of non-linear strain distribution in flange of T beam	87
5.7	Predicted axial load-moment interaction and axial load-curvature response	88
5.8	Influence of axial load on the moment curvature response of a column section	89
5.9	Influence of spalling on the response of a column section	90
5.10	Detailed analysis using the compression field theory	91
5.11	Simplified analysis using the compression field theory	91
5.12	Predicting axial load-moment-shear response	92
5.13	Spacing of inclined cracks	93
5.14	Equilibrium considerations for beam in shear	94
5.15	Stress-strain relationship for diagonallycracked concrete	95
5.16	Influence of axial load on shear response	97
5.17	Influence of moment to shear ratio on the response	98
5.18	Effect of bond-slip on deformation	99
5.19	Actual and idealized moment-rotation due to bond-slip	99
5.20	Determining bond-slip from assumed	100
5.21	Approximating bond-slip from assumed	102
5.22	Role of spandrel beam	104
5.23	Comparisons of moment-curvature predictions with experimental results for specimen Old K1.3	106
5.24	Comparisons of moment-curvature predictions with experimental results for specimen K1.3	107

5.25	Comparisons of moment-curvature predictions with	108
	experimental results for specimen K0.7	
5.26	Comparisons of predicted curvatures and shear strains.	109
	with experimental results for specimen Old K1.3	
5.27	Comparisons of predicted curvatures and shear strains.	110
	with experimental results for specimen K1.3	
5.28	Comparisons of predicted curvatures and shear strains	111
	with experimental results for specimen K0.7	
5.29	Comparison of predicted joint shear vs joint tie strain responses with	112
	experimental values for specimen SP7 tested by Uzumeri and Seckin [17]	
5.30	Comparison of predicted joint shear vs joint tie strain responses with	113
	experimental values for specimen 7 tested by Ehsani and Wight [22, 23, 24]	
5.31	Predicted and measured tip deflection components	114
6.1	Multi-linear force-displacement relationship	117
6.2	Computation of force increment [37].	118
6.3	Non-linear hysteretic behaviour.	120
6.4	Two-components element used to model beam-columns [28]	121
6.5	Yielding states and stiffness of inelastic component	121
	of parallel element	
6.6	Use of axial load-moment interaction curve to determine.	122
	yield point, adapted from Reference [27]	
6.7	Sample loading excursion with corresponding moment	122
	rotation response, adapted from Reference [27]	
6.8	Element degrees of freedom	123
6.9	Refined hysteretic model for reinforced concrete members	127
6.10	Definition of rotational ductility demand.	129
6.11	Definition of yield rotation.	130
6.12	Definition of curvature ductility demand.	131
7.1	Roof displacement time histories for different levels of maximum	144
	peak ground acceleration, a , for Old K=1.3 structure in Montreal	
7.2	Roof displacement time histories for different levels of maximum	145
	peak ground acceleration, a , for K=1.3 structure in Montreal	
7.3	Roof displacement time histories for different levels of maximum	146
	peak ground acceleration, a , for K=0.7 structure in Montreal	

7.4	Roof displacement time histories for different levels of maximum peak ground acceleration, a , for Old K1.3 structure in Vancouver . . .	147
7.5	Roof displacement time histories for different levels of maximum peak ground acceleration, a , for $K=1.3$ structure in Vancouver . . .	148
7.6	Roof displacement time histories for different levels of maximum peak ground acceleration, a , for $K=0.7$ structure in Vancouver . . .	149
7.7	Deformed shapes and corresponding types and locations of hinges, for $K=0.7$ structure in Montreal for the most critical motion	150
7.8	Summary of hinge types and locations during entire time history responses for Montreal structures	151
7.9	Summary of hinge types and locations during entire time history responses for Vancouver structures	152
7.10	Envelopes of lateral displacements for Old $K=1.3$ structure in Montreal	153
7.11	Envelopes of lateral displacements for $K=1.3$ structure in Montreal	154
7.12	Envelopes of lateral displacements for $K=0.7$ structure in Montreal	155
7.13	Envelopes of lateral displacements for Old K1.3 structure in Vancouver	156
7.14	Envelopes of lateral displacements for $K=1.3$ structure in Vancouver	157
7.15	Envelopes of lateral displacements for $K=0.7$ structure in Vancouver	158
7.16	Storey drift indices for Old $K=1.3$ structure in Montreal	159
7.17	Storey drift indices for Old $K=1.3$ structure in Montreal	160
7.18	Storey drift indices for $K=0.7$ structure in Montreal	161
7.19	Storey drift indices for Old $K=1.3$ structure in Vancouver	162
7.20	Storey drift indices for $K=1.3$ structure in Vancouver	163
7.21	Storey drift indices for $K=0.7$ structure in Vancouver	164
7.22	Estimated curvature ductilities and plastic hinge rotations for Old $K=1.3$ structure in Montreal	165
7.23	Estimated curvature ductilities and plastic hinge rotations for $K=1.3$ structure in Montreal	166
7.24	Estimated curvature ductilities and plastic hinge rotations for $K=0.7$ structure in Montreal	167
7.25	Estimated curvature ductilities and plastic hinge rotations for Old $K=1.3$ structure in Vancouver	168

7.26	Estimated curvature ductilities and plastic hinge rotations	169
	for K=1.3 structure in Vancouver	
7.27	Estimated curvature ductilities and plastic hinge rotations	170
	for K=0.7 structure in Vancouver	
7.28	Shear force envelopes for Old K=1.3 structure in Montreal	171
7.29	Shear force envelopes for K=1.3 structure in Montreal	172
7.30	Shear force envelopes for K=0.7 structure in Montreal	173
7.31	Shear force envelopes for Old K=1.3 structure in Vancouver	174
7.32	Shear force envelopes for K=1.3 structure in Vancouver	175
7.33	Shear force envelopes for Old K=0.7 structure in Vancouver	176
7.34	Summary of non-linear dynamic analyses for K=1.3 structure	177
	in Montreal with smaller columns	

LIST OF TABLES

2.1	Peak Ground Accelerations	25
4.1	Reinforcing Steel Properties	57
4.2	Concrete properties	57
4.3	Comparison of Failure Mode and Key Response Parameters	77
6.1	Δ_c Used to Estimate Damage	133
7.1	Peak Ground Accelerations	135
7.2	Predicted Peak Displacements for Montreal	137
7.3	Predicted Peak Displacements for Vancouver	138
7.4	Damage Estimates for Montreal Structures	138
7.5	Damage Estimates for Vancouver Structures	139
A.1	Distribution of Wind Loading Over Height for Montreal Buildings . .	191
A.2	Distribution of Wind Loading Over Height for Vancouver Buildings . .	191
A.3	Distribution of Earthquake Loading Over Height for Montreal Buildings	192
A.4	Distribution of Earthquake Loading Over Height for Vancouver Buildings	192
A.5	Beam Bending Moment (kN·m) at Joint A(B) Line 2 for Montreal K=1.3 Buildings	193
A.6	Beam Bending Moment (kN·m) at Joint (A)B Line 2 for Montreal K=1.3 Buildings	193
A.7	Beam Bending Moment (kN·m) at Joint B(C) Line 2 for Montreal K=1.3 Buildings	194
A.8	Beam Shear Force (kN) at Joint A(B) Line 2 for Montreal K=1.3 Buildings	194
A.9	Beam Shear Force (kN) at Joint (A)B Line 2 for Montreal K=1.3 Buildings	195
A.10	Beam Shear Force (kN) at Joint B(C) Line 2 for Montreal K=1.3 Buildings	195
A.11	Exterior Columns Bending Moments (kN·m) for Montreal K=1.3 Buildings	196

A.12	Interior Columns Bending Moments (kN·m)	196
	for Montreal K=1.3 Buildings	
A.13	Exterior Columns Shear Forces (kN) for Montreal K=1.3 Buildings . .	197
A.14	Interior Columns Shear Forces (kN) for Montreal K=1.3 Buildings . .	197
A.15	Beam Bending Moment (kN·m) at Joint A(B) Line 2	198
	for Montreal K=0.7 Building	
A.16	Beam Bending Moment (kN·m) at Joint (A)B Line 2	198
	for Montreal K=0.7 Building	
A.17	Beam Bending Moment (kN·m) at Joint B(C) Line 2	199
	for Montreal K=0.7 Building	
A.18	Beam Shear Force (kN) at Joint A(B) Line 2	199
	for Montreal K=0.7 Building	
A.19	Beam Shear Force (kN) at Joint (A)B Line 2	200
	for Montreal K=0.7 Building	
A.20	Beam Shear Force (kN) at Joint B(C) Line 2	200
	for Montreal K=0.7 Building	
A.21	Exterior Columns Bending Moments (kN·m)	201
	for Montreal K=0.7 Building	
A.22	Interior Columns Bending Moments (kN·m)	201
	for Montreal K=0.7 Building	
A.23	Exterior Columns Shear Forces (kN) for Montreal K=0.7 Building . .	202
A.24	Interior Columns Shear Forces (kN) for Montreal K=0.7 Building . .	202
A.25	Beam Bending Moment (kN·m) at Joint A(B) Line 2	203
	for Vancouver K=1.3 Buildings	
A.26	Beam Bending Moment (kN·m) at Joint (A)B Line 2	203
	for Vancouver K=1.3 Buildings	
A.27	Beam Bending Moment (kN·m) at Joint B(C) Line 2	204
	for Vancouver K=1.3 Buildings	
A.28	Beam Shear Force (kN) at Joint A(B) Line 2	204
	for Vancouver K=1.3 Buildings	
A.29	Beam Shear Force (kN) at Joint (A)B Line 2	205
	for Vancouver K=1.3 Buildings	
A.30	Beam Shear Force (kN) at Joint B(C) Line 2	205
	for Vancouver K=1.3 Buildings	

A.31	Exterior Columns Bending Moments (kN·m)	206
	for Vancouver K=1.3 Buildings	
A.32	Interior Columns Bending Moments (kN·m)	206
	for Vancouver K=1.3 Buildings	
A.33	Exterior Columns Shear Forces (kN) for Vancouver K=1.3 Buildings . .	207
A.34	Interior Columns Shear Forces (kN) for Vancouver K=1.3 Buildings . .	207
A.35	Beam Bending Moment (kN·m) at Joint A(B) Line 2	208
	for Vancouver K=0.7 Building	
A.36	Beam Bending Moment (kN·m) at Joint (A)B Line 2	208
	for Vancouver K=0.7 Building	
A.37	Beam Bending Moment (kN·m) at Joint B(C) Line 2	209
	for Vancouver K=0.7 Building	
A.38	Beam Shear Force (kN) at Joint A(B) Line 2	209
	for Vancouver K=0.7 Building	
A.39	Beam Shear Force (kN) at Joint (A)B Line 2	210
	for Vancouver K=0.7 Building	
A.40	Beam Shear Force (kN) at Joint B(C) Line 2	210
	for Vancouver K=0.7 Building	
A.41	Exterior Columns Bending Moments (kN·m)	211
	for Vancouver K=0.7 Building	
A.42	Interior Columns Bending Moments (kN·m)	211
	for Vancouver K=0.7 Building	
A.43	Exterior Columns Shear Forces (kN) for Vancouver K=0.7 Building . .	212
A.44	Interior Columns Shear Forces (kN) for Vancouver K=0.7 Building . .	212
A.45	Lateral Deflection Envelope under Specified Earthquake	213
	and Wind Load, mm, Montreal Buildings	
A.46	Lateral Deflection Envelope under Specified Earthquake	213
	and Wind Load, mm, Vancouver Buildings	

LIST OF SYMBOLS

A_b	area of bar
A_i	amplitude of i^{th} contributing sinusoid to earthquake motion
A_v	area of transverse reinforcement within distance s
a	peak horizontal ground acceleration; maximum aggregate size
$a(t)$	ground acceleration
a_0	scalar multiplier
a_1	scalar multiplier
b	total web width
b_v	web width resisting shear
b''	width of confined core measured to outside of hoops
b_0	width of shear flow path in a beam subjected to torsion
C	damping matrix
C_e	exposure factor
C_g	gust factor
C_p	external pressure coefficient
C_T	tangent damping matrix
c	distance from extreme compression fibre to neutral axis
D	dead load
DR	damage ratio
DR_c	damage threshold of 0.5%
DR_t	damage threshold of 50%
DR_w	window damage ratio
d	effective depth
d_b	nominal diameter of a bar
d_v	effective shear depth which can be taken equal to the flexural lever arm
E_c	modulus of elasticity of concrete
EI	flexural stiffness
E_s	modulus of elasticity of reinforcement
F	foundation factor
f	element local flexibility matrix
f_c	compressive stress in concrete
f'_c	crushing stress of concrete cylinder
f_{cr}	cracking stress of concrete
f_{c1}	average principal tensile stress in concrete
f_{c2}	principal compressive stress in concrete
f_{c2max}	maximum possible value of f_{c2}
f_{ij}	flexibility influence coefficient
f_s	steel stress
f_{su}	steel stress at ultimate
f_v	tensile stress in transverse reinforcement

g	acceleration due to gravity
I	importance factor
$I(t)$	intensity function
K	factor which reflects the type of construction, ductility and ability to dissipate energy
K	factor used in Equation 5.6
k_G	element geometric stiffness
K_T	structure global tangent stiffness matrix
k_T	element local tangent stiffness matrix
\bar{k}_T	combined element tangent stiffness matrix
k_{T0}	element tangent stiffness matrix at the beginning of a step
k_i^{sp}	stiffness of non-linear flexural spring acting at end i
L	live load
l_d	development length - distance beyond any section a reinforcing bar must extend in order to develop a given force at that section
l_{du}	development length at the ultimate stress
M	bending moment; magnitude of earthquakes on the Richter scale
M	mass matrix
M_{cr}	cracking moment
M_{el}	elastic moment
M_{max}	maximum bending moment
M_u	ultimate moment
M_y	yielding moment
m	integer; constant; factor used in Equation 5.3
m_i	mass
mpf	modal participation factor
N	axial force
N_p	axial force calculated from plane sections analysis
N_v	axial compression on concrete due to shear
p	external pressure coefficient
q	torsional shear flow
q	reference velocity pressure
r	factor used in Equation 5.3
\ddot{r}	acceleration vector
\dot{r}	velocity vector
r	displacement vector
\ddot{r}_g	ground acceleration
S	seismic response factor
S	external force vector
S_i	element force at beginning of cycle i
S_L	linear element force vector based on state of element at the beginning of the step
S_{NL}	non-linear force vector which accounts for changes in element tangent stiffness

S_U	unbalanced force vector resulting from change in element stiffness state
S_y	element force at yield
s	spacing of transverse reinforcement; factor used in Equation 5.3
s_h	spacing of hoops
s_{ml}	spacing of transverse cracks
s_{mv}	spacing of longitudinal cracks
$s_{m\theta}$	spacing of cracks inclined at θ
T	period of vibration; tension
T_{decay}	decay time of earthquake motion
T_n	period of n^{th} normal mode
T_{rise}	rising time of earthquake motion
$T_{sustained}$	sustained strong motion duration
t	time
u	bond stress
V	lateral seismic force
V	shear force
v	peak horizontal ground velocity
v	zonal velocity ratio
v_{ci}	shear stress on crack face
W	weight
W	wind load
w	crack width
Z	slope of assumed linear falling branch of concrete stress-strain curve
Z_a	acceleration related zone
Z_v	velocity related zone
z	distance from critical section of a beam to the point of contraflexure
Δ	increment; interstorey drift; drift index
Δ_c	ratio of interstorey drift to storey height corresponding to DR_c
Δ_f	component of the tip deflection of specimen tested corresponding to flexural yielding
Δ_j	component of the tip deflection of specimen tested associated with shear distortion of the joint together with bond slip of the flexural bars anchored into the joint
Δ_s	component of the tip deflection of specimen tested corresponding to shear distortion
Δ_t	ratio of interstorey drift to storey height corresponding to DR_t
δl	beam crack opening at the level of the longitudinal steel
δl_u	beam crack opening at the level of the longitudinal steel at ultimate
ϵ_c	concrete strain
ϵ_{cmax}	maximum strain at which concrete is assumed to crush
ϵ_{cr}	cracking strain of concrete
$\epsilon_{c_{top}}$	top fibre strain
ϵ_{co}	cylinder compressive strain at peak cylinder stress
ϵ_l	longitudinal strain

$\epsilon_{l, mid}$	longitudinal tensile strain at mid-depth of member
ϵ_s	steel strain
ϵ_{sh}	commencement of strain hardening
ϵ_{su}	strain in steel at ultimate moment
ϵ_u	ultimate strain
ϵ_v	tensile strain in transverse steel
ϵ_y	steel yield strain
ϵ_1	average principal tensile strain in concrete
ϵ_2	average principal compressive strain in concrete
ϵ_{20c}	strain factor used in Equation 5.1
ϵ_{50h}	strain factor used in Equation 5.1
ϵ_{50u}	strain factor used in Equation 5.1
μ_s	proportionality factor used in Equation 6.6
μ_ϕ	curvature ductility demand
μ_θ	rotational ductility demand
ω_i	undamped natural circular frequency
ϕ	curvature
ϕ_i	phase angle of i^{th} contributing sinusoid to earthquake motion
ϕ_u	ultimate curvature
ϕ_y	yield curvature
ρ_s	ratio of volume of transverse confining steel to volume of concrete core measured to outside of hoops
θ	rotation; angle of inclination of principal compressive stresses in concrete
θ_{max}	maximum rotation
θ_u	ultimate rotation
θ_y	yield rotation
ξ_n	damping ratio
■	end of algorithm

CHAPTER 1

INTRODUCTION

Earthquake resistant design provides a great challenge for structural engineers. As Newmark and Rosenblueth [1] point out "Earthquake effects on structures systematically bring out the mistakes made in design and construction, even the minutest mistakes." Lessons learned from past earthquakes such as San Francisco (1906), Long Beach (1933), El Centro (1940), Alaska (1964), Caracas (1967) and Managua (1972) have had a profound effect on North American codes. The recent 1985 Mexican earthquake further highlighted deficiencies in building codes and resulted in emergency changes to the Mexican building codes.

Experimental research on the reversed cyclic loading response of building components together with the recent development of non-linear dynamic analysis programs have provided basic tools for predicting the complete response of structures to strong ground motion. Although experiences from actual earthquakes provide the real test of building codes, the advent of these new analytical tools provide a means of evaluating design practice. The 1985 National Building Code of Canada [2] introduced new seismic zoning maps based on two parameters, the horizontal acceleration and the horizontal velocity. The 1984 Canadian Concrete Code [3] introduced new seismic design and detailing requirements for reinforced concrete structures. The design provisions for ductile moment resisting frame members were revised and new provisions were presented for members with "nominal ductility". Figure 1.1 summarizes some of the detailing requirements for the beams and columns corresponding to the level of "ductility" chosen in the design. The factor, K , reflects the type of construction, the degree of ductility and the energy dissipating capacity. In the light of these recent code changes there is a need for research in order to provide the following: a) experimental

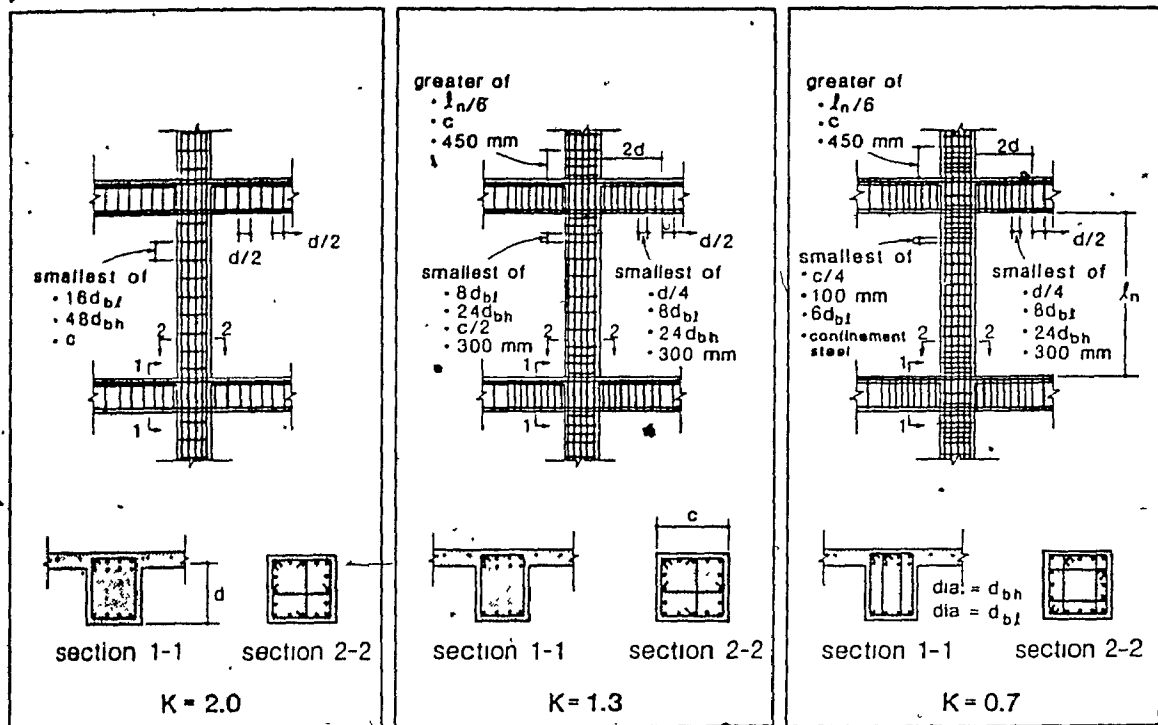


Fig. 1.1 Summary of detailing requirements for beams and columns

response data on large scale specimens designed and detailed according to the 1984 Canadian Concrete Code. b) non-linear response predictions of structures designed in different Canadian seismic zones with different levels of ductility.

1.1 PREVIOUS RESEARCH

In the field of earthquake engineering thousands of papers have been written on various subjects and research is still underway in many countries. The brief summary of previous research presented in this section will be restricted to research programmes which have had a direct influence on North American codes as well as on this research programme.

1.1.1 Seismic Risk Analysis and Seismic Zoning

The times of occurrence, the sizes and the locations of future earthquakes are uncertain and therefore should be described in probabilistic terms. The seismic zoning map introduced in the 1953 edition of the National Building Code [4] was only qualitative and based only on historical considerations. The first probabilistic seismic zoning map was introduced in the 1970 edition of the code [5]. This map developed from the work of Milne and Davenport [6], was based on the extreme value method and only the recurrence time was treated as a random variable. The seismic zoning maps, based on the Cornell method [7], given in the 1985 edition of National Building Code [2] represent a major departure from the previous code. Different maps are presented for peak horizontal ground acceleration and peak horizontal velocity, having a probability of exceedance of 10% in 50 years. The provision of two parameters (i.e., acceleration and velocity) for each location in Canada provides a more refined regional distinction and also provides a means of distinguishing between short and long period structural responses. More details on seismic risk analysis are given in Chapter 2.

1.1.2 Reversed Cyclic Loading Tests of Reinforced Concrete Components

Quasi-static reversed cyclic loading tests have been used to study the general responses of members under earthquake loading. Mahin and Bertero [8] have shown that the strain rate does not significantly affect the stiffness, the strength, the ductility nor the overall energy dissipating ability of reinforced concrete members. Hence quasi-static reversed cyclic loading tests are used to study the seismic responses of building components.

Early tests on beam-column connections were carried out by the Portland Cement Association and the University of Illinois in 1960 [9]. These experiments clearly demonstrated the benefits of confinement on the hysteretic response of beams. These tests however failed to simulate the complex behaviour of the beam-column joint region.

Ma, Bertero and Popov [10,11] reported the results of a series of tests carried out at the University of California at Berkeley on beam-column sub-assemblages. Some

of the test specimens included part of the slabs. Failure of the test specimens were either due to buckling of the bottom longitudinal bars and subsequent loss of load carrying capacity or due to loss of shear transfer across full depth open cracks in the beam. They concluded that the effect of the presence of the slab was to increase the negative moment capacity, which led to greater energy dissipation per cycle than was achieved in specimens without slabs. Increased compressive and shear forces due to the presence of the slabs were found to promote early buckling of the bottom longitudinal bars as well as to aggravate shear degradation. Supplementary ties in the beams to support compressed longitudinal bars increased the energy dissipation capacity. It was also found by the authors that the amount of bottom longitudinal steel had a significant effect on the energy dissipation capacity of the sections. They suggested that to improve the energy dissipation capacity of frames the ratio of compressive reinforcement to tensile reinforcement shall not be less than 0.75. The advantage of designing beams in frames with larger positive moment capacity has also been pointed out by Paulay [12]. Ma, Bertero and Popov also presented a detailed discussion of the effects of high shear in critical flexural regions. The pinching effect induced by high shear on the load-displacement relationship was clearly highlighted by the authors. A reduction in the energy dissipation capacity of more than 66% and a reduction in the plastic hinge rotation capacity of 30% occurred due to the presence of high shear.

Park [13] suggested that each beam bar in compression regions should be supported laterally by a corner of a tie. He recommended that the spacing of stirrup ties surrounding compression steel bars should not exceed six times the diameter of the longitudinal bar in order to prevent buckling of the longitudinal bars in plastic hinge zones.

Kent and Park [14] studied the influence of size and spacing of transverse ties in columns on the confinement of the concrete core of the column. They proposed an equation to modify the post peak stress-strain relationship of the concrete as a function of tie reinforcement ratio. Sheikh and Uzumeri [15] conducted a series of tests in which both the transverse reinforcement layout as well as the longitudinal reinforcement were varied. They found that both of these variables have a significant effect on the

confinement which could result in an increase in strength as well as ductility.

Uzumeri [16] at the University of Toronto and Uzumeri and Seckin [17] have performed a series of tests on beam-column connections to study the effect of the joint behaviour on the response of the sub-assemblages. The authors concluded from the results of tests on nine full-scale specimens that: 1) the energy dissipation capacity of beam-column sub-assemblages is dependent on the anchorage and confinement provided by the joint ties which therefore should be fully anchored in the core, 2) the assumption of rigid beam-column connections can lead to erroneous results in inelastic dynamic analysis of reinforced concrete frame structures, 3) the ductility achieved by the test specimens is affected by the strain in the joint ties, 4) the yielding of the joint steel should be prevented, and 5) the 45° truss analogy for the design of joint shear reinforcement does not predict the behaviour of the joint well.

Park and Paulay [13,18] give an excellent summary of the behavioural aspects of beam-column joints. Paulay, Park and Priestley [19] discussed the contribution of joint shear reinforcement and inclined concrete compressive struts on the joint shear resistance. Due to the yield penetration into the joint under cyclic loading it was suggested that the contribution of the concrete to the shear resistance of the joint should be neglected. It was also suggested that, in order to limit bond slip, the diameter of the beam longitudinal bars passing through the joint should be limited to $1/25$ of the column depth.

Zhu and Jirsa [20] studied the bond deterioration in beam-column joints and recommended that the beam bar diameter not exceed about $1/20$ of the column width and that the column bar diameter not exceed $1/22$ of the beam depth.

There are still some uncertainties in determining the effective width of the floor slabs and in particular the amount of slab reinforcement participating in the development of the flexural capacity of beams. Large differences in the measured and predicted responses of a seven-storey, one-fifth scale reinforced concrete frame-wall model tested under the U.S.-Japan Cooperative Research Program at the University of California at Berkeley [21] were attributed to the participation of the slab in the resistance of the model. In the past few years some studies have been undertaken to investigate the

behaviour of beam-column sub-assemblages with slabs and transverse beams. Ehsani and Wight [22,23,24] observed that the improved confinement provided by transverse beams prevented the pullout of the beam longitudinal bars. The authors noted that the ratio of column flexural strength to beam flexural strength may be over estimated by neglecting the contribution of the slab reinforcement in negative bending. It was suggested that the effective width of the slab in tension be taken at least equal to the width of the beam on each side of the column and that the ratio of the column flexural strength to beam flexural strength be no less than 1.4.

Hawkins and Lin [25] studied the reversed cyclic loading bond characteristics of reinforcing bars anchored in joints. They concluded that the deformations in joints must be considered and that the bond slip can be modelled by a rigid body rotation of the beam at the column face. They concluded that the bond-slip characteristics for bars are as important as their stress-strain characteristics in modelling member response.

1.1.3 Non-Linear Dynamic Analyses of Reinforced Concrete Structures

Non-linear dynamic analysis frame programs have been used to study the response of structures to earthquake loadings. These programs use beam elements with concentrated non-linear springs located at their ends. These springs are usually assigned some empirically derived hysteretic behaviour in the form of load-response rules. These load-response rules were typically determined from experiments. A few of the hysteretic models for reinforced concrete members are described below:

a) *Bi-linear model* - In the early stage of development elastic-perfectly plastic models which were successfully used to model steel members had also been applied to reinforced concrete structures. The improvement of this model by assigning a finite slope to the post yielding stiffness resulted in the bi-linear model as shown in Fig. 1.2 a. This model does not represent the degradation of the loading and unloading stiffnesses after yielding and therefore overestimates the energy dissipating capacity of reinforced concrete members. This model can be fully described by three load-response rules as shown in the figure.

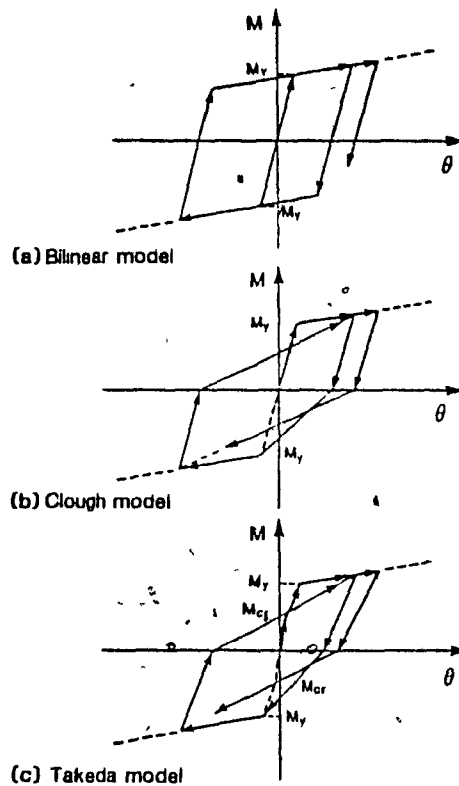


Fig. 1.2 Moment-Rotation hysteresis models

Veletsos and Newmark [26] have used the elasto-plastic model in the analysis of a single degree of freedom system. They found that the maximum displacement of this simple inelastic system was practically the same as that of an elastic system.

Mahin and Bertero [27] have used the bi-linear model in the analyses of the response of the following structures: 1) the Charaima building in Caracas, an eleven-storey moment resisting frame which partially collapsed during the 1967 Venezuelan earthquake, 2) the Olive View Hospital Main Building, a mixed structural system that suffered extensive damage during the 1971 San Fernando earthquake, and 3) the Banco de America building in Managua, an eighteen-storey building which had four shear wall cores as the principal lateral force resisting system and which sustained moderate damage to the core tie girders during the 1972 Nicaragua earthquake. The authors have tried to reconcile the analytical findings with the actual damage observed in the buildings after these earthquakes. They concluded that dynamic analyses can provide

additional information regarding the seismic response (e.g., displacements, interstorey drifts, maximum and residual inelastic deformations) not obtainable with conventional methods such as static analysis (linear or non-linear) or dynamic elastic analysis. They obtained better predictions of the performance of the buildings studied from the inelastic dynamic analyses than from the elastic analyses. The authors concluded however that in this type of analyses considerable engineering judgement was required in the following three areas: 1) modeling member mechanical characteristics, 2) estimating the energy dissipation capacity of the critical regions, and 3) selecting critical ground motions.

Clough, Benuska and Wilson [28,29] have used the bi-linear model in their study of the non-linear dynamic behaviour of a twenty-storey reinforced concrete structure in which the relative strengths of the beams and the columns were varied. The structure was subjected to the accelerogram for the North-South component of the 1940 El Centro earthquake. Some of the design conclusions from this study are: 1) A "weak girder - strong column" philosophy is preferred in order to arrive at reasonable ductility demands. The formation of plastic hinges in the beams does not seriously affect the vertical load carrying capacity of the structure. The formation of plastic hinges in the columns could lead to collapse of the structure. 2) Avoid localized zones of weakness in the structure because all of the inelastic action could take place in these locations, with the remainder of the structure remaining essentially elastic. A more appropriate structure, capable of absorbing more energy, would have a more uniform distribution of strength and stiffness such that yielding is more uniformly distributed over the structure. The same conclusions were arrived at by Park and Paulay [18] from their static collapse analyses of reinforced concrete frame structures. Paulay [30] reported the inelastic dynamic responses of three prototype frames designed according to New-Zealand capacity design procedures in order to evaluate the adequacy of these procedures. Load-response relationships were represented by elastic-perfectly plastic hysteresis loops without allowance for stiffness degradation.

b) *Clough's degrading stiffness model* - The early PCA concrete frame tests [9] demonstrated that reinforced concrete members have a completely different form of post

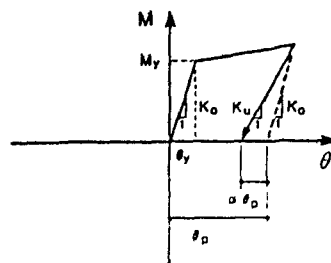
yielding response than the bi-linear model. Based on these tests, Clough and Johnston [31] proposed a model which could be completely described by six load-response rules. The first three rules are essentially the same as the elasto-plastic system, however after yielding the reloading stiffness is assumed to pass through the previous maximum response point. The energy dissipating capacity of this model is reduced significantly as can be seen by comparing Fig. 1.2a and 1.2b. A post yielding finite slope can be easily added to this model.

Clough and Johnston concluded from their study that: 1) The ductility requirements of systems modelled with degrading stiffness are not different from those obtained from the elasto-plastic models except for structures having a period of vibration less than 0.5 sec. 2) Systems modelled with degrading stiffness, representative of reinforced concrete frame members, have significantly different earthquake response characteristics from systems with elasto-plastic models. 3) The principal effect of the loss of stiffness resulting from yield deformations is an increase in period of vibration, modifying the response behaviour for long period structures and increasing the amplitude of displacements for short period structures.

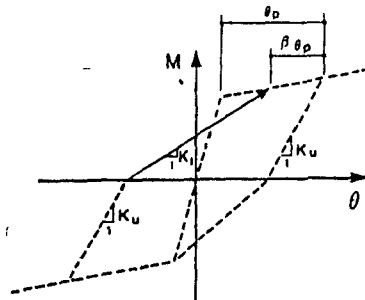
Clough [32] compared the response of a large scale, two-storey reinforced concrete frame structure to the response predicted by both the bi-linear and the Clough degrading stiffness models. The structure was tested on a shaking table and was subjected to the Taft 1952 earthquake motion [33]. He concluded that the degrading stiffness models gave a better representation of the response but noted that although good agreement was obtained further significant improvements could be made.

c) *Takeda's degrading stiffness model* – A more refined hysteresis model was developed by Takeda, Sozen and Nielsen [34] on the basis of experimental observations conducted at the University of Illinois. This improved model introduced stiffness change at flexural cracking and yielding, strain hardening past flexural yielding and an unloading stiffness which reduced as an exponential function of the previous maximum deformation. The set of 16 rules presented by the authors included detailed rules for load reversals (see Fig. 1.2c).

Otani and Sozen [35] simplified the Takeda model by removing the change of



(a) Reduced unloading stiffness



(b) Variable reloading stiffness

Fig. 1.3 Modified Takeda model, Litton [36]

stiffness at cracking of the concrete. Litton [36] and Powell [37] modified the Takeda model by also removing the change in stiffness at cracking and in addition introduced a reduction of the unloading stiffness by an amount which depends on the largest previous hinge rotation and a variable reloading stiffness which is larger than that of the Takeda model and which depends on the past loading history (see Fig. 1.3).

Otani and Sozen [35] compared the response of small scale three-storey one bay reinforced concrete frames that were tested on the University of Illinois earthquake simulator with their predictions using the Takeda model. They approximated member-end rotation due to bar slip with a concentrated hinge at the member end with load-deformation following a simplified bi-linear Takeda model without pinching. They found that the analytical model simulated the large amplitude oscillations well but failed to simulate the medium to low amplitude oscillations. They concluded that pinching of the hysteresis response curve due to bar slip and shear distortion needs to be incorporated in the analytical models.

Litton [36] compared responses of the two-storey, one bay reinforced concrete frame

that had been investigated by Clough [32,33] with the predictions using their modified Takeda model and the basic Takeda model. It was found that the maximum amplitude prediction was within 4% but the response predictions, although good at large amplitude oscillations, were poor at low-amplitude oscillations using the basic Takeda model. The predictions using the modified Takeda model were less accurate than with the basic Takeda model. The author concluded that further research was required before recommendations could be made on the use of either model.

A large number of interesting hysteresis models have been proposed in addition to the ones described above, particularly in Japan. Umemura and Takizawa [38] and Otani [39] have presented a very detailed and informative survey on the subject. One of the most interesting one is due to Takayanagi and Schnobrich [40]. They incorporated the effect of axial load variation in the Takeda model as well as pinching of the curve and a strength degradation feature. Takayanagi and Schnobrich compared the responses of ten-storey coupled shear walls that were tested on the University of Illinois earthquake simulator [41] with their predictions using their modified Takeda model. The Takeda-Takayanagi model with changing axial force was used for the wall element and the beam elements were modeled with the pinched model with a finite strength decay. The authors found that the predictions compared very well with the observed responses.

Recent analyses of frame-wall structures were carried out by Corley and Saatcioglu [42]. They used the Takeda-Takayanagi model with varying yield levels depending on the axial load acting on the walls. They studied the effects of axial load on the walls, pinching of the hysteretic response and shear yielding level.

Although non-linear dynamic analysis is mainly an analysis tool, guidance for its use in design is given by Fintel and Gosh [43]. This explicit inelastic design procedure attempts to investigate both the serviceability under the "design" earthquake and safety under the "hypothetical maximum credible" earthquake. Examples of applications of this procedure are given in References [44] and [45].

1.2 OBJECTIVES

The objective of this research program is to evaluate the seismic performance of reinforced concrete frame structures in two different regions of Canada. In particular the influence of design and detailing approaches is investigated. In order to meet this objective the following steps are taken:

- 1) A series of acceleration-time histories are generated for the Montreal and Vancouver regions.
- 2) A series of six-storey reinforced concrete frame structures are designed with different levels of ductility ($K=0.7$, $K=1.3$, $K=2.0$) for Montreal and Vancouver. The designs are carried out according to the 1985 National Building Code of Canada and the 1984 CSA Concrete Code.
- 3) Full scale sub-assemblages representing the exterior second storey beam-column connection with the three levels of ductility are tested. These sub-assemblages include part of the spandrel beams and the floor slab. The purpose of these tests is to study the reversed cyclic loading response of building components designed and detailed according to the latest code.
- 4) Analytical tools are developed to predict the test results. These analytical tools are then used to predict the responses of the building members.
- 5) In order to appropriately model the strength and stiffness degradation, as well as the pinching of the hysteresis response, a hysteresis model is developed and incorporated in the general purpose non-linear dynamic analysis program - DRAIN-2D [37].
- 6) Each of the six structures is analyzed for a series of acceleration-time histories using DRAIN-2D [37]. Four separate acceleration time history are scaled to three different levels of peak ground acceleration corresponding to "service", "design" and "ultimate" levels.
- 7) The results from the 72 time history analyses are evaluated in order to assess the structural damage, the ductility demand on the members and to provide a means of assessing the code design and detailing requirements.

The study is limited to symmetric frame structures founded on stiff soil. The structures are analyzed as two-dimensional frames with infinitely rigid floor diaphragms. The effects of all non-structural components are neglected in the analyses. Plastic hinges are assumed to form only at member ends.

The response predictions include the effects of:

- 1) bond-slip of reinforcing bars, anchored in the joint region,
- 2) joint shear distortion,
- 3) shear deformations of beams,
- 4) strain hardening of steel reinforcement,
- 5) effects of confinement on the stress-strain relationship of concrete,
- 6) participation of the slab reinforcement in the response,
- 7) strength degradation, stiffness degradation and pinching effects in the non-linear analyses.

CHAPTER 2

CANADIAN SEISMICITY AND GENERATION OF ACCELEROGRAMS

2.1 SEISMIC RISK ANALYSIS

Brief summaries of two well-known seismic risk analysis methods used to develop the seismic zoning maps in Canada are presented below.

2.1.1 Extreme Value Method – Milne and Davenport

The seismic zoning map used in the 1970 National Building Code of Canada [5] was based on the work of Milne and Davenport [6] and Witham, Milne and Smith [46], who used the extreme value method. The procedure followed in the derivation of this map is as follows:

- a) Based on historical data the probability of future ground motion occurrence at a given location is assumed equal to the average frequency in the past.
- b) A suitable attenuation law is assumed (e.g., Peak ground acceleration as a function of both magnitude and hypocentral distance).
- c) A relationship between acceleration versus probability of exceedance in any given year is assumed.
- d) Peak ground accelerations having a probability of exceedance of 0.01 per annum (corresponding to 40% probability of exceedance in 50 years) were computed for a large number of locations throughout Canada.
- e) The resulting contours were used to produce four seismic risk zones (see Fig. 2.1).

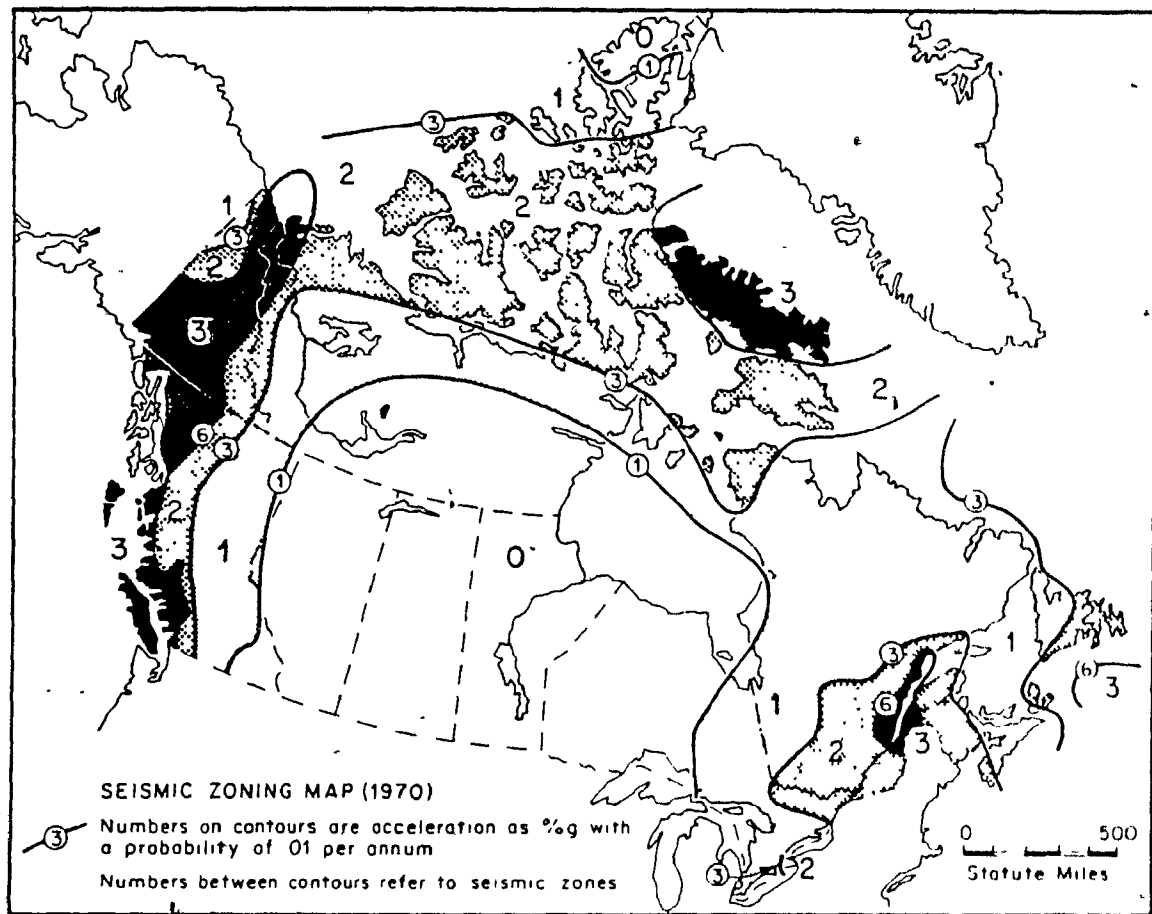


Fig. 2.1 1970 Seismic zoning map of Canada

Although the recurrence time is treated probabilistically in this method the random nature of the location and the size is not accounted for. One deficiency of maps derived with this method is that any change in either size or location can significantly alter the risk estimates.

2.1.2 Point Source Model – Cornell Method

The seismic zoning maps of the 1985 National Building Code of Canada [2] were derived based on the point source model developed by Cornell [7]. In essence the Cornell method combines information about times of occurrence of earthquakes, areal seismic activity supplemented by geological evidence and attenuation of motion intensity with distance, to give in probabilistic terms the seismic risk at a site. A complete analysis

includes the following four steps:

- a) Point, line or areal seismic sources are identified, based on seismic history as well as on geological evidence.
- b) A recurrence relationship is obtained or developed for each potential source. The relationship could be linear, bi-linear or truncated or non-linear.
- c) Forecasting future events is made by using a Poisson model. The Poisson model implies independence of arrival of the events, which have been found to be applicable on a worldwide basis, but not on a regional one.
- d) A suitable attenuation relationship linking a peak motion parameter (i.e., earthquake intensity, peak acceleration, velocity or displacement) is used to obtain the probable motion parameter at a site. The scatter of the peak motion parameters however is very large.

Such an analysis for a site would give for example a plot of peak motion characteristic (i.e., magnitude, acceleration, velocity or displacement) versus mean return period. Fig 2.2 presents the process followed to derive seismic zoning maps. Combining the results from a number of site risk analyses one can develop seismic probability maps or seismic zoning maps. The maps developed with the method have the following advantages:

- a) They account for randomness of times of occurrence, sizes and locations based on frequency of occurrence of various levels of seismic events.
- b) They include all available seismological data for potential sources.
- c) The probabilistic statement of the seismic parameters (i.e., magnitude, peak horizontal acceleration, peak horizontal velocity) at a site gives the engineer an estimate of the risk associated with it.
- d) Probable peak horizontal acceleration and velocity can be estimated corresponding to the economic life of a structure.
- e) An additional advantage of the method is the possibility to conduct sensitivity studies by varying the basic parameters used in the analysis [47,48] (see reference [49] for such an application in Canada). Cornell added the possibility of restricting the risk analysis to earthquakes presenting only damage threat at a site.

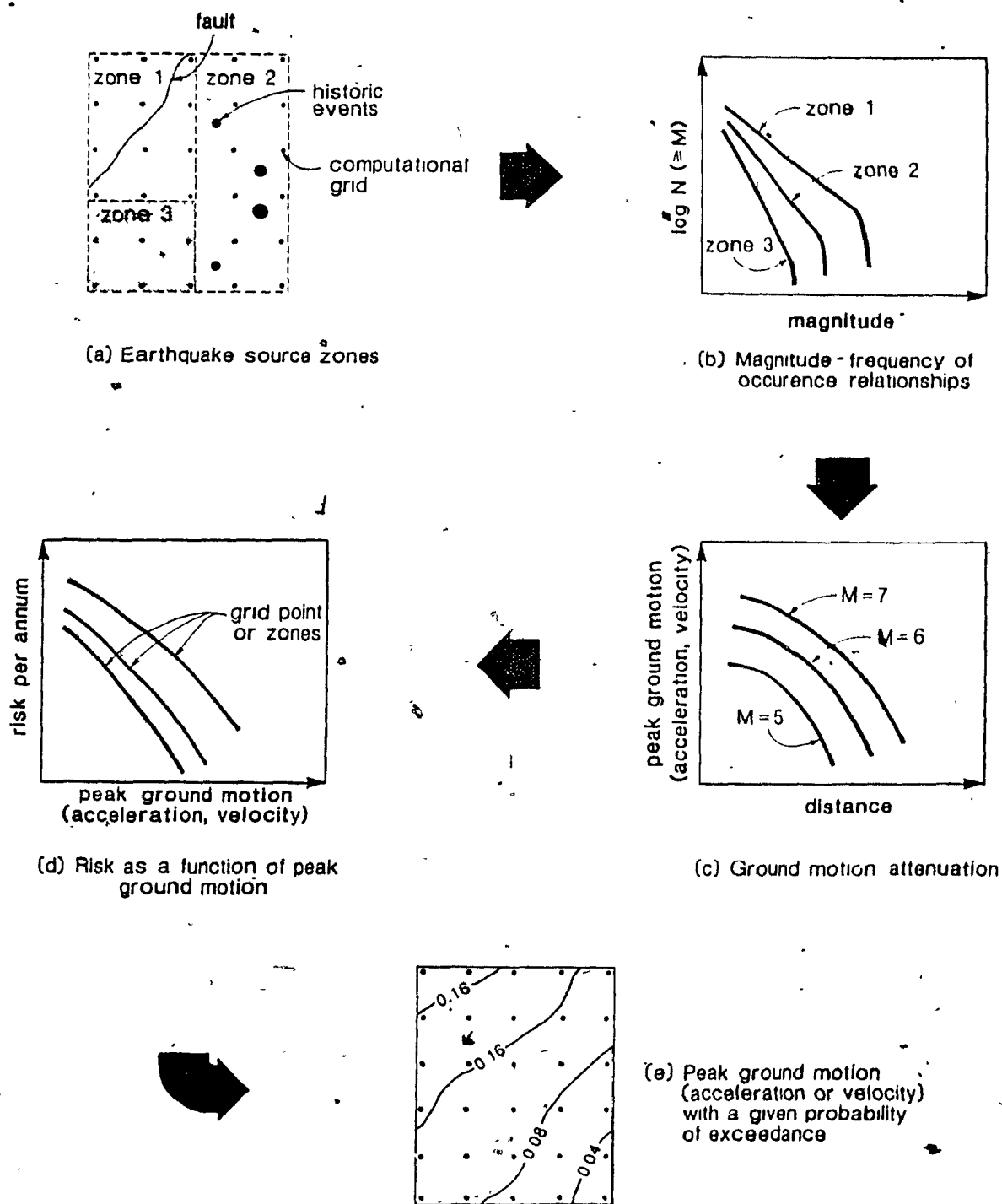


Fig. 2.2 Methodology for derivation of seismic zoning map

Up to the present time the duration of motion has not been included in the list of peak motion parameters. Another important motion parameter, the ground displacement, has not been used due to considerable scatter in the current attenuation relationships. This is unfortunate since both duration and displacement are of considerable importance in assessing structural performance.

2.2 THE 1985 SEISMIC ZONING MAP OF CANADA

To develop the new seismic zoning maps the country was divided into a grid of points. In addition the country and adjacent regions were divided into zones of earthquake occurrence. Wherever possible the boundaries of these zones were defined on the basis of geological and tectonic features. Figure 2.3 illustrates the zones of earthquake occurrence for the seismically active regions of Eastern Canada. In the absence of clearly defined active fault systems the zones were based on the distribution of historical seismicity. On the west coast there are clearly defined major fault systems as shown in Fig. 2.4. In the derivation of the maps different attenuation laws were used for Eastern and Western Canada to account for the much greater attenuation in Western Canada. Upper limits of magnitude were set deterministically for each zone. The resulting contours of peak horizontal accelerations and velocity, having a probability of exceedance of 10% in 50 years, were used to divide the country into seven seismic zones (see Fig. 2.5). The peak horizontal acceleration, a , and the peak horizontal velocity, v , give us information on both the distance from the anticipated earthquake sources and the frequency content of the motions. High frequency components of the motion (acceleration) attenuate more rapidly than lower ones (velocity, displacement). Therefore knowing the ratio of velocity to acceleration gives us an idea about the distances from the source. That is, the higher the v/a ratio, the greater the distance from the source. Since longer period structures are more affected by velocity, the higher the v/a ratio, the greater the influence on taller structures. Figure 2.6 illustrates the effects of velocity and acceleration ratios of different sites on the response spectra. A large v/a ratio indicates that the region is influenced by large earthquakes at great

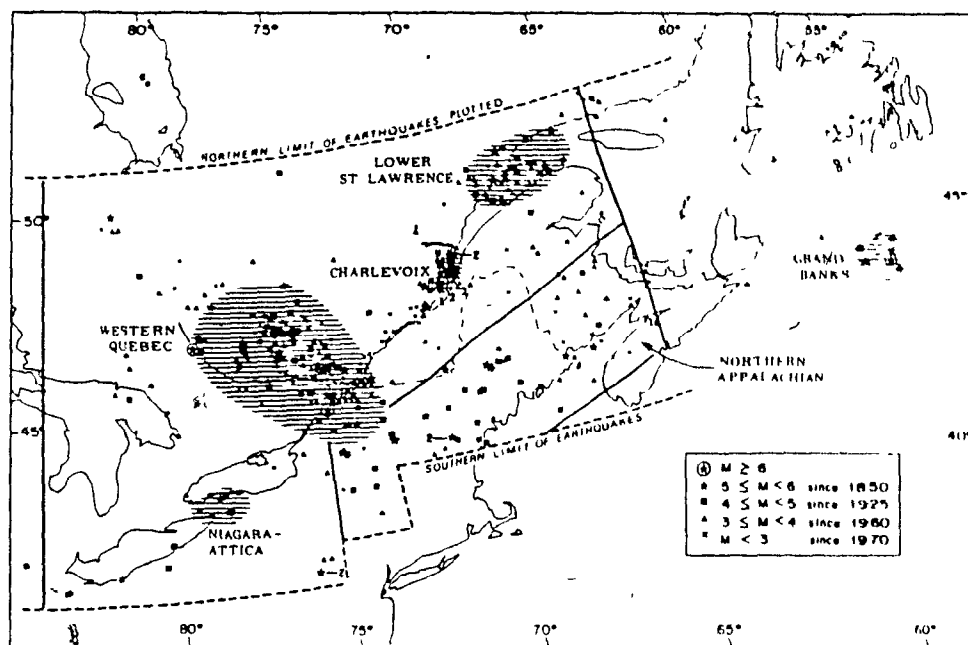


Fig. 2.3 Zones of earthquake occurrence and magnitudes (M) of earthquakes in Eastern Canada [49]

distances (e.g., Prince Rupert with $v/a = 2$). A low v/a ratio (e.g., Montreal with $v/a = 0.5$) indicates that the region is influenced by moderate earthquakes close-by.

2.3 GENERATION OF ACCELEROGRAMS

Non-linear dynamic analysis of structures is typically carried out with a number of different accelerograms. It has been demonstrated by Powell and Row [50] and by Biggs, Hansen and Holley [51] that the computed inelastic response of multi-degree of freedom systems vary greatly for different acceleration time-histories, even though the time histories have similar characteristics. It is generally agreed that the use of several accelerograms is necessary in order to adequately assess the non-linear dynamic performance of structures. For example Tso and Guru [52] have suggested that a minimum of eight records would provide a good estimate of the mean maximum response. The Applied Technology Council [53] suggests that four or five time histories be used. In their proposed "Explicit Inelastic Design Procedure", Fintel and Ghosh [43] suggest

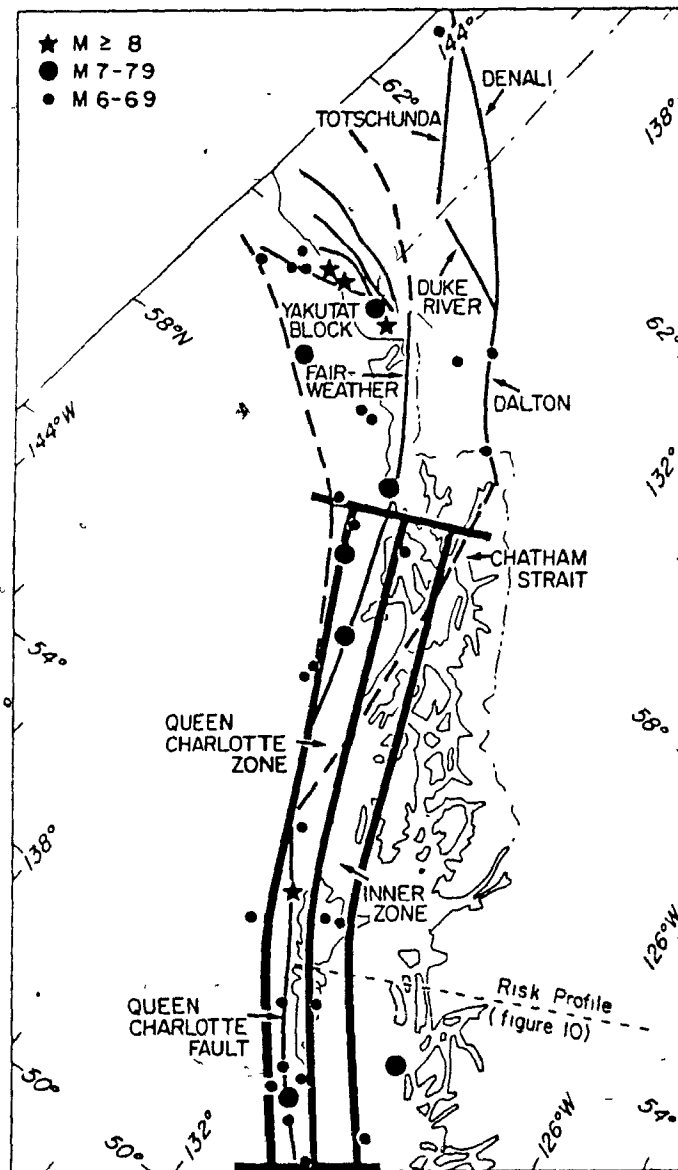
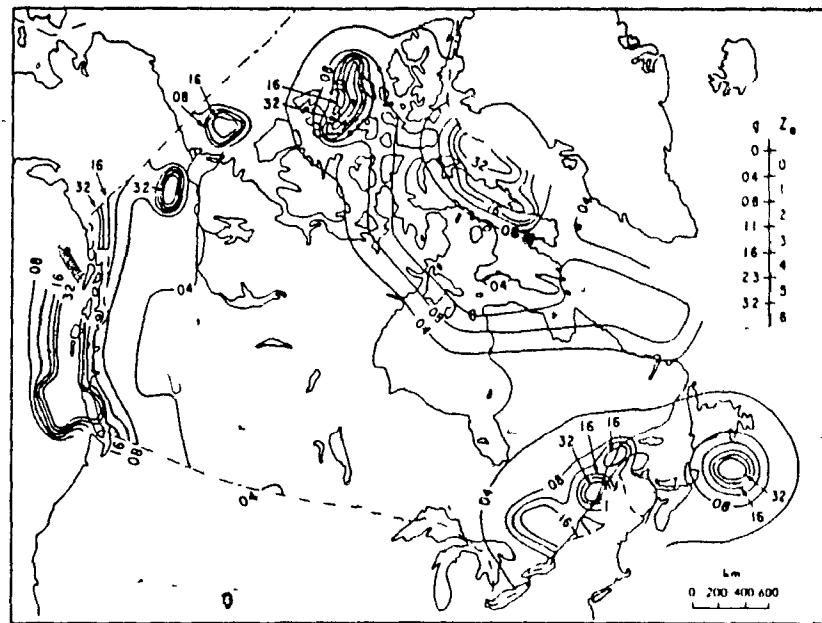


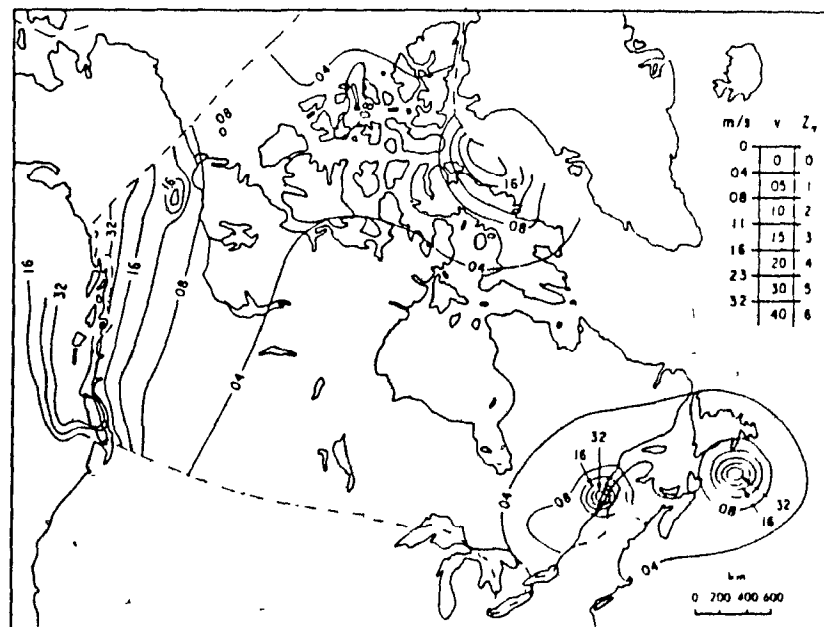
Fig. 2.4 Zones of earthquake occurrence and magnitudes (M) of Earthquakes in Western Canada [49]

that one or more earthquake accelerograms be selected from a number of records which "have frequencies with a potential to critically excite the structure". They further point out that the accelerogram that produces the maximum displacement is not necessarily the one which causes the largest forces in the members.

Newmark and Hall [54] stressed that, in the past, too much emphasis was placed on the peak horizontal ground acceleration. They have shown that high frequency



a) Acceleration related zones, Z_a , and contours of peak horizontal ground acceleration, in units of g , having a probability of exceedance of 10 per cent in 50 years



b) Velocity related zones, Z_v , and contours of peak horizontal ground velocities, in m/s, having a probability of exceedance of 10 per cent in 50 years

Fig. 2.5 1984 Seismic zoning maps of Canada [2]

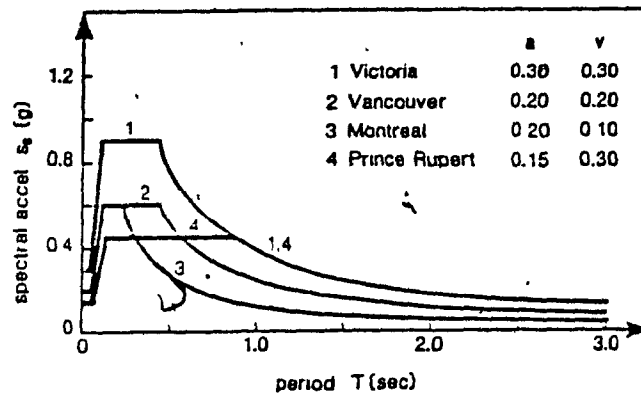


Fig. 2.6 Representative variation of response spectra for four different locations in Canada

spikes of acceleration do not significantly influence the response of structures and that strong energy content (related to velocity) is one of the most important parameters influencing the amount of damage. The use of both acceleration and velocity by code writing bodies [2,53] recognizes the important effects of velocity on the response.

It must be emphasized that no strong motion records are available for any region of Canada or the Eastern United States. It is therefore necessary to artificially generate a number of different acceleration time-histories. The computer program SIMQKE [55,56,57] is used to generate a series of spectrum compatible accelerograms. The generation is based on the concept that the motion consists of a summation of a large number, n , of random oscillatory functions of time. While the amplitude, A_i , of each oscillatory function is dependent on the target response spectrum, the phase angle, ϕ_i , is chosen randomly over the interval 0 to 2π . The basic equation describing the summation is given by:

$$a(t) = I(t) \sum_{i=1}^n A_i \sin(2\pi\omega_i t + \phi_i) \quad (2.1)$$

where $I(t)$ is a deterministic envelope intensity function which describes the overall character of the earthquake motion.

The intensity function defines such parameters as the rising time, T_{rise} , the strong motion duration, $T_{sustained}$, and the decaying time, T_{decay} , as shown in Fig. 2.7. Also

shown in Fig. 2.8 are the shape functions used in this study to describe the rising and decaying portions of the intensity function. The most important intensity function parameter is the duration of the sustained motion.

Housner [58] has proposed a relationship between earthquake magnitude, maximum acceleration and duration of sustained motion. For example, for maximum accelerations of $.15g$ and $.22g$ he suggests strong motion durations of 6 and 12 seconds respectively. Based on observations of records of various sites and seismic risk analyses Cornell and Merz [59] inferred that "the strong motion duration will be relatively short, about 5 sec., perhaps" for the Boston region. For Eastern Canada where one expects moderate earthquakes near-by it is assumed that the strong motion duration will be 5 seconds as shown in Fig. 2.8. For Western Canada where one expects larger earthquakes at greater distances it is assumed that the strong motion duration will be 9 seconds, with rise time and decay time as shown in Fig. 2.8. These values correspond to those used by Mahin and Bertero [27] for the San Fernando region in California. The strong motion durations assumed for Montreal and Vancouver are also about equal to those suggested by Housner [58].

Using the response spectra given in the 1980 Commentary to the National Building Code of Canada [60] as target spectra with velocity bound adjusted by multiplying by the v/a ratio corresponding to Montreal and Vancouver twelve different motions were generated for both locations. SIMQKE incorporates an iterative feature to improve the matching of the target spectrum. However when this feature was used, it was found that the ground displacements were strongly biased in one direction resulting in large residual displacements. Luyties, Anagnostopoulos and Biggs [61] decided not to use this additional iterative procedure in an attempt to obtain a more natural motion. Therefore in all subsequent generations of motions in this study this additional iterative procedure was not employed.

From the sets of twelve artificially generated motions, three motions were chosen for Montreal (see Fig. 2.9, 2.10 and 2.11) and for Vancouver (see Fig. 2.12, 2.13 and 2.14). The response spectra for the three motions are shown in Fig. 2.15 for Montreal

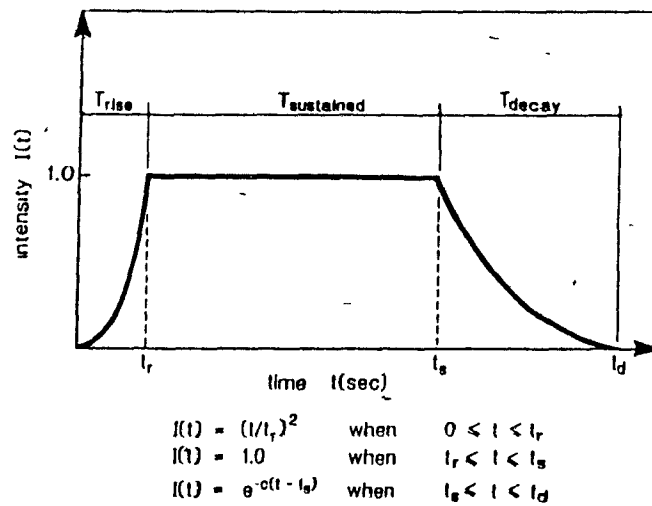
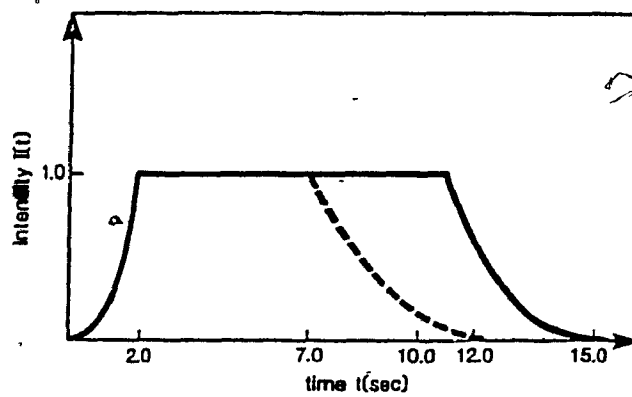


Fig. 2.7 General characteristics of intensity function



	T_{rise}	$T_{sustained}$	T_{decay}	α
Western Canada	2.0	9.0	4.0	0.5
Eastern Canada	2.0	5.0	5.0	0.5

Fig. 2.8 Intensity functions assumed for Western and Eastern Canada

and in Fig. 2.16 for Vancouver. The factors which influenced the choice of the motions are explained below:

- reasonably close matching of the target spectrum in the expected period range of the structures (see Fig. 2.15 and 2.16),
- small residual velocities and displacements at the end of the motion were preferred (see Fig. 2.9 to 2.14),
- although there was reasonably good matching of the target spectrum on the av-

erage, a concious effort was made to choose motions having responses above and below the target spectrum for the period range of interest.

In addition to the artificially generated motions the El Centro 1940 North-South earthquake motion was also included in the study in order to include a real earthquake motion.

All of the motions were scaled to desired maximum peak ground accelerations in order to produce "service", "design" and "ultimate" motions for both Montreal and Vancouver as shown in Table 2.1.

Table 2.1 Peak Ground Accelerations			
Region	Peak Ground Acceleration, g		
	Service	Design	Ultimate
Montreal	0.078	0.180	0.270
Vancouver	0.089	0.210	0.315

The design maximum acceleration corresponds to the peak horizontal acceleration having a probability of exceedance of 10% in 50 years. The service earthquakes were assumed to have a maximum acceleration having a probability of exceedance of about 40% in 50 years. This service earthquake is used to study the response of the structures under small earthquakes having large probabilities of occurrence in the life of the structure. The ultimate maximum accelerations were assumed to be 1.5 times the design maximum acceleration. It was felt that these maximum acceleration level would produce significant non-linear actions in the structures and would represent a large earthquake having a low probability of occurrence in the life of the structure. It is noted that it is impossible to estimate the probability of occurrence of such large events in Canada due to the lack of data.

• SIMULATED MOTION FOR MONTREAL AREA ($V/A=0.539$)
MOTION MATCHING NBC 80 RESPONSE SPECTRUM FOR 0.05 OF CRITICAL DAMPING
⊙ PEAK VALUES : ACC = 981.0 CM/SEC/SEC VEL = 85.7 CM/SEC DIS = 47.7 CM

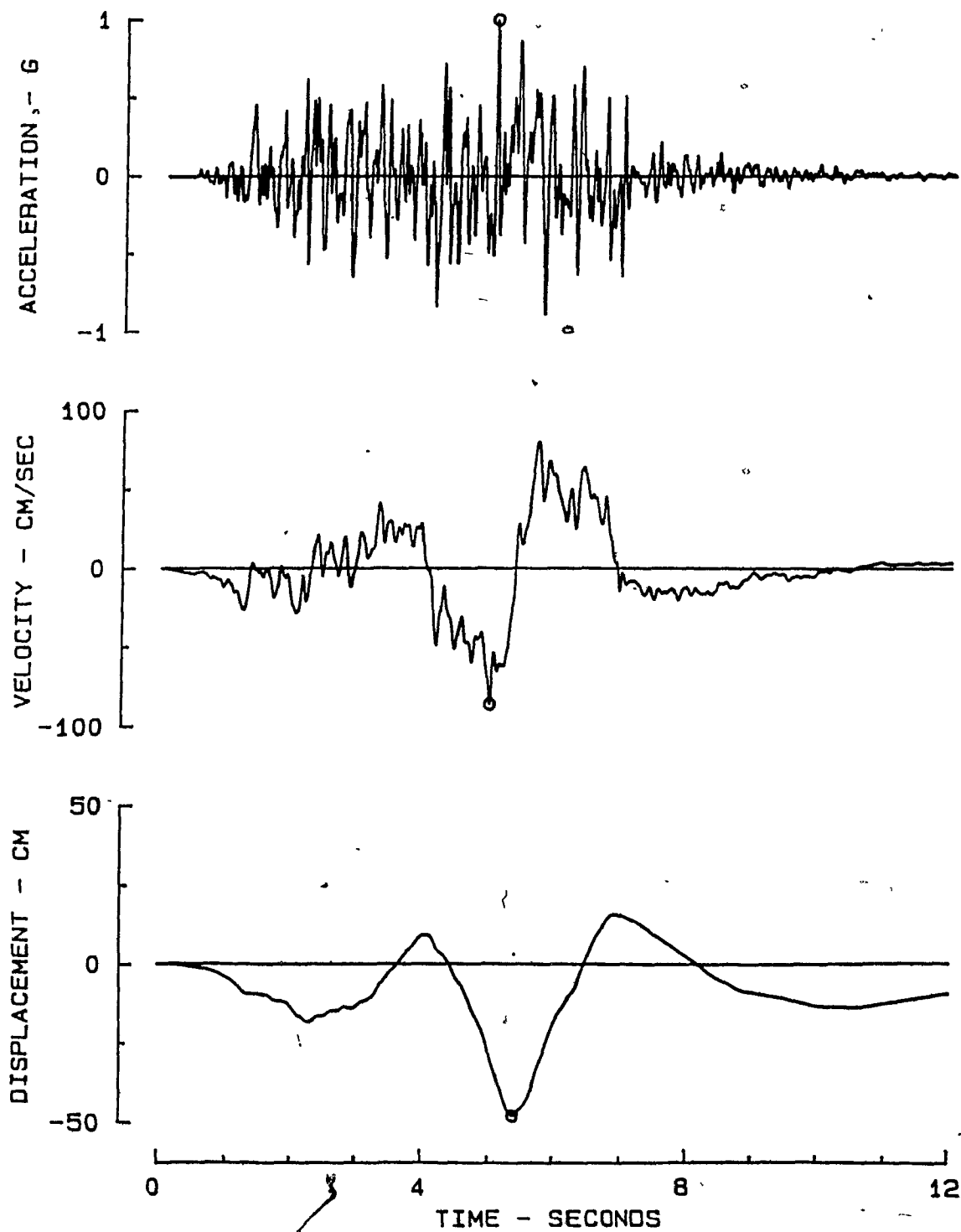


Fig. 2.9 Simulated ground motion 1-Montreal region

SIMULATED MOTION FOR MONTREAL AREA ($V/A=0.539$)
MOTION MATCHING NBC 80 RESPONSE SPECTRUM FOR 0.05 OF CRITICAL DAMPING
⊙ PEAK VALUES : ACC = 981.0 CM/SEC/SEC VEL = 81.7 CM/SEC DIS = 40.1 CM

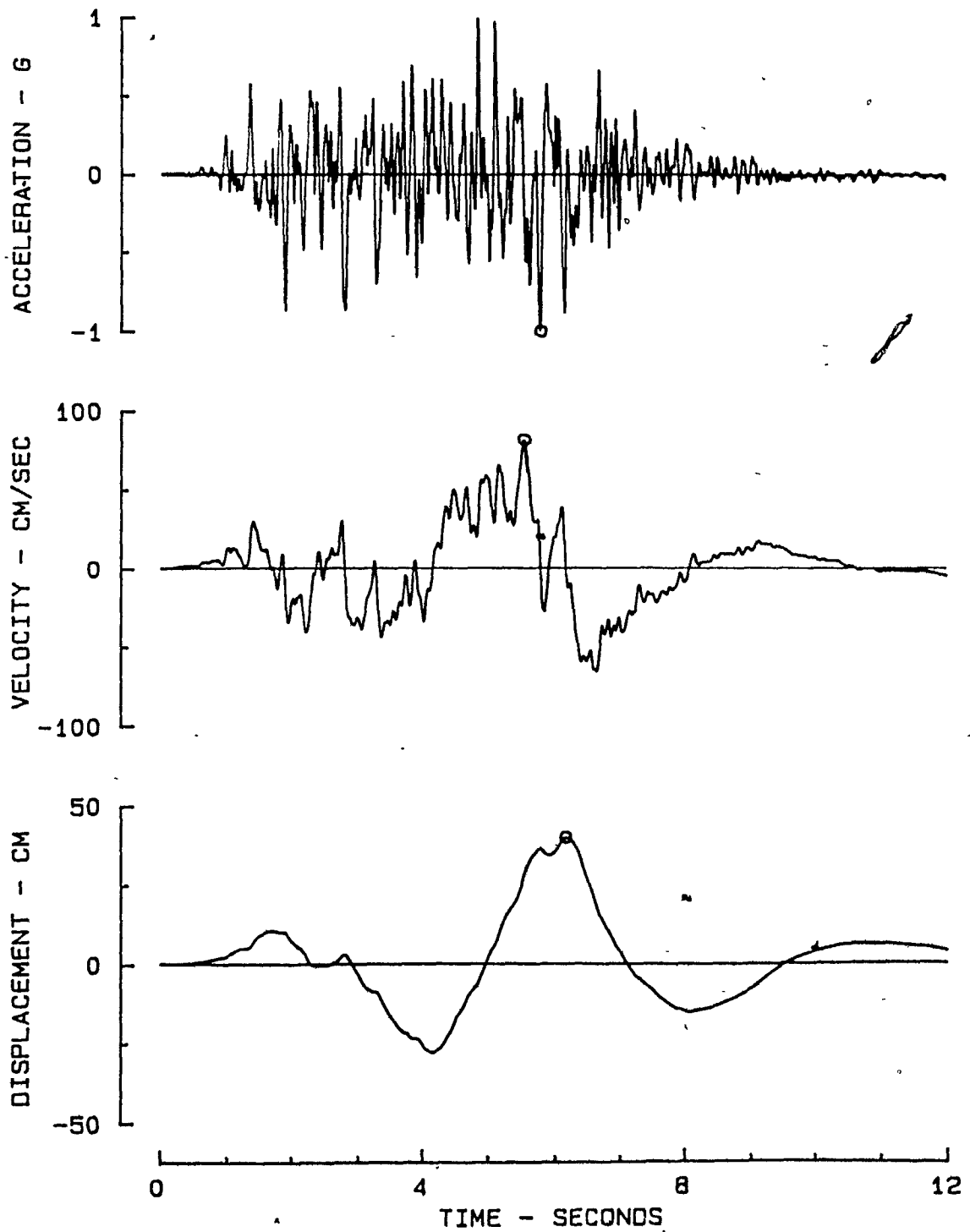


Fig. 2.10 Simulated ground motion 2-Montreal region

^ SIMULATED MOTION FOR MONTREAL AREA ($V/A=0.539$) -
MOTION MATCHING NBC 80 RESPONSE SPECTRUM FOR 0.05 OF CRITICAL DAMPING
⊙ PEAK VALUES : ACC = 981.0 CM/SEC/SEC VEL = 68.3 CM/SEC DIS = 22.8 CM

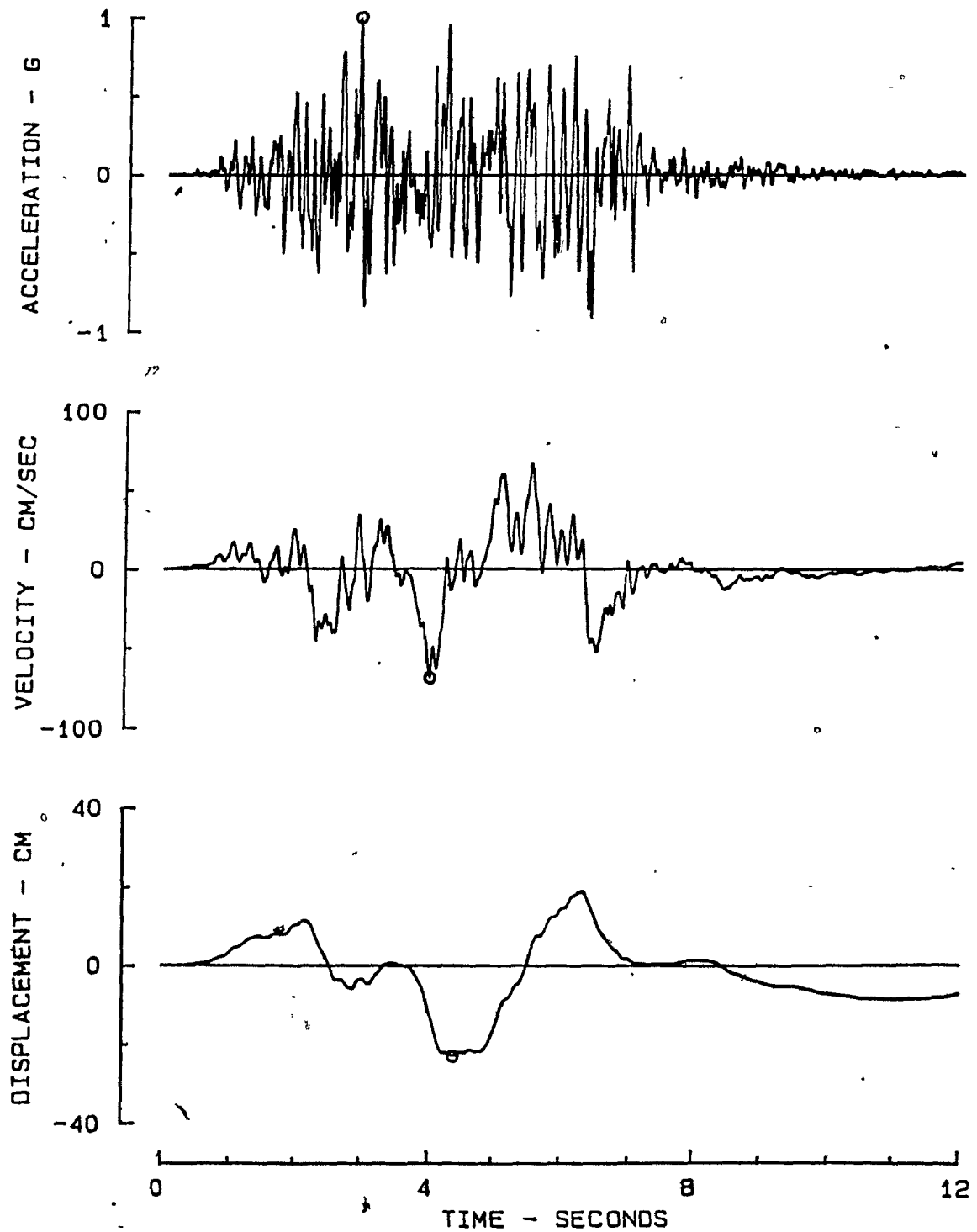


Fig. 2.11 Simulated ground motion 3-Montreal region

SIMULATED MOTION FOR VANCOUVER AREA ($V/A=1.000$)
MOTION MATCHING NBC 80 RESPONSE SPECTRUM FOR 0.05 OF CRITICAL DAMPING
⊙ PEAK VALUES : ACC = 206.0 CM/SEC/SEC VEL = 26.7 CM/SEC DIS = 16.3 CM

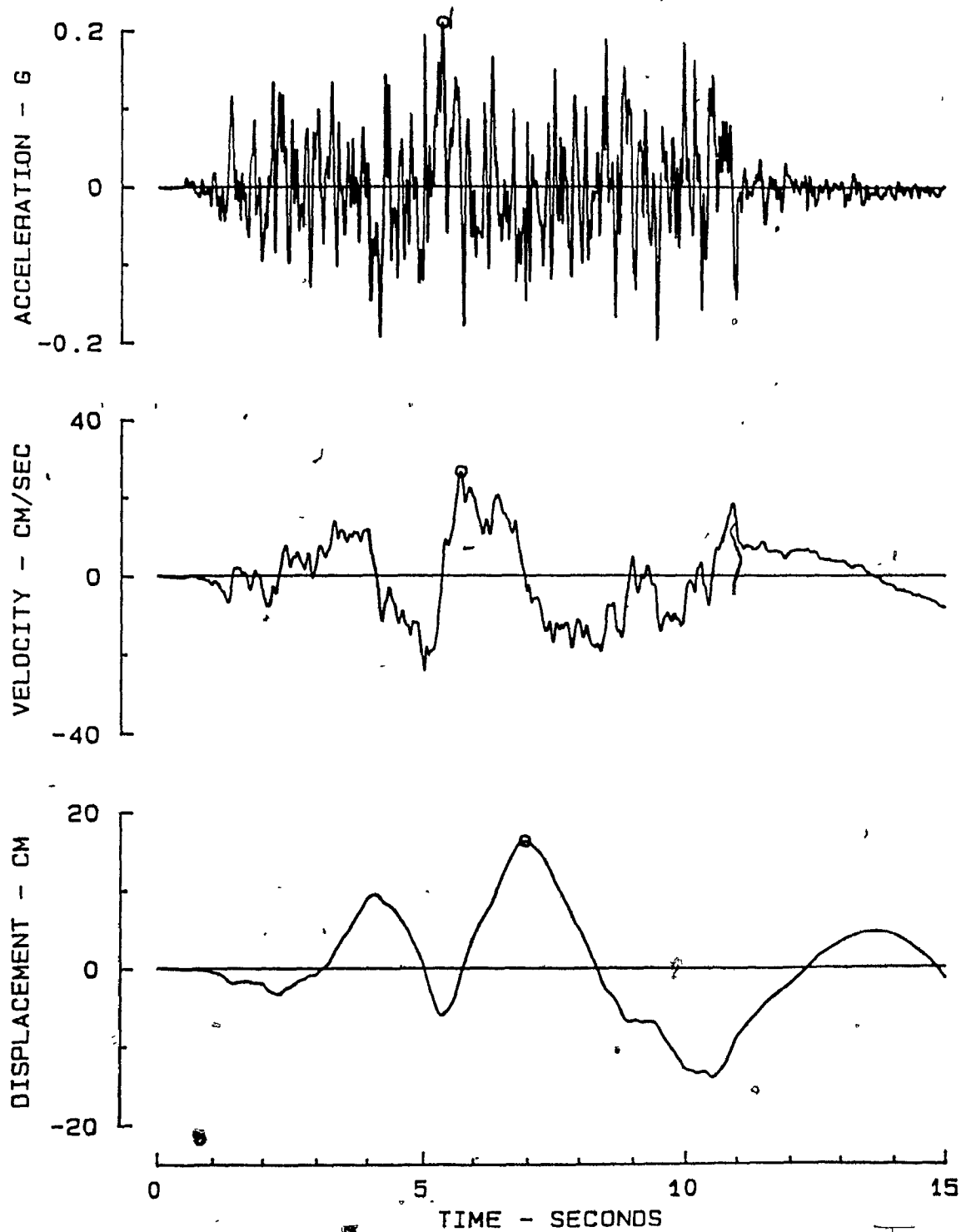


Fig. 2.12 Simulated ground motion 1-Vancouver region

SIMULATED MOTION FOR VANCOUVER AREA ($V/A=1.000$)
MOTION MATCHING NBC 80 RESPONSE SPECTRUM FOR 0.05 OF CRITICAL DAMPING
@ PEAK VALUES : ACC = 206.0 CM/SEC/SEC VEL = 42.2 CM/SEC DIS = 45.6 CM

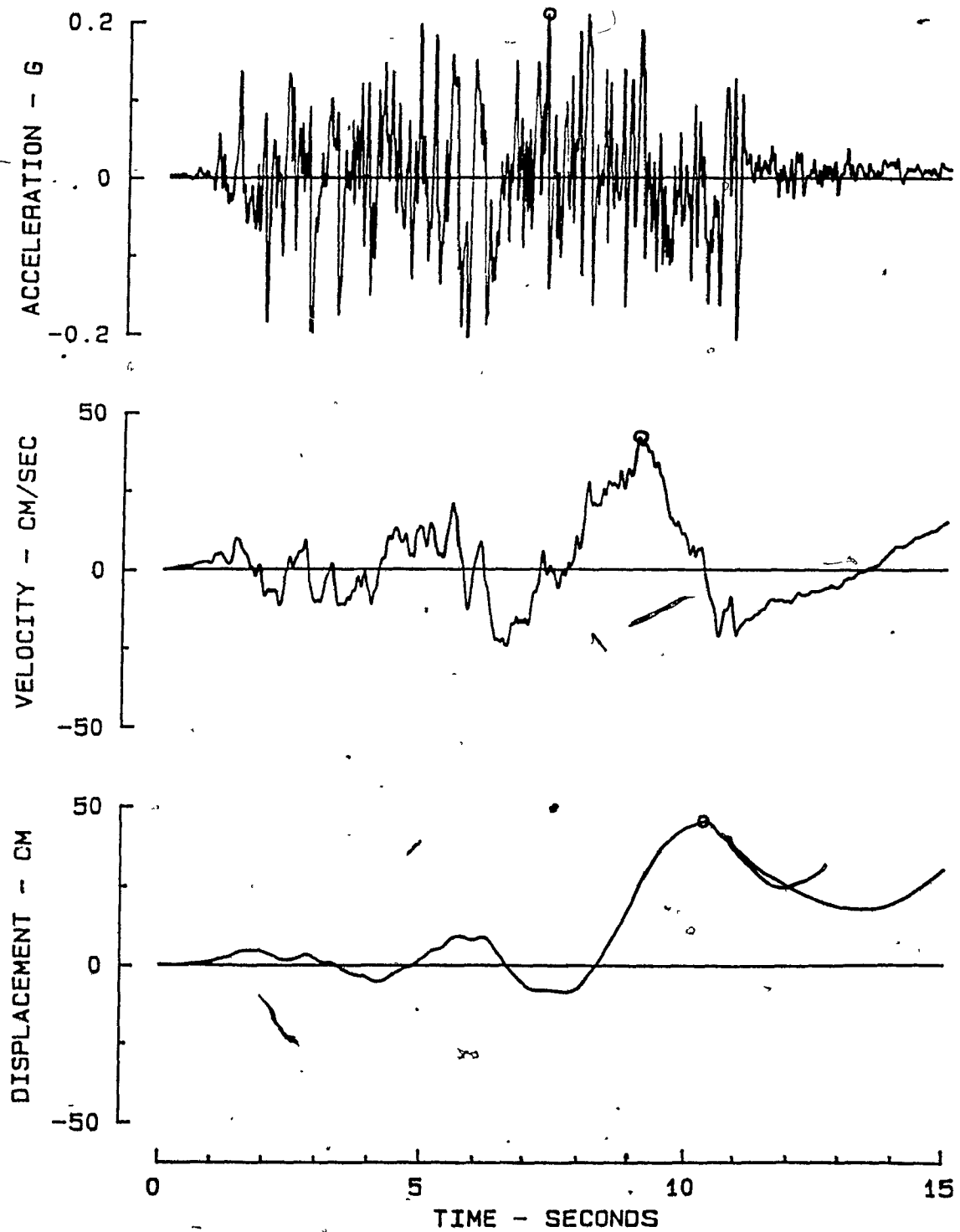


Fig. 2.13 Simulated ground motion 2-Vancouver region

SIMULATED MOTION FOR VANCOUVER AREA ($V/A=1.000$)
MOTION MATCHING NBC 80 RESPONSE SPECTRUM FOR 0.05 OF CRITICAL DAMPING
⊙ PEAK VALUES : ACC = 206.0 CM/SEC/SEC VEL = 23.8 CM/SEC DIS = 11.3 CM

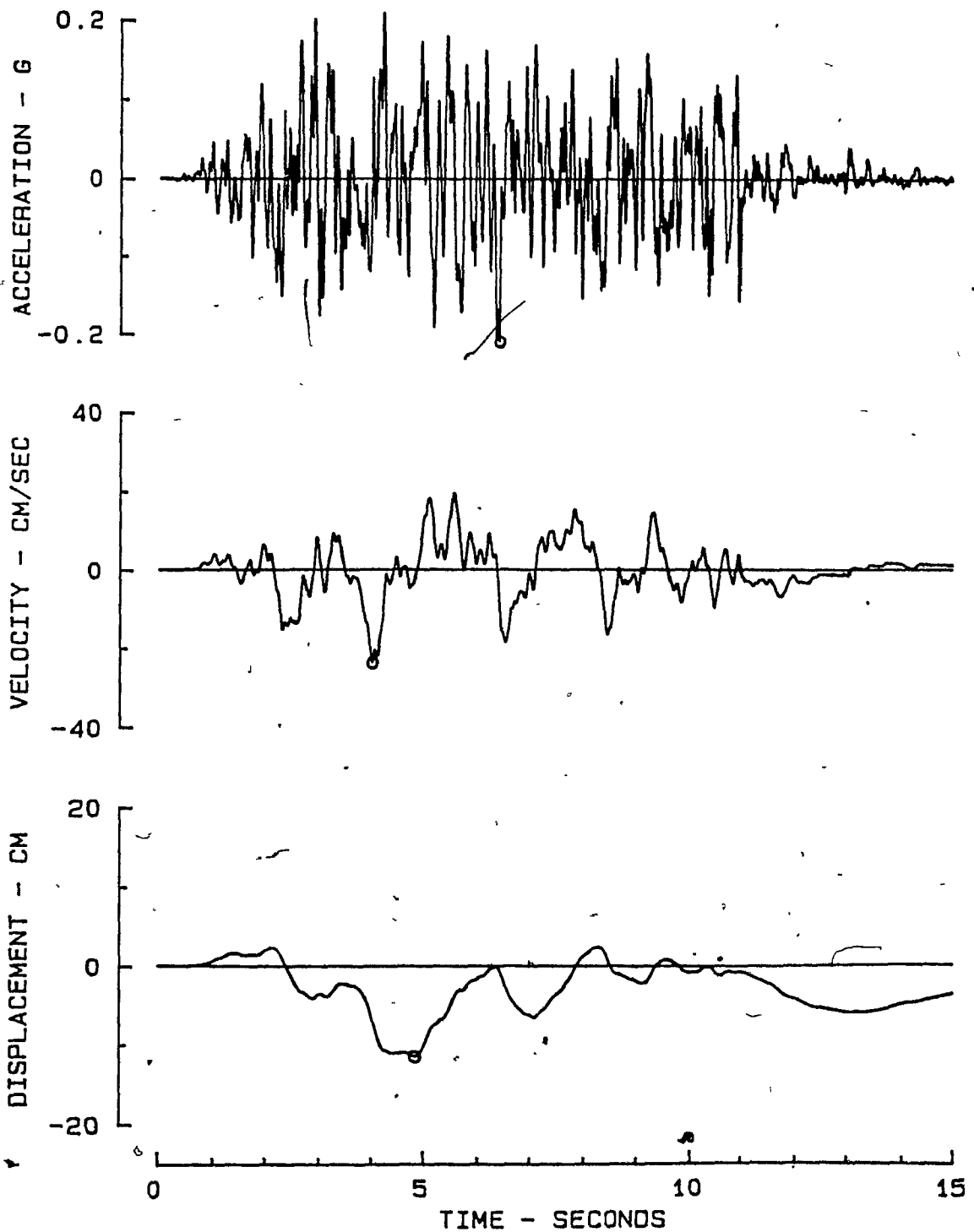


Fig. 2.14 Simulated ground motion 3-Vancouver region

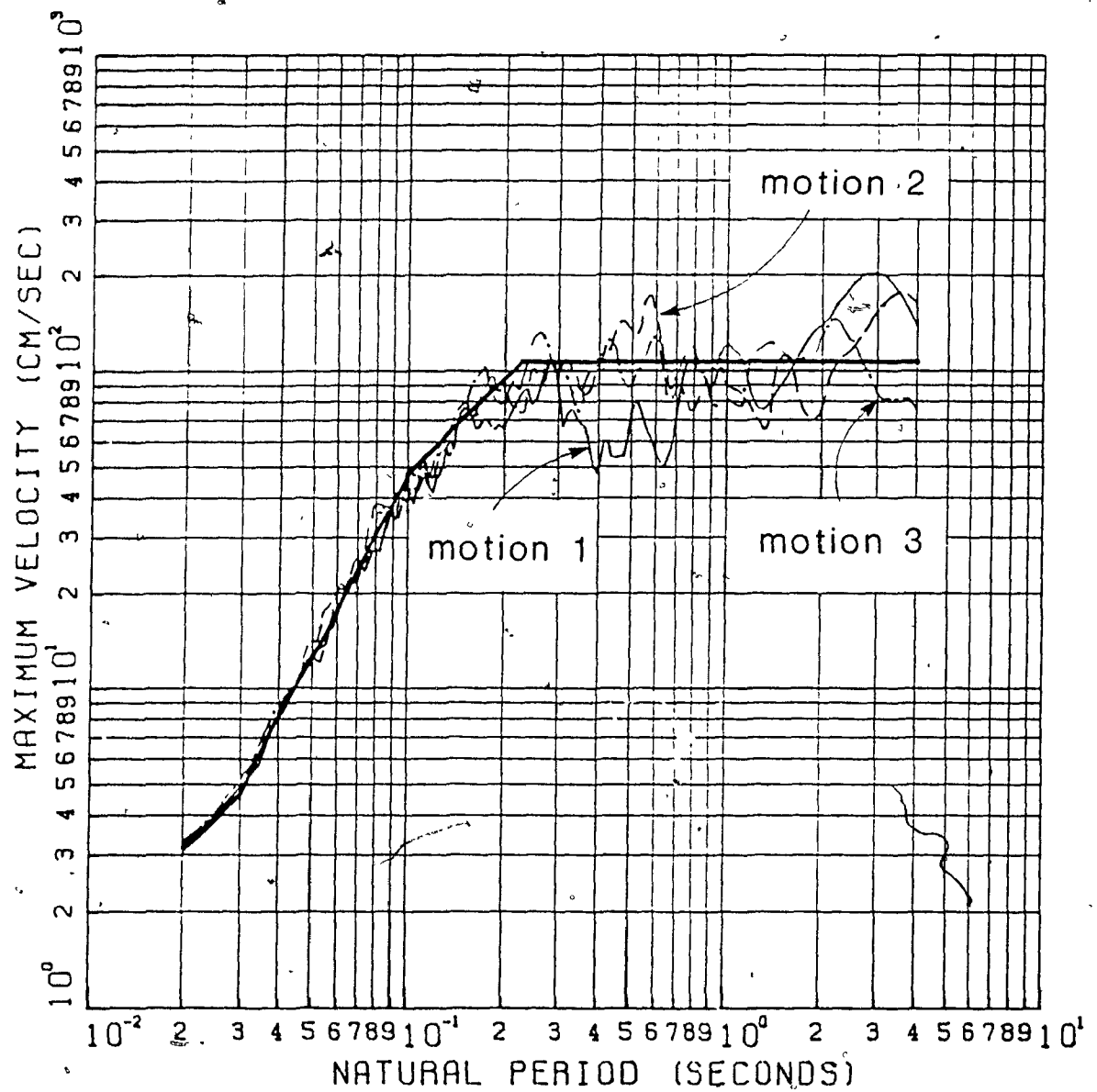


Fig. 2.15 Pseudo-velocity response spectra—Montreal region

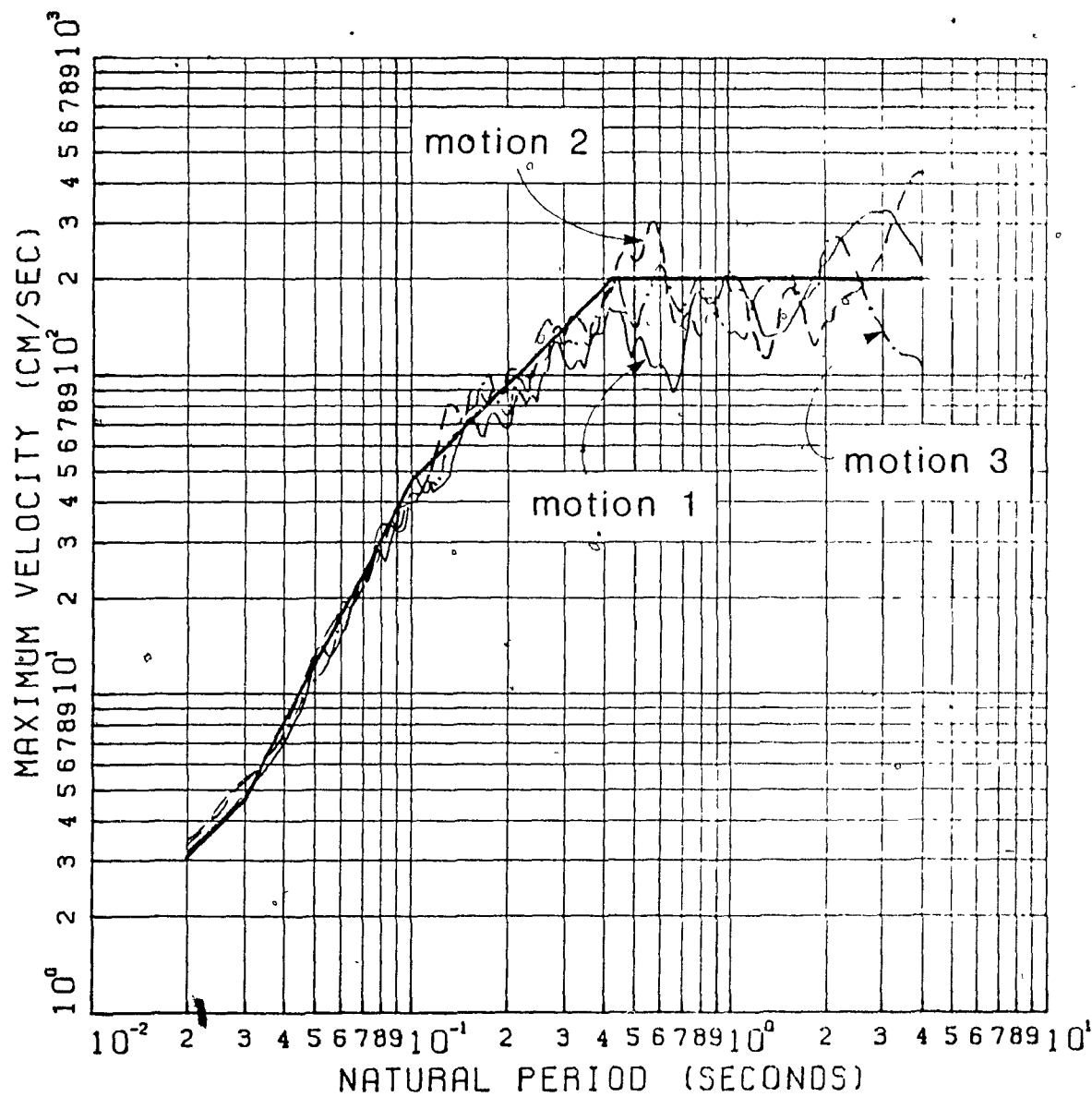


Fig. 2.16 Pseudo-velocity response spectra-Vancouver region

CHAPTER 3

MOMENT RESISTING FRAME STRUCTURES DESIGNED FOR MONTREAL AND VANCOUVER

3.1 GEOMETRY OF STRUCTURES

Two six-storey reinforced concrete moment resisting frame buildings located in Montreal and Vancouver were designed with $K=1.3$ and $K=0.7$ according to the 1985 National Building Code of Canada [2] and the 1984 Canadian Concrete Code, CSA CAN3-A23.3-M84 [3]. In addition, to enable an evaluation of older concrete buildings, a third building was designed with force levels corresponding to $K=1.3$ and reinforcing details according to earlier concrete codes (e.g. the 1977 Canadian Concrete Code, CSA CAN3-A23.3-M77 [62]). It should be pointed out that this last building also enables the evaluation of $K=2.0$ buildings as defined in the 1984 Canadian Concrete Code, since the detailing requirements for $K=2.0$ are similar to older $K=1.3$ code requirements. The overall building dimensions were chosen to be the same for Montreal and Vancouver and are typical of office buildings built in Canada. Figure 3.1 shows the plan and elevation view of the buildings.

The six-storey reinforced concrete office buildings have 7-6 m bays in the longitudinal (N-S) direction and 3 bays in the transverse direction (E-W), consisting of 2 - 9 m external office bays with 1.5 m cantilevers and a central 6 m corridor bay. The storey height is 4.85 m for the ground floor and 3.65 m for all the other floors. It is assumed that the central roof bay supports machinery.

3.2 DESIGN PARAMETERS

The dead loads and live loads conform to the 1985 National Building Code of Canada [2] and are summarized below:

Dead loads	Density of concrete	24 kN/m ³
	Partitions on all floors	1.00 kN/m ²
	Mechanical services and	
	Suspended ceilings	0.50 kN/m ²
Floor live loads :	Office floor loading	2.40 kN/m ²
	Corridor bay loading	4.80 kN/m ²
Roof live loads :	Mechanical services loading	
	on 6m wide (N-S) interior bay	1.60 kN/m ²
	Snow load - Montreal	2.20 kN/m ²
	- Vancouver	1.50 kN/m ²
Wind loading :	Montreal top 4 storeys	1.03 kN/m ²
	bottom 2 storeys	0.95 kN/m ²
	Vancouver top 4 storeys	1.53 kN/m ²
	bottom 2 storeys	1.42 kN/m ²
Seismic loadings :	Montreal K = 1.3, base shear, V = 0.037W	
	K = 0.7, base shear, V = 0.020W	
	Vancouver K = 1.3, base shear, V = 0.074W	
	K = 0.7, base shear, V = 0.040W	

where W is total weight (dead + 25% of snow load) of the building.

Tables of wind and earthquake loading are presented in Appendix A. For seismic analysis, the partitions on all floor and the mechanical services were considered as permanent loads and thus were included in the calculation of the weight of the building.

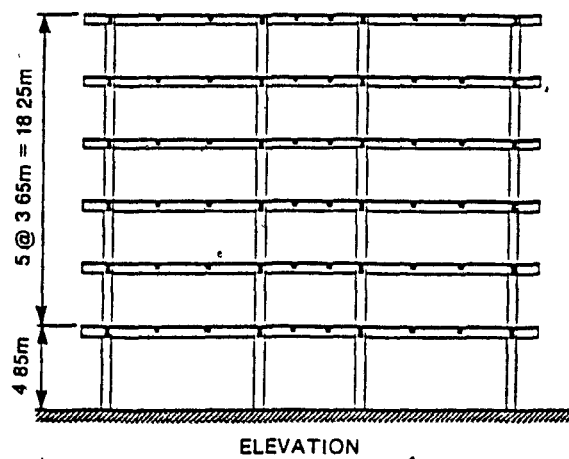
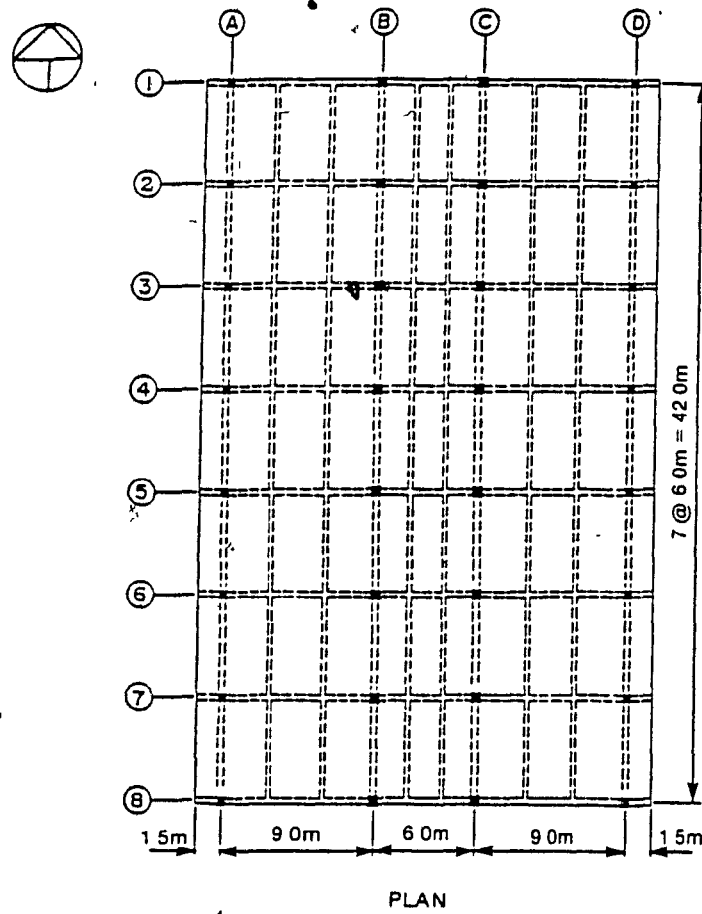


Fig. 3.1 Elevation and plan view of prototype structure

3.3 ANALYSIS ASSUMPTIONS AND IDEALIZATION

The structural system of each building consists of eight identical frames, and since the floor diaphragms were assumed to be rigid, the analysis was reduced to the study of a single frame subjected to one-eighth of the lateral loading. To account for the reduction of stiffness after cracking of the concrete, member stiffnesses were assumed to be 0.5 of the gross EI for all beams and 0.8 of the gross EI for all columns. A micro computer plane frame analysis program, CMPT Frame 2D [63], was used to determine member forces. Finite size of beam column joints were accounted for by the "node-offset" feature of the program. This feature allowed all beam forces to be obtained at the face of the columns and all column forces to be obtained at the faces of the beams (see Figure 3.2). All ground floor columns were assumed to be rigidly fixed at their bases. Gravity load analysis was made for each floor level by assuming the far ends of the columns to be fixed at the floor levels above and below the level under consideration. Pattern loading was used to find maximum forces.

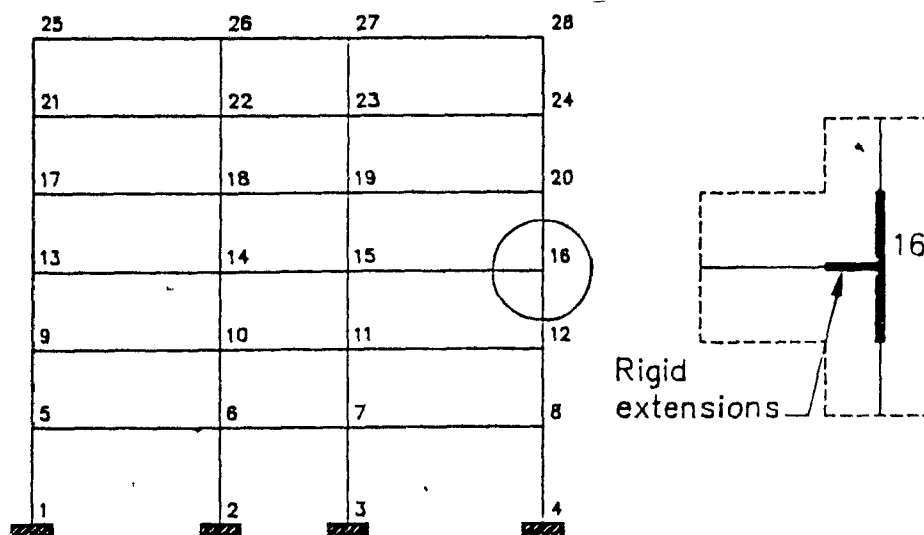


Fig. 3.2 Mathematical model for CMPT FRAME-2D program

3.4 LOAD COMBINATION AND LOAD EFFECTS

Member end forces were calculated for four basic loading cases, that is dead, live, wind and earthquake loads. A computer program was written to read directly the binary file containing the member forces created by the frame program and to perform load combinations as prescribed by the 1985 National Building Code of Canada [2]. A total of thirteen load cases were considered for each member. The loading cases considered were:

- 1) 1.25 D
- 2) 1.50 L
- 3) 1.50 W
- 4) 1.50 Q
- 5) 1.25 D + 1.50 L
- 6) 1.25 D + 1.50 W
- 7) 1.25 D + 1.50 Q
- 8) 1.25 D + 0.70(1.50 L + 1.50 W)
- 9) 1.25 D + 0.70(1.50 L + 1.50 Q)
- 10) 0.85 D + 1.50 W
- 11) 0.85 D - 1.50 W
- 12) 0.85 D + 1.50 Q
- 13) 0.85 D - 1.50 Q

The load combination program also included an option to redistribute the bending moments of continuous beams as allowed by the 1984 Canadian Concrete Code [3]. Although it is possible to redistribute bending moments resulting from earthquake loading, in the design of these buildings study only bending moments from vertical loads were redistributed.

In Appendix A tables A.5 to A.44 present summaries of the load combinations for the buildings in Montreal and Vancouver. For the Montreal buildings ($K=1.3$ old, $K=1.3$ and $K=0.7$) the beam design was controlled by load combination 9, (1.25 D + 0.70(1.50 L + 1.50 Q)), which gave the maximum member forces at all floor levels but

the roof. Load combination 5, $(1.25 D + 1.50 L)$, gave the maximum member forces at the roof level. The load combination 7, $(1.25 D + 1.5 Q)$ gave the maximum interior column moments and shear forces. For the exterior columns the maximum member forces were given by load combination 7 for the first two storeys and by load combination 9 elsewhere. The controlling load combinations for $K=0.7$ buildings in Vancouver were the same as those that controlled the design of the Montreal buildings. However due to the large increase in earthquake loading for $K=1.3$ buildings in Vancouver load combination 7 gave maximum column and beam forces in nearly all floor levels and storey levels.

Lateral deflections at specified load levels (i.e. unfactored loads) for earthquake and wind loading were well below the suggested code limit of $1/500$ th of the height (see tables A.45 and A.46 in Appendix A).

In order to calculate the dynamic properties of the buildings a micro computer program was written to calculate the periods of vibration of the structure and the corresponding mode shapes. This program was linked to the frame program and therefore used the same mathematical model. The calculations of the eigenvalues are based on the Jacobi method. All vertical degree of freedom were eliminated in the vibration analysis. Figures 3.3 and 3.4 presents the first three mode shapes for the Montreal and Vancouver buildings. It can be seen that the calculated periods differ largely from the computed code period (0.6 sec.). This difference should be expected, since the analysis was based on a bare frame. The calculated periods are not unrealistic however for buildings with light curtain glass walls. The periods are essentially the same for buildings with $K=1.3$ and $K=0.7$.

3.5 DESIGN SUMMARY AND COMPARISONS

In all analyses the beam moments of inertia were calculated with slab flanges included in the cross section. This resulted in higher bending moments in the beams than would have been predicted by conventional analysis with rectangular cross sections assumed. Although cracked section properties were used in the specified-load analyses

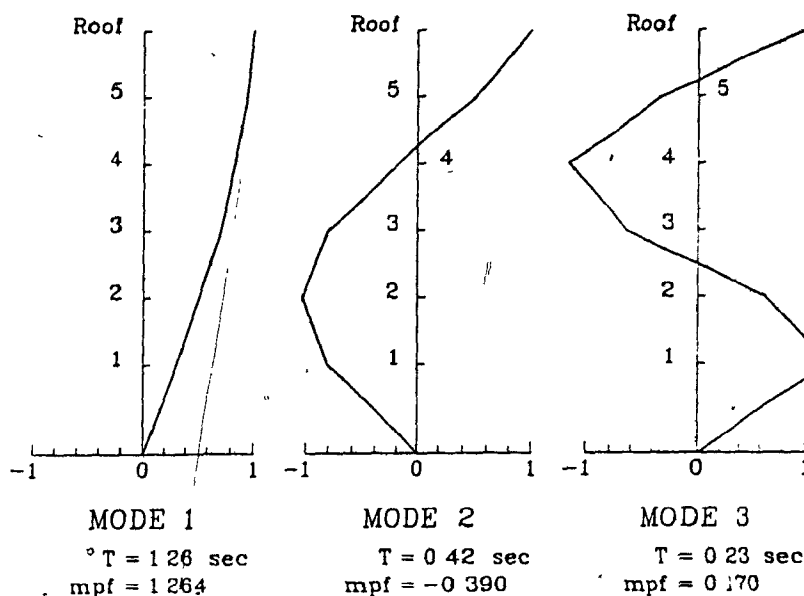
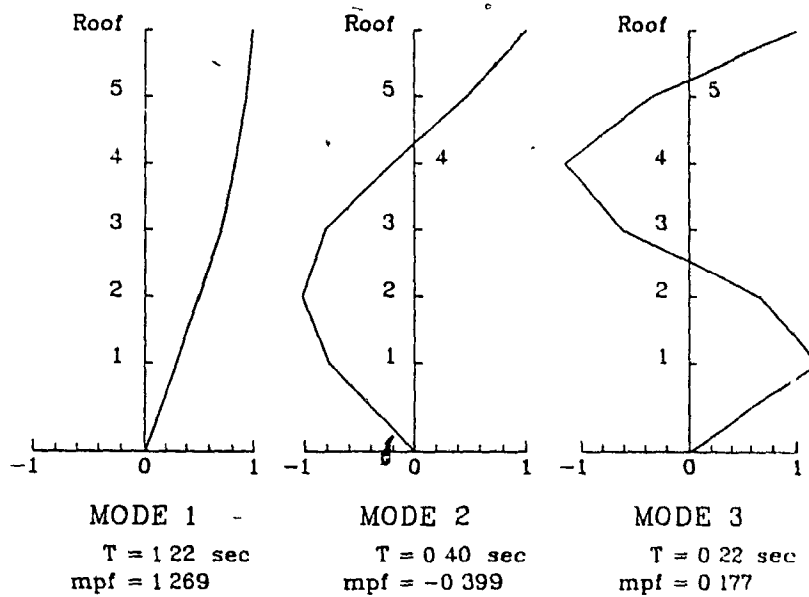


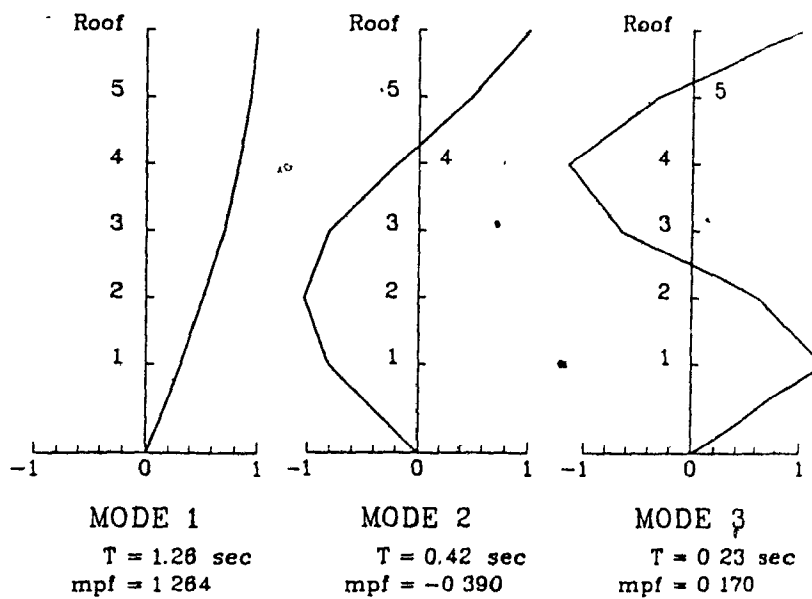
Fig. 3.3 Mode shapes and natural periods of vibration for Montreal buildings including modal participation factors (*mpf*)

the lateral deflections were not a controlling factor in the design of the buildings. For the old $K=1.3$ structures imperial sized bars were used. Although there is not much difference in the flexural design of members containing either SI bar sizes or comparable imperial bar sizes, there is a significant effect on the amount of shear and tie reinforcement due to the sizeable difference between a #3 imperial bar and a No. 10 SI bar. For design purposes it was assumed that the specified yield stress for all steel was 400 MPa and the concrete strength was 30 MPa.

Figures 3.5 and 3.6 present summaries of the designs for the buildings in Montreal and Vancouver. With a judicious redistribution of bending moments due to gravity loads (up to a maximum of 20% as allowed by the code) an almost constant design resistance was achieved at all beam joints. For the beam design the longitudinal bars within four slab thicknesses from the face of the beam were assumed to contribute to the beam strength for the $K=1.3$ and $K=0.7$ buildings. For the old $K=1.3$ building the slab bars were neglected in the flexural design as was the design practice for older buildings. The beam reinforcement was kept constant for three floor levels. This resulted in some overdesign at the roof level and slight underdesign at the first floor level. All first floor



a) $K = 1.3$ structures



b) $K = 0.7$ structure

Fig. 3.4 Mode shapes and natural periods of vibration for Vancouver buildings including modal participation factors (mpf)

beams were slightly underdesigned (5% maximum) in order to have flexural capacities as close as possible to the required capacities. The details of the reinforcement for the beams given in Fig. 3.5 and 3.6 are for the regions of the beams close to the columns. Note that for the case of $K=0.7$, four legged No.10 hoops at a spacing of $d/4$ were used for the transverse reinforcement in the beams. Although the $K=1.3$ structure required the same spacing, the transverse reinforcement consisted of only two legged No.10 stirrups. In contrast the transverse reinforcement in the old $K=1.3$ structure consisted of two legged #3 stirrups at a spacing of $d/2$.

Column sizes were kept constant over the height of the building. For these six-storey buildings the column size was chosen such that close to minimum amounts of longitudinal steel governed the design for most of the columns except for those at the first floor level. In all the buildings the longitudinal reinforcement ratio was kept under 3%. For the $K=0.7$ structures the transverse reinforcement in the columns consisted of hoops which satisfied the confinement requirements of the code in potential plastic hinge regions. All first storey columns of the $K=0.7$ buildings contained confinement reinforcement over their entire clear height. The columns in the $K=1.3$ structures contained ties and cross ties as their transverse reinforcement. For these structures, since the columns were stronger than the beams, no additional confinement reinforcement was required near the end of the columns. The old $K=1.3$ structure contained #3 ties and cross ties as required by previous codes.

The transverse reinforcement in the joint for the $K=0.7$ structures consisted of 6 sets of No.10 hoops as shown in Fig. 3.5 and 3.6. Confinement requirements of the code control the choice of this transverse reinforcement. Although specific requirements for joint transverse reinforcement are not given in Clause 21.9 of the CSA code [3] it was decided to provide three sets of No.10 ties as shown in Fig. 3.5 and 3.6. This amount of transverse reinforcement was chosen such that the shear strength of the joint was sufficient to develop the beam bars framing directly into the column. The joint reinforcement for the old $K=1.3$ structures consisted of three sets of #3 ties which were chosen to satisfy minimum shear reinforcement requirements. It is noted that in many of these old $K=1.3$ structures joint reinforcement might not have been provided.



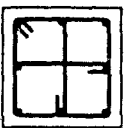
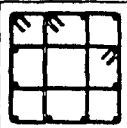
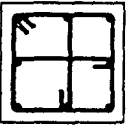

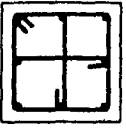
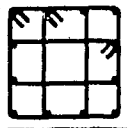

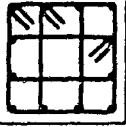

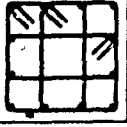
Structure	Column details		Joint details		Beam details	Slab details No. of bars within 4 slab thickness from beam side
	Exterior	Interior	Exterior	Interior		
Old $K=1.3$	<ul style="list-style-type: none"> - 450x450 mm - 8 # 6 (1.1%) - # 3 square ties + single cross-ties at 190 mm 	<ul style="list-style-type: none"> - 500x500 mm - 1st-6th storey - 12 # 6 (1.4%) - # 3 square + rectangular ties at 190 mm 	<ul style="list-style-type: none"> - 450x450 mm - 3 sets - # 3 square ties + single cross-ties 	<ul style="list-style-type: none"> - 500x500 mm - 3 sets - # 3 square + rectangular ties 	<ul style="list-style-type: none"> - 2nd-4th floor 400x600 mm - 8 # 6 top - 2 # 6 bot - 2 legged stirrups # 3 at 250 mm - 5th floor-Roof 400x550 mm - 8 # 6 top - 2 # 6 bot - 2 legged stirrups # 3 at 230 mm 	<ul style="list-style-type: none"> - 110 mm thick - 4 # 3 top - 4 # 3 bot
$K=1.3$	<ul style="list-style-type: none"> - 450x450 mm - 8 No. 20 (1.2%) - No. 10 square ties + single cross-ties at 190 mm 	<ul style="list-style-type: none"> - 500x500 mm - 1st-6th storey - 12 No. 20 (1.4%) - No. 10 square + rectangular ties at 190 mm 	<ul style="list-style-type: none"> - 450x450 mm - 3 sets - No. 10 square ties + single cross-ties 	<ul style="list-style-type: none"> - 500x500 mm - 3 sets - No. 10 square + rectangular ties 	<ul style="list-style-type: none"> - 2nd-4th floor 400x600 mm - 8 No. 15 top - 4 No. 15 bot - 2 legged stirrups No. 10 at 130 mm - 5th floor-Roof 400x550 mm - 8 No. 15 top - 4 No. 15 bot - 2 legged stirrups No. 10 at 115 mm 	<ul style="list-style-type: none"> - 110 mm thick - 4 No. 10 top - 4 No. 10 bot
$K=0.7$	<ul style="list-style-type: none"> - 450x450 mm - 8 No. 20 (1.2%) - No. 10 square + diamond hoops at 80 mm near joint at 190 mm elsewhere 	<ul style="list-style-type: none"> - 500x500 mm - 12 No. 20 (1.4%) - No. 10 square + rectangular ties at 100 mm near joint at 200 mm elsewhere 	<ul style="list-style-type: none"> - 450x450 mm - 6 sets - No. 10 square + diamond hoops 	<ul style="list-style-type: none"> - 500x500 mm - 6 sets - No. 10 square + rectangular ties 	<ul style="list-style-type: none"> - 2nd-4th floor 400x600 mm - 4 No. 20 top - 4 No. 20 bot - 4 legged hoops No. 10 at 130 mm - 5th floor-Roof 400x550 mm - 4 No. 20 top - 4 No. 20 bot - 4 legged hoops No. 10 at 115 mm 	<ul style="list-style-type: none"> - 110 mm thick - 4 No. 10 top - 4 No. 10 bot

Fig. 3.5 Reinforcement Details for Montreal Buildings

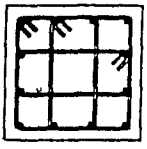
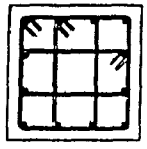
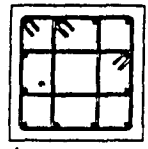
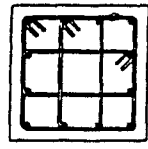
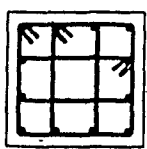
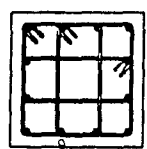
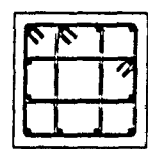
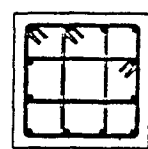
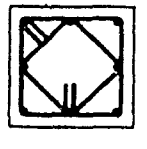
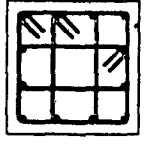
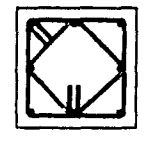
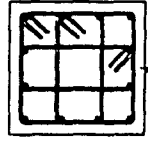
Structure	Column details		Joint details		Beam details	Slab details No. of bars within 4 slab thickness from beam side
	Exterior	Interior	Exterior	Interior		
Old $K=1.3$	- 500x500 mm - 1st storey 12 # 8 (2.4%) - 2nd-6th storey 12 # 6 (1.4%) - #3 square + rectangular ties at 200 mm 	- 500x500 mm - 1st storey 18 # 8 (3.3%) - 2nd-6th storey 12 # 6 (1.4%) - #3 square + rectangular ties at 200 mm 	- 500x500 mm - 3 sets #3 square + rectangular ties 	- 500x500 mm - 3 sets #3 square + rectangular ties 	- 2nd-4th floor 400x600 mm 8 # 8 top 2 # 8 bot. 2 legged stirrups # 3 at 250 mm - 5th floor-Roof 400x550 mm 8 # 8 top 2 # 8 bot 2 legged stirrups # 3 at 230 mm	- 110 mm thick 4 # 3 top 4 # 3 bot.
$K=1.3$	- 500x500 mm - 1st storey 12 No. 25 (2.4%) - 2nd-6th storey 12 No. 20 (1.4%) - No. 10 square + rectangular ties at 200 mm 	- 500x500 mm - 1st storey 16 No. 25 (3.2%) - 2nd-3rd storey 16 No. 20 (1.9%) - 4th-6th storey 12 No. 20 (1.4%) - No. 10 square + rectangular ties at 200 mm 	- 500x500 mm - 3 sets No. 10 square + rectangular ties 	- 500x500 mm - 3 sets No. 10 square + rectangular ties 	- 2nd-4th floor 400x600 mm 4 No. 25 top 4 No. 20 top 4 No. 20 bot 2 legged stirrups No. 10 at 125 mm - 5th floor-Roof 400x550 mm 8 No. 20 top 4 No. 20 bot 2 legged stirrups No. 10 at 115 mm	- 110 mm thick 4 No. 10 top 4 No. 10 bot.
$K=0.7$	- 450x450 mm - 8 No. 20 (1.2%) - No. 10 square + diamond hoops at 80 mm near joint at 190 mm elsewhere 	- 500x500 mm - 1st-3rd storey 12 No. 25 (2.4%) - 4th-6th storey 12 No. 20 (1.4%) - No. 10 square + rectangular hoops at 100 mm near joint at 200 mm elsewhere 	- 450x450 mm - 6 sets No. 10 square + diamond hoops 	- 500x500 mm - 6 sets No. 10 square + rectangular hoops 	- 2nd-4th floor 400x600 mm 8 No. 15 top 4 No. 20 bot. 4 legged hoops No. 10 at 130 mm - 5th floor-Roof 400x550 mm 8 No. 15 top 4 No. 20 bot. 4 legged hoops No. 10 at 115 mm	- 110 mm thick 4 No. 10 top 4 No. 10 bot.

Fig. 3.6 Reinforcement Details for Vancouver Buildings

CHAPTER 4

REVERSED CYCLIC LOADING TESTS OF FULL SCALE CONCRETE FRAME SUBASSEMBLAGES

This chapter presents details of three full scale specimens tested in the Jamieson Structures Laboratory of the Department of Civil Engineering and Applied Mechanics at McGill University as part of this research project. Additional information on specimens with $K=1.3$ and $K=0.7$ can be found in Reference [64].

4.1 DESIGN OF TEST SPECIMENS

The 1984 Canadian Concrete Code (CSA CAN3-A23.3-M84) [3] contains specific clauses for the design and detailing of building components for different levels of "ductility". The changes that occurred in this code represent a major departure from past Canadian codes. While the new design and detailing requirements of the CSA Code were influenced by the 1983 ACI [65] and the 1982 New-Zealand [66] codes, the requirements for "nominally ductile" ($K=1.3$) building members are completely new. Two full scale test specimens designed and detailed according to the 1984 Canadian Concrete Code with ductility factors, K , of 1.3 and 0.7 were constructed and subjected to reversed cyclic loading until failure. In addition a third specimen with details corresponding to an older structure having a $K=1.3$ (Specimen Old $K1.3$) was also built and tested. The purpose of these tests was to evaluate the behaviour under reversed cyclic loading of realistic building components in order to assess the adequacy of these new code provisions and to assess the performance of older structures. This study would also provide

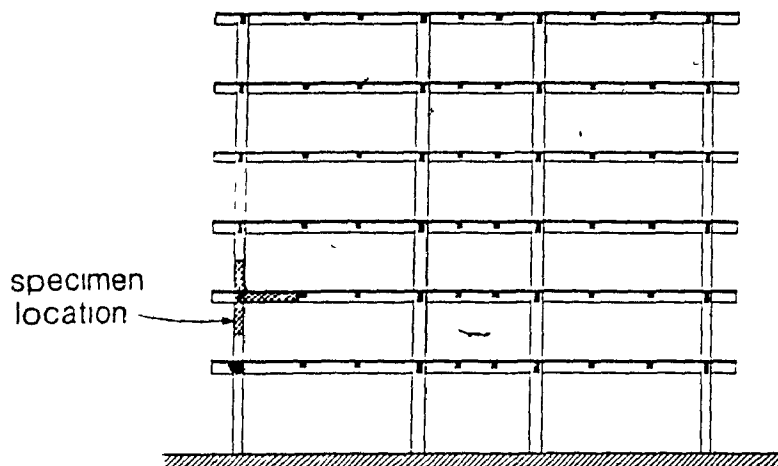


Fig. 4.1 Specimen location

key behavioural parameters necessary in modelling the non-linear dynamic response of structures.

The three full scale test specimens represent second storey external beam-slab-column connections of the six storey moment resisting frame structures described in Chapter 3 (see Fig. 4.1). The overall test specimen dimensions and the test set up shown in Fig. 4.2 were designed to simulate the points of contraflexure in the beams and the columns. The 1500 mm exterior cantilever slab and beam were not included in the test subassemblages in order to study the response of the subassemblages without the beneficial effects of these cantilevers on the exterior joint behaviour.

In order to study the effects of the slab and its reinforcement on the response it was necessary to include as large a portion of the slab as possible. Although the code does not give specific effective slab widths when the slab is acting in tension, the effects of slab reinforcement within a distance three times the slab thickness measured from the beam faces must be included in determining the nominal resistances of beams. Park and Paulay [18] suggest that reinforcement within 4 times the slab thickness from the beam faces is effective in tension. The effective flange width in compression calculated from the Canadian Code varies from 1500 mm to 2000 mm for the 6000 mm and 9000 mm spans respectively. The chosen 1900 mm slab width was the largest width that could

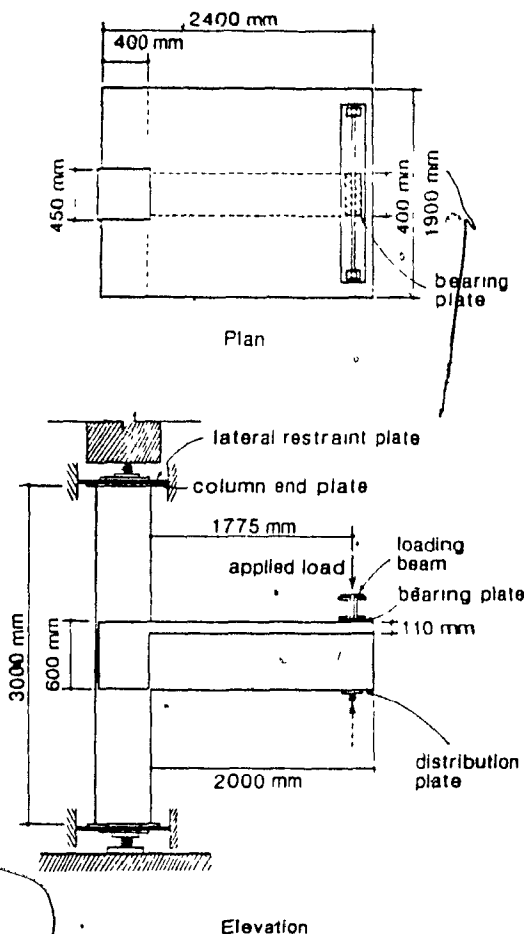


Fig. 4.2 Test specimen dimensions and test set-up

be accommodated in the testing apparatus.

It is noted that the design was performed for the prototype structure assuming a specified yield stress in all reinforcement of 400 MPa and a concrete strength of 30 MPa.

4.2 DETAILS OF TEST SPECIMENS

4.2.1 Test Set-Up

Each test specimen consisted of a 450×450 mm column with a total height of 3000 mm. A constant compressive axial load of 1076 kN corresponding to 90% of the dead load acting on the prototype structures was applied at the top of the column

by a universal testing machine. The load was transmitted by a 76 mm diameter roller bearing against two load distribution plates. Two 6 mm thick steel plates were welded to the reinforcing bars at the ends of the columns. The ends of the columns were heavily reinforced in the transverse direction to control vertical splitting. To simulate points of contraflexure and to provide lateral restraints, two flexible 6 mm thick plates were bolted to the end plates of the columns and to the reaction frame (see Fig. 4.2).

The 400×600 mm main beam extended a distance of 2000 mm from the face of the column as shown in Fig. 4.2. The 110 mm thick slab had a width of 1900 mm. Two 400×600 mm spandrel beams framed into the sides of the columns and extended over the full slab width.

The lateral loading was simulated by applying a vertical force near the tip of the beam at a location of 1775 mm from the face of the column. A downward load, resulting in negative bending moment in the beam, was produced by pulling down on two tie rods reacting against a distribution beam as shown in Fig. 4.2. Care was taken to ensure that the vertical load was transferred totally to the main beam by means of a 400 mm wide bearing plate (see Fig. 4.2). An upward load, producing positive bending moment in the beam, was applied directly to the bottom face of the beam by two hydraulic rams as shown in Fig. 4.2. Figure 4.3 shows a general view of test specimen Old K1.3 before testing.

4.2.2 Details of Reinforcement

Figure 4.4 shows the reinforcement details of all three specimens, Old K1.3, K1.3 and K0.7 (this specimen designation indicates the K factor used in the design). In all specimens the slab was reinforced with No. 10 top and bottom transverse bars at a spacing of 300 mm. A 20 mm concrete cover was provided for the slab bars and a clear concrete cover of 40 mm was provided for beam and column steel. Extra transverse bars and beam hoops were provided at the free end of the slab and beam near the point of application of the loads. A discussion of the details of the three specimens follow.

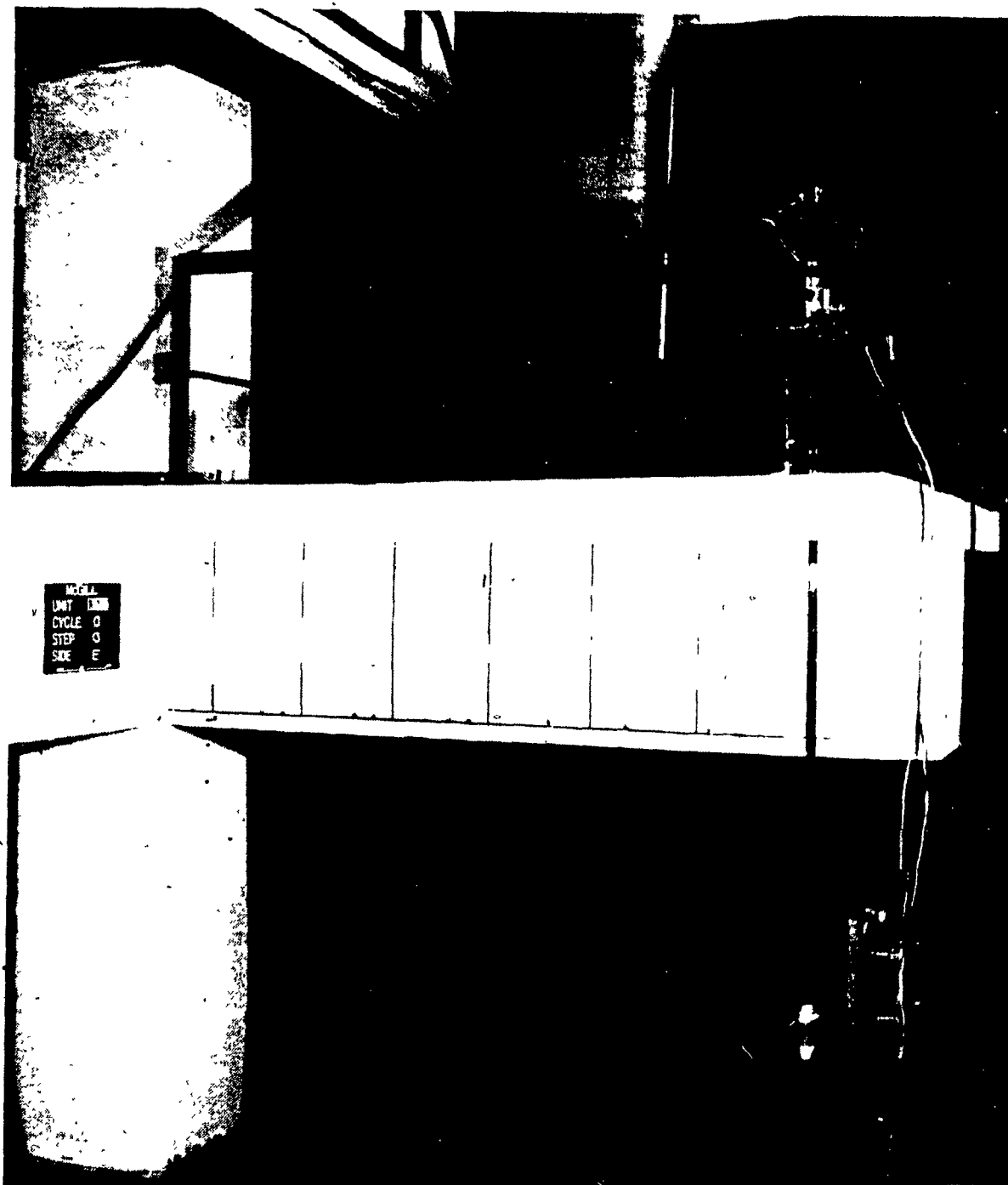


Fig. 4.3 Photograph of test set-up for specimen Old K1.3

	elevation	beam and slab	column
Old K=1.3	<p>6 sets at 190 mm 2 2 6 sets at 190 mm 8 sets of U-stirrups at 260 mm</p>	<p>No. 10 at 300 mm top and bottom of slab 3 stirrups 8 No. 15 4 No. 15 SECTION 1-1</p>	<p>No. 10 ties 8 No. 20 SECTION 2-2</p>
K=1.3	<p>6 sets at 190 mm 2 2 6 sets at 190 mm 8 sets of U-stirrups at 130 mm 4 sets of U-stirrups at 260 mm</p>	<p>No. 10 at 300 mm top and bottom of slab No. 10 stirrups 8 No. 15 4 No. 15 SECTION 1-1</p>	<p>No. 10 ties 8 No. 20 SECTION 2-2</p>
K=0.7	<p>3 sets at 90 mm 7 sets at 80 mm 6 sets at 70 mm 7 sets at 80 mm 3 sets at 90 mm 8 sets of double legged hoops at 130 mm 7 sets of double legged stirrups at 130 mm</p>	<p>No. 10 at 300 mm top and bottom of slab No. 10 stirrups 4 No. 20 4 No. 20 SECTION 1-1 No. 10 at 300 mm top and bottom of slab No. 10 stirrups 4 No. 20 4 No. 20 SECTION 2-2</p>	<p>No. 10 hoops 8 No. 20 SECTION 3-3</p>

Fig. 4.4 Reinforcement details of specimens

4.2.2.1 Specimen Old K1.3

Figure 4.5 shows two views of the reinforcing cage near the joint for specimen Old K1.3. This specimen was designed without incorporating special seismic design and detailing requirements. The design resulted in 8-No. 20 longitudinal bars in the column. Transverse reinforcement consisted of No. 10 square peripheral ties and single leg ties as shown in Fig. 4.4, and spaced at 190 mm (i.e., a spacing equal to half the effective depth of the column, $d/2$). The peripheral ties had 135° bend anchorages with straight bar end extensions of $6d_b$. The cross-ties were anchored with 135° bends at one end and 90° bends at the other end with free end extensions of $6d_b$. The end with the 90° bend was alternated with the end with the 135° bend along the column height (see Fig. 4.5).

The longitudinal reinforcement in the main beam consisted of 8-No. 15 bars placed in two rows at the top and 4-No. 15 bars in one row at the bottom. The beam shear reinforcement consisted of #3 (9.5 mm diameter) open U-stirrups spaced at 260 mm (i.e., a spacing equal to half the effective depth of the beam, $d/2$).

The longitudinal bars in the spandrel beam consisted of 4-No. 15 bars top and bottom. Closed #3 (9.5 mm diameter) stirrups spaced at 200 mm were provided in the spandrel beam due to the presence of torsion.

The minimum shear reinforcement was provided in the joint according to Clause 7.7.3 [3] which resulted in three sets of peripheral ties and single leg ties within the joint region.

4.2.2.2 Specimen K1.3

Figure 4.6 shows two views of the reinforcing cage near the joint for specimen K1.3. This specimen was designed according to the "nominal ductility" requirements of Clause 21.9 of the 1984 Concrete Code [3]. The column design was similar to the Old K1.3 specimen. In the main beam 8-No. 15 top bars placed in two rows and 4-No. 15 bottom bars were provided. This amount of bottom reinforcement was chosen to satisfy Clause 21.9.2.1.1, which requires that the positive moment resistance of the

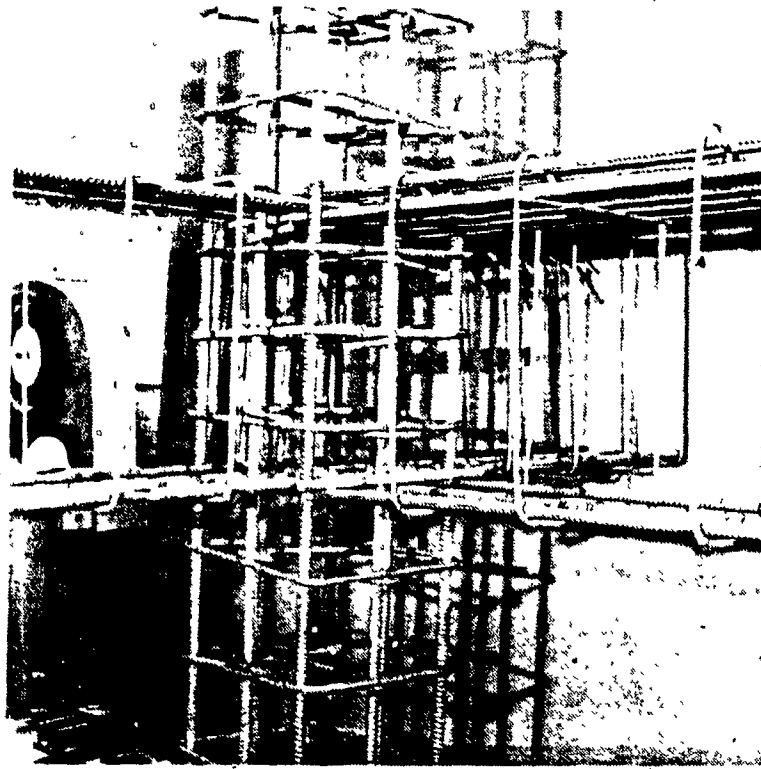
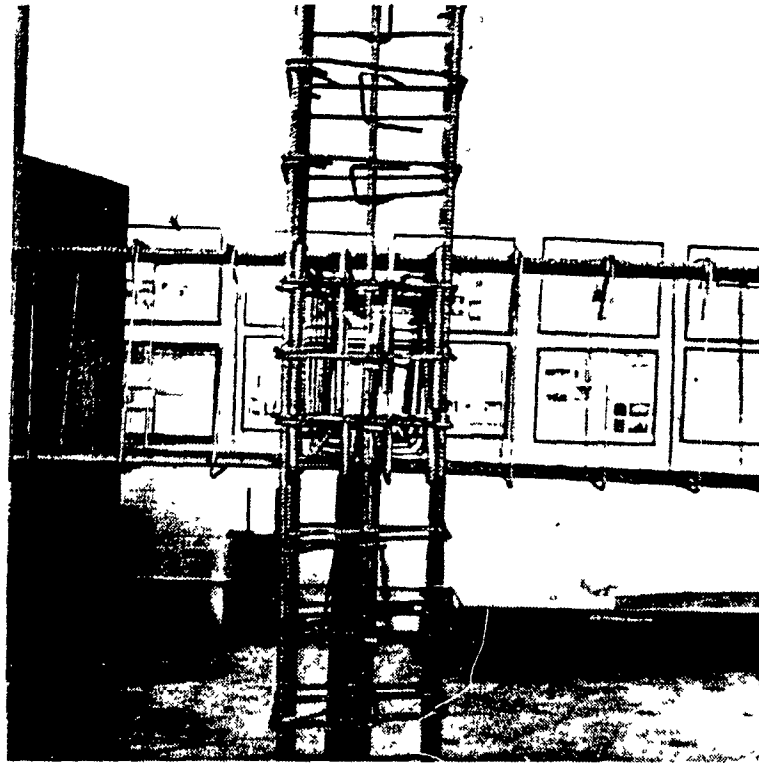


Fig. 4.5 Photograph of reinforcing cage for specimen Old K1.3

beam at the joint be at least one third of the negative moment resistance. To satisfy Clause 21.9.2.1.2, open U-stirrups spaced at 130 mm (i.e., $d/4$) were provided over a length equal to twice the effective depth of the beam. Stirrups spacing was increased to 260 mm (i.e., $d/2$) in the remainder of the beam.

The longitudinal bars in the spandrel beam consisted of 4-No. 15 bars at both top and bottom. Closed stirrups spaced at 125 mm (i.e., $d/4$) were used in the spandrel beam to satisfy the requirements for "nominal ductility".

After investigation of the column and beam resistance, including the effects of the slab reinforcement within a distance of four slab thickness, it was found that the factored resistances of the columns exceeded 1.1 times the nominal resistance of the beam and therefore the more stringent column tie spacing, required by Clause 21.9.3.1 [3], was not necessary.

4.2.2.3 Specimen K0.7

Figure 4.7 shows two views of the reinforcing cage near the joint for specimen K1.3. This specimen was designed according to the "ductile" moment-resisting frame requirements of Clause 21 of the 1984 CSA Code [3]. The column contained 8-No. 20 longitudinal bars. Transverse column reinforcement consisted of closed square hoops together with supplementary diamond-shaped hoops spaced at 80 mm (see Fig. 4.4). As required by the Code [3] the hoops had 135° bend anchorages with straight bar extensions of 10 times the bar diameter. These closely spaced hoops were provided over a distance equal to one sixth of the clear height of the column, i.e., 508 mm. The hoops were spaced at 190 mm, i.e., half the effective depth, d , of the column outside of the region with closely spaced hoops. Due to the concentration of transverse reinforcement, the factored shear resistance of the column far exceeds the shear corresponding to the development of the probable moment resistance, M_{pr} , in the beam.

The beam longitudinal reinforcement consisted of 4-No. 20 bars at both top and bottom in addition to the slab reinforcement. This amount of bottom reinforcement was necessary to satisfy the requirement of the Code [3] that the positive moment resistance at the joint be at least equal to one-half of the negative moment resistance

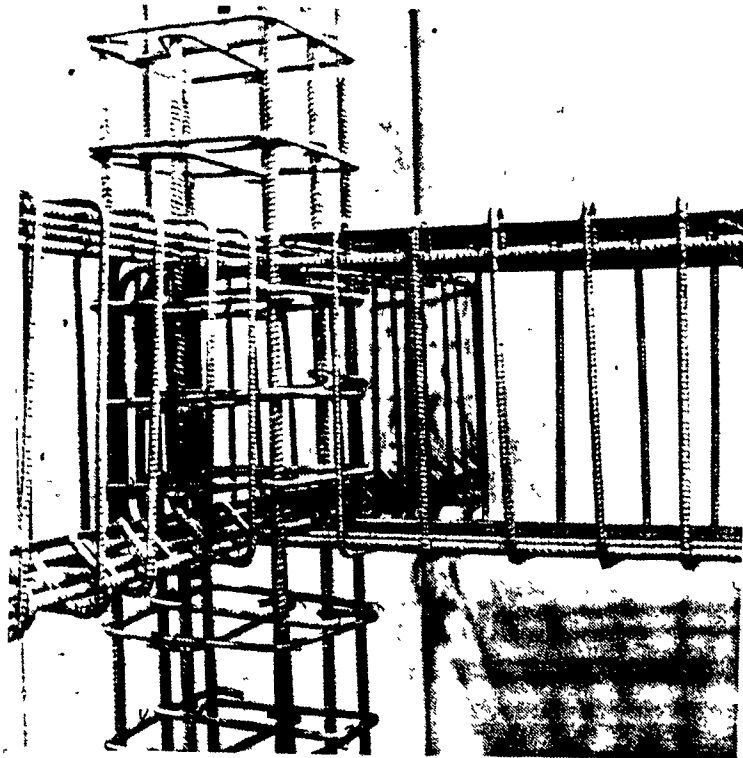
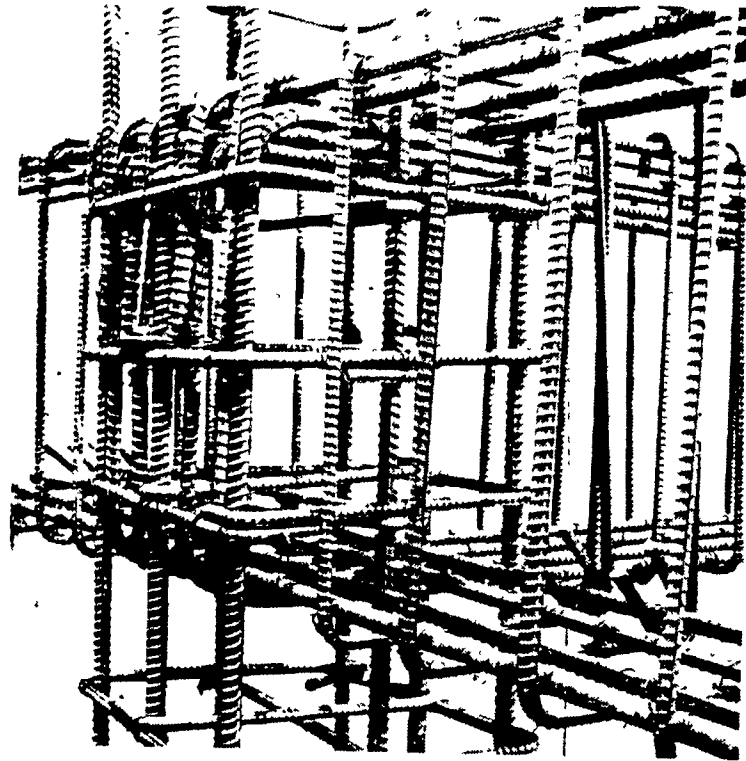


Fig. 4.6 Photograph of reinforcing cage for specimen K1.3

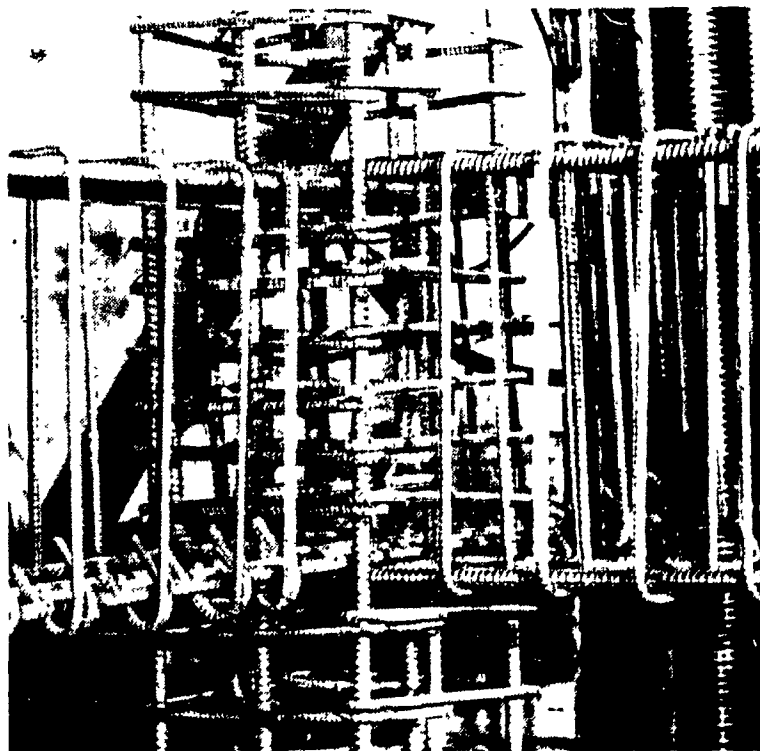
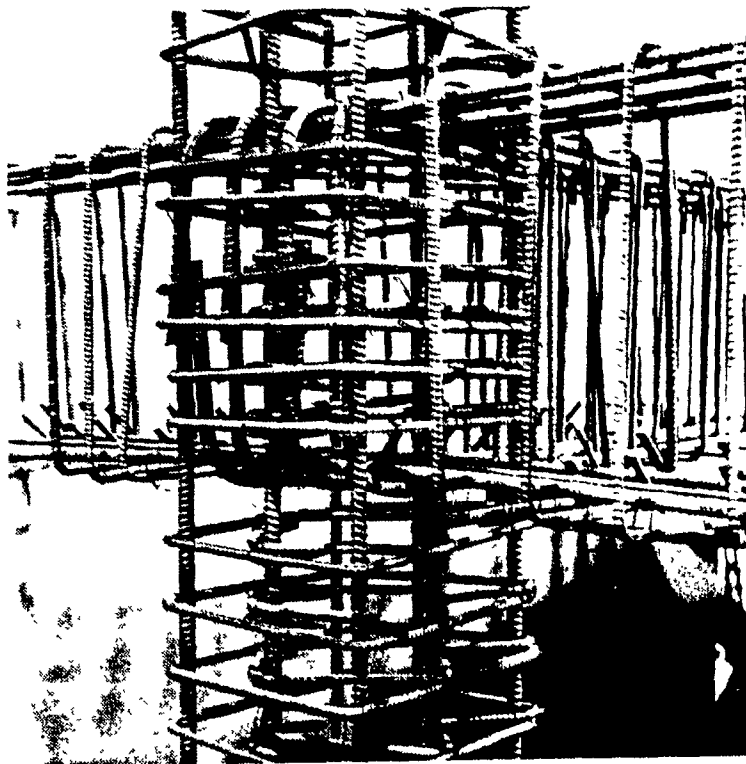


Fig. 4.7 Photograph of reinforcing cage for specimen K0.7

(Clause 21.3.2.2).

The main beam transverse reinforcement consisted of peripheral rectangular closed hoops together with supplementary U-shaped stirrups spaced at 130 mm over a distance equal to twice the effective depth, $2d$, from the column face. The resulting four stirrup legs are intended to prevent lateral buckling of the longitudinal bars in the beam. The first set of transverse reinforcement was placed at 50 mm from the face of the column. The spacing of these transverse reinforcement was limited to $d/4$ as required by Clause 21.3.3.3. The transverse reinforcement also satisfied the requirement that the beam be capable of resisting the shear due to the development of the probable moment resistance, M_{pr} , at the column face. For the remainder of the beam the closed hoops were replaced by U-shaped stirrups at a spacing of 130 mm as required for shear strength.

4.2.3 Material Properties

4.2.3.1 Steel

In accordance with Clause 21.2.5.1. of the 1984 Canadian concrete code [3], reinforcing bars conforming to CSA Standard G30.16-M 1977 [67] were used in specimen K1.3 and K0.7. In the case of specimen Old K1.3 reinforcing bars conforming to the requirements of CSA standard G30.12-M 1977 [68] were used. Tension tests were performed on 300 mm long specimens cut from each bar size. The strains were determined from an extensometer, having a gauge length of 50 mm, clamped to each test bar. The resulting average values of stresses and strains obtained from three test samples for each bar size are given in Table 4.1.

4.2.3.2 Concrete

Two batches of concrete were used in the fabrication of each specimen; the first batch was used to cast the lower column, the beams and the slab, while the second batch was cast one day later for the upper column. High early strength ready mix concrete with a minimum specified strength of 30 MPa was ordered. The maximum

Table 4.1 Reinforcing Steel Properties

Bar	Area	f_y , MPa	ϵ_{sh}	f_u , MPa	ϵ_u
#3	71	489†	-	655	0.030
No. 10 ‡	100	492	0.0120	622	0.200
No. 10	100	480	0.0125	622	0.220
No. 15 ‡	200	400	0.0135	578	0.280
No. 15	200	471	0.0120	774	0.200
No. 20	300	478	0.0100	763	0.160

† value taken at 2% offset; rounded stress-strain curve

‡ specimen Old K1.3 only

aggregate size was 20mm and the specified slump was 100 mm. At least 6 - 150×300 mm and 6 - 100×200 mm cylinders were prepared from each concrete batch. Compression tests and splitting tests were performed to determine the compressive strength f'_c and the tensile strength f_t of the concrete respectively. The testing of specimen Old K1.3 was performed 15 days after casting, specimen K1.3 was tested 30 days after casting and specimen K0.7 was tested 37 days after casting. Table 4.2 presents the average compressive and the average tensile strengths of the concrete batches for each specimen. The average compressive and tensile strengths were obtained from 3 - 150×300 mm specimens.

Table 4.2 Concrete properties

Specimen	Batch	f'_c , MPa	f_t , MPa
Old K1.3	1	39.8	2.8
	2	31.1	2.1
K1.3	1	39.5	2.8
	2	40.0	2.8
K0.7	1	40.4	2.6
	2	36.2	2.6

4.2.4 Instrumentation and Experimental Procedure

Deflection at the loading point was obtained from two Linear Voltage Differential Transformers (LVDT's) which were arranged to measure vertical displacements of ± 150 mm from the unloaded position. The LVDT's were attached to a special frame

which was fixed at the base of the top column (see Fig. 4.8). The use of this outrigger frame removes the contribution of the column rotation to the tip deflection of the beam. Readings were continuously recorded by the OPTILOG data acquisition system linked to an IBM PC.

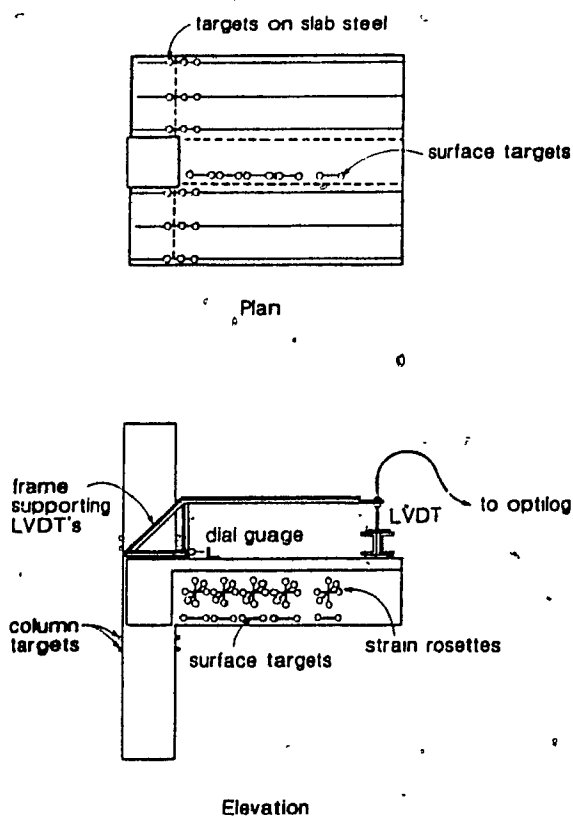


Fig. 4.8 Specimen instrumentation

Two load cells were used to record the force in the tie rods for downward loading and two other load cells were used to record the force transmitted by the hydraulic jacks used for upward loading.

Slab bar strains were obtained by means of mechanical extensometers measuring the displacement between sets of two brass targets glued directly to the steel reinforcing bars 140mm apart and accessible through small holes formed in the concrete cover of the slab (see Fig. 4.8).

Longitudinal strains in the main beam were obtained at several locations along the beam by measuring with mechanical extensometers the displacement between sets of two targets glued directly to the concrete surface. These targets were located at the level of the bottom longitudinal steel in the beam and at the top concrete surface (see Fig. 4.8) and had gauge lengths of 200 mm.

Shear strains as well as principal strains along the beam were determined by 45° strain rosettes formed by targets glued to the surface of the web of the beam as shown in Fig. 4.8. The rosettes were centred at mid-depth of the beam and consisted of individual readings with gauge lengths of 200 mm.

Column strains were measured with targets glued to the interior and exterior faces of the column, both above and below the joint region, in order to monitor strain distributions in the column.

A dial gauge was clamped to the column, 60 mm above the top surface of the slab. This horizontal gauge measured the movement of a point on the slab 90 mm away from the column face (see Fig. 4.8). This measurement enabled the contribution of the bond slip and joint shear distribution to the tip deflection to be estimated.

The load deflection responses were plotted during the experiment. Figure 4.9 shows an example loading and deflection history. Full measurements were taken systematically for each half cycle at zero load, at the maximum load reached in the previous cycle, at the new maximum load, at half the maximum load upon unloading and at zero load again (see Fig. 4.9). In addition more frequent readings of loads and deflections were taken in order to obtain a complete load history response. Downwards loads and deflections at the tip of the beam are taken as positive values.

In the first cycle, loading was applied to a peak load such that the full service moment level (about 20% larger than the cracking moment) was reached in the beam at the column face. The load was increased in the next loading cycle until strain readings confirmed that first yielding of the flexural reinforcement in the beam was achieved. General yielding of the flexural reinforcement was used to determine the next peak load. General yielding was determined when a significant change in the load deflection response was observed. The deflections corresponding to general yielding (Δ_{yp} and Δ_{yn})

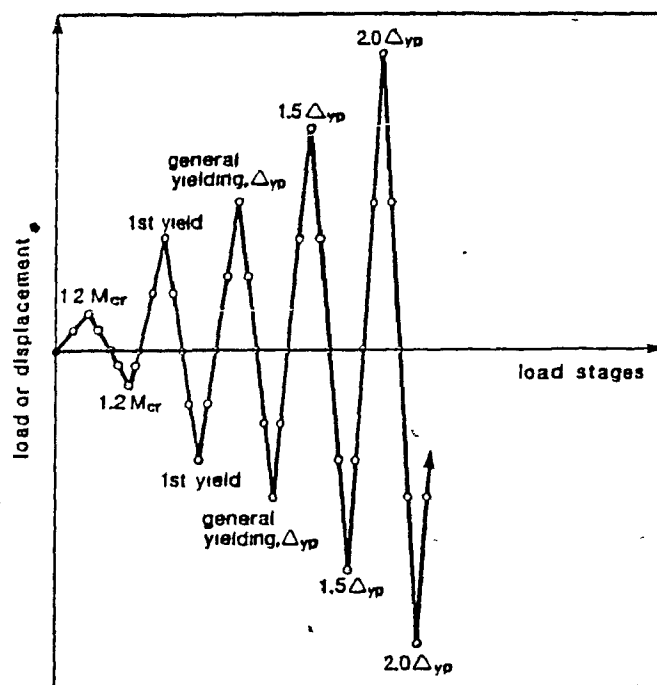


Fig. 4.9 Loading and deflection history

for downwards and upwards deflections respectively) were noted. The peak loading in subsequent cycles was controlled by deflection, with maximum deflection levels taken to be multiples of Δ_{yp} and Δ_{yn} . This procedure was continued until failure was reached.

The instrumentation enabled the different tip deflection components to be estimated at each load stage. The flexural tip deflection component was calculated from the measured longitudinal strains at the top and bottoms of the beam at different locations along the beam length. After general yielding a plastic hinge length was estimated from an examination of the longitudinal strain distributions in the beam. Knowing this plastic hinge length together with the calculated curvatures at a number of points enabled the curvature distributions to be estimated. The shear strains were calculated from the measured rosette strains at the mid-height of the beam at different locations along the beam length. The resulting shear strain distributions were integrated to estimate the contribution of the shear to the tip deflection. The horizontal dial gauge readings measuring movement of the slab relative to the column enabled an

estimate of the combined contribution of both bond-slip and joint shear distortion to the tip deflection. The measured movement over the gauge length was first corrected to remove the component from flexural strains in the beam and then converted into a concentrated rotation at the column face. Thus the tip deflection component was computed as the product of this concentrated rotation and the beam length.

4.3 EXPERIMENTAL RESULTS AND OBSERVATIONS

4.3.1 Specimen Old K1.3

The hysteretic load-tip deflection response for specimen Old K1.3 is shown in Fig. 4.10. First yielding of the top steel occurred at a load of 198 kN and a corresponding deflection of 8 mm. First yielding (also "general yielding") in the negative direction occurred at a load of 110 kN and a deflection of 6 mm. General yielding occurred at a load of 322 kN and a deflection of 21 mm in the positive direction. The hysteresis loops remained stable up to a displacement ductility of 3 at a load of 345 kN and a deflection of 58 mm. At this stage a significant shear crack, crossing four sets of stirrups, had developed with a crack opening of 3 mm causing yielding of these stirrups. As can be seen from Fig. 4.11 b significant fanning of the diagonal compression had occurred which started to cause spalling of the concrete near the bottom of the beam in the flexural compression zone. After this stage one can observe a significant decrease (about 50%) in load carrying capacity as well as large stiffness reduction and severe pinching of the response curve and therefore reduction of the energy dissipating capacity of the beam. This was due to both the shear distress and severe buckling of the bottom longitudinal bars between the widely spaced stirrups (see Fig. 4.12). The peak positive load was 340 kN corresponding to a moment at the face of the column of 634 kN·m (including dead load effects) and a tip deflection of 60 mm. The peak negative load was 129 kN corresponding to a moment at the column face of 229 kN·m and to a tip deflection of 30 mm. The maximum positive deflection achieved was 100 mm, however the load, as can be seen from Fig. 4.10, was only 165 kN, or 51% of the load at general yielding. The maximum negative deflection achieved was 40 mm corresponding to a

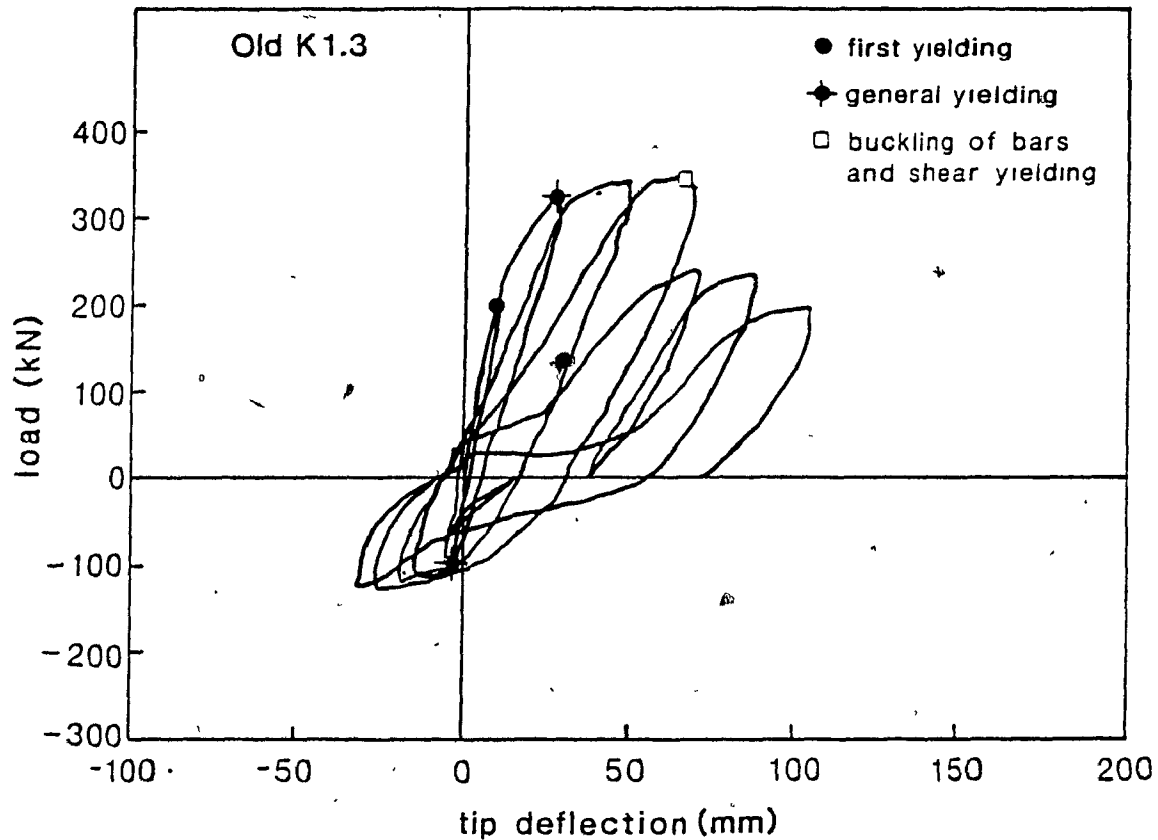


Fig. 4.10 Hysteretic load-tip deflection response for Specimen Old K1.3

load of 129 kN.

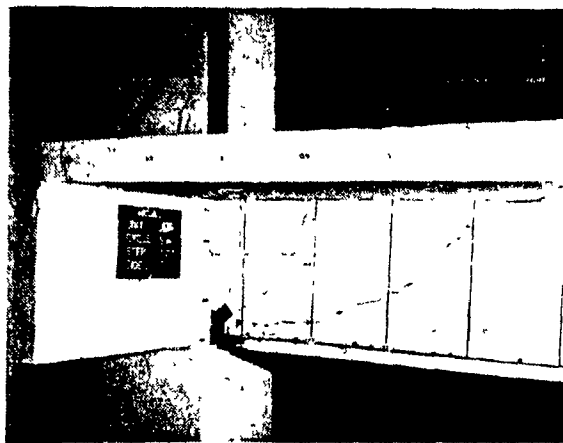
From the measurements of the steel slab strains it was determined that the full slab width (i.e., all 8 bars) was effective in carrying the load as can be seen from Fig. 4.13.

There was significant torsion in the spandrel beam with spalling of the concrete cover and severe torsional cracking. In addition the cover concrete spalled in the column near the joint and cracking extended into the column.

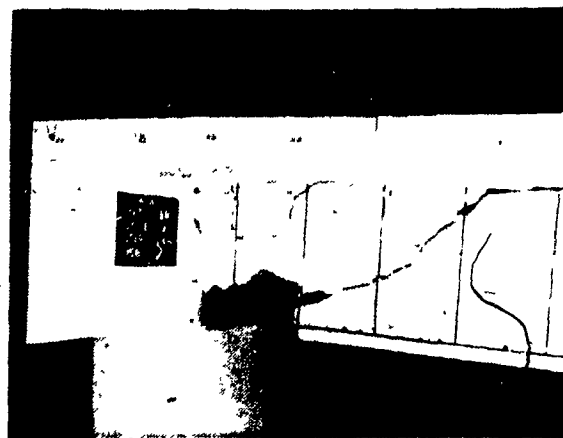
Figure 4.14 shows the load versus measured tip deflection response together with components of the tip deflection corresponding to flexural curvatures, Δ_f , shear distributions in the beam, Δ_s , and the deflection component, Δ_j , associated with shear distortion of the joint together with bond slip of the flexural bars anchored in the joint. A plastic hinge length of 180mm was estimated from the longitudinal strain readings



a) General yielding, $P = 322 \text{ kN}$



b) Ultimate, $P = 332 \text{ kN}$



c) Near end of test, $P = 240 \text{ kN}$

Fig. 4.11 Specimen Old K1.3 at different load stages



Fig. 4.12 Buckling of longitudinal reinforcement in main beam of Specimen Old K1.3

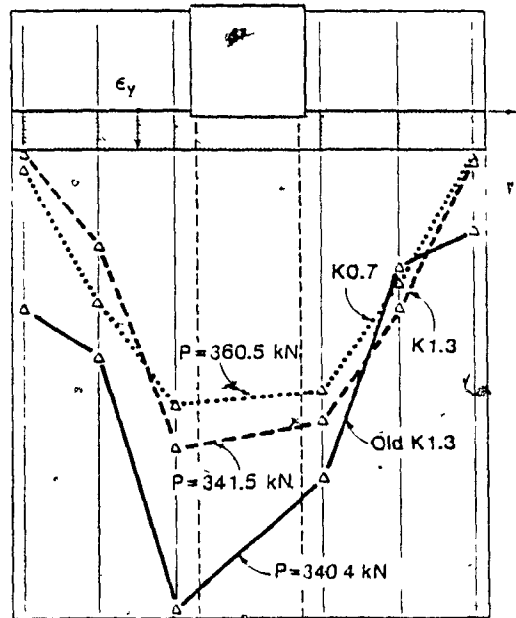


Fig. 4.13 Strain distribution in slab longitudinal reinforcement for all three specimens

for the computation of Δ_f after general yielding. As can be seen from Fig. 4.14 the shear component of the deflection was very significant at general yielding due to the large shear cracking that had developed. After general yielding, both the large curvature due to buckling of the compression bars and the extremely severe shear cracking and yielding of the stirrups controlled the response. As can be seen from Fig. 4.14 the contribution of Δ_f to the tip deflection was limited because the buckling of the bottom beam bars and shear yielding of the beam limited the total shear force transferred to the joint.

4.3.2 Specimen K1.3

The hysteretic load-tip deflection response for specimen K1.3 is shown in Fig. 4.15. First yielding of the top steel occurred in the second cycle at a load of 231 kN and a corresponding tip deflection of 14 mm. First yielding occurred in the negative direction at a load of 90 kN and a corresponding tip deflection of 3 mm. General yielding occurred at a load of 327 kN and a deflection of 28 mm in the positive direction and at a load of

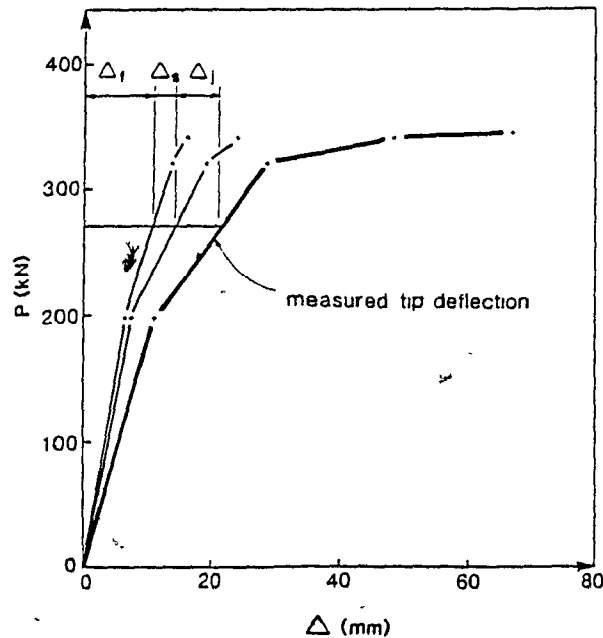


Fig. 4.14 Beam tip deflection components for Specimen Old K1.3

137 kN and a deflection of 8 mm in the negative direction as can be seen from Fig. 4.15. The hysteresis loops remained stable for the duration of the test. After a displacement ductility of 3 a slight loss in the load carrying capacity of the specimen in the positive direction is noticeable. This was due to the spalling of the concrete cover which began in the 8th cycle. The loss of concrete cover in the bottom of the beam extended along the beam a distance of 180 mm from the column face. At the end of the test (see Fig. 4.16 c) the region of spalling was still small and buckling of the 4 No. 15 bottom longitudinal bars was observed. Shear cracking was well controlled by the closely spaced stirrups and the hysteresis loops do not show any sign of pinching. The peak positive load was 348 kN corresponding to a moment at the face of the column of 640 kN·m including the dead load effects and to a tip deflection of 81 mm. The peak negative load was 144 kN corresponding to a moment at the column face of 233 kN·m and to a tip deflection of 30 mm. The maximum positive deflection achieved was 140 mm, however the load, as can be seen from Fig 4.15, was 314 kN or 96% of the load at general yielding. The maximum negative deflection achieved was 41 mm corresponding to a load of 132 kN.

The measurements of the steel strains in the slab reinforcing bars indicated that

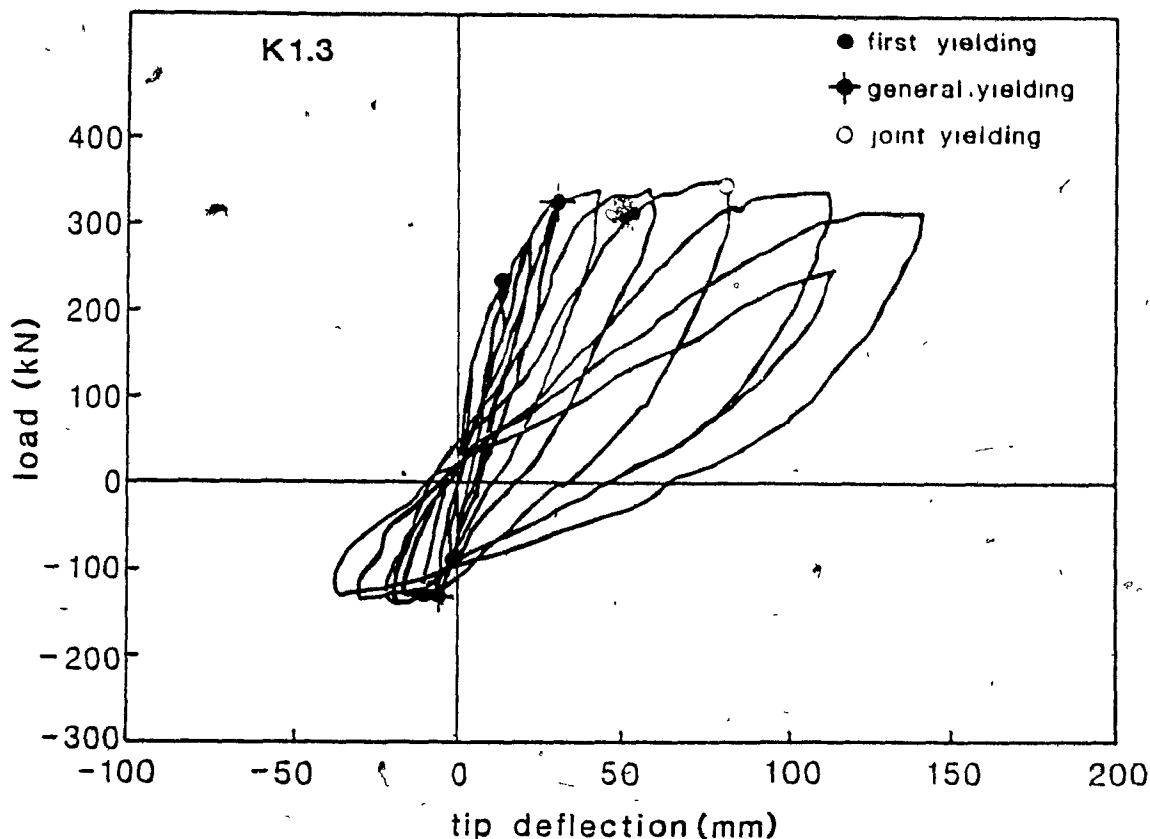
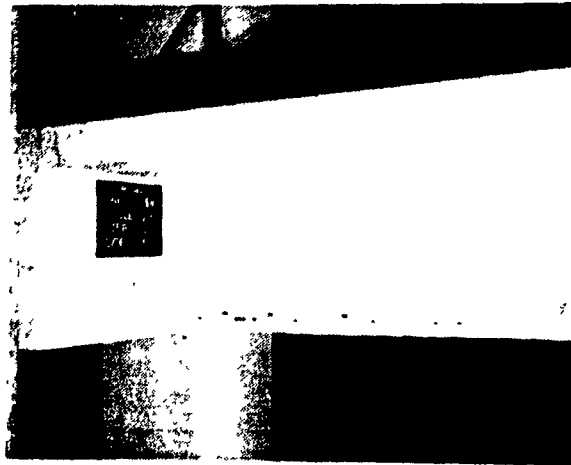


Fig. 4.15 Hysteretic load-tip deflection response for Specimen K1.3

at general yielding the slab bars within a distance of 4 times the slab thickness from the beam face have yielded. At the maximum load level, all of the bars across the entire slab width experienced strains exceeding the yield strain. Fig. 4.13 shows the measured strain distribution of the slab bars at a load level of 341.5 kN reached during the 6th cycle (displacement ductility of 2).

Figure 4.17 shows the external face of the column and the spandrel beam at the end of the test. The column cover concrete in the joint region had spalled off completely and one can notice from the photograph that the 90° hooks of the No. 15 longitudinal bars were tending to straighten out causing the free end extension to protrude from the reinforcing cage. At this stage torsional spalling extended over a region of about 100 mm from the column face. The spalling of the back concrete cover started at the peak downwards deflection in the seventh cycle (displacement ductility of 3). The



a) Near first yielding, $P = 90 \text{ kN}$



b) General yielding, $P = 327 \text{ kN}$



c) Near end of test, $P = 314 \text{ kN}$

Fig. 4.16 Specimen K1.3 at different load stages

diagonal torsional cracks in the spandrel beam extended into the joint core. It is clear from the large crack width and severe spalling (Fig. 4.17) that the spandrel beam had yielded in torsion.

Figure 4.18 shows the load versus measured tip deflection together with components of the tip deflection corresponding to flexural curvatures, Δ_f , shear distributions in the beam, Δ_s , and the deflection component, Δ_j , associated with shear distortion of the joint together with bond slip of the flexural bars anchored in the joint. After general yielding a plastic hinge length of 480 mm was estimated and used in determining Δ_f . As can be seen from Fig 4.18 the sum of the calculated tip deflection components agrees remarkably well with the measured tip deflection. The horizontal dial gauge connected to the column above the slab indicated that at a load level of 338.9 kN, a cycle after general yielding, the joint tip deflection component jumped to 24 mm (double the previous value). At the maximum load level of 348 kN this component had increased to 53 mm. These large increases in deflection indicate significant joint distress. In addition to the joint distress it was noticed that the curvature of the top column increased dramatically after general yielding. Testing had to be discontinued because of concern over the stability of the subassembly due to the large rotations in the joint and high local column rotations immediately above the joint (see Fig. 4.16 c).

4.3.3 Specimen K0.7

Figure 4.19 shows the hysteretic response for specimen K0.7. First yielding of the top steel occurred at a load of 219 kN and a corresponding deflection of 11 mm. First yielding in the negative direction occurred at a load of 142 kN and a corresponding deflection of 7 mm. General yielding in the positive direction occurred at a load of 273 kN and a deflection of 15 mm. In the negative direction general yielding occurred at a load of 177 kN and a deflection of 11 mm. The hysteresis loops remained stable throughout the duration of the test. In addition the specimen maintained its load carrying capacity for the duration of the test with peak loads in either direction for each cycle exceeding the loads at general yielding. Slight pinching of the hysteresis loops is noticeable during unloading after the fourth cycle. The peak positive load was 360 kN

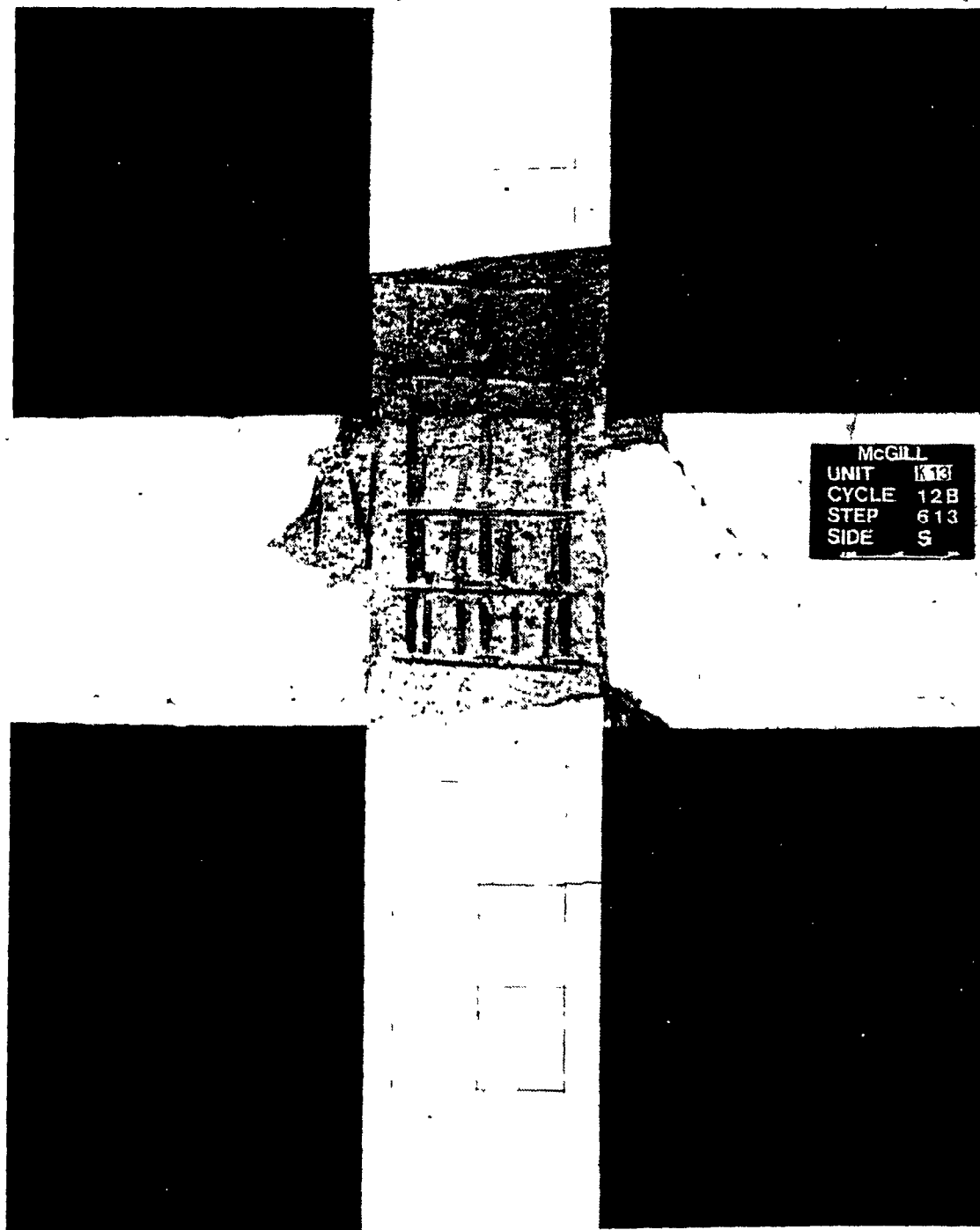


Fig. 4.17 Exterior face of specimen K1.3 at end of test

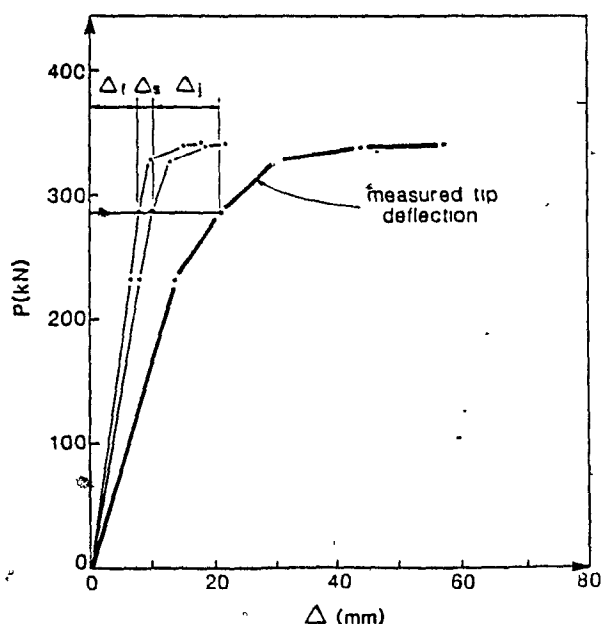


Fig. 4.18 Beam tip deflection components for specimen K1.3

in the eight cycle corresponding to a moment at the face of the column of 662 kN·m including dead load effects. The peak negative load was 244 kN corresponding to a moment at the column face of 433 kN·m. The maximum positive deflection achieved was 177 mm or a displacement ductility of 8. The corresponding load was 328 kN or 122% of the load at general yielding. The maximum negative deflection was 77 mm (displacement ductility of 8) corresponding to a load of 245 kN.

The measurements of the slab steel strains indicate, as in the case of specimens Old K1.3 and K1.3, that the first two rows of slab bars on either side of the longitudinal beam had yielded, as assumed in the design, at general yielding (at a load of 273 kN). Fig. 4.13 shows the distribution of the measured strains in the slab steel across the width of the slab at a load of 360 kN along with the yield strain of the No. 10 slab bars. It can be seen that the strain distribution is highly non-linear with the highest strains closer to the column and main beam beam. One can notice that at a load of 360 kN all the slab bars had yielded.

Figure 4.21 shows the external face of the column and the spandrel beam. As can be seen from this figure, due to the significant torsion in the spandrel beam, loss of

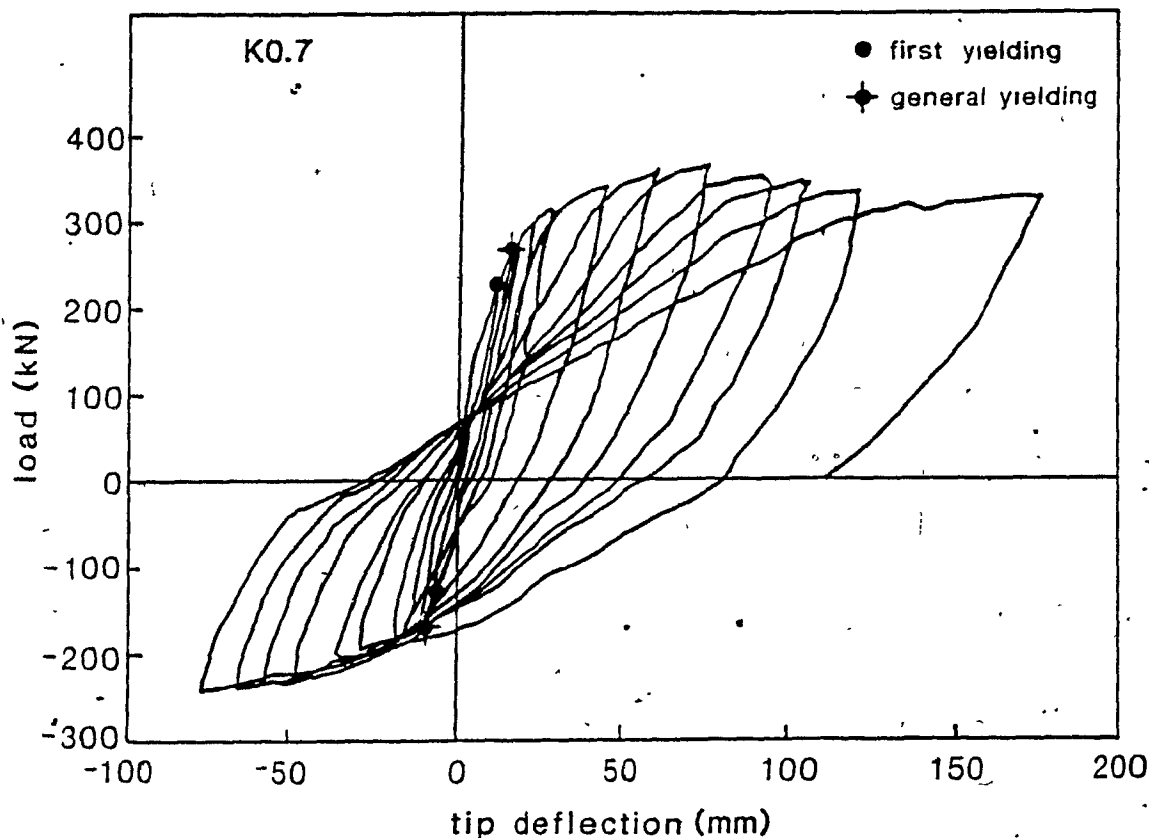
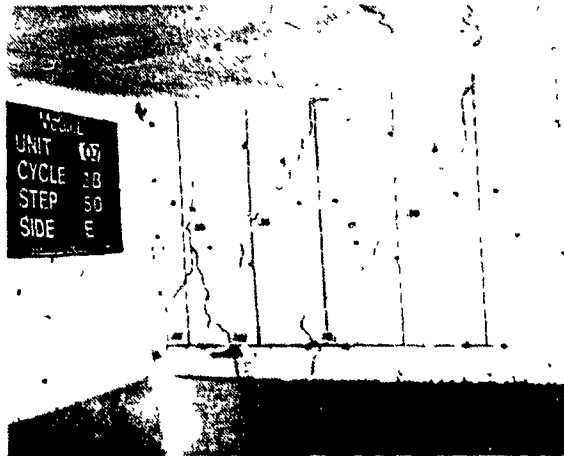


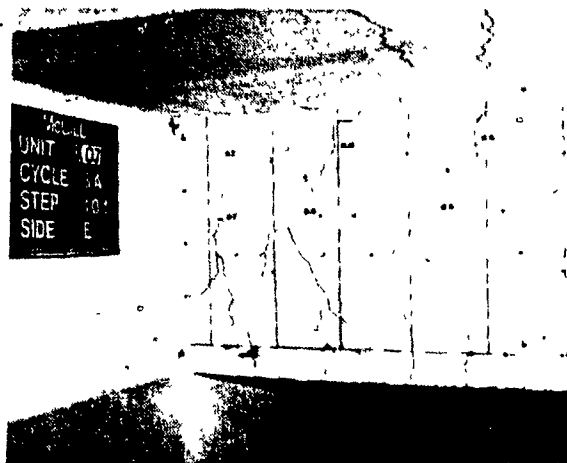
Fig. 4.19 Hysteretic load-tip deflection response for Specimen K0.7

concrete cover in the beam over a length of 150 mm on the east side had occurred at a displacement ductility of 7. There was also onset of spalling of the concrete cover on the west side. These large crack widths and extensive spalling in the spandrel beams indicated that torsional yielding of the spandrel beams had occurred.

Figure 4.22 shows the load versus measured tip deflection response along with components of the tip deflection corresponding to flexural curvatures, Δ_f , shear deformations in the beam, Δ_s , and the deflection component, Δ_j , associated with shear distortion of the joint together with bond-slip of the flexural bars anchored in the joint. As can be seen the contribution of the shear strains in the beam are relatively small during the complete response due to the large amount of transverse reinforcement in the beam. After general yielding the combined contribution of joint distortion and bond-slip becomes more significant (about 50% of the total). Once again, the sum of



a) Near first yielding, $P = 51 \text{ kN}$



b) General yielding, $P = 273 \text{ kN}$



c) Near end of test, $P = 318 \text{ kN}$

Fig. 4.20 Specimen K0.7 at different load stages

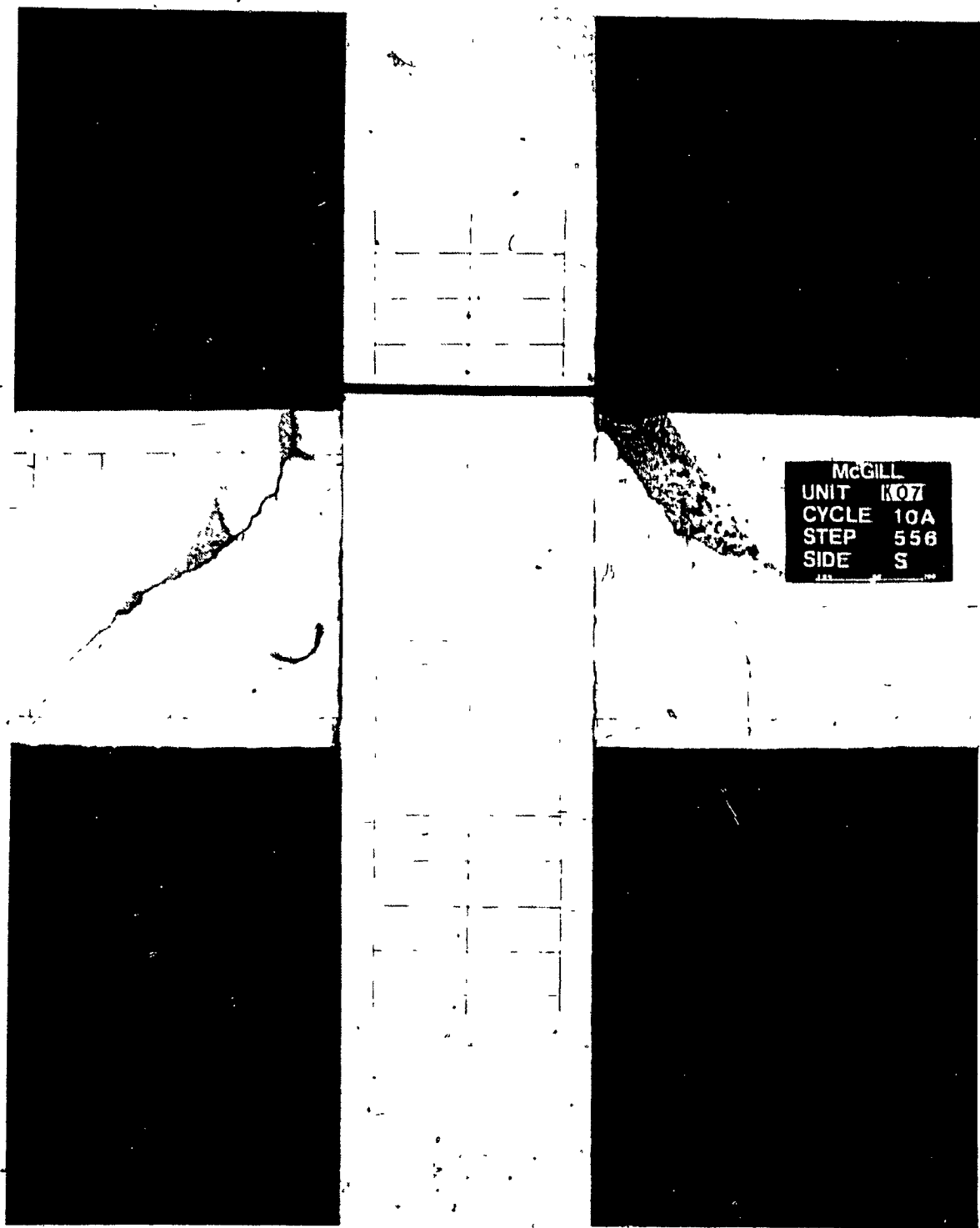


Fig. 4.21 Exterior face of specimen K0.7 at end of test

the calculated tip components agrees remarkably well with the measured tip deflection (see Fig. 4.22). No significant joint distortions were observed during the test.

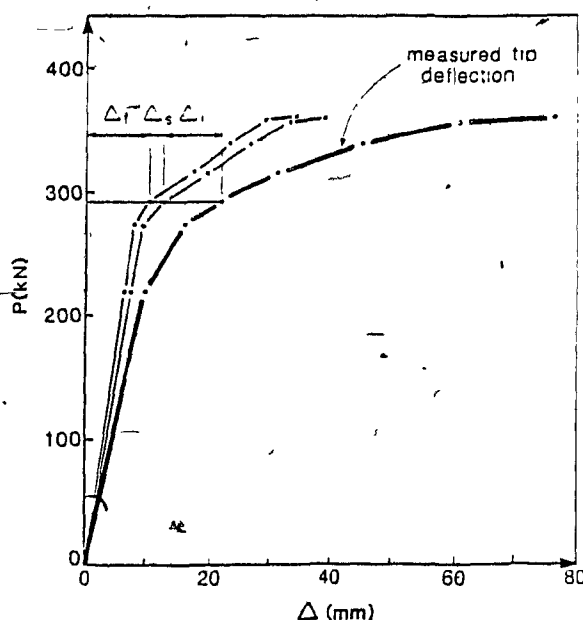


Fig. 4.22 Beam tip deflection components for specimen K0.7

Figure 4.23 shows the condition of the beam at the peak positive deflection in the eleventh cycle. As can be seen from this figure slight buckling of the longitudinal bars between the closely spaced stirrups occurred at this peak deflection. Comparing the state of these bars to similar ones in specimen Old K1.3 it can be concluded that the additional stirrups are effective in controlling the buckling of the longitudinal bars. From the measured curvatures in post yielding cycles, it was found that the length of the plastic hinge reached 400 mm.

Testing was stopped at a positive deflection of 177 mm due to lack of further travel of the loading jacks.

4.4 COMPARISON OF EXPERIMENTAL RESULTS

Table 4.3 compares the overall behaviour of the three specimens tested. As can be seen the "ductility factor", K , influences the failure modes, and hence the "ductility",



Fig. 4.23 Specimen K0.7 close to failure

the ability to maintain load after general yielding and the overall response stiffnesses. The reported ductilities in Table 4.3 were calculated from the ratio of the maximum displacement, Δ_u , reached while still maintaining load levels greater than general yielding to the displacement, Δ_y , at general yielding. As a measure of the ability to maintain load after general yielding the ratio of the load corresponding to Δ_u to the load at general yielding (i.e., P_u/P_y) is presented. The ratio of the overall response stiffness to the stiffness at general yielding (i.e., K_u/K_y) was determined for the "ultimate" and the "yield" cycles from the slope of the line joining the negative and positive peak values. The "ductility" achieved was 2.8, 5 and over 8 for specimens Old K1.3, K1.3 and K0.7 respectively. Specimen K0.7 demonstrated the ability to maintain the load carrying capacity much better than specimens Old K1.3 and K1.3. As can be seen from Table 4.3 as the ductility is increased a significant drop in the stiffness at ultimate occurs.

Table 4.3 Comparison of Failure Mode and Key Response Parameters

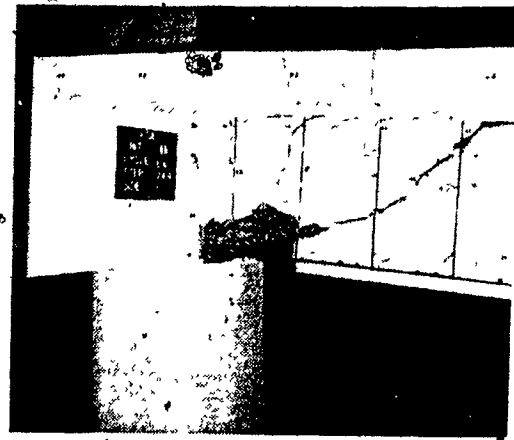
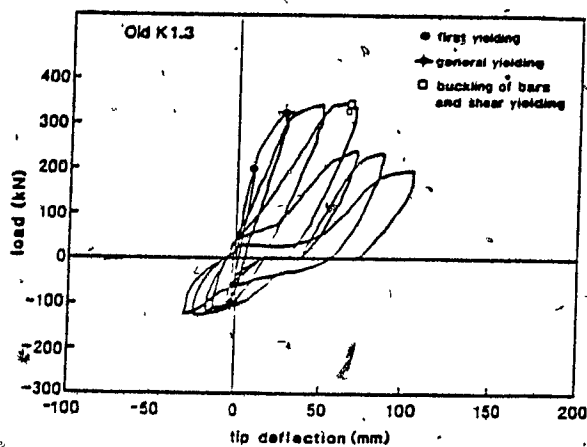
Specimen	Failure mode	Ductility	P_u/P_y	K_u/K_y
Old K1.3	Beam shear failure Longitudinal bar buckling	2.8	1.07	0.31
K1.3	Joint yielding Column hinging	5	1.06	0.22°
K0.7	Beam flexural yielding	8†	1.22	0.18

† testing was stopped due to lack of travel in loading rams

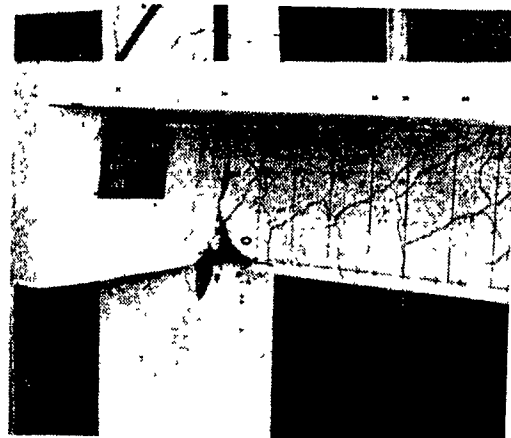
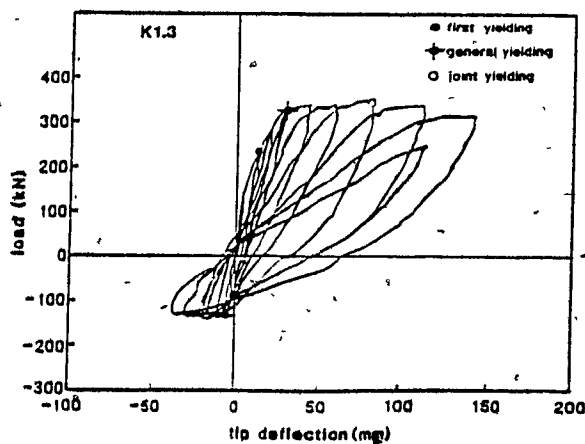
Figure 4.24 compares the hysteretic responses of the three specimens along with photographs of each specimen at failure. As can be seen Specimen Old K1.3 displayed a pinched hysteretic response with a significant drop in the load carrying capacity after a displacement ductility of about 3. This behaviour is a result of the buckling of the bottom longitudinal bars between the stirrups as well as severe shear distress in the main beam. Specimen K1.3 displayed much improved response with an absence of pinching and ability to maintain the load up to a displacement ductility of about 5. Although the longitudinal bars in the beam did not buckle and the beam did not suffer significant shear distress the test was stopped due to severe shear distortion in the joint and commencement of column hinging (see Fig. 4.24 b). The stable hysteresis

loops and the excellent ability to maintain the load level up to a displacement ductility greater than 8 for specimen K0.7 is evident from Fig. 4.24c. As can be seen from Fig. 4.24 c inelastic action was concentrated in the main beam with the design and detailing preventing a) buckling of the longitudinal bars, b) yielding of the shear reinforcement in the beam, c) yielding of the joint reinforcement and d) hinging in the column.

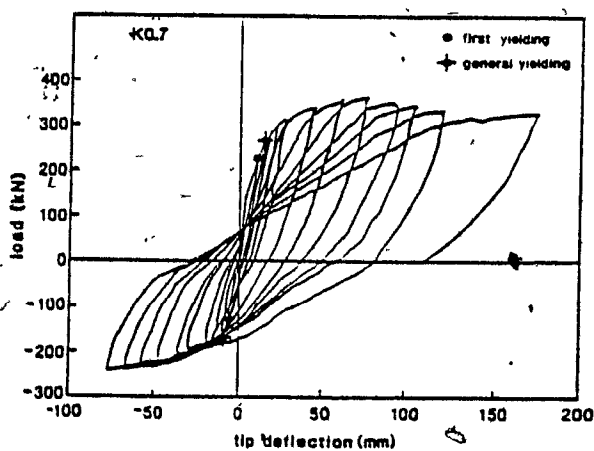
Figure 4.25 compares the load-deflection response envelopes of the three specimens. As can be seen from this figure the overall response is improved as the ductility increases. Specimen Old K1.3 has low energy dissipating capacity due to the low level of ductility and the relatively small area enclosed by the response envelope. There is significant improvement in the overall response of specimen K1.3 which was designed and detailed according to the "nominal ductility" requirements of the 1984 CSA Concrete Code [3]. It is important to realize that the apparent ductility displayed by specimen K1.3 might not be attainable in a structure because of the joint rotations and column hinging. These effects will be investigated in the non-linear dynamic analysis reported in Chapter 7. The improved response of specimen K0.7 in both the positive and negative loading direction is evident in Fig. 4.25. The much improved negative loading response is due mainly to the requirement that the positive moment resistance of the beam at the column face be at least 50% of the negative moment capacity.



a) Specimen Old K1.3



b) Specimen K1.3



c) Specimen K0.7

Fig. 4.24 Comparisons of responses and appearance of specimens near failure

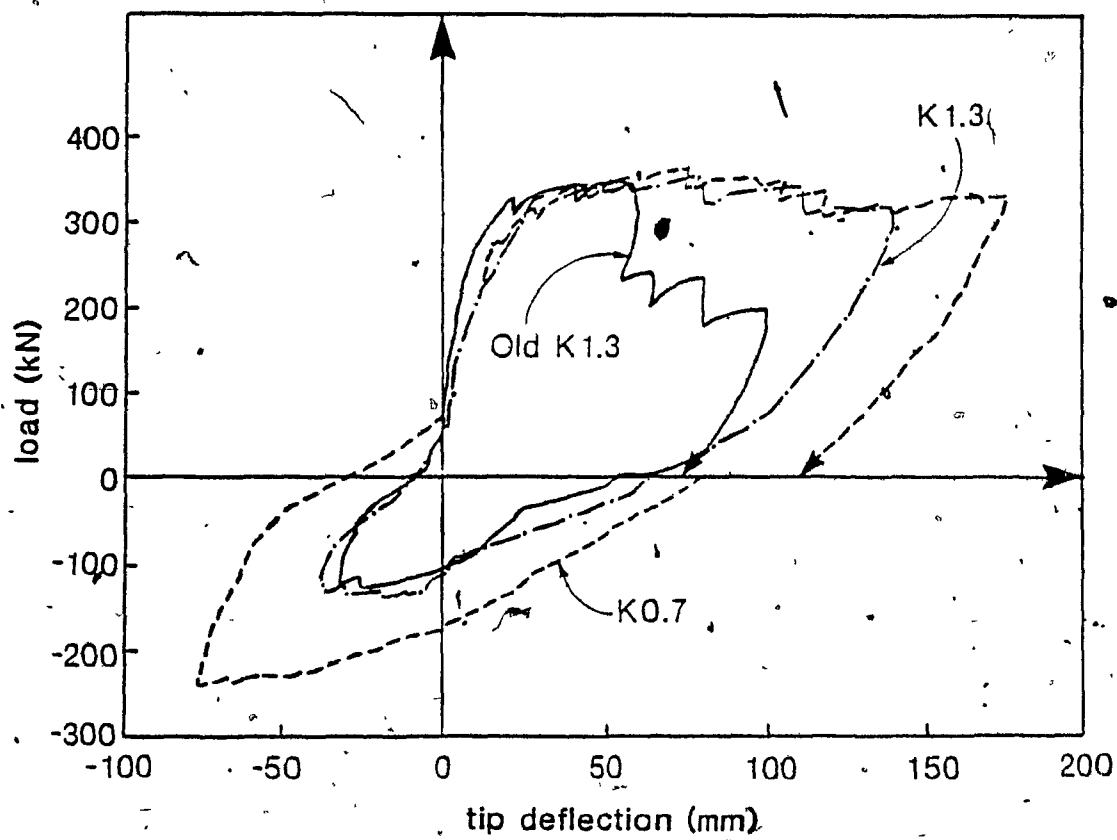


Fig. 4.25 Envelopes of responses

CHAPTER 5

PREDICTIONS OF MEMBER BEHAVIOUR AND COMPARISONS WITH TEST RESULTS

5.1 PREDICTING FLEXURE AND AXIAL LOAD RESPONSE

The complete moment-curvature response of a section of a member provides useful information necessary to understand the flexural response. Therefore an analytical procedure had to be developed to predict the moment-curvature relationship while accounting for the following effects:

- 1) the complete stress-strain relationship of the steel including strain hardening,
- 2) the non-linear stress-strain relationship for the concrete including confinement effects in compression and tension stiffening effects in tension,
- 3) changes in the geometry of the section due to progressive spalling of the concrete cover at higher strains,
- 4) non-linear strain distribution in flanged sections.

A computer program, called MNPHI, having the above capabilities was developed on a micro-computer (IBM PC/XT/AT) to predict the moment-curvature responses.

The analysis is based on idealized stress-strain relationships for the materials (see Fig. 5.1) and ensures compatibility of strains and equilibrium of forces.

In order to predict the response the cross section of the member is divided into a number of concrete strips parallel to the neutral axis of the section as shown in Fig. 5.1 b. For each concrete strip it is necessary to give the total width and the width of the confined portion. If the strip is in compression this enables the modelling of progressive spalling of the concrete cover and also enables the modelling of the beneficial effects of

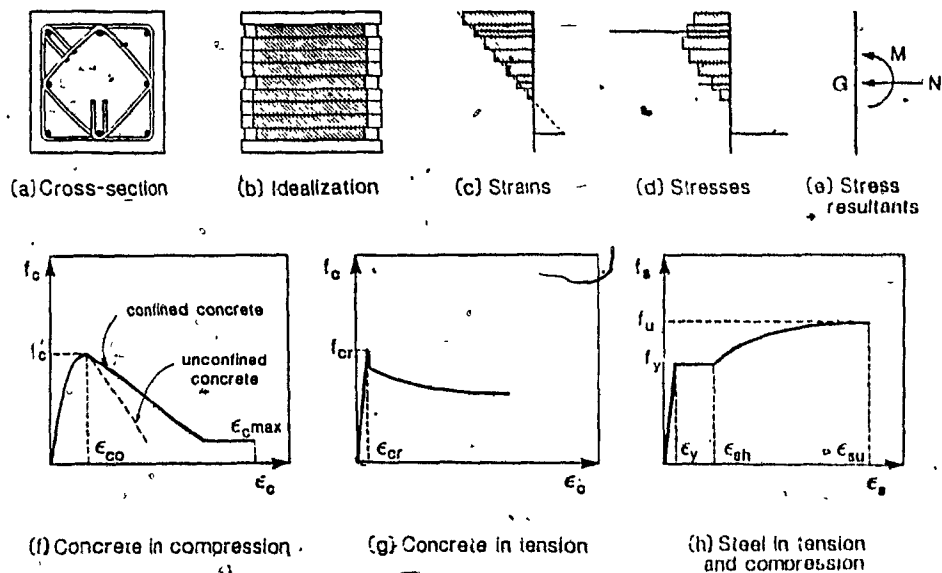


Fig. 5.1 Predicting flexural response

confinement in the confined region of each strip. The strain at which the unconfined concrete cover is assumed to spall (i.e. carries no stress) can be set independently but is given a default strain value of -0.004. This spalling strain corresponds to that assumed by Park and Paulay [16]. As can be seen from Fig. 5.1f the compressive stress-strain relationship of the concrete depends on the degree of confinement. The manner in which the amount of confinement provided by rectangular hoops affects the stress-strain relationship, as developed by Kent and Park [14], is illustrated in Fig. 5.2.

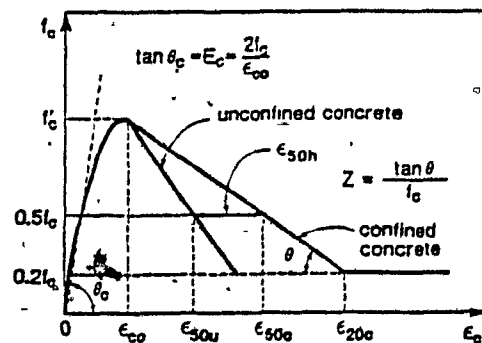


Fig. 5.2 Stress-strain relationship for concrete confined by rectangular hoops, Kent and Park [14]

The concrete stress can be found from:

$$f_c = \begin{cases} f'_c \left[\frac{2\epsilon_c}{\epsilon_{co}} - \left(\frac{\epsilon_c}{\epsilon_{co}} \right)^2 \right], & \text{for } \epsilon_{co} \leq \epsilon_c \leq 0.0 \\ f'_c [1 - Z(\epsilon_c - \epsilon_{co})], & \text{for } \epsilon_{20c} \leq \epsilon_c \leq \epsilon_{co} \\ 0.2f'_c, & \text{for } \epsilon_c \leq \epsilon_{20c} \end{cases} \quad (5.1)$$

where

$$Z = \frac{0.5}{\epsilon_{50u} + \epsilon_{50h} - \epsilon_{co}}$$

$$\epsilon_{50u} = \frac{3 + \epsilon_{co} f'_c}{f'_c - 1000}$$

$$\epsilon_{50h} = \frac{3}{4} \rho_s \sqrt{\frac{b'}{s_h}}$$

It is noted that in the above expressions all compressive strains and stresses are taken as negative quantities.

The maximum strain, $\epsilon_{c_{max}}$, at which the confined concrete is assumed to "crush" (i.e. carries no stress) can also be set independently. Guidance to calculate this maximum strain was given by Corley [69] and simplified by Mattock [70] as:

$$\epsilon_{c_{max}} = -0.003 - 0.002 \frac{b}{z} - 0.2\rho_s \quad (5.2)$$

where b is the width of the beam, z is the distance from the critical section to the point of contra-flexure, and ρ_s is the ratio of the volume of confining steel (including compression steel) to the volume of the concrete core.

The steel is modelled as concentrated areas located at the appropriate positions in the cross section. The stress-strain relationship including strain hardening is assumed to be that given by Park and Paulay [18] (see Fig 5.3).

The steel stress can be found from:

$$f_s = \begin{cases} \epsilon_s E_s, & \text{for } 0.0 \leq \epsilon_s \leq \epsilon_y \\ f_y, & \text{for } \epsilon_y \leq \epsilon_s \leq \epsilon_{sh} \\ f_y \left[\frac{ms + 2}{60s + 2} + \frac{s(60 - m)}{2(30r + 1)^2} \right], & \text{for } \epsilon_{sh} \leq \epsilon_s \leq \epsilon_u \end{cases} \quad (5.3)$$

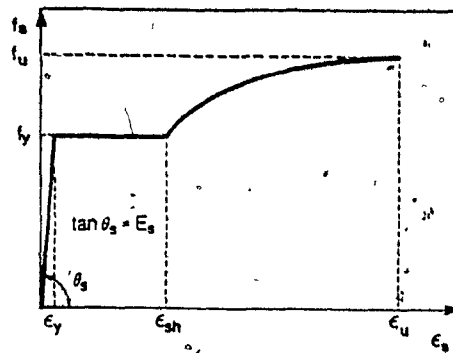


Fig. 5.3 Idealization for the stress-strain relationship for steel in tension or compression, Park and Paulay [18]

where

$$r = \epsilon_u - \epsilon_{sh}$$

$$s = \epsilon_s - \epsilon_{sh}$$

$$m = \frac{(f_u/f_y)(30r + 1)^2 - 60r - 1}{15r^2}$$

The effect of tension stiffening in the concrete after cracking is accounted for in specified concrete layers. The average tensile stress in the concrete after cracking as given by Vecchio and Collins [71,72] is shown in Fig 5.4.

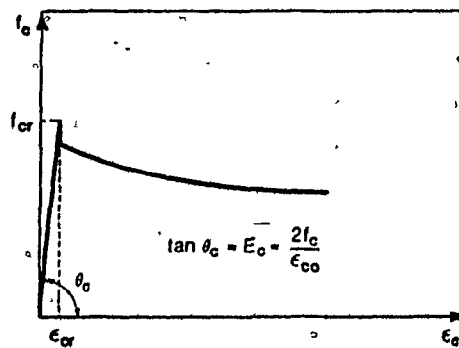


Fig. 5.4 Average stress-strain relationship for cracked concrete in tension, Vecchio and Collins [71]

The average tensile stress in the concrete can be found from:

$$f_c = \begin{cases} 2 \frac{f'_c}{\epsilon_{co}} \epsilon_c, & \text{for } 0.0 \leq \epsilon_c \leq \epsilon_{cr} \\ \frac{f_{cr}}{1 + \sqrt{200\epsilon_c}}, & \text{for } \epsilon_c > \epsilon_{cr} \end{cases} \quad (5.4)$$

In addition MNPHI incorporates stress-strain relationships which include bi-linear elasto-plastic, tri-linear as well as inverse Ramberg-Osgood [73] relationship for modelling of highly curved stress-strain relationships (e.g. small diameter bars and prestressing steel).

The analysis procedure with reference to Fig. 5.1 is as follows:

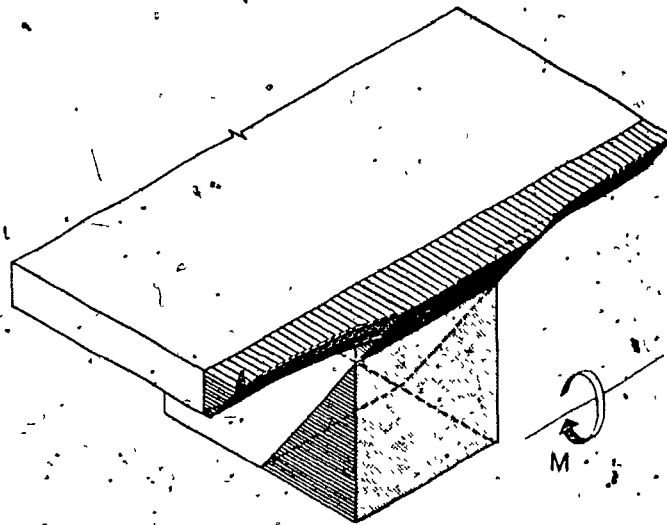
- M1. Assume a top fibre strain, $\epsilon_{c, top}$.
- M2. Assume the value of the depth to the neutral axis, c .
- M3. Compute all stress resultants in the concrete and the steel for the assumed strain distribution and accounting for spalling of the cover concrete.
- M4. Iterate on c until equilibrium is satisfied to a specified accuracy.
- M5. Calculate the resultant moment, axial load and curvature.
- M6. Increment the top fibre strain and repeat steps M2 through M5. ■¹

The above procedure is carried out including the effect of average tensile stresses in the concrete. Another separate analysis is carried out with no tension stiffening effects in order to limit the maximum moment that can be carried at a crack location. The complete response assumed follows the analysis with tension stiffening up to the maximum moment that the section can carry at a crack location.

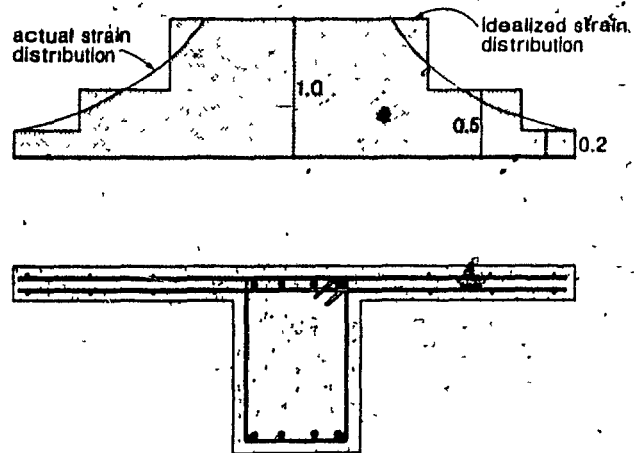
For flanged sections MNPHI permits the user to specify a variation of strain across the width of the flange as shown in Fig. 5.5 a. This is carried out in the layered analysis shown in Fig. 5.1 by separating each flange layer into different horizontal parts, each part having a specified strain participation factor. An example of the use of this participation factor is given in Fig. 5.5 b.

For determining the axial load-moment interaction curve the same procedure given above is followed for a number of different levels of axial load. In determining the axial

¹ ■ indicates end of algorithm



a) Variation of strain across the width of the flange



b) Strain participation factor

Fig. 5.5 Accounting for variation of strains across the flange of T section

load-moment strength interaction curve two options are available: i) assume that the capacity occurs when a fixed value of maximum compressive strain is reached (the traditional assumption is $\epsilon_{c_{max}} = -0.003$), ii) for a range of maximum compressive concrete strains find the maximum moment. In both cases tensile steel yielding is traced allowing an evaluation of available ductility.

Figure 5.6 shows the predicted moment-curvature responses of the main beam of specimen K0.7 subjected to negative bending moment. The lower curve is the prediction of the response assuming the non-linear strain distribution across the flange as shown and the upper curve is the prediction assuming a uniform strain distribution across the full width of the flange. The non-linear strain distribution results in a more "rounded" response due to progressive yielding of the top reinforcement. It should be noted that the curves are essentially the same after yielding of all bars. In the curves first yielding of the tensile and compressive reinforcement, onset of spalling and crushing of the concrete are reported. The effect of the steel strain hardening after a curvature of about 25×10^{-3} rad/m can also be seen.

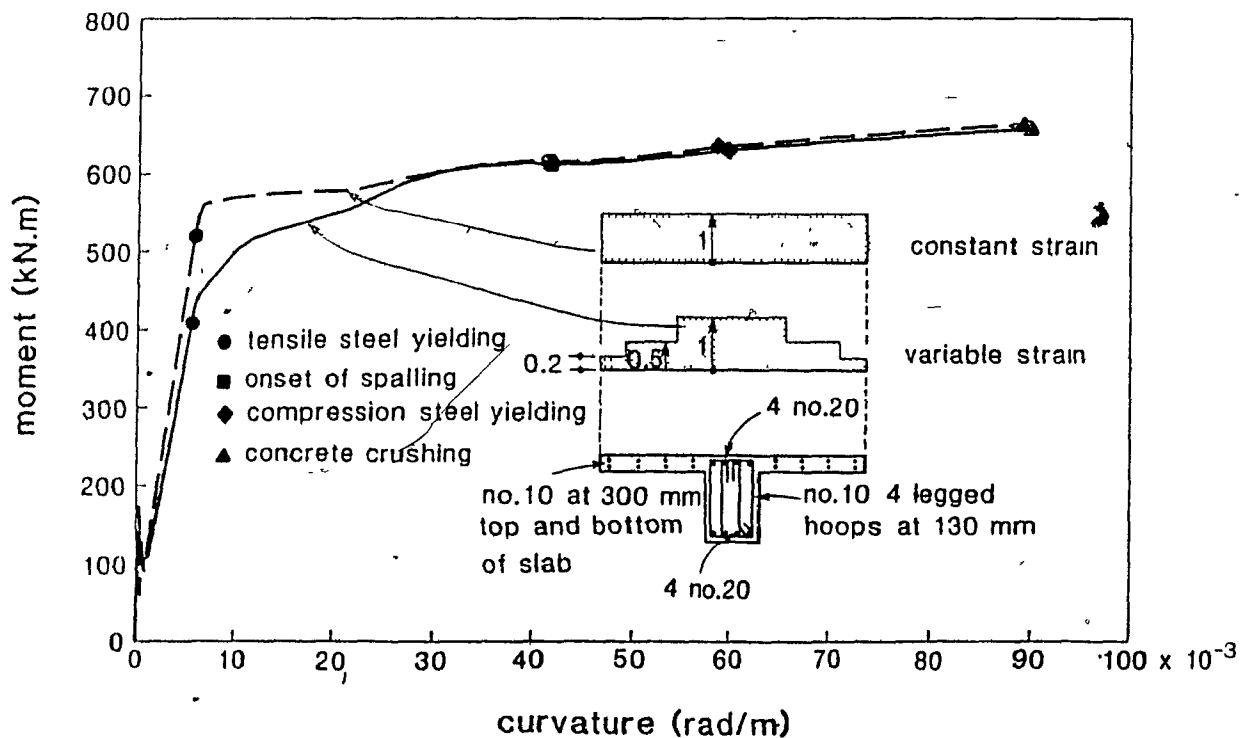


Fig. 5.6 Influence on moment-curvature response of non-linear strain distribution in flange of T beam

Figure 5.7 presents the predicted axial load-moment interaction diagram for the column section used in specimen K0.7 together with the predicted axial load-curvature response. Since the ultimate axial load-moment interaction diagram was obtained by

searching for the maximum possible moment obtainable for different axial load levels the corresponding extreme fibre compressive strain will not be constant at ultimate. As can be seen the resulting extreme compressive fibre strains are within the limiting strain of -0.01 as calculated from Eq. 5.2. Fig. 5.7 shows the variation in strain distribution for different levels of axial loads. The dashed lines in Fig. 5.7 represent values at first yielding of the tensile reinforcement. The ratio ϕ_u/ϕ_y represents the curvature ductility of the cross section. It can be seen that at an axial load of -2200 kN the moment at first yielding equals the ultimate moment, and therefore the balanced condition exists. At this balanced condition the curvature ductility ϕ_u/ϕ_y is equal to 1.0 . For lower levels of axial compression the curvature ductility increases.

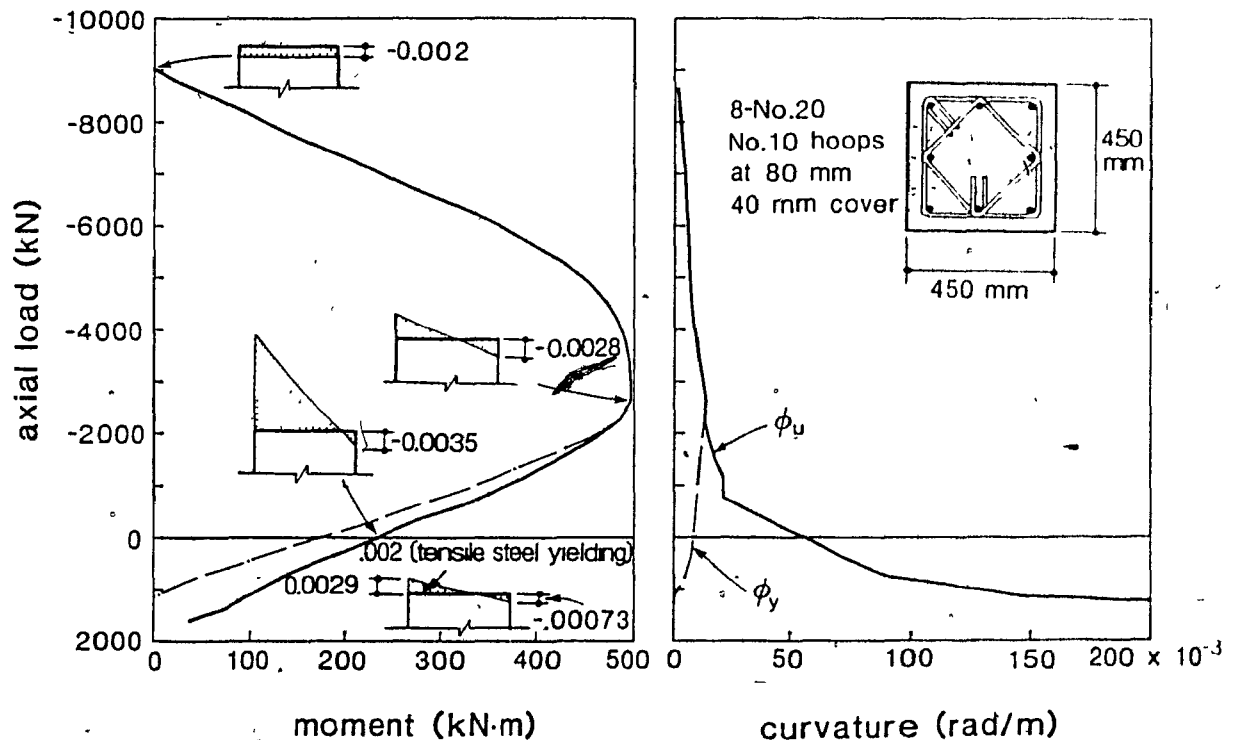


Fig.5.7 Predicted axial load-moment interaction and axial load-curvature response

Figure 5.8 shows the influence of axial load on the moment curvature response for the section shown in Fig. 5.7 (specimen K0.7). It can be seen that the strength increases with increasing levels of compressive axial load but the ductility decreases.

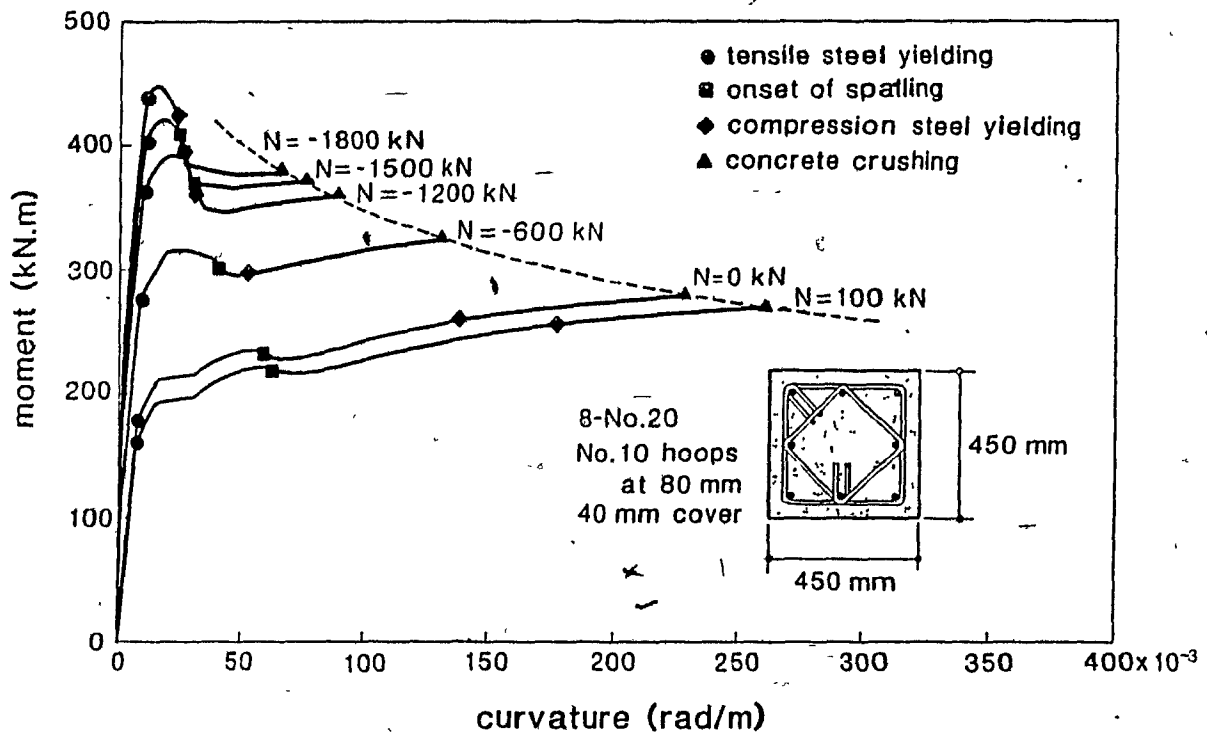


Fig. 5.8 Influence of axial load on the moment curvature response of a column section

Figure 5.9 shows the predicted axial load-moment and predicted axial load-curvature interaction diagrams for the column section of specimen K0.7 in its unspalled and fully spalled conditions. The unspalled predictions were obtained by limiting the maximum compressive strain to -0.004 (i.e. the strain at which the unconfined concrete is assumed to spall). The fully spalled predictions were obtained by neglecting the unconfined concrete cover on all sides of the section and by limiting the maximum compressive strains to -0.01 .

5.2 PREDICTING MOMENT-AXIAL LOAD-SHEAR RESPONSE

When shear is present with moment and axial load it is no longer possible to determine directly the longitudinal stresses in the concrete from a flexural sectional analysis as described in Section 5.1. The compression field theory [74,75,76] provides a rational way of predicting the response of reinforced concrete sections subjected to

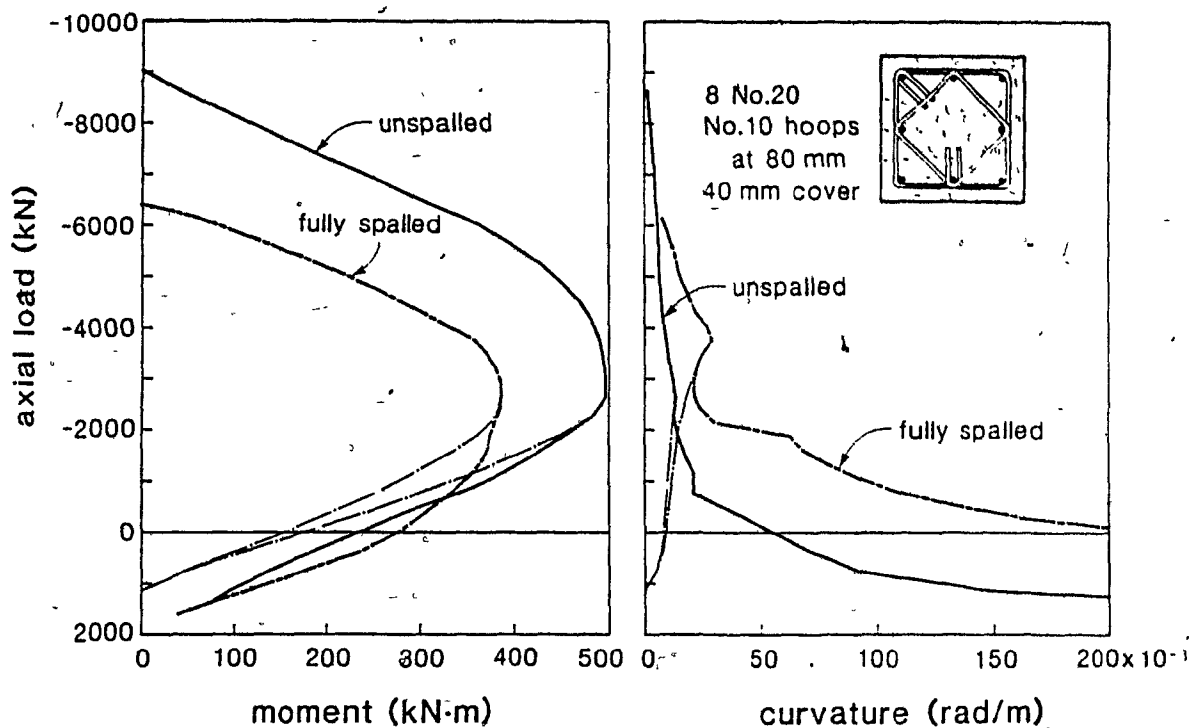


Fig. 5.9 Influence of spalling on the response of a column section

combined flexure, shear and axial load. In its most general form the analysis can account for both a non uniform shear stress distribution as well as changes in direction of principal compressive stresses in the concrete over the depth of the section (see Fig. 5.10). In this study however a more direct approach proposed by Collins and Mitchell [77,78] will be used. In this procedure (see Fig. 5.11) the shear stresses are assumed to be uniformly distributed over the effective shear area, b_v wide and d_v deep, and the direction of the principal compressive stresses (defined by the angle θ) is assumed to remain constant over the depth d_v .

The combination of shear, flexure and axial load results in a longitudinal strain distribution as shown in Fig. 5.11. The longitudinal strain, $\epsilon_{l,m,d}$, at mid-height of the web due to the combined loading effects is used as an indicator of how severely strained the web is due to these effects.

The procedure adopted follows that described by Collins and Mitchell [77,78] and involves an incremental analysis using the Modified Compression Field Theory which

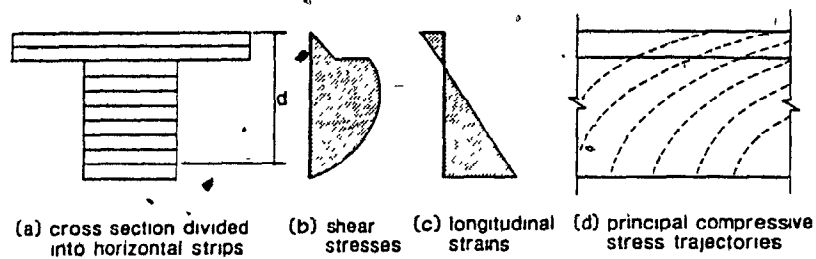


Fig. 5.10 Detailed analysis using the compression field theory

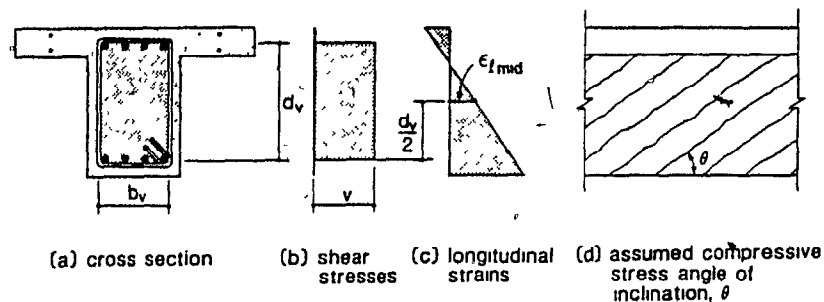


Fig. 5.11 Simplified analysis using the compression field theory

considers equilibrium, strain compatibility and utilizes the non-linear stress-strain characteristics of both the concrete and the steel.

Figure 5.12 illustrates the manner in which the full response of a beam can be determined using plane section analysis linked to the modified compression field theory. The incremental analysis is performed by first choosing the principal tensile strain, ϵ_1 , at mid-height of the web (see Fig. 5.13) and estimating the angle of inclination of principal compression, θ . The strains (including $\epsilon_{l\text{mid}}$), the stresses in the steel and the concrete, and the corresponding shear V together with the equivalent axial tension, N_v , are then determined. A flexural sectional analysis (MNPFI) is then performed by imposing a mid-height longitudinal strain, $\epsilon_{l\text{mid}}$, determined from the shear analysis. For this mid-height longitudinal strain, $\epsilon_{l\text{mid}}$, and for the applied moment M the necessary curvature is determined. For the strain distribution corresponding to this curvature the axial load is then determined. If this axial load, N_p , equals the applied axial load

plus the equivalent axial tensile load, N_v , due to shear then the estimated value of θ is correct and the corresponding strain distribution is found. If longitudinal equilibrium is not achieved a new estimate of θ is made and the process repeated. The complete response is obtained by performing the above procedure for a range of principal tensile strain ϵ_1 .

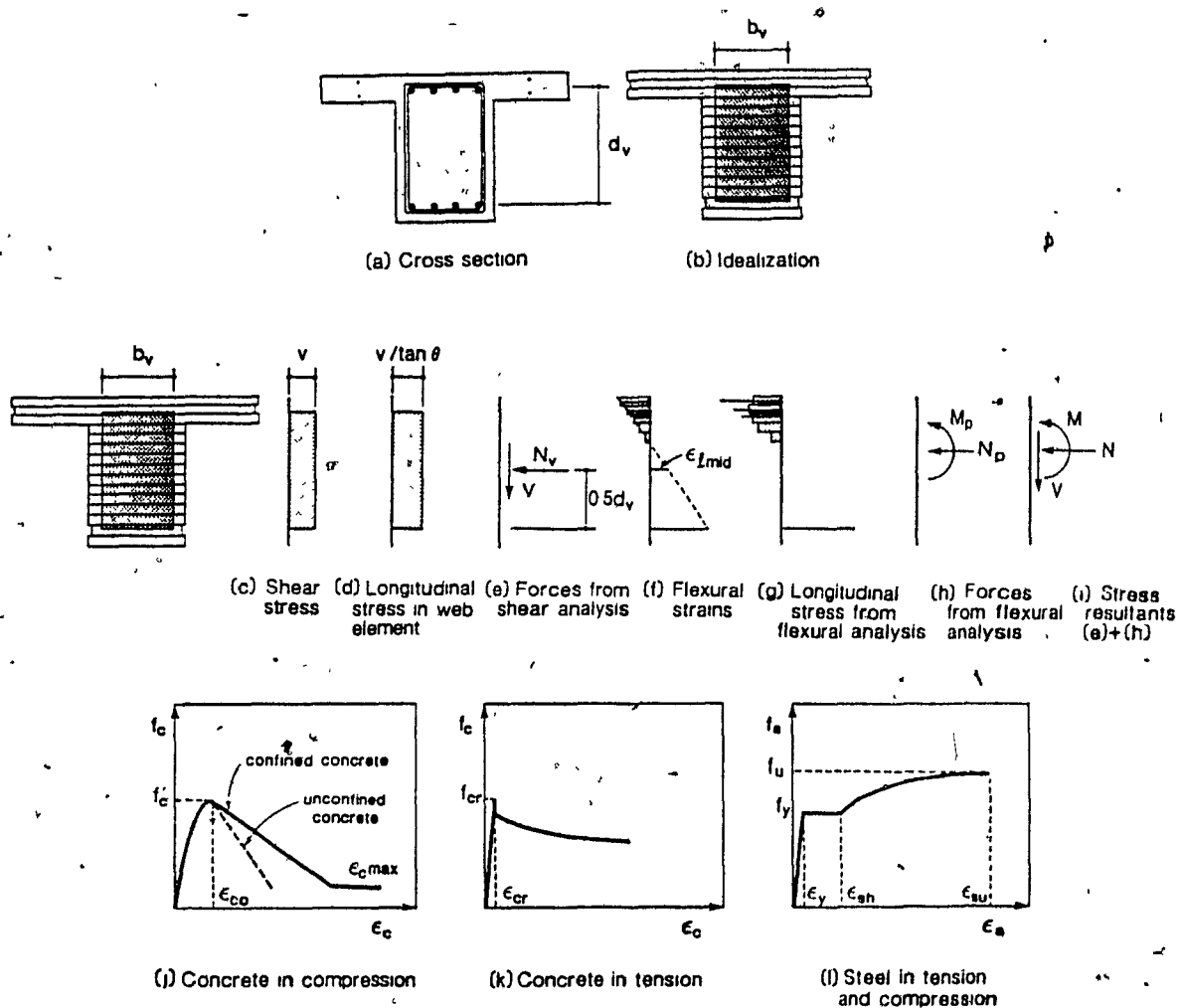


Fig. 5.12 Predicting axial load-moment-shear response

This procedure is described with reference to Fig. 5.12 in the following steps.

- V.1. Choose a value of principal tensile strain, ϵ_1 , at which to perform the calculations

V2. Estimate angle of inclination, θ , of principal compressive stress.

V3. Calculate average crack width, w

$$w = s_{m\theta} \epsilon_1 \quad (5.5)$$

where

$$s_{m\theta} = \frac{1}{\frac{\sin \theta}{s_{m,l}} + \frac{\cos \theta}{s_{m,v}}}$$

in which $s_{m,l}$ and $s_{m,v}$ are crack spacings indicative of the reinforcement details in the longitudinal and transverse directions respectively (see Fig. 5.13).

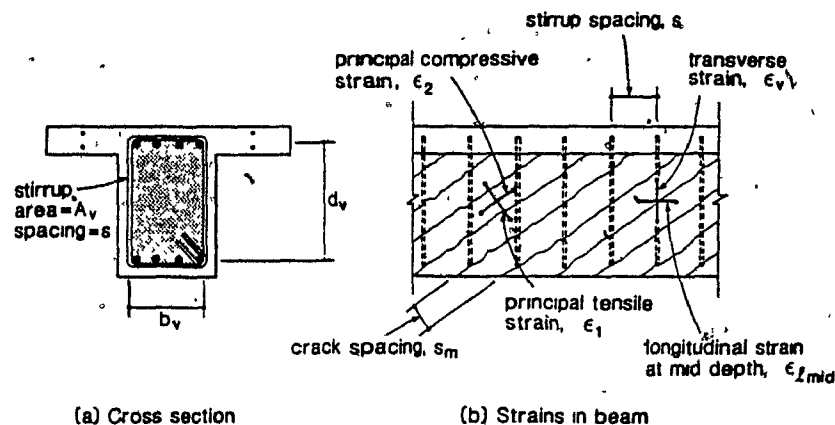


Fig. 5.13 Spacing of inclined cracks

V4. Estimate average stress in the transverse reinforcement, f_v .

V5. Calculate average principal tensile stress in the concrete, f_{c1} , from Eq.

5.4. These relations account for the reduction in average tensile stress that occurs between cracks after cracking.

However, the value of f_{c1} is limited by the ability of the steel and the cracked concrete to transmit stresses across the cracks. This limit given by Collins and Mitchell is:

$$f_{c1} \leq \frac{\sqrt{f'_c}(0.18 + 0.3K^2) \tan \theta}{0.31 + \frac{24w}{16+a}} + \frac{A_v}{b_v s} (f_{vv} - f_v) \quad (5.6)$$

where

$$K = \frac{1}{\tan \theta - 1.64} \geq 0$$

In which a is the maximum aggregate size, f'_c is the concrete strength, and f_{vv} is the yield stress of transverse steel.

- V6. Calculate the shear, V , corresponding to the estimated average stress in the transverse reinforcement, f_v , in step V4 and estimated principal compressive stress angle of inclination, θ , in step V2. The equilibrium condition is described in Fig. 5.14 and is described below:

$$V = \frac{A_v f_v}{s} \frac{d_v}{\tan \theta} + \frac{f_{c1} b_v d_v}{\tan \theta} \quad (5.7)$$

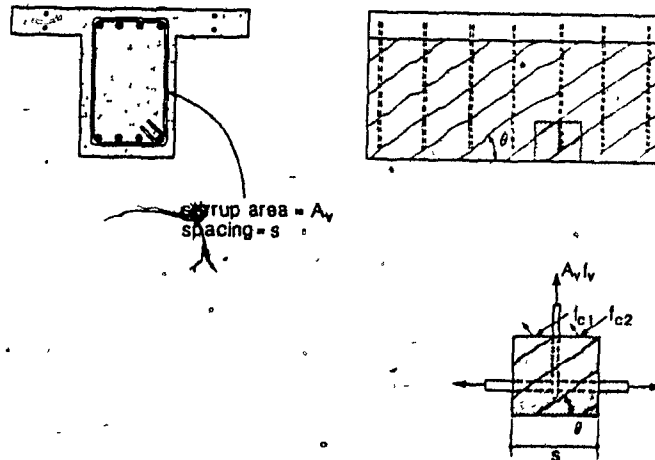
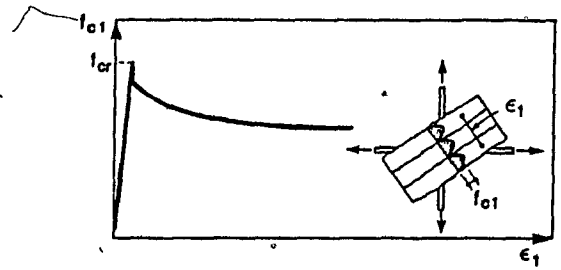
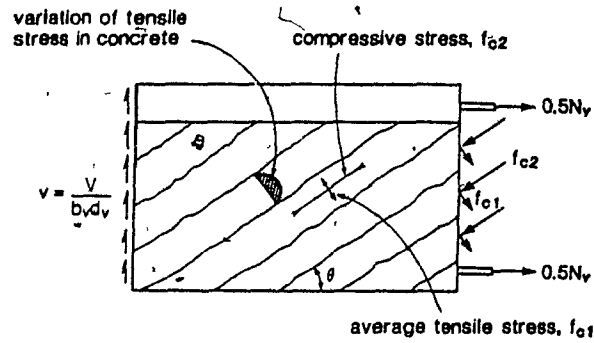
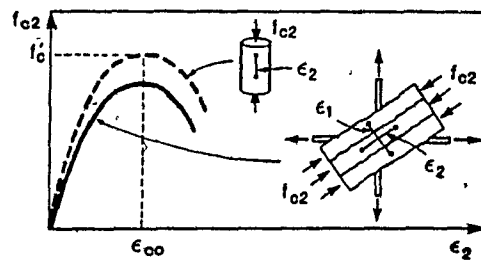


Fig. 5.14 Equilibrium considerations for beam in shear

- V7. Calculate the principal compressive stress, f_{c2} (see Fig. 5.14) from the following relationship:



(b) Average stress-strain relationship for cracked concrete in tension



(c) Average stress-strain relationship for cracked concrete in compression

Fig. 5.15 Stress-strain relationship for diagonally cracked concrete

$$f_{c2} = f_{c1} - v \left(\tan \theta + \frac{1}{\tan \theta} \right) \quad (5.8)$$

V8. Calculate the maximum strength of the concrete (see Fig. 5.15) which is diagonally cracked and subjected to a principal tensile strain, ϵ_1 from the following expression [71,76]:

$$f_{c2_{max}} = \frac{f'_c}{0.8 - 0.34 \frac{\epsilon_1}{\epsilon_{c0}}} \quad (5.9)$$

- V9. If $|f_{c2}| > |f_{c2_{max}}|$, return to step V2 and choose a larger value of θ .
- V10. Calculate principal compressive strain, ϵ_2 , corresponding to principal compressive stress, f_{c2} , from:

$$\epsilon_2 = \epsilon_{co} \left(1 - \sqrt{1 - \frac{f_{c2}}{f_{c2_{max}}}} \right) \quad (5.10)$$

- V11. Calculate the transverse strain, ϵ_t , from compatibility of strain:

$$\epsilon_t = \frac{\epsilon_1 + \epsilon_2 \tan^2 \theta}{1 + \tan^2 \theta} \quad (5.11)$$

- V12. Calculate the stress in transverse reinforcement, f_v , corresponding to the calculated strain, ϵ_v , and from the stress-strain relationship for the transverse reinforcement.
- V13. If f_v calculated in step V12 does not agree with the estimated f_v in step V4, return to step 4 with the new calculated value of f_v .
- V14. Calculate the longitudinal strain, ϵ_l

$$\epsilon_l = \epsilon_1 + \epsilon_2 + \epsilon_v \quad (5.12)$$

- V15. Call MNPHI (flexural sectional analysis program) with the strain at mid-depth, $\epsilon_{l_{mid}}$, equal to the calculated value of ϵ_l in step V14. Find the strain distribution corresponding to desired the moment, M , and then determine the corresponding axial load, N_p , as shown in Fig. 5.12 h. The desired moment may be specified by the user or may be calculated internally by the program from a specified M/V ratio.
- V16. Calculate the equivalent axial tensile load, N_v , due to shear (see Fig. 5.12 e)

$$N_v = f_{c1} b_v d_v - \frac{V}{\tan \theta} \quad (5.13)$$

- V17. Calculate the equivalent axial load on the section, N

$$N = N_v + N_p \quad (5.14)$$

V18.. Check if the calculated value of N agrees with the axial load acting on the section. If these values do not agree, make a new estimate of θ and return to step V2 (increasing θ increases N).

V19. Return to step V1, increment ϵ_1 . ■

Figure 5.16 shows the influence of different levels of axial load on the shear response for the column section used in specimen K0.7 under a constant bending moment of 180 kN·m. These different axial load levels correspond to the column axial loads for the different storeys in the six storey frame structure under study. It can be seen that the capacity increases with increasing axial compression. For high axial load the capacity is governed by the yielding of the flexural steel. For lower levels of axial load it is governed by yielding of the shear reinforcement.

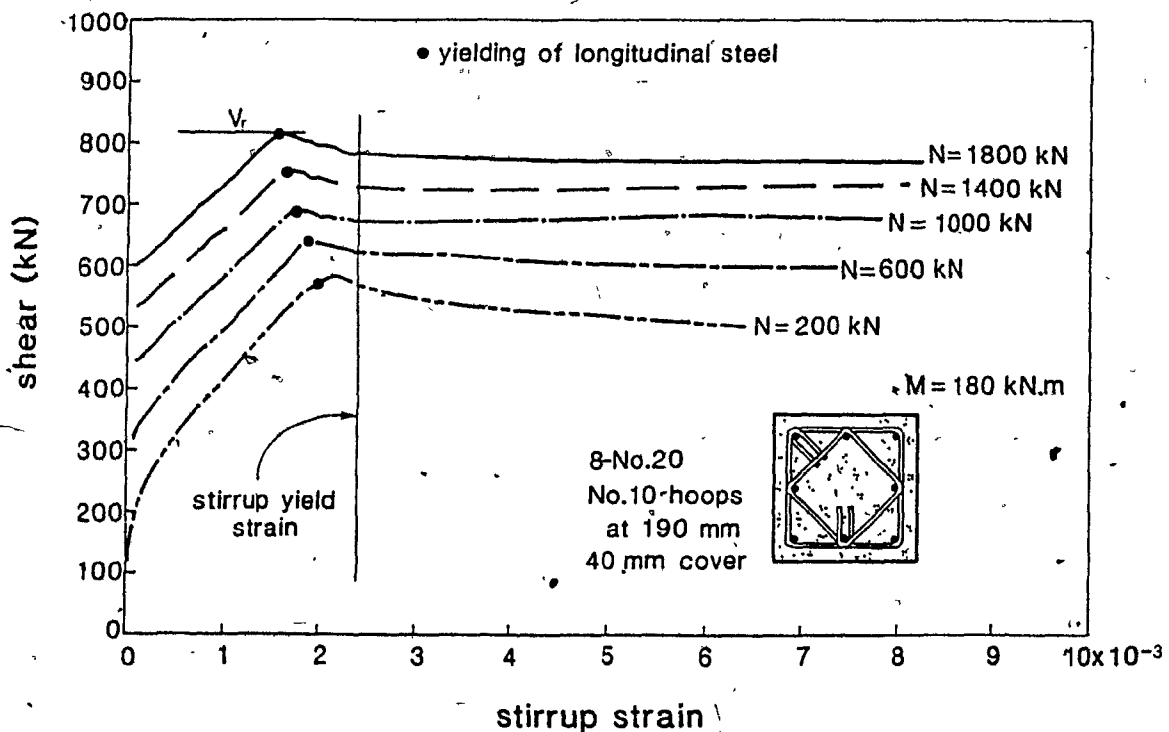


Fig. 5.16 Influence of axial load on shear response

Figure 5.17 illustrates the use of the option available in the program of specifying a moment to shear ratio, M/V . The curves represent the predicted shear vs. stirrup

strains for different sections of the cantilever beam from specimen K0.7. It can be seen that due to the small stirrup spacing at section 1 and due to the large moment to shear ratio the stirrups did not yield and failure is predicted to be caused by diagonal crushing of the concrete after the flexural reinforcement is well beyond yield. The influence of moment can be seen by comparing the response of section 2, 3 and 4 which experience flexural yielding before stirrup yielding. Since section 5 has a smaller amount of reinforcement and also a smaller moment to shear ratio, it experiences yielding of the shear reinforcement.

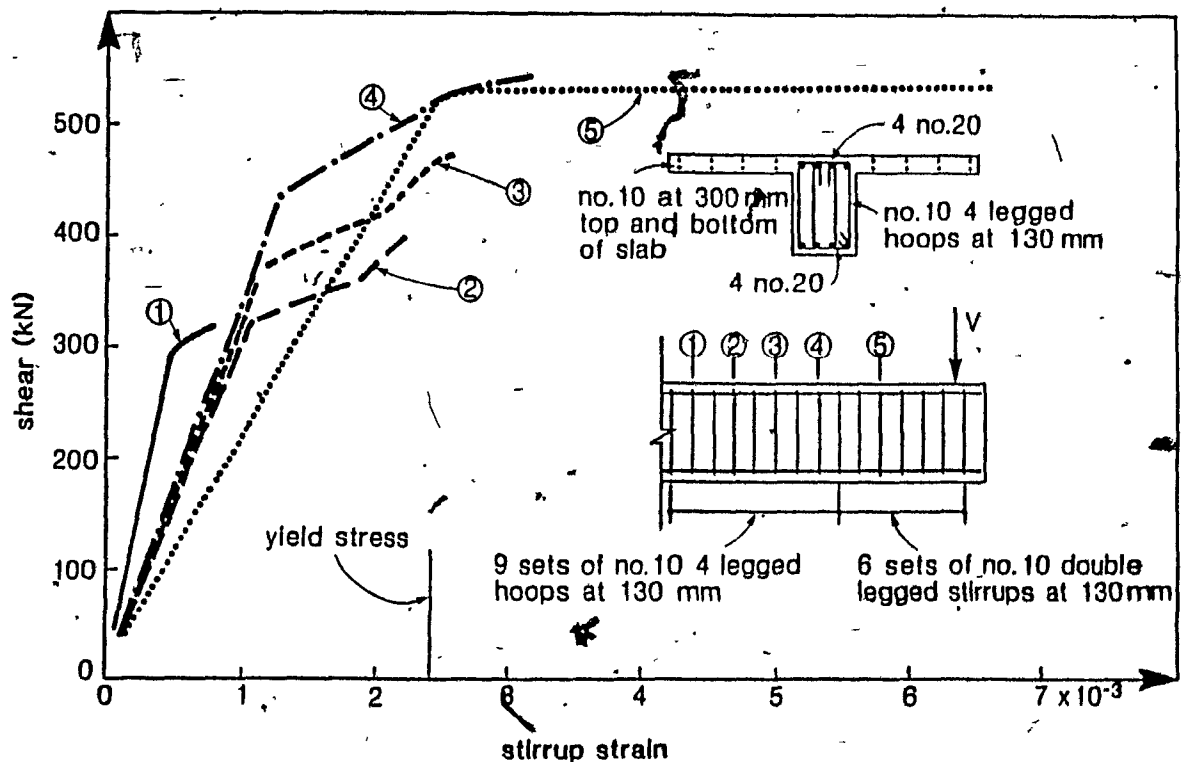


Fig. 5.17 Influence of moment to shear ratio on the response

5.3 ACCOUNTING FOR BOND-SLIP EFFECTS

In accounting for bond-slip it is assumed that a crack forms right at the face of the column and that a concentrated rotation takes place at that location as shown in Fig. 5.18. This approximation is similar to that suggested by Park and Paulay [18].

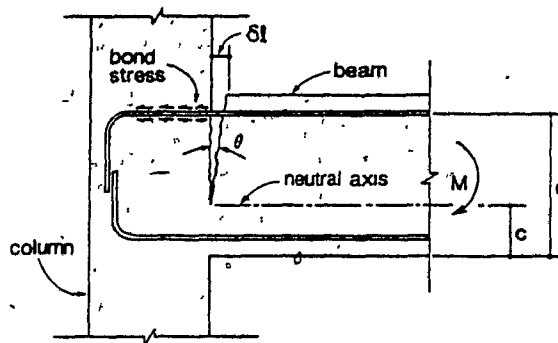


Fig. 5.18 Effect of bond-slip on deformation

The moment-rotation relationship due to bond-slip for monotonic loading can be described by a tri-linear curve with critical points defined by cracking (M_{cr}), yielding (M_y, θ_y) and ultimate (M_u, θ_u) conditions. In this research a bi-linear idealization will be assumed as shown in Fig 5.19.

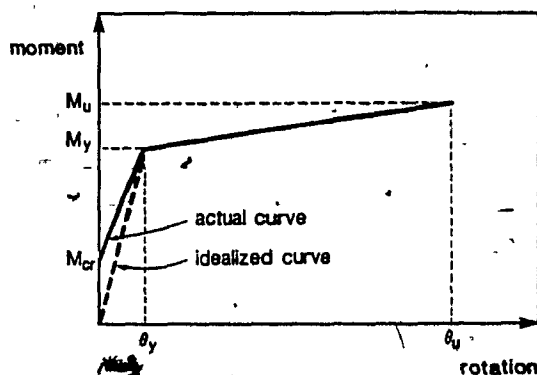


Fig. 5.19 Actual and idealized moment-rotation due to bond-slip

In this research project a simplified model, for determining the bond-slip of the beam bars anchored in the joint, was used. This model assumes a uniform bond stress distribution along the development length of the reinforcement (see Fig. 5.20). Although more complex, empirically derived, bond-slip relationships have been proposed (e.g., Ref. 25) the simplified approach illustrated in Fig. 5.20 and Fig. 5.21 were found

to be sufficiently accurate for predicting the bond-slip response of the specimens tested.

Fig. 5.20 shows the assumed bond stress distribution at yielding of a bar. The bar tension, T is transmitted to the concrete by the bond stress, u , over the development length, l_d . Assuming the average bond stress to be uniformly distributed along l_d , the steel strain varies linearly up to the yield strain at the critical section. The development length, l_d , from equilibrium is:

$$l_d = \frac{A_b f_y}{\pi d_b u} \quad (5.15)$$

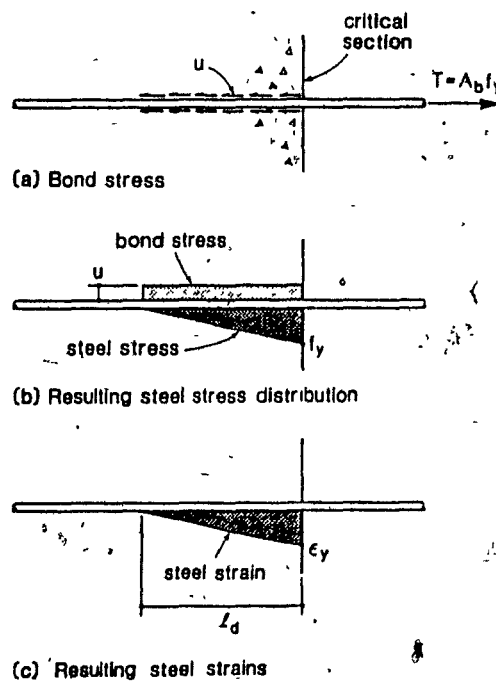


Fig. 5.20 Determining bond-slip from assumed bond-stress distribution

If we assume that the steel elongation contributes to the crack opening at the face of the column, then the opening of the crack at the level of the steel is given by the integration of the steel strain distribution over the development length, l_d (see Fig. 5.20). Thus at yielding:

$$\delta l = \frac{1}{2} \epsilon_s l_d = \frac{1}{2} \frac{l_d f_y}{E_s} \quad (5.16)$$

Combining Eqs. 5.15 and 5.16 we obtain the following expression for the crack opening

$$\delta l = \frac{1}{8} \frac{d_b}{E_s u} f_y^2 \quad (5.17)$$

The concentrated rotation of the beam at the column face due to bond-slip is given by:

$$\theta = \frac{\delta l}{d - c} \quad (5.18)$$

If we assume the following linear relationship between steel stress and moment:

$$\frac{f_s}{f_y} = \frac{M}{M_y} \quad (5.19)$$

Then the additional rotation of the beam at a moment M is given by

$$\theta = \frac{1}{8} \frac{d_b}{E_s u} \left(\frac{f_y}{M_y} \right)^2 M^2 \frac{1}{d - c} \quad (5.20)$$

and at the yielding moment

$$\theta_y = \frac{1}{8} \frac{d_b}{E_s u} \frac{f_y^2}{d - c} \quad (5.21)$$

The development length increases when the reinforcement stress exceeds the yield stress. It can be calculated from equilibrium knowing the steel stress. At the ultimate stress the development length is given by

$$l_{du} = \frac{A_b f_{su}}{\pi d_b u} \quad (5.22)$$

The steel elongation can be calculated knowing the stress strain relationship. Assuming a tri-linear stress-strain relationship with a yield plateau and constant strain

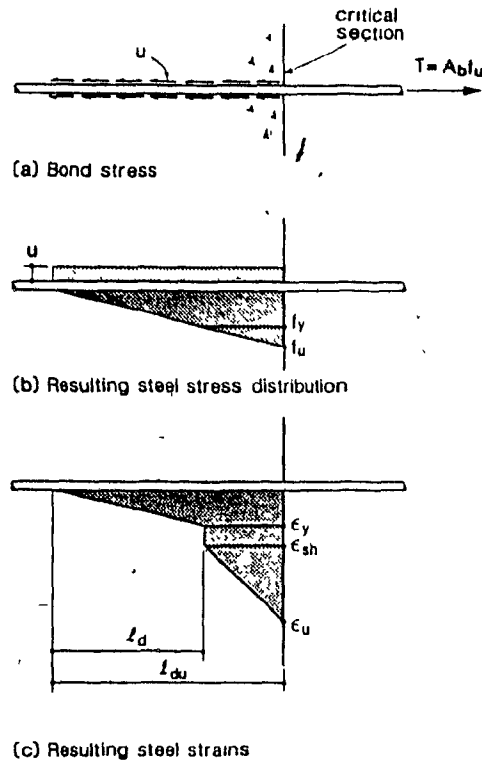


Fig. 5.21 Approximating bond-slip from assumed bond-stress distribution

hardening we have at ultimate the stress and strain distribution along the development length l_{du} illustrated in Fig. 5.21.

The assumption of a constant, uniform bond stress gives:

$$l_{du} = \frac{f_{su}}{f_y} l_d \quad (5.23)$$

The total elongation of the reinforcement is equal to the area under the strain curve and is given by

$$\delta l_u = \frac{1}{2} l_d \left[\left(\frac{f_{su}}{f_y} - 1 \right) (\epsilon_{su} + \epsilon_{sh}) + \epsilon_y \right] \quad (5.24)$$

The concentrated rotation of the beam due to bond-slip at ultimate is given by:

$$\theta_u = \frac{1}{2} \frac{l_d}{d - c} \left[\left(\frac{f_{su}}{f_y} - 1 \right) (\epsilon_{su} + \epsilon_{sh}) + \epsilon_v \right] \quad (5.25)$$

The 1984 Canadian Concrete Code [3] expressions for development length for bar sizes up to a No. 20 bar imply a bond stress value of 4.3 MPa for concrete compressive strengths over 20 MPa. This value of bond stress was used in Eqs. 5.15 and 5.22 to determine l_d and l_{du} .

5.4 RESPONSE OF SUBASSEMBLAGES

5.4.1 Role of Spandrel Beam

Figure 5.22 illustrates the flow of the forces from the main beam and the slab into the spandrel beam and into the joint region. The tensions in the slab bars create torsion in the spandrel beams on each side of the column. The spandrel beam transmits both direct shear and torsional shear flow to the side faces of the joint as shown in Fig. 5.22. The total tension in the slab bars will therefore be limited by the torsional capacity of the spandrel beams.

For example the torsional capacity of the spandrel beam in specimen K1.3 is about 99000 kN·m and since the slab bars are located 245 mm above the centre of the beam the maximum tensile force that will cause torsional yielding is $99000/0.245 = 404$ kN on each side of the column. The yield force of a No. 10 slab bar is $100 \text{ mm}^2 \times 480 \text{ MPa} = 48$ kN. Hence the yielding of $404/48 = 8.4$ bars is required to cause torsional yielding of the spandrel beam. From the strain measurements on the slab reinforcement all 6 slab bars on each side of the column yielded at failure as shown in Fig. 4.13. It is evident from this figure that some of the slab bars reached strain hardening. Due to the large torsional cracks observed in the spandrel beams of all three specimens it is clear that they all yielded in torsion (e.g. see Fig. 4.17, 4.21).

Further examination of Fig. 5.22 reveals that the top reinforcing bars in the main beams transfer horizontal shear directly into the joint. The spandrel beam transfers horizontal shear from the tensions in the slab bars as well as torsional shear flow

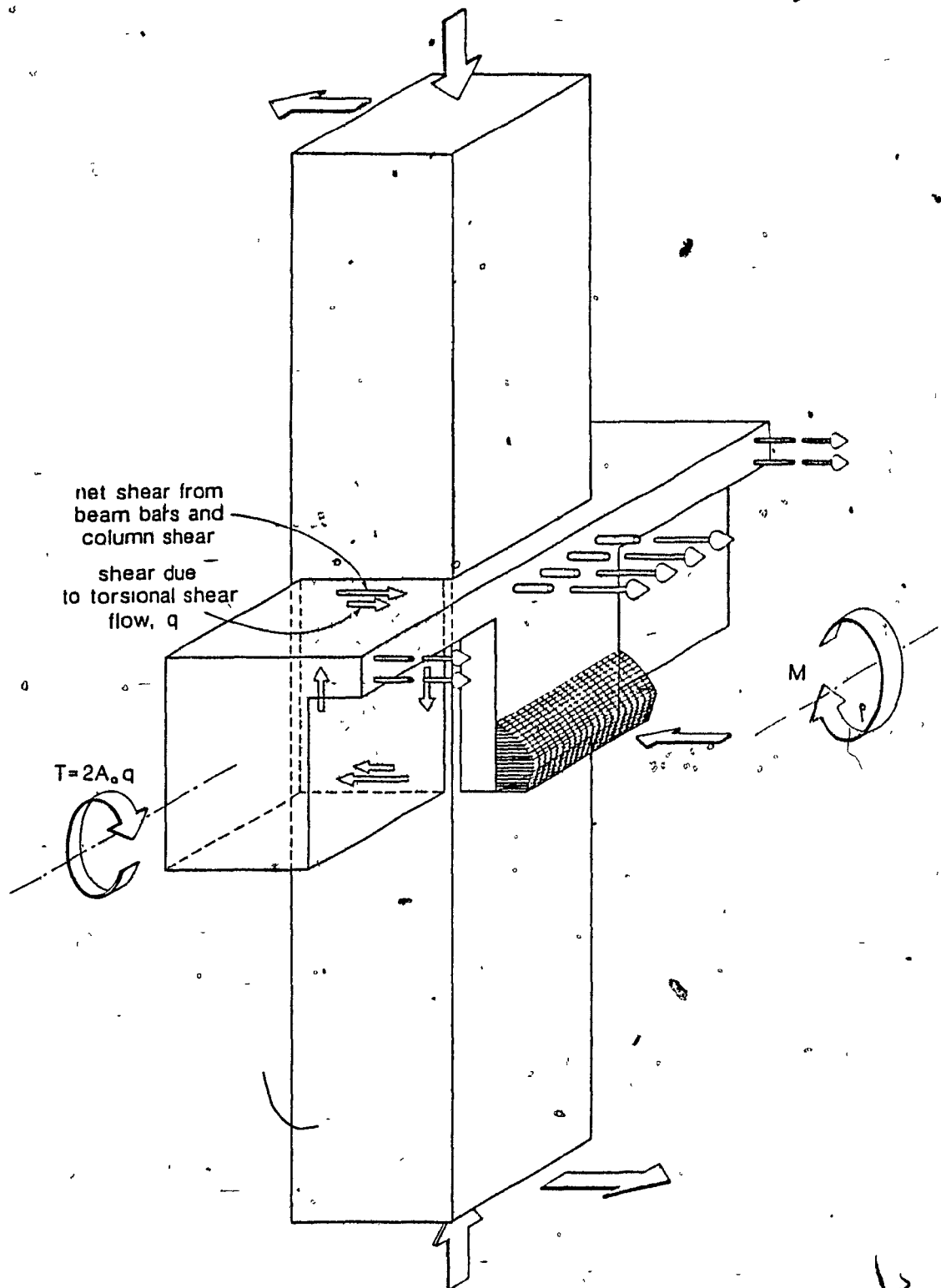


Fig. 5.22 Role of spandrel beam

to the side faces of the joint. Due to the vertical shear from the main beam the axial compression in the joint increases from a minimum at the top of the joint to a maximum at the bottom of the joint. If it is assumed that the critical section is at the top of the joint then the axial load acting on the joint equals the axial load acting in the column above the joint and the resultant shear force is equal to the sum of the forces in the top beam bars, minus the column shear, plus the shear due to torsional shear flow, q , in the spandrel beam (i.e. $q \times b_0$, where b_0 is the length of the shear flow path on the side face).

These three specimens illustrate clearly how the effective flange width is limited by the torsional yielding of the spandrel beam. In addition the spandrel beam also affects the flow of the shear into the joint region.

5.4.2 Beam Responses

Figures 5.23, 5.24 and 5.25 compare the predicted moment-curvature responses with the moment-curvature responses determined from the longitudinal strain readings taken at the top and bottom of the beam near the column face. The predictions shown in these figures are for a) a rectangular beam with only the beam reinforcement considered, b) a T beam with an effective flange width equal to three times the slab thickness, c) a T beam with an effective flange width equal to four times the slab thickness, d) a variable strain distribution acting on the total slab width of the specimen (see Fig. 5.5 and 5.6), and e) a constant strain distribution across the total slab width. As can be seen from these figures it is unrealistic to ignore the contribution of the reinforcement in the slab. As illustrated in Section 5.4.1 the spandrel beam controls the effective width of the slab. For these specimens the effective width is greater than 4 times the slab thickness as shown in Section 5.4.1. Although the strengths of the specimens are predicted well by using a constant strain distribution across the full slab width, the best predictions of the entire responses are with a variable strain distribution across the full slab width (case d above).

Figures 5.26, 5.27 and 5.28 give the predicted curvature distributions and the

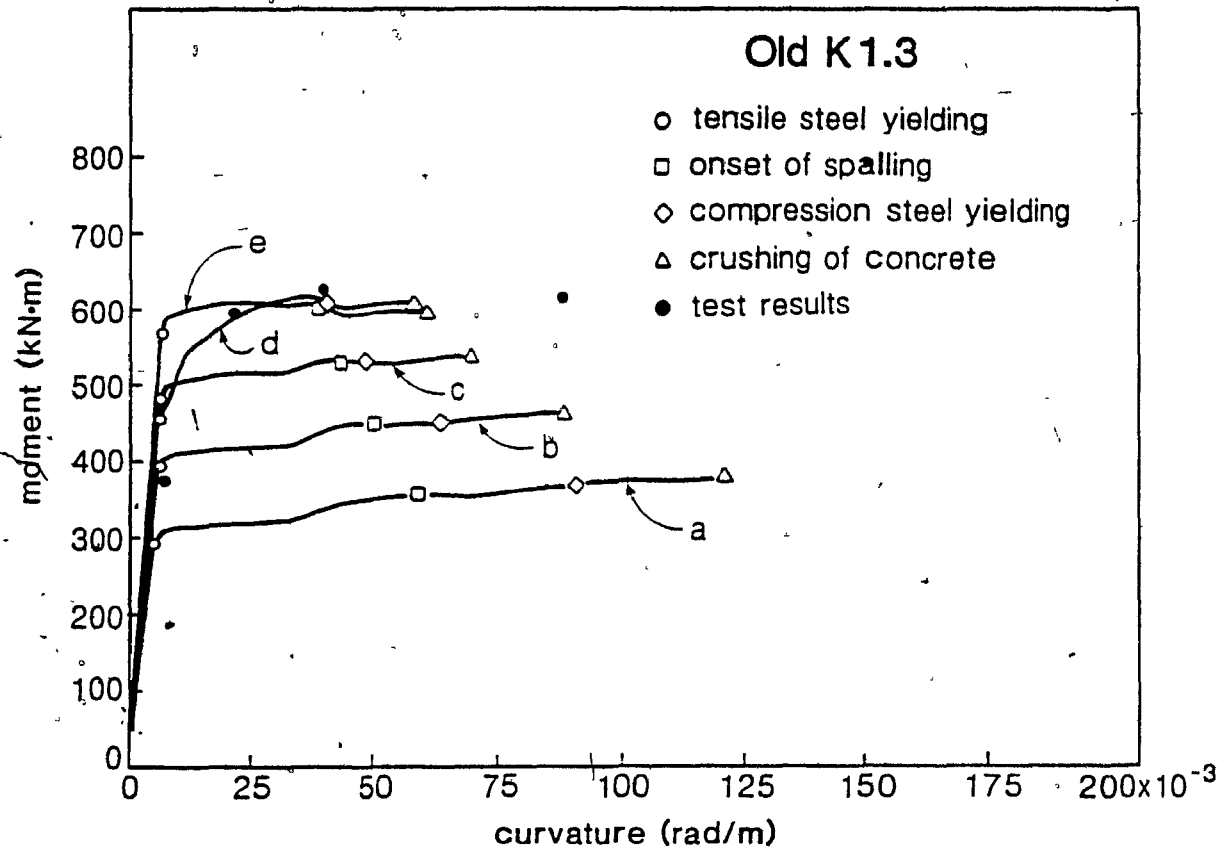


Fig.5.23 Comparisons of moment-curvature predictions with experimental results for specimen Old K1.3

predicted shear strain distributions along the length of the three test specimens. Also shown are the curvatures obtained from the longitudinal strain measurements at the top and bottom of the beams together with the shear strains obtained from the strain rosette readings located on the sides of the beams. The predicted and experimentally determined deformations given in these three figures are for load levels close to the ultimate strengths of the beams. As expected there is considerable scatter in the test values due to the discrete nature of the cracking. The predictions of curvatures and shear strains were made neglecting tension stiffening in the concrete in order to approximate the influence of cyclic loading. Also shown in Fig. 5.26, 5.27 and 5.28 are the predicted tip deflections obtained by integrating the curvatures and the shear strains. The experimental values of the shear strains for specimen Old K1.3 are not shown since the major shear cracks did not pass through the strain rosettes. As expected

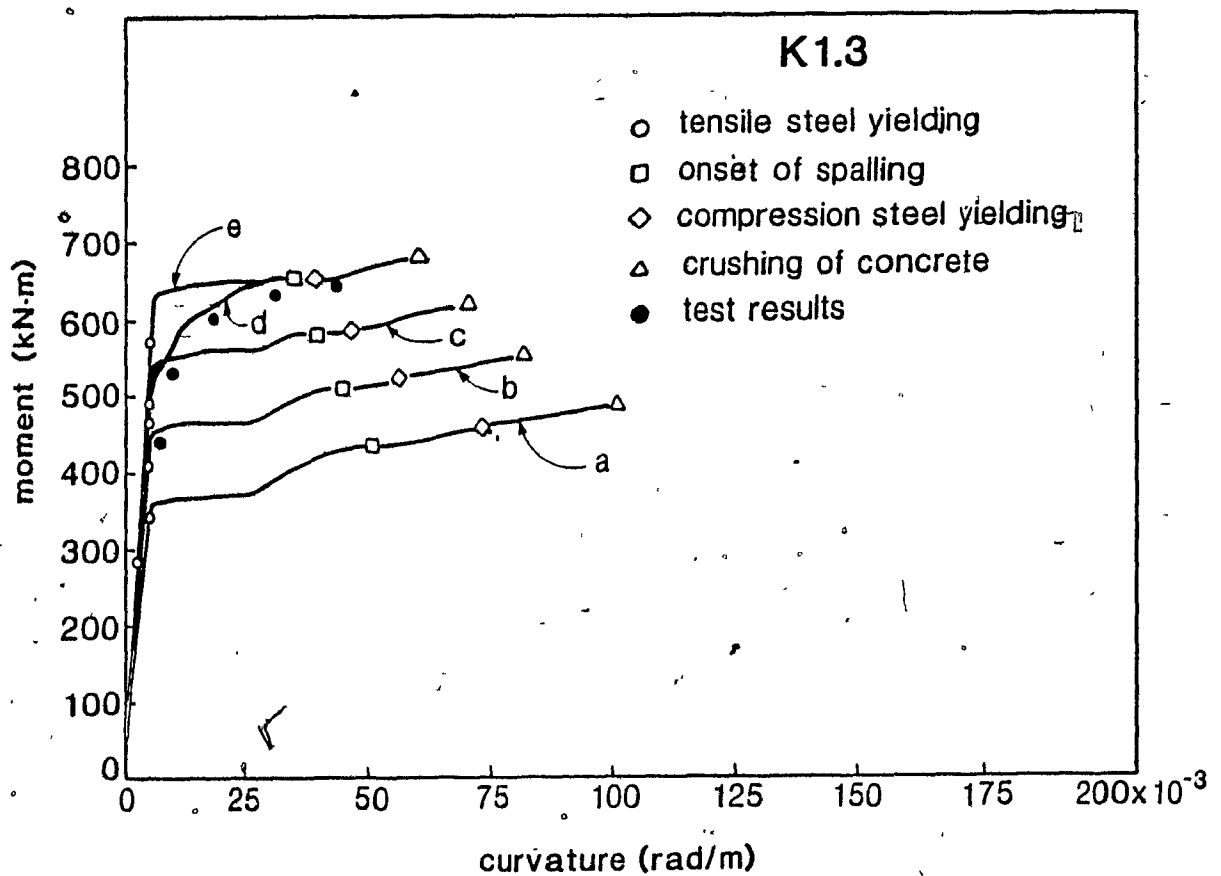


Fig. 5.24 Comparisons of moment-curvature predictions with experimental results for specimen K1.3

as the amount of transverse reinforcement is increased the contribution of the shear strains to the tip deflection decreases. These analyses were carried out for the three specimens in order to determine the flexure and shear response of the beams. The results will be discussed in more detail in Section 5.4.4.

5.4.3 Column and Joint Responses

Using the analysis procedure described in Section 5.1 the axial load moment interaction diagrams together with the corresponding moment curvature responses were predicted for all three specimens (e.g., see Fig. 5.7 to 5.9). In all three cases the columns were predicted to be stronger than the beams. It is noted that for specimen K1.3 the spalled strength of the column above the joint is close to the strength demand

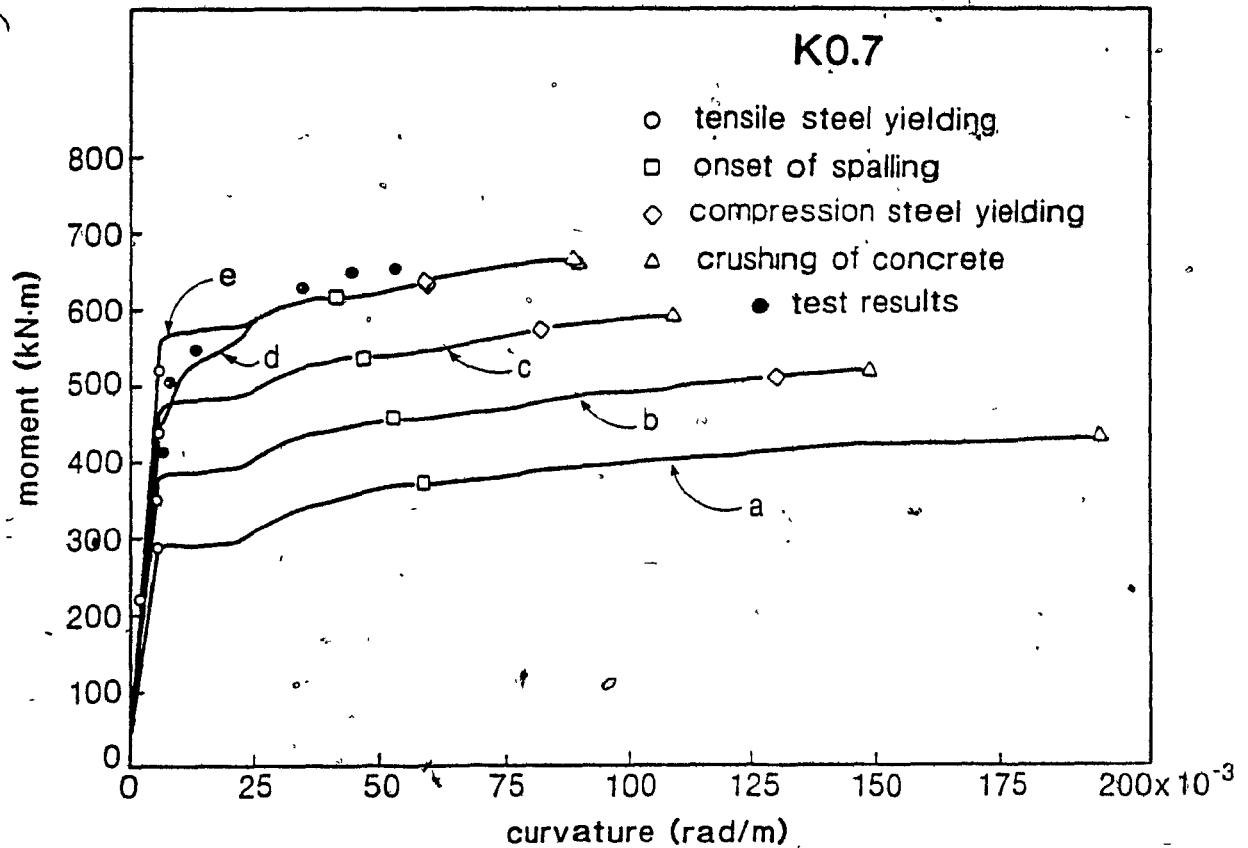


Fig. 5.25 Comparisons of moment-curvature predictions with experimental results for specimen K0.7

resulting from the beam hinging.

Using the procedure described in Section 5.2 it is possible to predict the axial load-moment-shear response of the joint region. In these predictions it is assumed that the shear is resisted by a field of compressive stresses in the concrete. In order to predict the response of a joint region it is necessary to account for the cross sectional properties of the joint region, the amount of transverse reinforcement in the joint, the amount and distribution of the column longitudinal steel passing through the joint, and the shear to moment ratio in the joint. In the analysis of the joint it is assumed that the critical section is close to the top of the joint region where the axial load is the lowest.

In order to demonstrate the capabilities of the analytical procedure, it was used to predict the joint shear versus the stirrup strain response of a beam-column joint tested by Uzumeri and Seckin [17] shown in Fig. 5.29. This exterior beam-column joint did

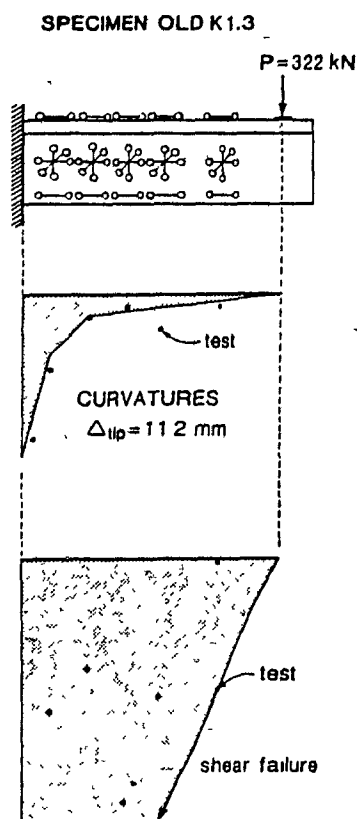


Fig. 5.26 Comparisons of predicted curvatures and shear strains with experimental results for specimen Old K1.3

not have any transverse beams nor any slab framing into the joint and hence provides an excellent test of the analysis, since no assumptions need to be made concerning the flow of the forces into the joint region. As can be seen from Fig. 5.29 two predictions of the response were made: one with tension stiffening ($f_{c1} > 0$) and one with no tension stiffening ($f_{c1} = 0$). Due to the cyclic loading the response approaches the case with no tension stiffening.

Figure 5.30 compares the predictions of the joint shear versus stirrup strain with the experimental results obtained by Ehsani and Wight [22, 23, 24]. This exterior beam column joint contained transverse beams and a slab and thus provides a useful test of both the analytical predictions of the joint shear response and the assumed role of the spandrel beam (see section 5.4.1). It is noted that yielding of the longitudinal column bars in the joint region is predicted to occur before yielding of the tie reinforcement.

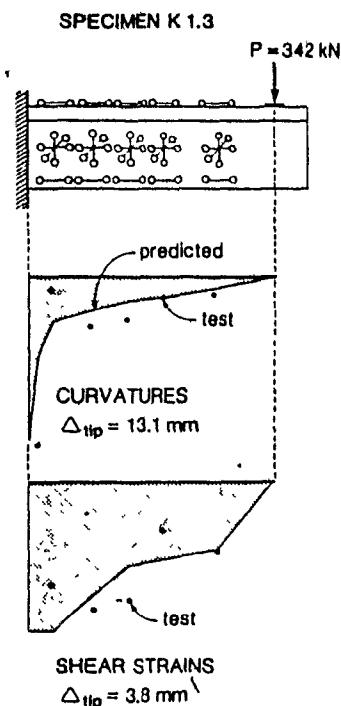


Fig. 5.27 Comparisons of predicted curvatures and shear strains with experimental results for specimen K1.3

The procedures described above were used to predict the axial load-moment-shear response of the joint regions of the three specimens tested. In the case of specimen K1.3 shear failure of the beam was predicted to occur before any significant distress in the joint. However yielding of the longitudinal column bars, followed closely by yielding of the tie reinforcement, is predicted to occur before beam hinging in specimen K1.3. Due to the confinement reinforcement provided in the joint region of specimen K0.7 no joint yielding is predicted before full beam hinging. The tip deflection components corresponding to joint shear strain were predicted throughout the full loading responses of all three specimens and are discussed in the following section.

5.4.4 Total Responses

The flexural components, Δ_f , and the shear components, Δ_s , of the beam tip deflection were calculated from the integration of the curvature and shear strain dis-

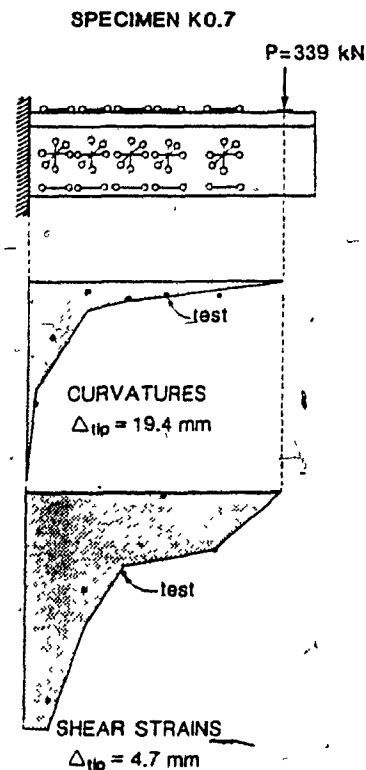


Fig. 5.28 Comparisons of predicted curvatures and shear strains with experimental results for specimen K0.7

tributions. The contribution to the tip deflection due to a concentrated rotation at the column face, Δ_j , were determined from the predicted bond slips and joint shear strains.

Figure 5.31 compares the measured contributions of the components (i.e., Δ_f , Δ_j , and Δ_s) to the beam tip deflection with those predicted. As can be seen the predicted components and the overall responses are in good agreement. It is apparent that particularly after general yielding bond slip and joint distortion contribute significantly (about 50%) to the total deformation. The improved performance of specimen K0.7 is again evident from these plots.

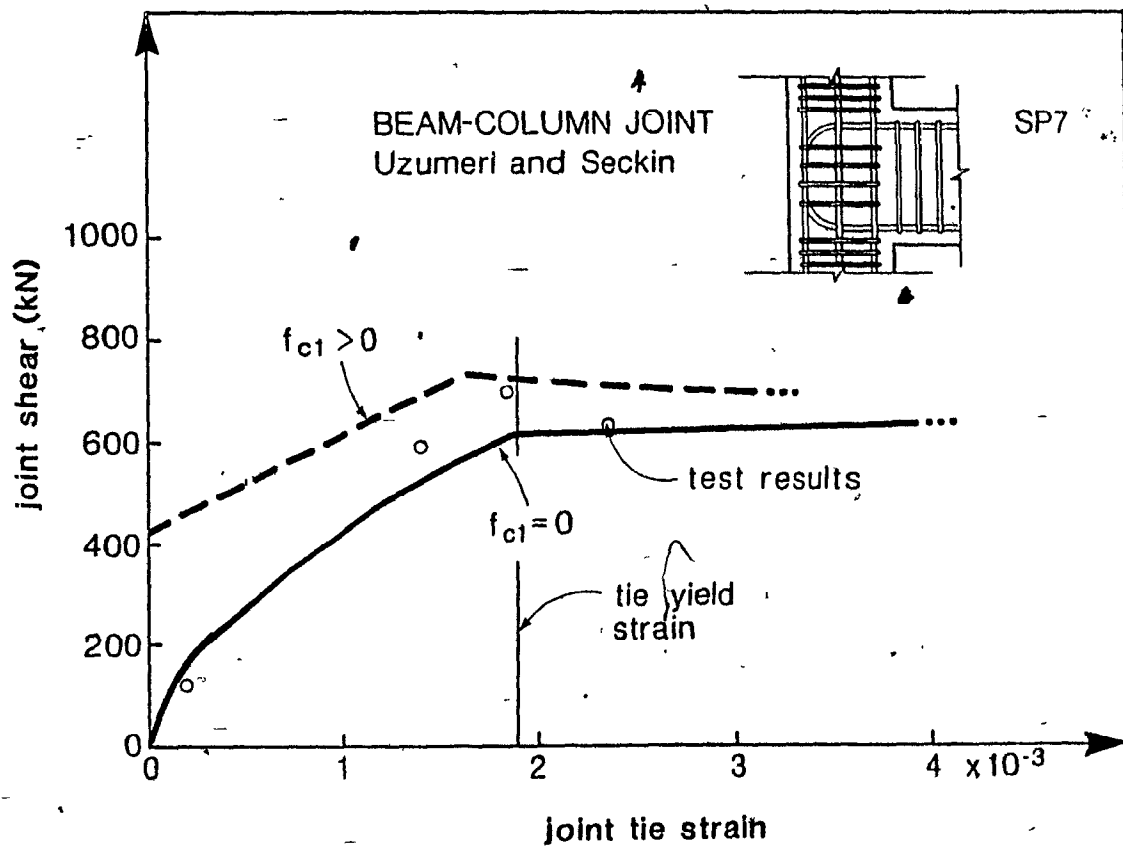


Fig. 5.29 Comparison of predicted joint shear vs joint tie strain responses with experimental values for specimen SP7 tested by Uzumeri and Seckin [17]

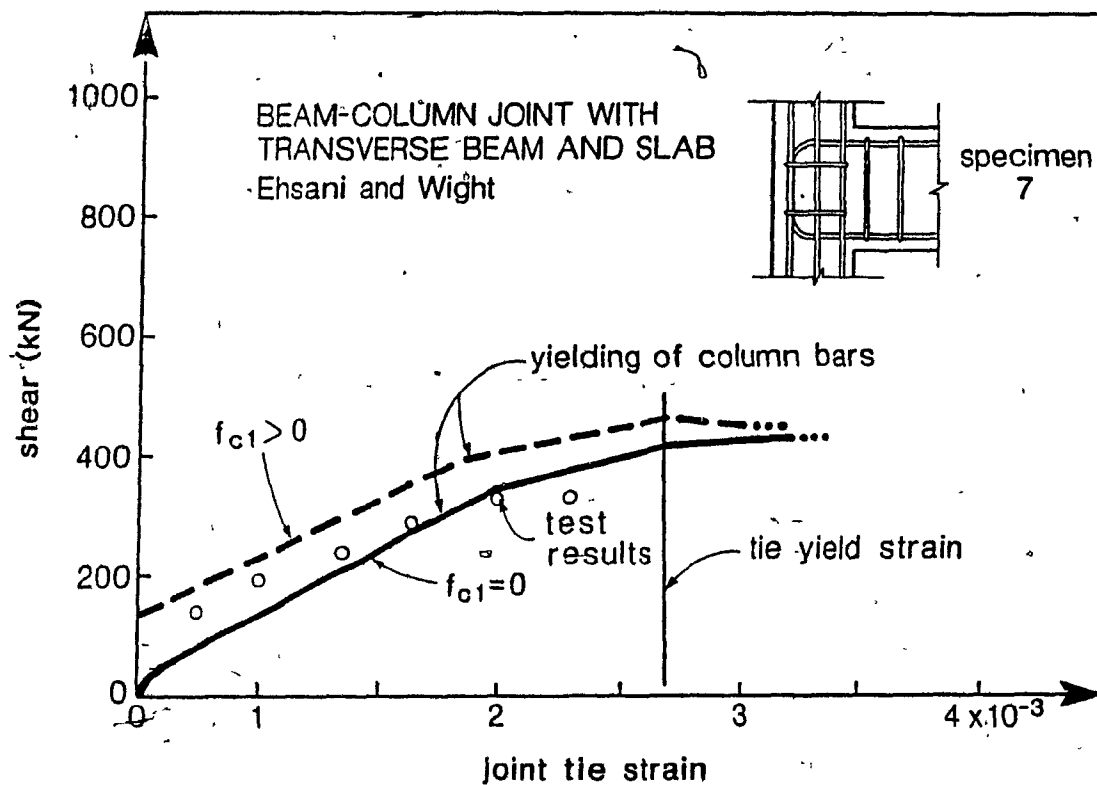
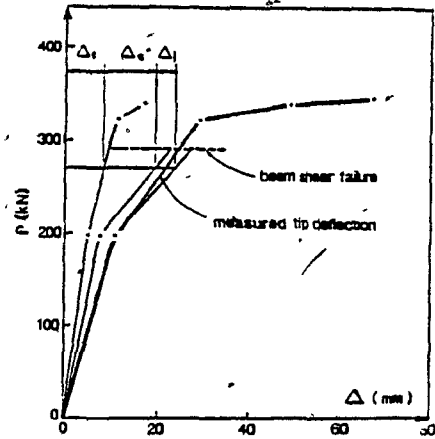
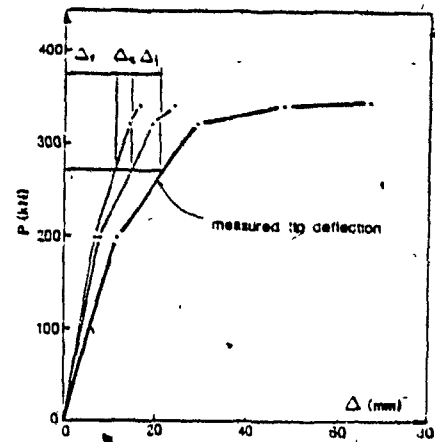


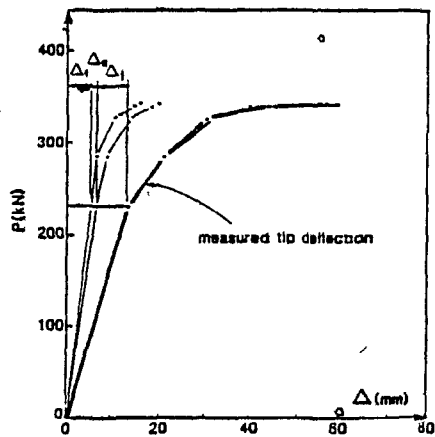
Fig. 5.30 Comparison of predicted joint shear vs joint tie strain responses with experimental values for specimen 7 tested by Ehsani and Wight [22, 23, 24]



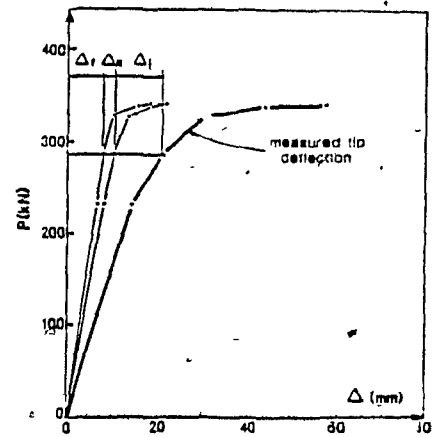
a) Specimen Old K1.3, predicted values



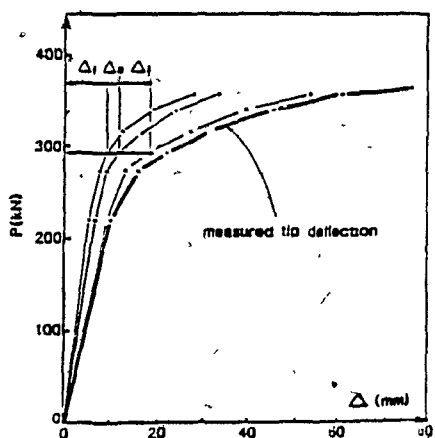
b) Specimen Old K1.3, measured values



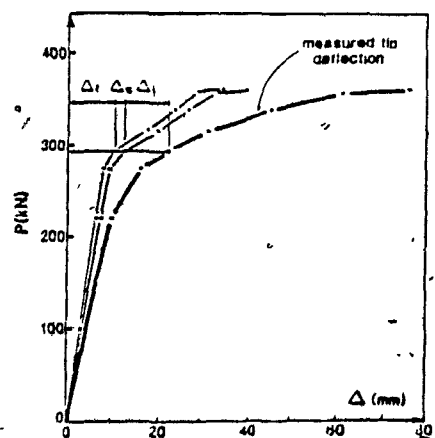
c) Specimen K1.3, predicted values



d) Specimen K1.3, measured values



e) Specimen K0.7, predicted values



f) Specimen K0.7, measured values

Fig. 5.31 Predicted and measured tip deflection components

CHAPTER 6

PREDICTING NON-LINEAR DYNAMIC RESPONSE OF CONCRETE STRUCTURES

This chapter briefly summarizes some of the important aspects of non-linear dynamic analysis used in this study. The analysis techniques used in the computer program DRAIN-2D [37] are discussed and a refined hysteretic model capable of predicting the response of poorly detailed reinforced concrete components is described. Different means of assessing damage of structures from the predicted non-linear responses are also described.

6.1 NON-LINEAR DYNAMIC ANALYSIS USING DRAIN-2D

6.1.1 Equations of Motion

For a structural system responding non-linearly, the dynamic incremental equations of equilibrium for earthquake motions can be written for a finite time step Δt as:

$$M\Delta\ddot{r} + C_T\Delta\dot{r} + K_T\Delta r = -M\Delta\ddot{r}_g \quad (6.1)$$

in which $\Delta\ddot{r}$, $\Delta\dot{r}$ and Δr are finite increments of acceleration, velocity and displacement relative to the ground and $\Delta\ddot{r}_g$ is the finite increment of ground acceleration; M is the constant mass matrix; and C_T and K_T are the tangent values of the damping and stiffness matrix for the structure in its current state.

The computer program DRAIN-2D uses the Newmark "constant average acceleration method" over a time step, Δt , chosen by the user. This method has been found to be unstable for systems responding non-linearly when relatively large time steps are used [80]. In order to avoid this problem a maximum time step size equal to about 1/10 of the smallest natural period of the structure was chosen. A number of additional analyses were carried out with smaller time increments in order to verify that the response did not change appreciably.

6.1.2 Solution Procedure

The DRAIN-2D program uses a solution scheme based on the evaluation of the tangent stiffness matrix for a given time step and on the corresponding load vector which is corrected for the out-of-balance loads resulting from any change in the tangent stiffness matrix [37].

Because DRAIN-2D was designed to accept additions to the library of existing non-linear elements it is helpful to briefly discuss the general solution technique used in the program. In order to implement a new element it must conform to the requirements of the solution technique which is briefly described below.

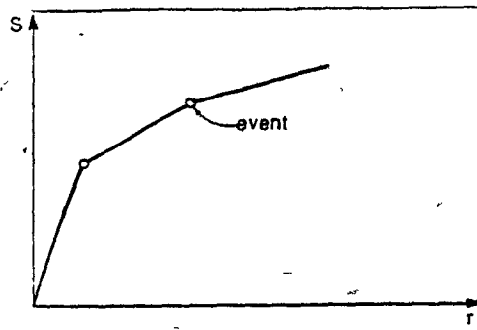
The element tangent stiffness matrix, k_T , is defined by the following relationship.

$$dS = k_T dr \quad (6.2)$$

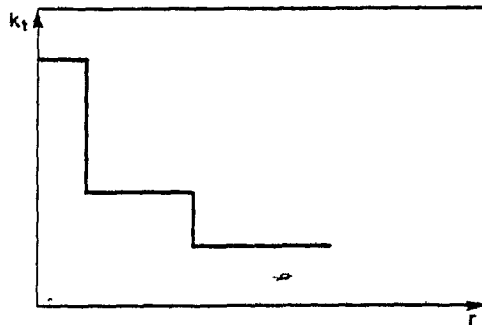
In which dS is the increment of external forces acting on the nodes of the element, and dr is the corresponding increment of nodal displacements.

All the elements in the DRAIN-2D program must have a multi-linear force vs displacement representation (see Fig. 6.1 a) which results in sudden changes in stiffness at every change in state, referred to as event (see Fig 6.1). The structure stiffness matrix, K_T , is then formed by addition of the element tangent stiffness according to direct stiffness matrix procedures.

The incremental state determination, i.e., the new state of force and deformation in each element, is determined in the following way (see Fig. 6.2):



a) Multi-linear load vs displacement



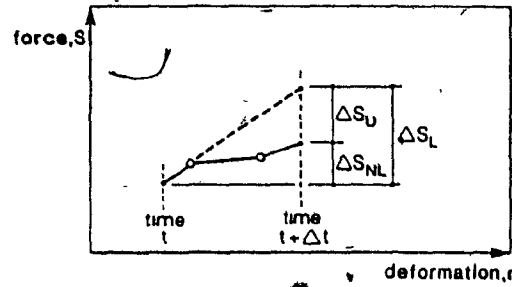
b) Multi-linear stiffness vs displacement

Fig. 6.1 Multi-linear force-displacement relationship

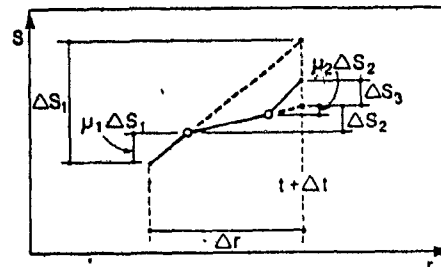
- 1) Given the calculated increment in the element nodal displacements, Δr , calculate the increment of internal element deformations.
- 2) From the non-linear (piece-wise linear) force-deformation relationship calculate the internal element force.
- 3) From the new internal element force calculated, the unbalanced force is determined from:

$$\Delta S_U = \Delta S_L - \Delta S_{NL} \quad (6.3)$$

where ΔS_U is the external nodal loads required to satisfy element equilibrium, ΔS_L is the linear element force increment based on the state of the element at the beginning of the step, and ΔS_{NL} is the non-linear element force increment which accounts for



a) Definition of linear and non-linear force increment



b) Computation of non-linear force increments

Fig. 6.2 Computation of force increment [37]

changes in the element tangent stiffness k_T within the step. The linear force increment, ΔS_L , is given by:

$$\Delta S_L = k_{T0} \Delta r \quad (6.4)$$

where k_{T0} is the element tangent stiffness at the beginning of the step and which was used to calculate Δr .

The non-linear force increment, ΔS_{NL} , is dependent on the number of changes in state within a given time step. If there are n changes in state then the non-linear force increment can be calculated as:

$$\Delta S_{NL} = k_{T0} \Delta r_1 + k_{T1} (\Delta r_2 - \Delta r_1) + \dots + k_{Tn} (\Delta r - \Delta r_n) \quad (6.5)$$

DRAIN-2D approximates ΔS_{NL} in equation 6.5 as:

$$\Delta S_{NL} = \mu_1 \Delta S_1 + \mu_2 \Delta S_2 + \dots + \Delta S_n^a \quad (6.6)$$

in which the proportion, μ_i , of element force increment which is required to produce the next "event" is given by (see Fig. 6.2):

$$\mu_i = \frac{S_y - S_i}{\Delta S_i} \quad (6.7)$$

where S_y is element force at yield, S_i is element force at beginning of sub-increment i , and ΔS_i is the computed sub-increment of element force.

6.1.3 Mass Matrix

Although the mass of a building system is distributed throughout the structure it is customary in dynamic analysis of buildings to assume the entire mass to be concentrated at floor slabs and to neglect rotational inertia. Since only lateral effects of earthquake are considered in this study and since all the nodes in a floor are assumed to have identical lateral displacement, the mass matrix reduces to the following diagonal matrix:

$$\mathbf{M} = \begin{bmatrix} m_1 & 0 & \dots & 0 \\ 0 & m_2 & \dots & 0 \\ \vdots & \vdots & \ddots & \vdots \\ 0 & 0 & \dots & m_n \end{bmatrix} \quad (6.8)$$

where m_i is the mass corresponding to storey i and n is the number of storeys.

6.1.4 Tangent Stiffness Matrix

The program lumps the plasticity in zero-length plastic hinges concentrated at the ends of the element. The multi-linear force-deformation relationship enables very complex responses to be modelled.

With this representation non-linear hysteretic behaviour can be formulated, in which the force depends on the past history of deformation as well as on the current state of deformation. The essential requirement is that the formulation must be

complete, i.e., the tangent stiffness k_T can always be defined depending on the past history and the present state of deformation. To achieve completeness a set of force-displacement rules must be defined such that for any state in the response (e.g., point r on line 2 in Fig. 6.3) the lower and the upper limits must be known (points l and u), the adjacent lines (lines 1 and 3) must also be known as well as the line defining the unloading state (line 4)

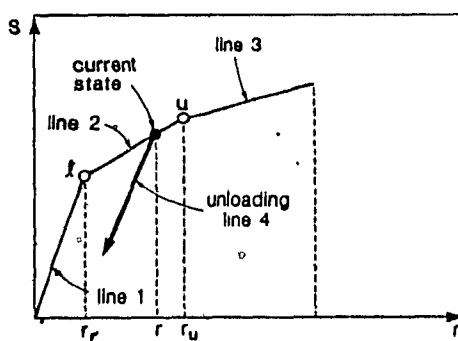


Fig. 6.3 Non-linear hysteretic behaviour

To perform the analyses of the building structures two elements of the general purpose computer program DRAIN-2D are used. They fall into the parallel element and the physical hinge element formulation. A brief description of the formulation of these elements follows in the next two sections.

6.1.4.1 Dual Component Element – Beam-Column Model

This element possesses both flexural and axial stiffness. Shear deformation can be accounted for and finite rigid links can be used at the ends of the members. The use of rigid links forces the inelastic deformation to take place at the face of the adjoining elements.

The element is idealized as an elastic member acting in parallel with an elastoplastic element (see Fig. 6.4). This two-component parallel element has been developed by Clough and Wilson [28]. Yielding can occur only at the ends of

the element. The four possible states of flexural yielding of the inelastic element are illustrated in Fig. 6.5.

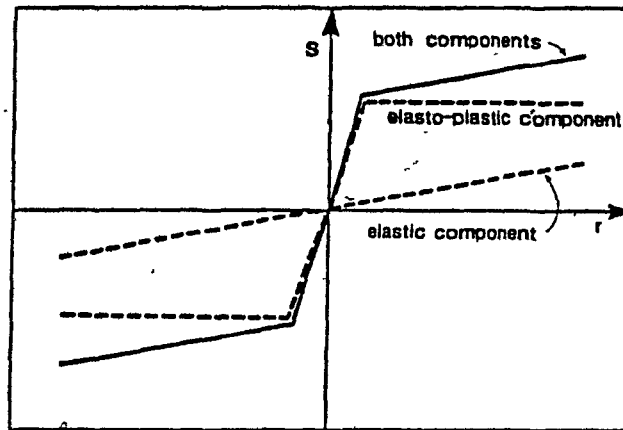


Fig. 6.4 Two-component element used to model beam-columns [28]

yielding state of inelastic element	stiffness matrix, k_T
	$[k_T] = \frac{2EI}{L} \begin{bmatrix} 2 & 1 \\ 1 & 2 \end{bmatrix}$
	$[k_T] = \frac{3EI}{L} \begin{bmatrix} 0 & 1 \\ 0 & 0 \end{bmatrix}$
	$[k_T] = \frac{3EI}{L} \begin{bmatrix} 1 & 0 \\ 0 & 0 \end{bmatrix}$
	$[k_T] = \begin{bmatrix} 0 & 0 \\ 0 & 0 \end{bmatrix}$

Fig. 6.5 Yielding states and stiffness of inelastic component of parallel element.

To determine if yielding occurs in a column an axial load-moment interaction diagram of the form shown in Fig. 6.6 is used. During yielding, internal forces are

constrained to remain on the interaction curve as illustrated by the loading excursions shown in Fig. 6.7. While the flexural stiffness is affected by yielding and the axial load level, the axial stiffness is assumed invariant. This can lead to inconsistencies such as resulting in an axial load in excess of the axial load capacity of a column. This condition has been checked in all the columns because its occurrence is definitely a sign of severe column distress. Because of the formulation of the element, the hysteretic response assumed for the columns does not account for stiffness degradation.

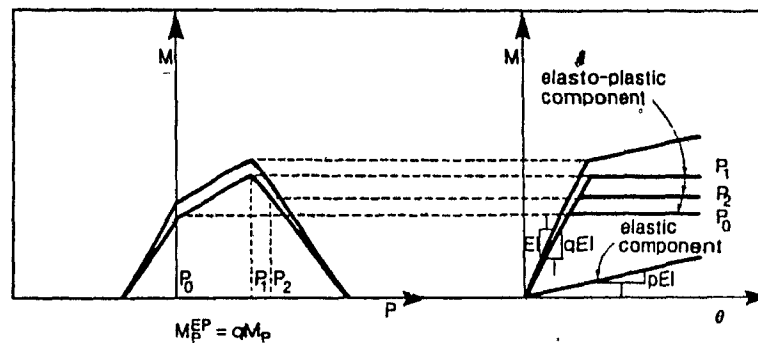


Fig. 6.6 Use of axial load-moment interaction curve to determine yield point, adapted from Reference [27]

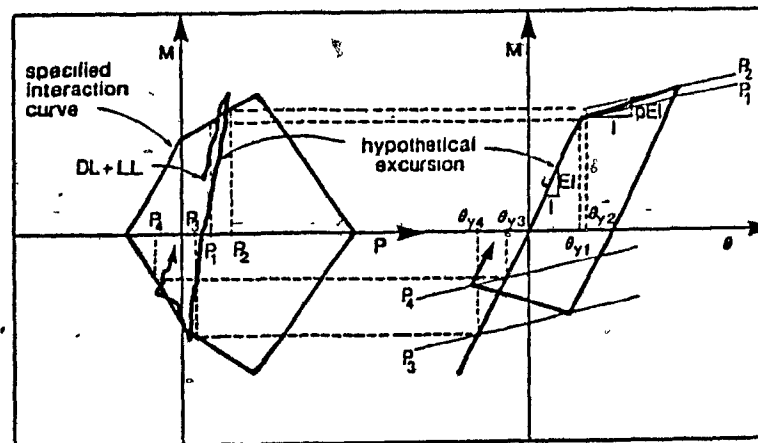


Fig. 6.7 Sample loading excursion with corresponding moment rotation response, adapted from Reference [27]

6.1.4.2 Single Component Element – Physical Hinge Beam Model

The beam element possesses flexural and axial stiffness. Shear distortion can be accounted for as well as finite rigid zone at the ends of the member.

The beam element consists of an elastic line element in series with two inelastic springs at the ends. The degrees of freedom for the springs are condensed at the element level so that the resulting degrees of freedom are a rotation at each end and an axial deformation (see Fig. 6.8).

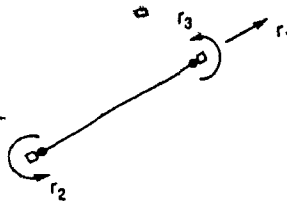


Fig. 6.8 Element degrees of freedom

The complete element tangent stiffness matrix is formed by first inverting the rotation stiffness matrix of the elastic line element into its flexibility form, then the current flexibilities of the rotational springs are added. The flexibility matrix, \mathbf{f} , takes the following form:

$$\mathbf{f} = \begin{bmatrix} f_{ii} + \frac{1}{k_i^{sp}} & f_{ij} \\ f_{ji} & f_{jj} + \frac{1}{k_j^{sp}} \end{bmatrix} \quad (6.9)$$

where f_{ii} , f_{ij} , f_{ji} , f_{jj} are flexibility influence coefficients, and k_i^{sp} , k_j^{sp} are stiffnesses of the non-linear flexural springs.

The resulting element flexibility is finally inverted to the current element tangent stiffness matrix, \mathbf{k}_T . Initially the inelastic springs are infinitely rigid and do not affect the element stiffness matrix before yielding.

As for the dual component model, yielding can only take place at the ends of the element but no interaction between axial load and moment is considered in determining

yielding. All plastic deformations are introduced by means of the moment-rotation relationships for the inelastic rotational springs.

6.1.4.3 P - Δ Effects - Geometric Stiffness

P - Δ is accounted for by subtracting the geometric stiffness from the element stiffness as follows [79]:

$$\bar{k}_T = k_T - k_G \quad (6.10)$$

The following linear approximation of the geometric stiffness, exact for truss elements however, is used for all elements in the DRAIN-2D.

$$k_G = \frac{N}{L} \begin{bmatrix} 1 & -1 \\ -1 & 1 \end{bmatrix} \quad (6.11)$$

where N is the axial-force component acting in the element and L is the element length. In Equation 6.11, only the non-zero shear terms are presented. The matrix is expanded to a 6×6 matrix by addition of rows and columns of zero terms before addition to the element stiffness matrix.

6.1.5 Damping Matrix

Damping is modelled in two different forms. Hysteretic damping forces that are in phase with the velocity but proportional to the displacements are accounted for directly at the element level when inelastic actions take place. Viscous damping is assumed to model damping from non-structural components, friction and any other sources. Because the basic energy-loss mechanisms in real structures are not yet fully understood one relies on experimental methods to determine the damping in most structural systems. Newmark and Hall [54] suggest a value of 7 to 10% of critical damping for concrete structures at or just below yielding and 3 to 5% at service load levels. The NBC supplement [2] suggests a value of 5% of critical damping for concrete structures.

It is assumed in the solution process that the structure's damping matrix is of the Rayleigh type, i.e., can be represented by a linear combination of the mass and the stiffness matrices of the form

$$C = a_0 M + a_1 K_T \quad (6.12)$$

where a_0 and a_1 are scalar multipliers.

The damping ratio as a percentage of critical damping for the n^{th} mode can be expressed in terms of the scalar multipliers and the modal frequency ω_n as:

$$\xi_n = \frac{a_0}{2\omega_n} + \frac{a_1 \omega_n}{2} \quad (6.13)$$

If the damping ratios ξ_m and ξ_n corresponding to modal frequencies ω_m and ω_n are known, one can calculate the proportionality factors with the following formula:

$$a_0 = \frac{2\omega_m \omega_n (\omega_n \xi_m - \omega_m \xi_n)}{\omega_n^2 - \omega_m^2} \quad (6.14)$$

$$= \frac{4\pi(T_m \xi_m - T_n \xi_n)}{T_m^2 - T_n^2} \quad (6.15)$$

$$a_1 = \frac{-2\omega_m \xi_m + 2\omega_n \xi_n}{\omega_n^2 - \omega_m^2} \quad (6.16)$$

$$= \frac{T_m T_n (T_m \xi_n - T_n \xi_m)}{\pi(T_m^2 - T_n^2)} \quad (6.17)$$

In all the analyses it was assumed that the modal damping ratios were equal for the 1st and the n^{th} mode of vibration, where n is the number of storeys. This damping ratio was calculated by an iterative procedure to find a damping ratio close to 5% of critical damping at the code specified period, but was not allowed to be greater than 8.5% of critical damping.

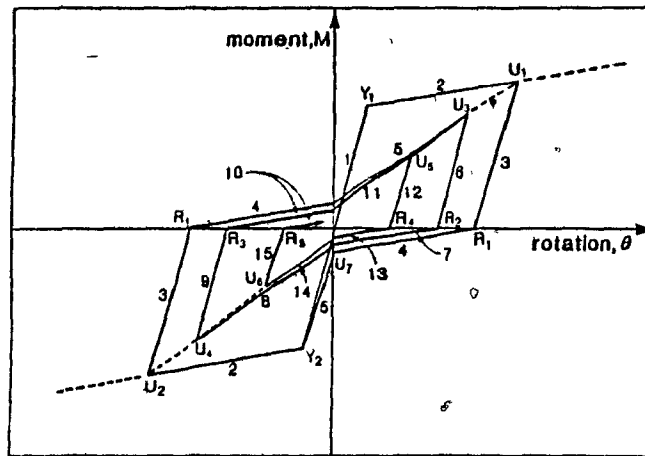
6.2 REFINED HYSTERETIC MODEL

A refined hysteretic model was developed in order to more accurately model the response of reinforced concrete members. This was necessary due to the significant

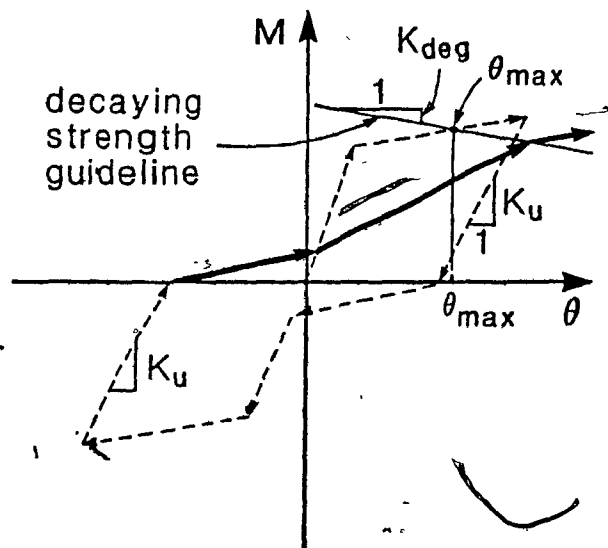
strength degradation, stiffness degradation and pinching of the response relationship observed in experimental responses of beam-column connections. In particular in this study specimen Old K1.3 exhibited a drop in capacity of about 50% and severe pinching of the response curves due to shear distress, bond-slip of the longitudinal beam bars as well as buckling of the bottom flexural bars in the beam.

The multi-linear hysteresis model which was developed to account for the above effects is described below by a series of 19 response Rules (see Fig. 6.9):

- R1. [Elastic stage.] *Loading* - if $M(p) \leq M(Y_1/Y_2)$, go to step R1; otherwise go to step R2. *Unloading and load reversal* - go to step R1.
- R2. [Loading on the primary curve after yielding.] *Loading* - If rotation greater than specified maximum rotation then calculate drop in strength from specified strength degradation slope (as a per cent of post yield slope) and go to step R2. *Unloading* - save point U_1/U_2 and go to step R3.
- R3. [Unloading from point U_1/U_2 on the primary curve.] *Loading* - if $M(p) \leq M(U_1/U_2)$, go to step R3; otherwise go to step R2. *Unloading* - go to step R3. *Load reversal* - save reversal point R_1 and go to step R4.
- R4. [Loading from reversal point R_1 after rule R3.] *Loading* - if $M(p) \leq M(U_7)$, go to step R4; otherwise go to step R5. *Unloading* - save unloading point U_8 and go to step R16.
- R5. [Loading toward point U_1/U_2 on the primary curve.] *Loading* - if $M(p) \leq M(U_1/U_2)$, go to step R5; otherwise go to step R2. *Unloading* - Save unloading point U_3 and go to step R6.
- R6. [Unloading from point U_3 after rule R5.] *Loading* - if $M(p) \leq M(U_5)$, go to step R6; otherwise go to step R5. *Unloading* - go to step R6. *Load reversal* - Save reversal point R_2 and go to step R7.
- R7. [Loading from reversal point R_2 after rule R6.] *Loading* - if $M(p) \leq M(U_7)$, go to step R7; otherwise go to step R8. *Unloading* - save unloading point U_8 and go to step R17.
- R8. [Loading toward point U_1/U_2 (opposite rule R4/R5).] *Loading* - if



a) Response rules



b) Strength degradation

Fig. 6.9 Refined hysteretic model for reinforced concrete members

$M(p) \leq M(U_1/U_2)$, go to step R8; otherwise go to step R2. *Unloading* – save unloading point U_4 and go to step R9.

R9. [Unloading from point U_4 after rule R8.] *Loading* – if $M(p) \leq M(U_4)$, go to step R9; otherwise go to step R8. *Unloading* – go to step R9. *Load*

reversal – save reversal point R_3 and go to step R10.

- R10. [Loading from reversal point R_3 after rule R9.] *Loading* – if $M(p) \leq M(U_8)$, go to step R10; otherwise go to step R11. *Unloading* – save unloading point U_9 and go to step R18.
- R11. [Loading toward point U_3 .] *Loading* – if $M(p) \leq M(U_3)$, go to step R11; otherwise go to step R5. *Unloading* – save unloading point U_5 and go to step R12.
- R12. [Unloading from point U_5 after rule R11.] *Loading* – if $M(p) \leq M(U_5)$, go to step R12; otherwise go to step R11. *Unloading* – go to step R12. *Load reversal* – save reversal point R_4 and go to step R13.
- R13. [Loading from reversal point R_4 after rule R12.] *Loading* – if $M(p) \leq M(U_7)$, go to step R13; otherwise go to step R14. *Unloading* – save unloading point U_9 and go to step R19.
- R14. [Loading toward point U_4 .] *Loading* – if $M(p) \leq M(U_6)$, go to step R14; otherwise go to step R8. *Unloading* – save unloading point U_8 and go to step R15.
- R15. [Unloading from point U_8 after rule R14.] *Loading* – if $M(p) \leq M(U_8)$, go to step R15; otherwise go to step R14. *Unloading* – go to step R15. *Load reversal* – save reversal point R_5 and go to step R10.
- R16. [Unloading from point U_8 after rule R4.] *Loading* – if $M(p) \leq M(U_8)$, go to step R16; otherwise go to step R4. *Unloading* – go to step R16. *Load reversal* – save reversal point R_6 and go to step R8.
- R17. [Unloading from point U_8 after rule R7.] *Loading* – if $M(p) \leq M(U_8)$, go to step R17; otherwise go to step R7. *Unloading* – go to step R17. *Load reversal* – save reversal point R_7 and go to step R11.
- R18. [Unloading from point U_9 after rule R10.] *Loading* – if $M(p) \leq M(U_9)$, go to step R18; otherwise go to step R10. *Unloading* – go to step R18. *Load reversal* – save reversal point R_8 and go to step R14.
- R19. [Unloading from point U_9 after rule R13.] *Loading* – if $M(p) \leq M(U_9)$, go to step R19; otherwise go to step R13. *Unloading* – go to step R19.

Load reversal – save reversal point R_9 and go to step R11. ■

6.3 ESTIMATING DAMAGE

6.3.1 Member Damage

In order to estimate member damage both “rotational ductility” and “curvature ductility” will be used in this study. These two approaches are discussed below.

a) *Rotational ductility demand* – Rotational ductility demand, μ_θ , is defined as the ratio of maximum rotation reached in a member, θ_{max} , to the yield rotation θ_y , see Fig. 6.10. That is:

$$\mu_\theta = \frac{\theta_{max}}{\theta_y} \quad (6.13)$$

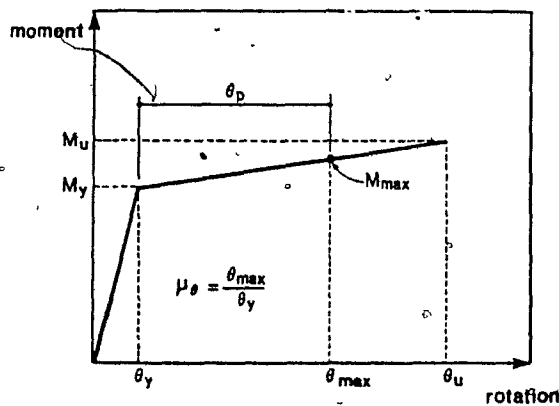


Fig. 6.10 Definition of rotational ductility demand

The assumption of anti-symmetric bending of the element (see Fig. 6.11) permits an estimate of the yield rotation, θ_y , as follows:

$$\theta_y = \frac{M_y L}{6EI} \quad (6.18)$$

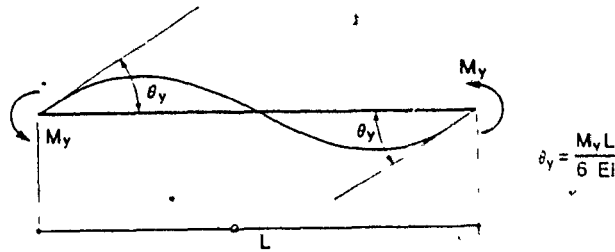


Fig. 6.11 Definition of yield rotation

where M_y is the yielding moment corresponding to θ_y , L is the length of the member and EI is the flexural stiffness prior to yielding. Hence the rotational ductility can be written as:

$$\mu_\theta = 1 + \frac{\theta_p}{\theta_y} = 1 + \frac{\theta_p}{M_y L / 6EI} \quad (6.19)$$

where θ_p is the plastic hinge rotation (see Fig. 6.10). Equation 6.19 is convenient since DRAIN-2D determines the plastic hinge rotation in every element that is yielding at each time step.

The assumption of a constant θ_y due to anti-symmetric bending is valid when only lateral load is acting. When gravity load is also acting θ_y will vary with time. This definition of ductility is not appropriate for columns where the value of M_y is not constant but varies with the level of axial load. In spite of these limitations the rotational ductility gives some indication of the relative amount of inelastic action displayed by different members.

a) *Curvature ductility demand* – Since curvature ductility demand depends on the sectional response only it can be determined for a given applied moment, M_{max} , if the moment-curvature response is known. It is defined as the ratio of maximum curvature to yield curvature as shown in Fig. 6.12. Hence

$$\mu_\phi = \frac{\phi_{max}}{\phi_y} \quad (6.20)$$

In the "elastic" range, i.e., prior to yielding, where $M_{max} < M_y$ the curvature ductility demand is less than 1.0 and can be expressed as:

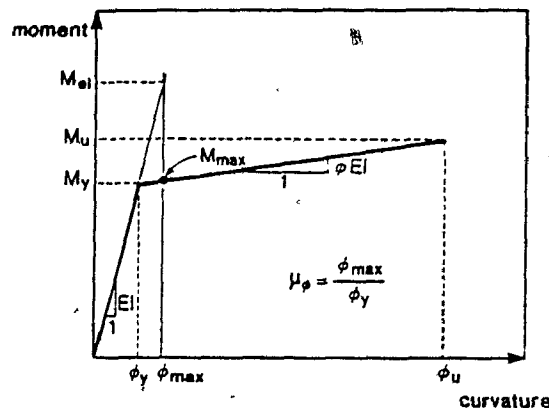


Fig. 6.12 Definition of curvature ductility demand

$$\mu_\phi = \frac{M_{max}}{M_y} \quad (6.21)$$

In the inelastic range where $M_{max} > M_y$ the curvature ductility demand is defined as the ratio of the moment that would exist if the member had remained elastic, M_{el} , to the yield moment, M_y , and can be written:

$$\mu_\phi = \frac{M_{el}}{M_y} = 1 + \frac{M_{max} - M_y}{pM_y} \quad (6.22)$$

where p is the ratio of the post yield stiffness to the initial elastic stiffness. This method is expected to give good estimates of curvature ductility.

6.3.2 Structural and Non-Structural Damage

The estimation of structural and non-structural damage of a building subjected to a number of different acceleration-time histories is a difficult task. Damage depends on the type of structure, the specific details of the structural components, the type of non structural components (partitions, windows etc.), the quality of construction and maintenance, history of previous events and the duration of motion. The 1971 San-Fernando earthquake provided a large amount of data on the seismic performance of buildings in the Los Angeles area. The studies done by Hasselman and Wiggins [80] are particularly useful in estimating the correlation between interstorey drift and

expected structural and non-structural damage. The methods suggested by Hasselman and Wiggins are used in this study and are summarized below.

This approach uses Bayesian statistics to combine actual earthquake damage data with estimates of structural damage. The actual earthquake damage for a number of structures following the 1971 San Fernando earthquake was transformed into damage ratios. The damage ratio, DR , is defined as the repair cost divided by the replacement cost. The authors categorized the types of buildings into three groups, i.e., steel frame buildings, reinforced concrete frame buildings and reinforced concrete shear-wall buildings. Each category was further subdivided into three different sub-categories (good, average and poor) according to the quality and year of construction. In order to develop a relationship between damage ratio and interstorey drift, regression analyses were first carried out on the available damage data (mostly low damage states) and was corrected by prior estimates done by experts for higher damage states. The resulting damage ratio vs interstorey drift relationship which is assumed to be linear on a log-log plot is given as:

$$\log DR = \log DR_t + \left(\frac{\log DR_c - \log DR_t}{\log \Delta_c - \log \Delta_t} \right) (\log \Delta - \log \Delta_t) \quad (6.23)$$

In the above relationship DR is the damage ratio, Δ is the interstorey drift to storey height ratio, DR_c is the damage threshold of 0.5%, DR_t is the damage threshold of 50%, Δ_c is the interstorey drift to storey height ratio corresponding to DR_c and Δ_t is the interstorey drift to storey height ratio corresponding to DR_t . Hasselman and Wiggins reported good correlation between their predicted damage ratios and the actual observations of damage in a number of structures after the 1971 San Fernando earthquake.

The term Δ_t was taken as 0.00085 as recommended by Hasselman and Wiggins[80]. In this study the quality of construction for the reinforced concrete frame structures was judged to be "good" for $K=0.7$, "average" for $K=1.3$ and "poor" for Old $K=1.3$. These qualitative categories were arrived at by comparing the overall structural responses of the specimens tested and by comparing the Canadian Code requirements with the

corresponding requirements used in California. The term Δ_c which depends on the quality of construction and the duration of motion were determined for the Montreal and Vancouver structures for the different levels of peak ground acceleration. These values are based on the relationships given by Hasselman and Wiggins [80] for assumed values of earthquake magnitudes and are given in Table 6.1.

Table 6.1 Δ_c Used to Estimate Damage

Location	K	Peak horizontal ground acceleration, g	Δ_c , mm/mm
Montreal	0.7	0.27	0.0934
		0.18	0.1540
		0.078	0.2540
	1.3	0.27	0.0323
		0.18	0.0532
		0.078	0.0878
	Old 1.3	0.27	0.0081
		0.18	0.0133
		0.078	0.0219
Vancouver	0.7	0.27	0.0567
		0.18	0.0934
		0.078	0.1540
	1.3	0.27	0.0196
		0.18	0.0323
		0.078	0.0532
	Old 1.3	0.27	0.0049
		0.18	0.0081
		0.078	0.0133

In assessing the predicted damage ratios it is helpful to realize that a damage ratio of 50% represents significant damage and would likely result in the building being replaced.

An additional consideration in assessing the damage to structures is the resulting damage to windows. The equation for the window damage ratio DR_w as given below was derived from a log-log plot from reference [81].

$$\log DR_w = 2.35 \log \Delta + 6.3 \quad (6.23)$$

in which Δ is the interstorey drift. Unlike the structural damage ratio the window damage ratio as given by Hasselman, Eguchi and Wiggins [81] is a function of the drift index only.

CHAPTER 7

EVALUATION OF PREDICTED RESPONSES

This chapter presents a summary of the responses of the three Montreal and the three Vancouver buildings. Each of these six-storey buildings was subjected to three different levels of peak ground accelerations. For each level of acceleration there were three artificially generated accelerograms as well as the 1940 North-South El-Centro accelerogram scaled appropriately.

Table 7.1 presents the peak horizontal ground accelerations used to scale the different accelerograms to obtain the "service", the "design", and the "ultimate" motions.

Table 7.1 Peak Ground Accelerations			
Region	Peak Ground Acceleration, g		
	Service	Design	Ultimate
Montreal	0.078	0.180	0.270
Vancouver	0.089	0.210	0.315

In the non-linear analysis the effects of the dead load and the live load were first determined. The live load was taken as the full unfactored live loading reduced by the live load reduction factors of the National Building Code of Canada [2].

Due to the large number of figures required to summarize the response predictions, these figures are presented at the end of the chapter for all 6 structures analyzed.

7.1 ROOF DISPLACEMENT TIME HISTORIES

Figures 7.1 to 7.6 present the roof displacement time histories for the three Montreal structures and the three Vancouver structures for the three different levels of peak

horizontal ground acceleration. Tables 7.2 and 7.3 summarize the results in the form of the maximum predicted roof displacements and approximate structural periods. It is interesting to note that even with significant inelastic action occurring for the highest level of ground acceleration the resulting displacements for the different acceleration time histories are approximately proportional to the levels of acceleration. As can be seen from Table 7.2 and Table 7.3 there was no significant change in the period for different levels of acceleration. The slightly higher periods for the K1.3 and the Old K1.3 structures reflect the influence of joint deformation, bond-slip and shear distortion.

7.2 LOCATIONS AND TYPES OF PLASTIC HINGES

In the analyses the time histories of all member responses and the degree of inelastic action were saved at each time step. Figure 7.7 illustrates the deformed shapes and the corresponding locations and types of plastic hinges at three different times for the $K=0.7$ Montreal structure.

In order to summarize the large amount of data concerning the locations and types of plastic hinges the aggregate of all inelastic actions for the most critical motion is presented for each structure.

As can be seen from Fig. 7.8 a and 7.9 a only flexural hinges formed in the beams in the $K=0.7$ structures as expected. While there was no yielding of the columns in the Montreal structure some yielding is predicted to occur at the base of the columns for the Vancouver structure.

Figures 7.8 b and 7.9 b illustrate the locations of plastic hinges in the $K=1.3$ structures. As can be seen there are a large number of connections where yielding of the joint reinforcement has taken place. These hinges formed mainly in the top storey due to the low level of axial load in these columns. In addition a few flexural hinges developed in the beams and some yielding occurred at the column bases in the Vancouver structure.

Figures 7.8 c and 7.9 c illustrate that a large number of joint yielding occurred in both the Montreal and Vancouver structures as well as some shear yielding in the interior bay beams in the Vancouver structure. This shear distress in the beams in

the interior bay is caused by the larger shear in this relatively short beam and by the presence of only minimum shear reinforcement.

7.3 ENVELOPES OF LATERAL DISPLACEMENTS

The envelopes of lateral displacements for the six structures studied are presented in Fig. 7.10 to 7.15. As can be seen from these envelopes the first mode dominated except for some higher mode effects in the upper two storeys as expected. It is evident that the maximum response depends strongly on the motion since a wide range of envelopes is predicted for each level of ground motion. Powell and Row [50] have made the same observations concerning the importance of the ground motion characteristics on the response. A summary of the predicted maximum roof displacements and predicted periods is presented in Tables 7.2 and 7.3.

Table 7.2 Predicted Approximate Periods and Maximum Roof Displacements for Montreal Buildings

K	Peak horizontal ground acceleration, g	Approximate period T , sec	Maximum roof displacement, mm
0.7	0.27	1.83	125
	0.18	1.83	83
	0.078	1.83	36
1.3	0.27	2.10	178
	0.18	2.10	118
	0.078	2.10	51
Old 1.3	0.27	2.13	178
	0.18	2.13	118
	0.078	2.13	51

7.4 INTERSTOREY DRIFTS AND DAMAGE ESTIMATES

Figures 7.16 to 7.21 show the envelopes of the interstorey drift index (i.e., the ratio of the interstorey drift to the storey height) for the six structures studied. Also shown in these figures is the interstorey drift ratio, Δ/h , corresponding to the 1/200 limit recommended in the supplement to the 1985 National Building Code of Canada [2]. As expected there is considerable variation in the drifts depending on the characteristics of

Table 7.3 Predicted Approximate Periods and Maximum Roof Displacements for Vancouver Buildings

K	Peak horizontal ground acceleration, <i>g</i>	Approximate period <i>T</i> , sec	Maximum roof displacement, mm
0.7	0.27	1.81	212
	0.18	1.81	141
	0.078	1.81	60
1.3	0.27	2.12	231
	0.18	2.12	154
	0.078	2.12	65
Old 1.3	0.27	2.33	230
	0.18	2.33	154
	0.078	2.33	65

the ground motions. The $K=0.7$ structures display essentially a flexural type response with the interstorey drift increasing toward the base. The $K=1.3$ and the Old $K=1.3$ structures display larger drifts in the middle storeys probably due to the significant contribution of joint shear distortions and bond-slip to the response. It is interesting to note that for the lower level earthquakes all of the structures displayed maximum interstorey drift ratios, Δ/h , less than about 0.003. At the design level of earthquake the $K=0.7$ structure displays a maximum interstorey drift ratio of about 1/200 while the $K=1.3$ and Old $K=1.3$ structures have drift ratios considerably greater than 1/200. The maximum and average structural and window damage ratios for the Montreal and Vancouver structures are presented in Tables 7.4 and 7.5.

Table 7.4 Damage Estimates for Montreal Structures

K	Peak horizontal ground acceleration, g	Structural damage, %		Window damage, %	
		Average	Maximum	Average	Maximum
0.7	0.27	13.0	14.5	12.5	19.4
	0.18	9.9	10.9	4.8	7.4
	0.078	6.6	7.3	0.7	1.0
1.3	0.27	22.0	23.6	33.1	37.6
	0.18	14.8	15.7	11.8	14.7
	0.078	8.7	9.2	1.6	2.0
Old 1.3	0.27	53.0	62.8	28.5	39.6
	0.18	25.5	27.9	11.8	14.7
	0.078	11.0	11.8	1.6	2.0

Table 7.5 Damage Estimates for Vancouver Structures

K	Peak horizontal ground acceleration, <i>g</i>	Structural damage, %		Window damage, %	
		Average	Maximum	Average	Maximum
0.7	0.315	17.5	20.5	28.3	50.0
	0.21	13.6	15.0	15.5	23.0
	0.089	8.4	9.2	2.1	3.0
1.3	0.315	32.9	37.2	52.3	73.5
	0.21	19.9	22.1	20.7	29.6
	0.089	10.4	11.5	2.7	3.9
Old 1.3	0.315	97.5	100.0	53.5	76.4
	0.21	46.8	55.1	20.8	29.3
	0.089	15.1	15.1	2.7	2.7

The variation of the damage ratios over the height of the structures is related to the variation of the interstorey drift. As can be seen from Tables 7.4 and 7.5 there is significantly higher structural and window damage as the "ductility" assumed in the design decreases. The old $K=1.3$ structures for both Montreal and Vancouver are predicted to be so severely damaged under the "ultimate earthquakes" that total replacement of the structure will likely be necessary. The $K=1.3$ structures in Montreal and Vancouver are predicted to sustain average structural damage ratios of 22% and 33% respectively for the "ultimate earthquakes". The predicted window damage is considerably higher. The $K=0.7$ structures are predicted to sustain relatively light structural damage for the "ultimate earthquakes" with some significant window damage.

It is interesting to note that considerable structural and window damage is predicted to occur in the Old $K=1.3$ structures under the "design" earthquakes.

As expected, for the relatively low level earthquakes that may occur several times during the life of the structure very little structural and window damage is predicted and the damage is not strongly effected by the quality of construction and the choice of K used in design. For earthquakes exhibiting higher peak ground accelerations with a lower probability of occurrence during the life of the structure the quality of construction and the choice of K used in design have significant effects on the predicted damage levels.

7.5 INELASTIC DEFORMATION AND FLEXURAL STRENGTH DEMANDS

Because very little inelastic deformation occurs in the columns (only at the column bases of the Vancouver structures as shown in Fig. 7.8 and 7.9) we will describe in some detail the predicted inelastic deformations in the beams. The predicted curvature ductilities and plastic hinge rotations for the six different structures are illustrated in Fig. 7.22 to 7.27. The curvature ductility and rotational ductility values are calculated using the expressions given in Section 6.4. Due to the definitions of these terms they both give the same value of "ductility" before yielding but give very different values after yielding. The maximum plastic hinge rotations and the cumulative plastic hinge rotations give the same values only if a single inelastic excursion has taken place. If the cumulative plastic hinge rotation is significantly higher than the maximum plastic rotation then this indicates that there have been a number of inelastic excursions.

The predicted inelastic deformation demands on the beams for the $K=0.7$ structures (see Fig. 7.22 and 7.27) indicate that significant yielding has taken place in the beams of the bottom two storeys and that some beams in the upper storeys are close to flexural yielding. It is important to note that specimen K0.7 displayed a hinge rotation capacity of at least 0.090 rad. Paulay [12] has determined that a well detailed beam can sustain a minimum plastic hinge rotation of 0.035 rad. It is clear from these figures that the $K=0.7$ structures are capable of providing the necessary plastic hinge rotations. It can be seen that the beams in the $K=0.7$ structures do not undergo flexural yielding when subjected to lower level earthquakes. The beams are however close to flexural yielding for the "design" earthquakes.

In the analyses of the $K=1.3$ and Old $K=1.3$ structures the effect of the bond-slip of the longitudinal bars anchored in the joint and the effect of shear deformation of the beams was included in the flexural hinge properties. Therefore the hinge rotations plotted for these cases include these two effects. This explains why there are predicted hinge rotations even though no flexural yielding is predicted. In assessing the performance of the beams it is therefore necessary to realize that the flexural component of these rotations is about 50% of the total hinge rotation predicted. Test specimens K1.3

and Old K1.3 displayed plastic hinge rotation capacities of 0.063 rad and 0.018 rad respectively. It is evident from the predicted hinge rotations in Fig. 7.23, 7.24, 7.26 and 7.27 that they are considerably less than those required to cause failure. However it must be emphasized that in the K=1.3 and Old K=1.3 structures significant structural damage was predicted (see Tables 7.4 and 7.5).

If the responses for the three Montreal structures and the responses for the three Vancouver structures are compared for the "ultimate" earthquake then it is evident that the Vancouver structures require rotations that are about 4 times larger than those predicted for the Montreal structures. It is interesting to note that the maximum hinge rotations are about the same for the Old K=1.3, the K=1.3 and the K=0.7 structures, i.e., about 0.002 rad for Montreal and about 0.005 rad for Vancouver.

7.6 LATERAL FORCES AND SHEAR STRENGTH DEMANDS

Figures 7.28 to 7.33 illustrate the predicted column shears for the four different earthquakes, the factored static design column shears and the predicted column shear capacities. The figures compare the above values for exterior and interior columns for three different levels (i.e., "ultimate", "design" and "service") of earthquakes. The static design column shears given in these figures correspond to the factored earthquake lateral loads ($1.5Q$) and do not include shears due to live load and dead load.

It is evident from Fig. 7.28 to 7.33 that the shear capacities of both the interior and exterior columns are significantly greater than the shears predicted at each storey level for all the buildings. The shear capacities were determined using the procedures described in Chapter 5 and accounted for the combined effects of shear, axial load and moment. As can be seen the shear capacities increase toward the bottom of each structure due to the increasing levels of compressive axial load. In the determination of the shear capacities axial loads corresponding to 85% of the dead load were assumed. It is noted that the first storey columns for the K=0.7 structures have significantly higher shear capacities than the columns in the upper storeys due to the presence of confinement reinforcement over the entire clear storey height of the first storey columns.

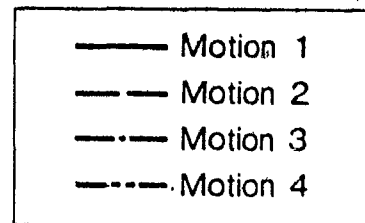
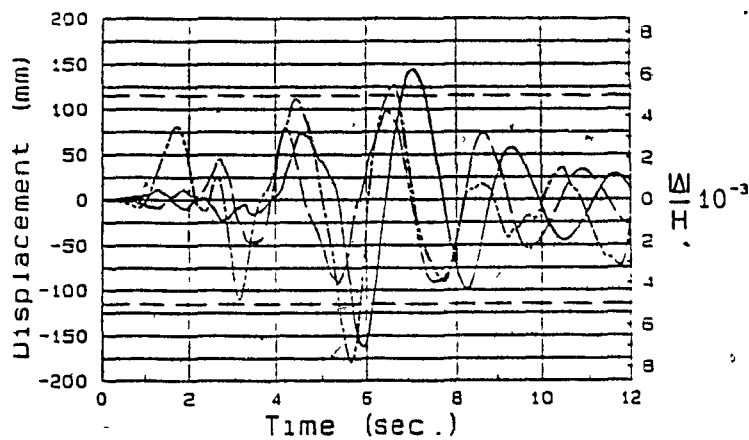
The column shears predicted using non-linear dynamic analysis for the "service" level earthquake (i.e., with a horizontal peak ground acceleration of about 40% of the acceleration corresponding to a probability of exceedance of 10% in 50 years) are about equal to the factored static design shears in the first storey columns. It is noted that the non-linear dynamic analyses give column shears larger than the computed factored earthquake shears for the "design" and "ultimate" motions. As mentioned above the shear capacities of the columns are much larger than the shear resulting from the non-linear analysis. The only columns that experienced flexural yielding were those at the base of the $K=0.7$ structure in Vancouver. One factor which increased the capacity of the column in both shear and flexure was the use of probable resistances for the concrete and the steel. Another factor which influence the flexural capacity of the columns was the need to provide minimum amount of longitudinal reinforcement which governed the choice of the longitudinal steel.

It is noted that it is possible with some $K=1.3$ and Old $K=1.3$ structures that the columns may yield before the beams and this may cause significant damaging storey drifts possibly only in one storey. This could result in very little energy dissipation and possible collapse for very severe earthquakes.

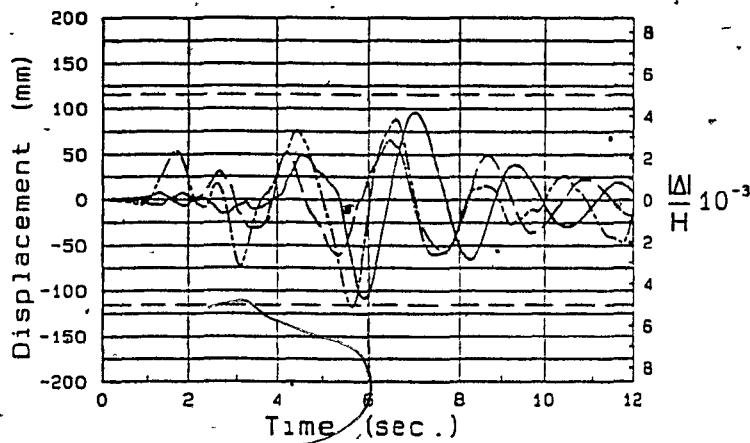
7.7 INFLUENCE OF COLUMN SIZE ON THE RESPONSE

In order to investigate the influence of the size of the columns on the response a design was carried out on the Montreal structure designed with $K=1.3$ which resulted in smaller columns. For this structure all the columns were chosen to be 450×450 mm instead of 500×500 mm. Due to the smaller dimensions of these columns the longitudinal reinforcement in the interior ground floor columns had to be increased to 2.4%. In this design the columns were stronger than the beams. The results of the non-linear dynamic analyses [82] are summarized in Fig. 7.34. It is interesting to note that the reduction in column size for the interior columns has led to an increase in the number of joint hinges from just four at the top storey to a total of ten as shown in Fig. 7.34 a. The large amount of longitudinal reinforcement in the first storey columns prevented joint hinges from forming at the first storey level. The reduction in column size led to

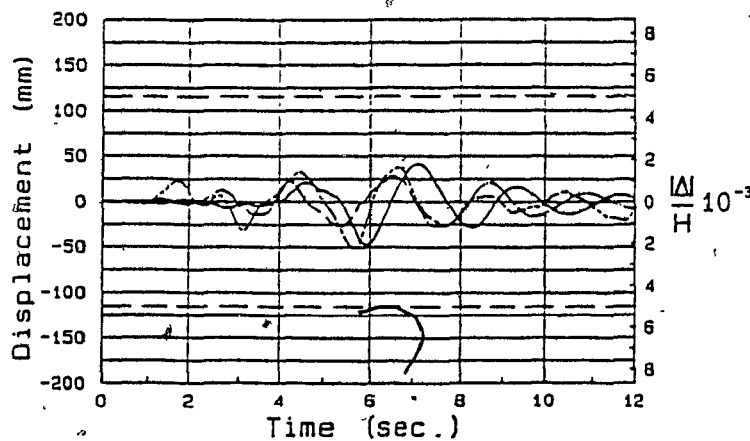
an increase of 16% in the top storey deflection (see Fig. 7.34 b) and a 25% increase in the interstorey drift of the first floor level (see Fig. 7.34 c). This 25% increase in the interstorey drift results in a significant increase in the structural and non-structural damage estimates. In addition the shear in the interior column at the first storey level doubled (see Fig. 7.34 d). The results of this study emphasize the need to avoid yielding of the joints by choosing sufficiently large columns and by providing sufficient joint reinforcement. The sensitivity of the responses to joint yielding creates greater concern about the adequacy of older structures in resisting significant earthquakes.



a) peak ground acceleration = $0.27g$

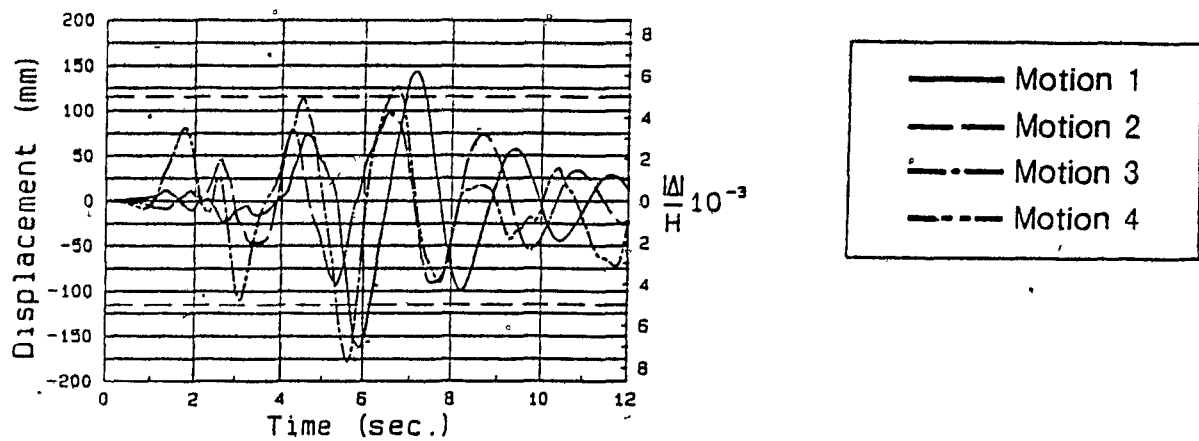


b) peak ground acceleration = $0.18g$

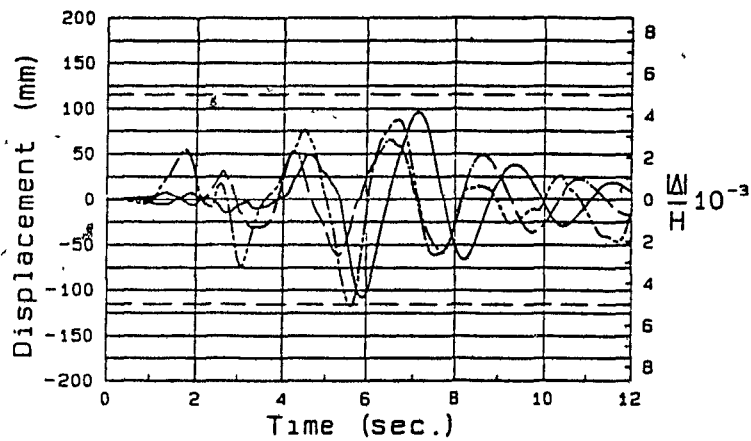


c) peak ground acceleration = $0.078g$

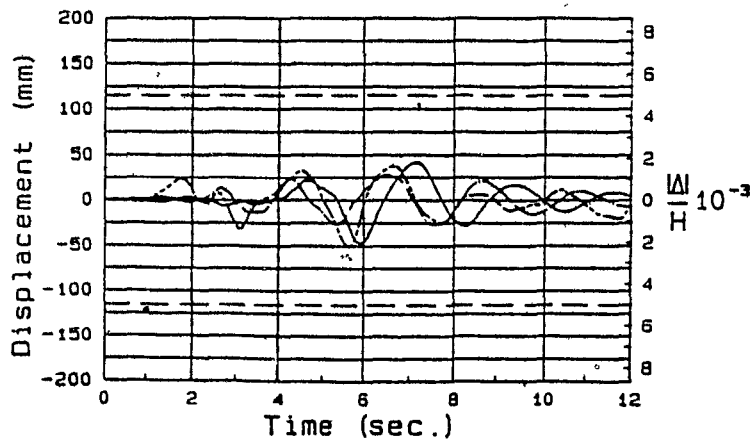
Fig. 7.1 Roof displacement time histories for different levels of maximum peak ground acceleration, a , for Old $K=1.3$ structure in Montreal



a) peak ground acceleration = 0.27g

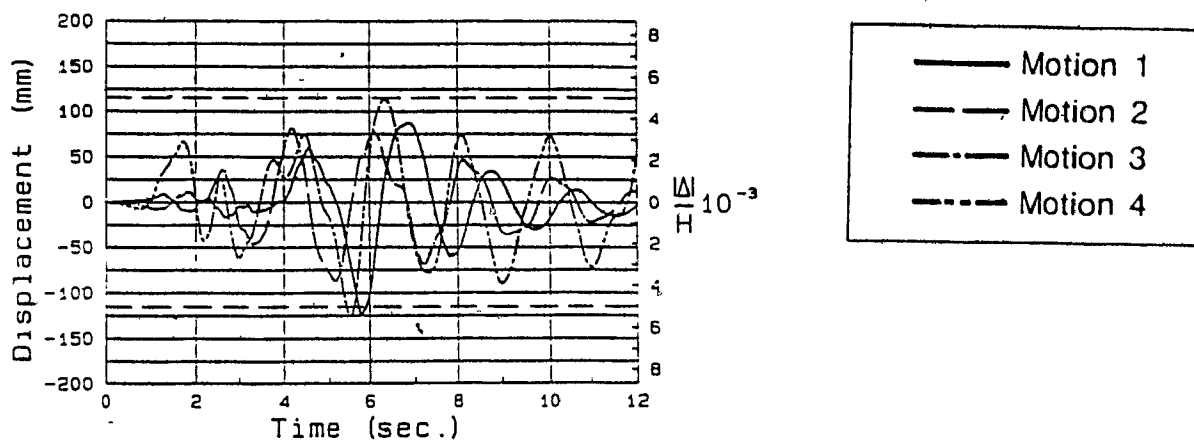


b) peak ground acceleration = 0.18g

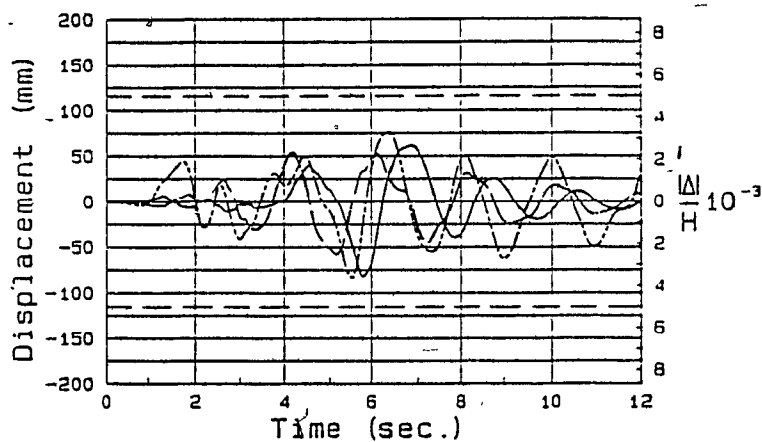


c) peak ground acceleration = 0.078g

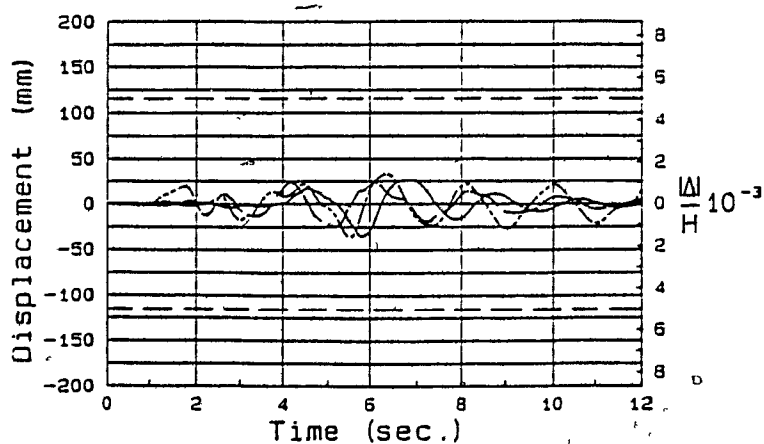
Fig.7.2 Roof displacement time histories for different levels of maximum peak ground acceleration, a , for $K=1.3$ structure in Montreal



a) peak ground acceleration = 0.27g

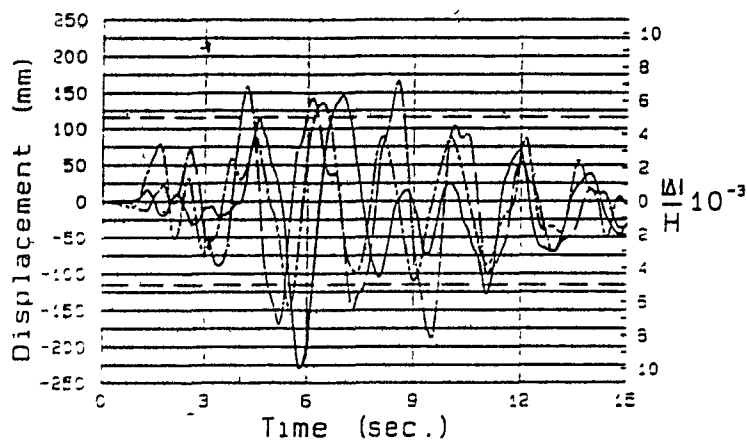


b) peak ground acceleration = 0.18g

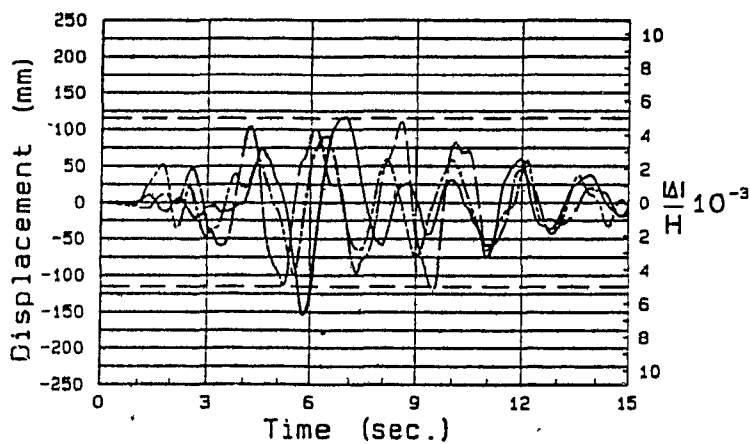


c) peak ground acceleration = 0.078g

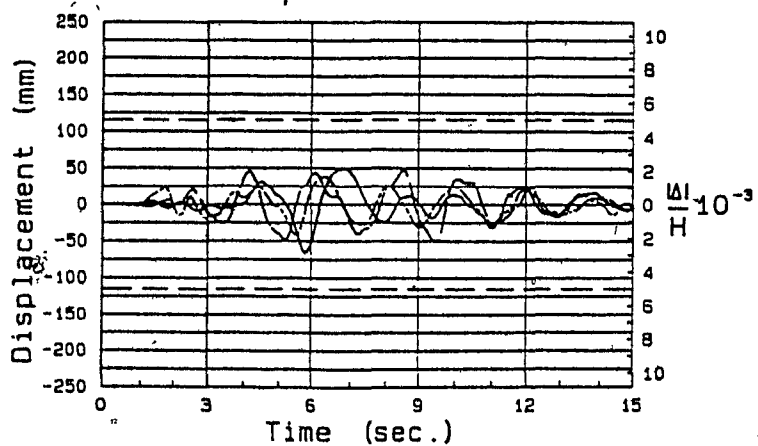
Fig. 7.3 Roof displacement time histories for different levels of maximum peak ground acceleration, a , for $K=0.7$ structure in Montreal



a) peak ground acceleration = 0.315g

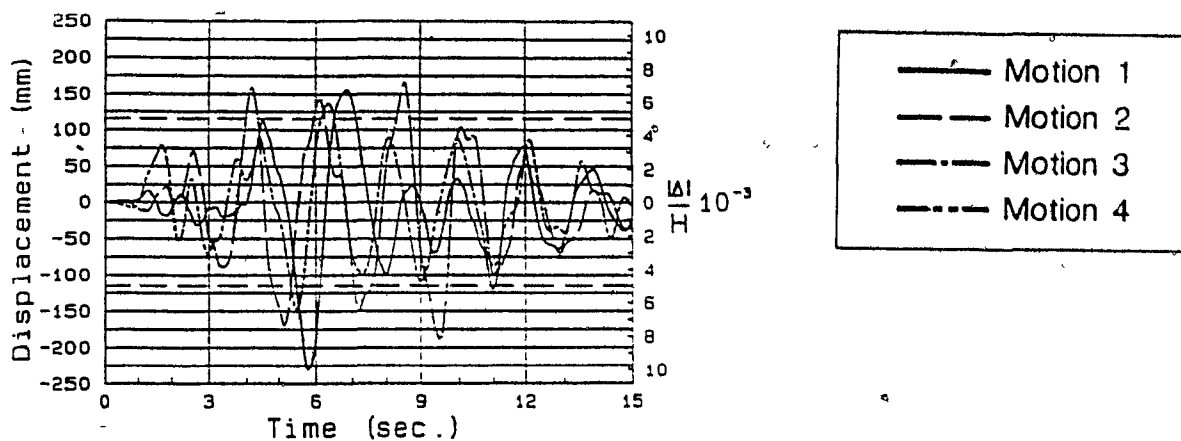


b) peak ground acceleration = 0.21g

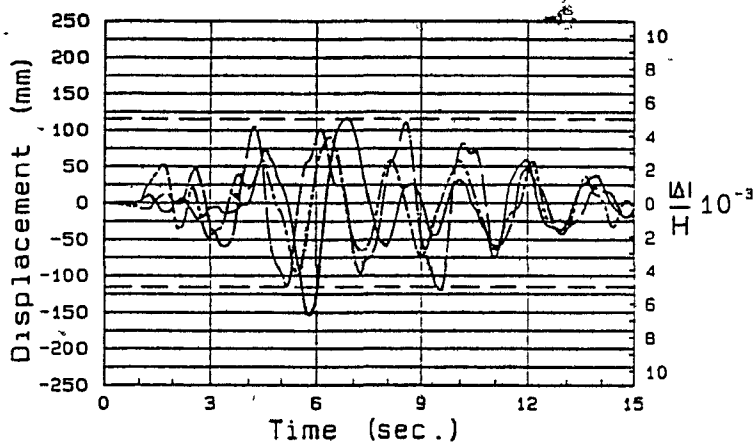


c) peak ground acceleration = 0.089g

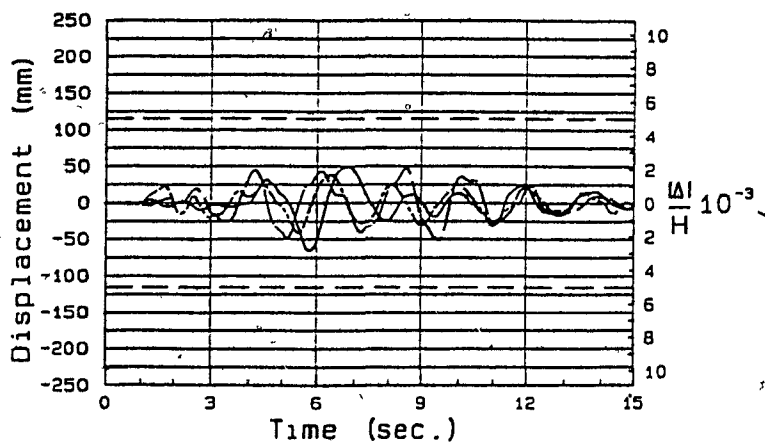
Fig. 7.4 Roof displacement time histories for different levels of maximum peak ground acceleration, a , for Old K=1.3 structure in Vancouver



a) peak ground acceleration = 0.315g

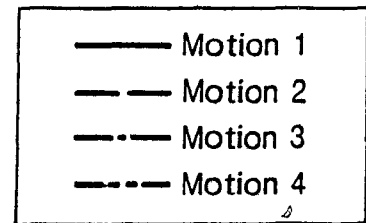
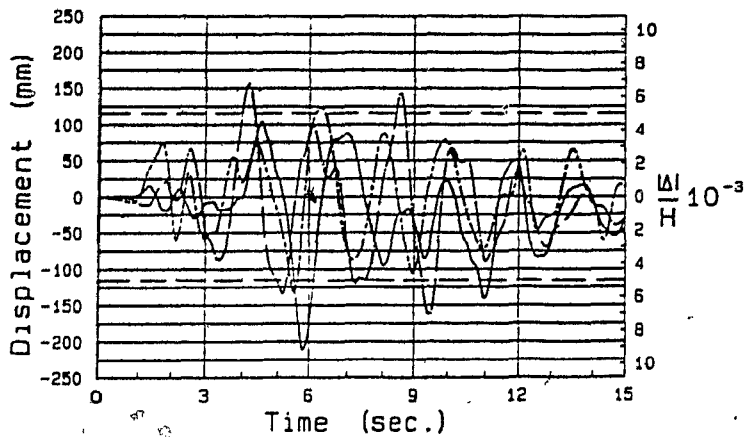


b) peak ground acceleration = 0.21g

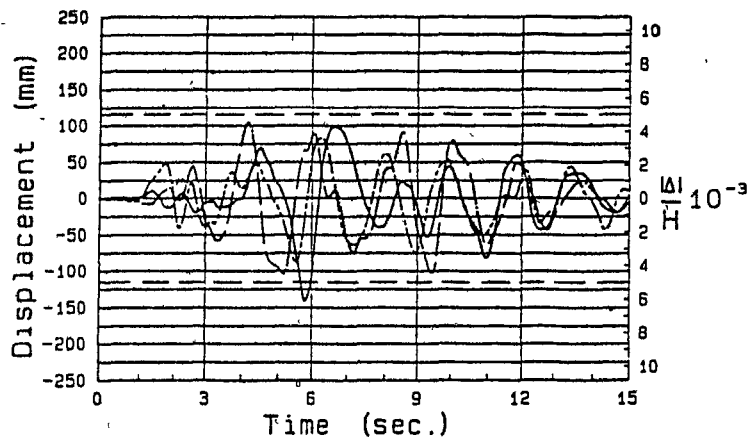


c) peak ground acceleration = 0.089g

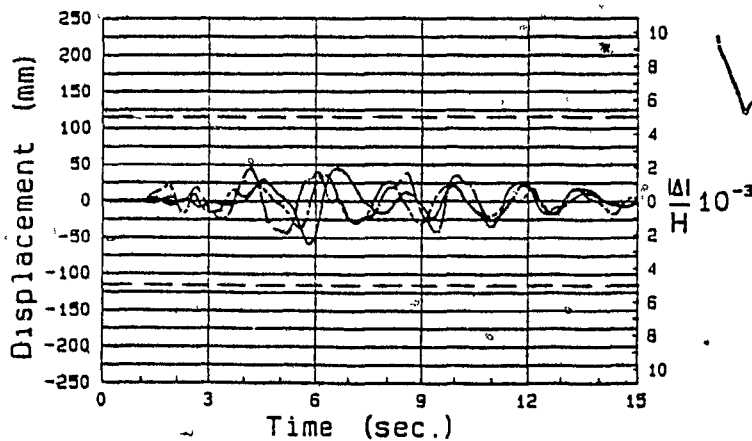
Fig. 7.5 Roof displacement time histories for different levels of maximum peak ground acceleration, a , for $K=1.3$ structure in Vancouver



a) peak ground acceleration = 0.315g



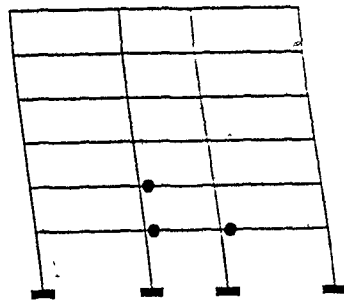
b) peak ground acceleration = 0.21g



c) peak ground acceleration = 0.089g

Fig. 7.6 Roof displacement time histories for different levels of maximum peak ground acceleration, a , for $K=0.7$ structure in Vancouver

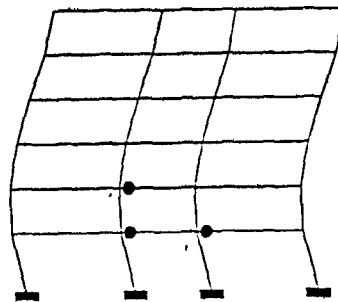
- Negative moment hinge
- Positive moment hinge



a)

Time = 5.51 sec.

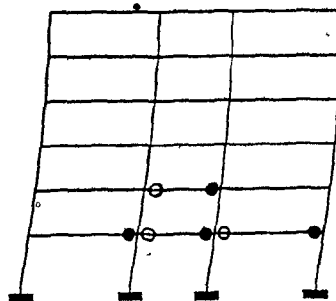
Δ roof = -124.70 mm



b)

Time = 5.89 sec.

Δ roof = 5.89 mm



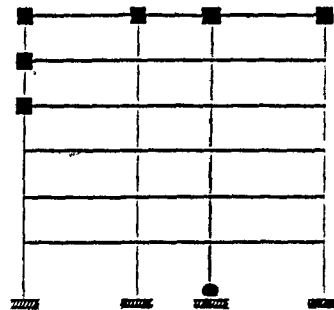
c)

Time = 6.32 sec.

Δ roof = 112.47 mm

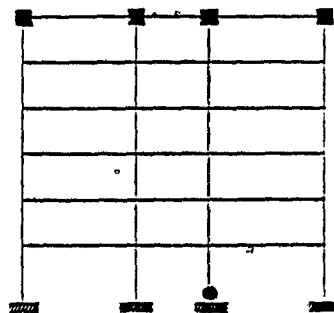
Fig.7.7 Deformed shapes and corresponding types and locations of hinges, for $k=0.7$ structure in Montreal for the most critical motion

- joint "yielding"
- moment hinging
- ✕ shear "yielding"



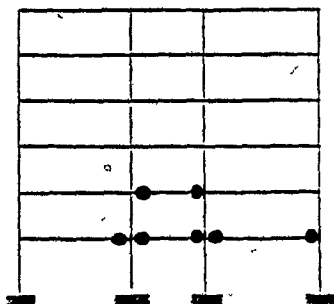
a)

Old $K=1.3$



b)

$K=1.3$

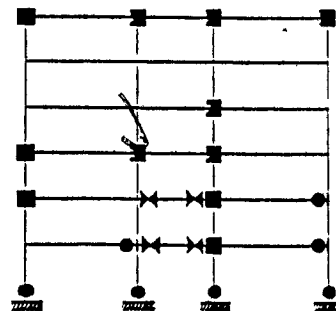


c)

$K=0.7$

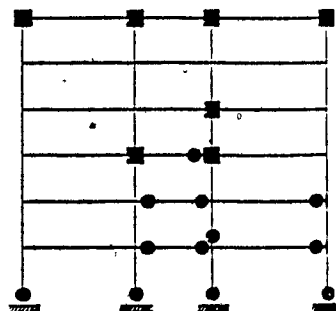
Fig. 7.8 Summary of hinge types and locations during entire time history responses for Montréal structures

- joint "yielding"
- moment hinging
- ✕ shear "yielding"



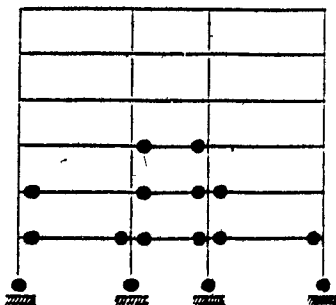
a)

Old $K=1.3$



b)

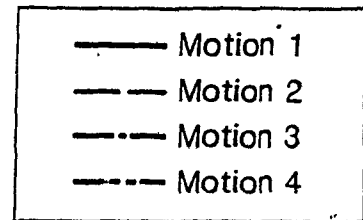
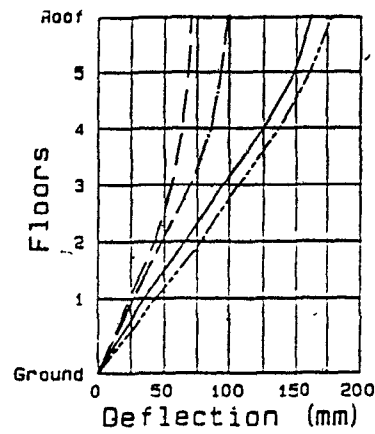
$K=1.3$



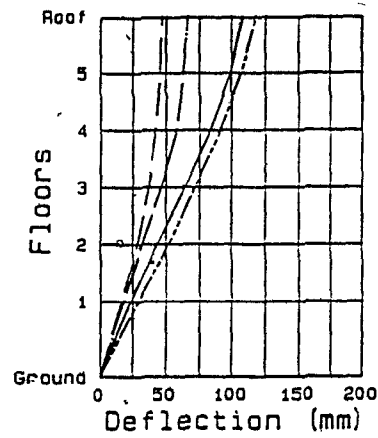
c)

$K=0.7$

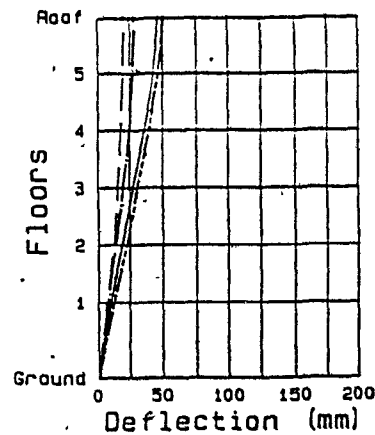
Fig. 7.9 Summary of hinge types and locations during entire time history responses for Vancouver structures



a) peak ground acceleration = 0.27g

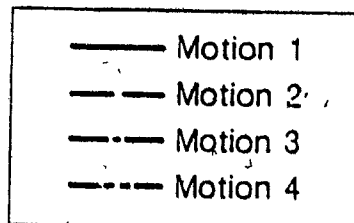
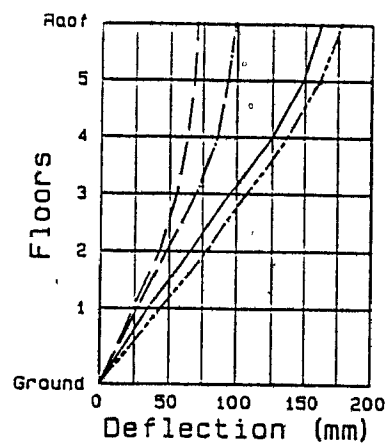


b) peak ground acceleration = 0.18g

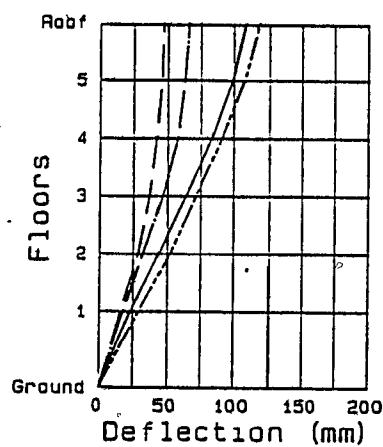


c) peak ground acceleration = 0.078g

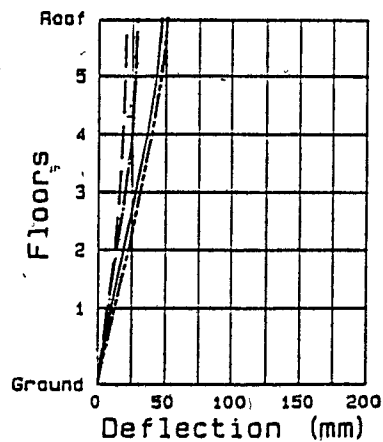
Fig. 7.10 Envelopes of lateral displacements for Old K=1.3 structure in Montreal



a) peak ground acceleration = 0.27g

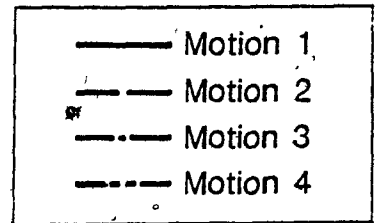
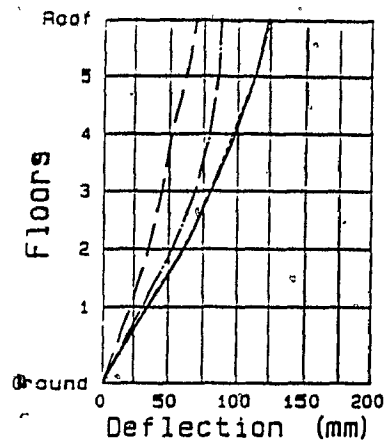


b) peak ground acceleration = 0.18g

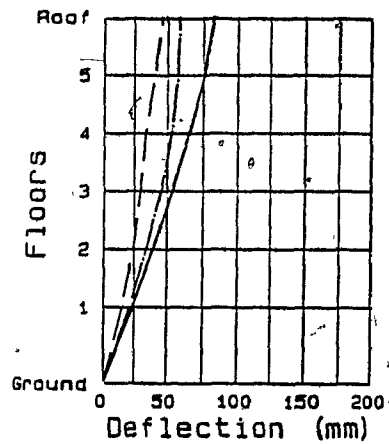


c) peak ground acceleration = 0.078g

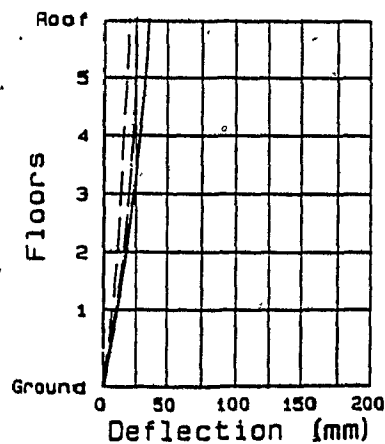
Fig. 7.11 Envelopes of lateral displacements for $K=1.3$ structure in Montreal



a) peak ground acceleration = 0.27g

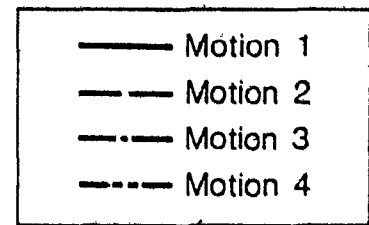
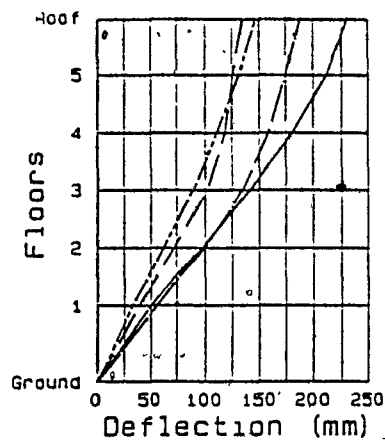


b) peak ground acceleration = 0.18g

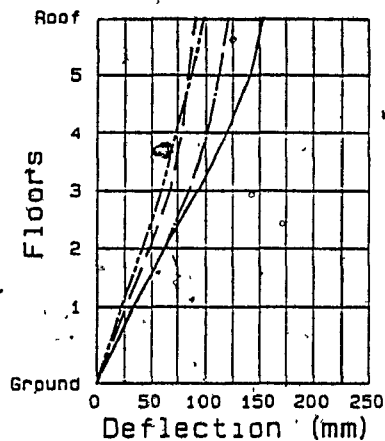


c) peak ground acceleration = 0.078g

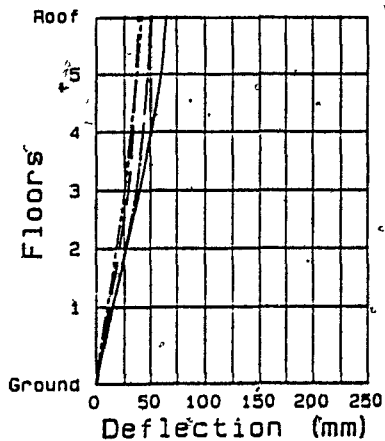
Fig. 7.12 Envelopes of lateral displacements for $K=0.7$ structure in Montreal



a) peak ground acceleration = 0.315g

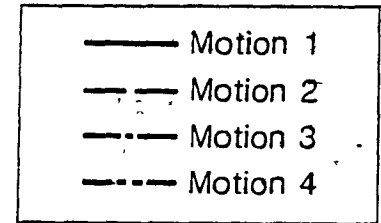
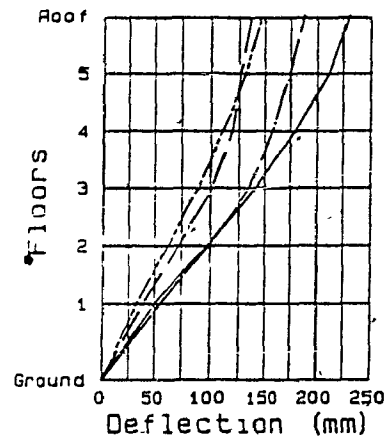


b) peak ground acceleration = 0.21g

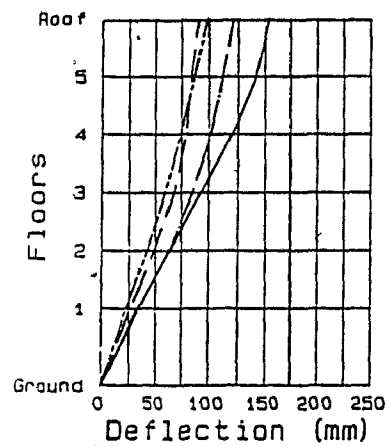


c) peak ground acceleration = 0.089g

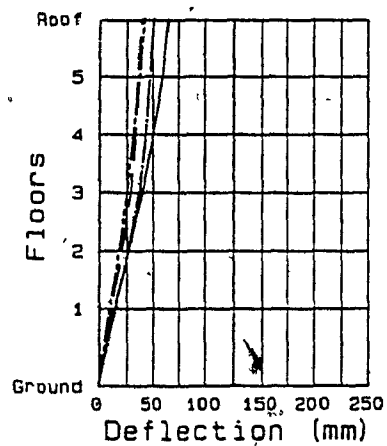
Fig. 7.13 Envelopes of lateral displacements for Old K=1.3 structure in Vancouver.



a) peak ground acceleration = 0.315g

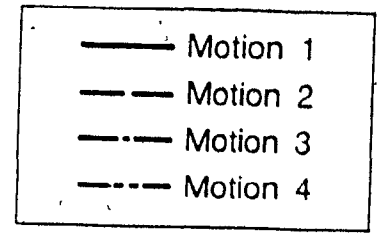
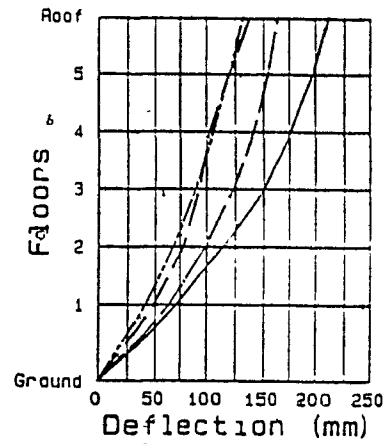


b) peak ground acceleration = 0.21g

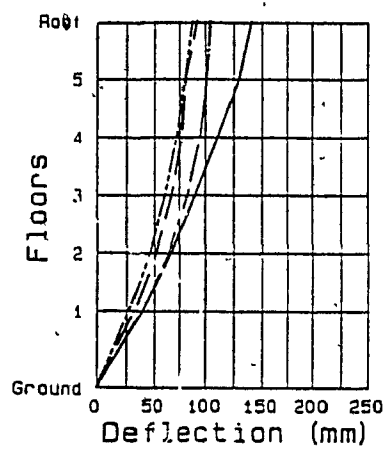


c) peak ground acceleration = 0.089g

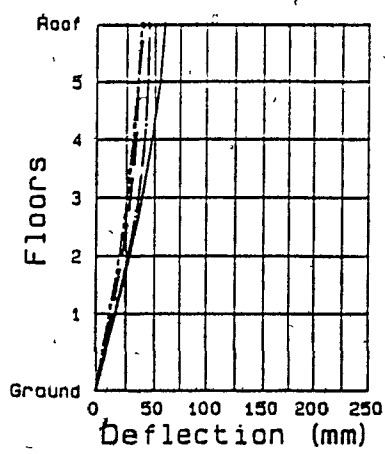
Fig. 7.14 Envelopes of lateral displacements for K=1.3 structure in Vancouver



a) peak ground acceleration = 0.315g

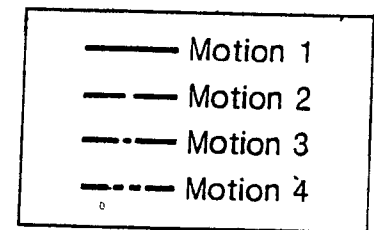
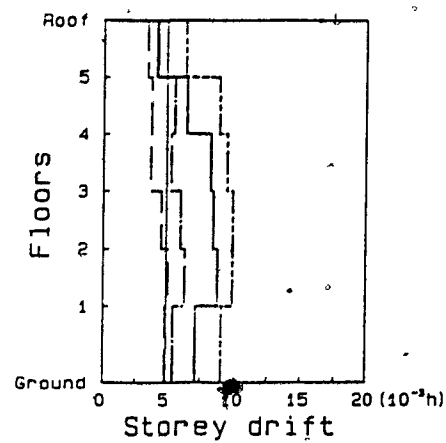


b) peak ground acceleration = 0.21g

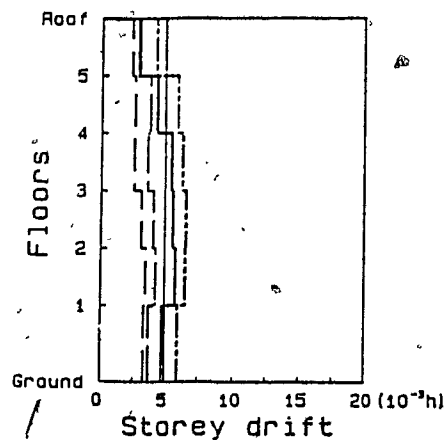


c) peak ground acceleration = 0.089g

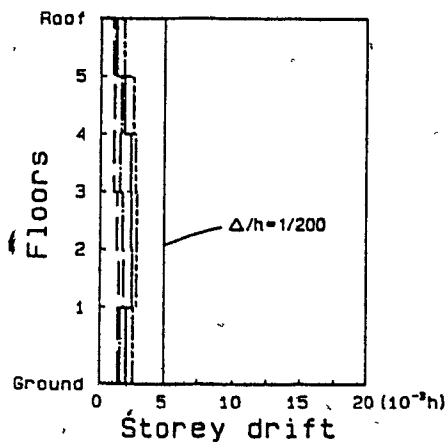
Fig. 7.15 Envelopes of lateral displacements for K=0.7 structure in Vancouver



a) peak ground acceleration = 0.27g

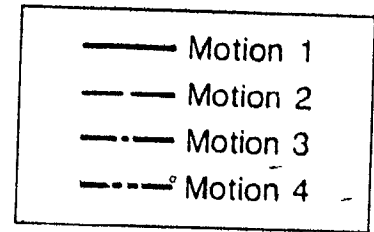
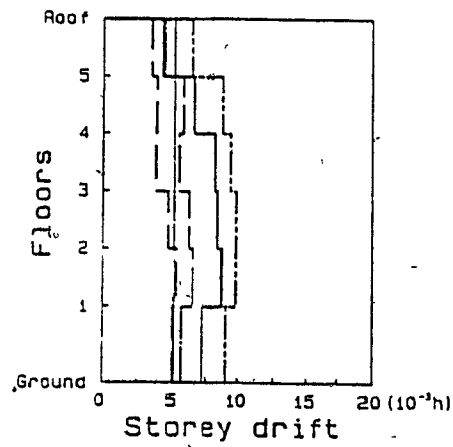


b) peak ground acceleration = 0.18g

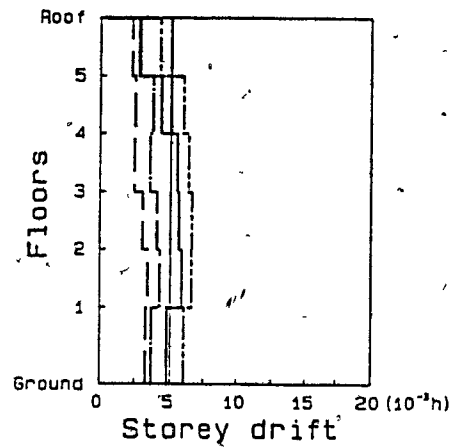


c) peak ground acceleration = 0.078g

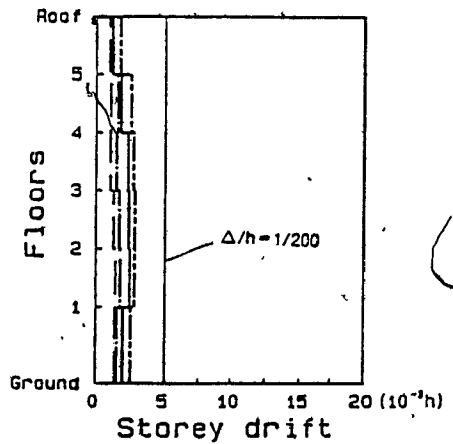
Fig. 7.16 Storey drift indices for Old K=1.3 structure in Montreal



a) peak ground acceleration = 0.27g

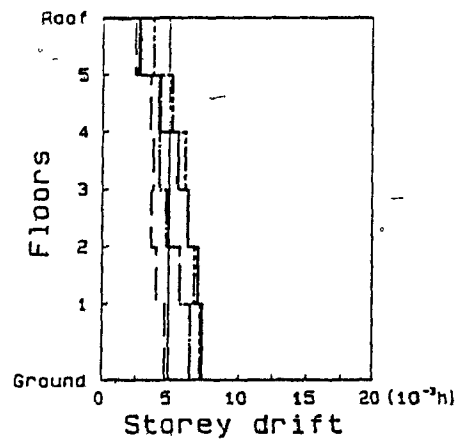


b) peak ground acceleration = 0.18g

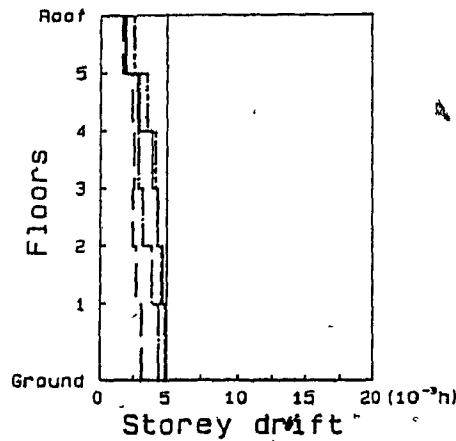


c) peak ground acceleration = 0.078g

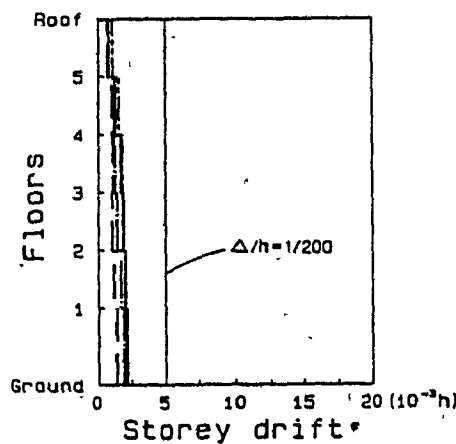
Fig. 7.17 Storey drift indices for $K=1.3$ structure in Montreal.



a) peak ground acceleration = 0.27g.

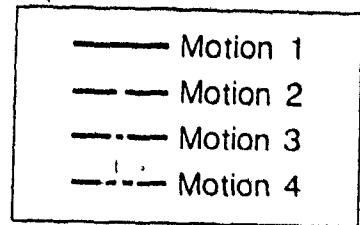
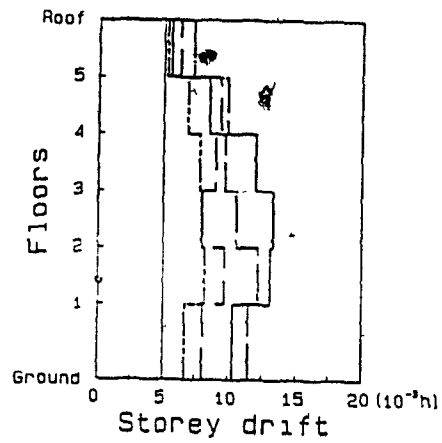


b) peak ground acceleration = 0.18g

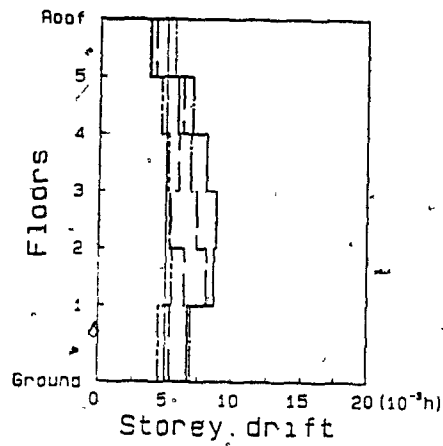


c) peak ground acceleration = 0.078g

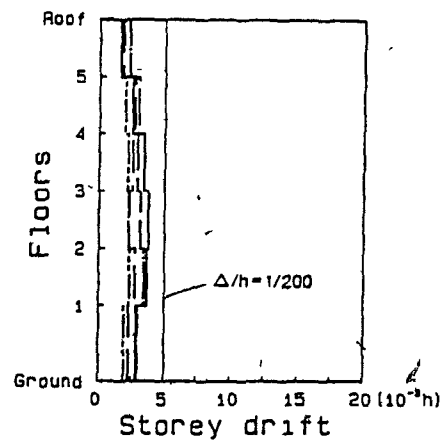
Fig. 7.18 Storey drift indices for K=0.7 structure in Montreal



a) peak ground acceleration = 0.315g

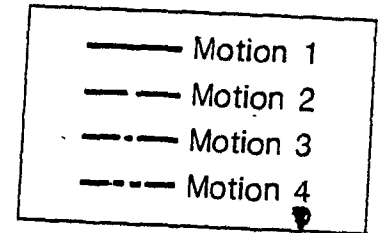
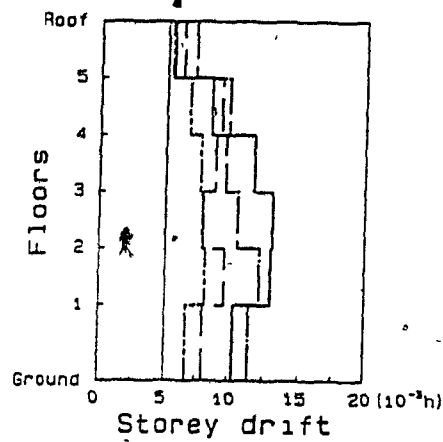


b) peak ground acceleration = 0.21g

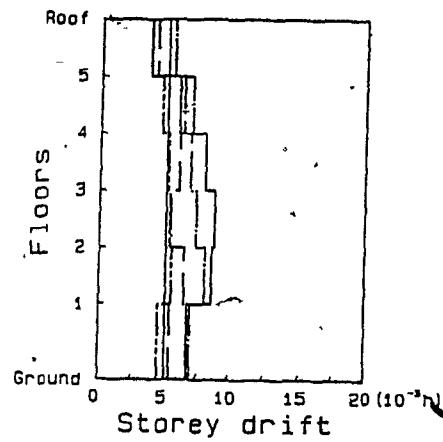


c) peak ground acceleration = 0.089g

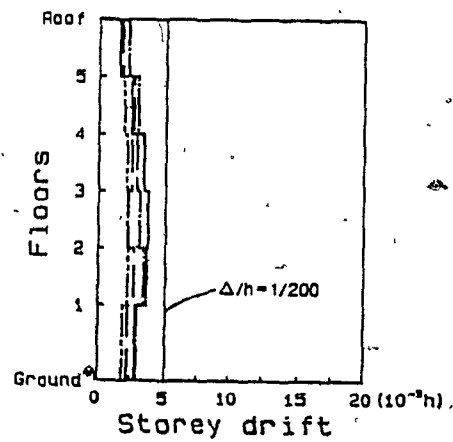
Fig. 7.19 Storey drift indices for Old K=1.3 structure in Vancouver



a) peak ground acceleration = 0.315g

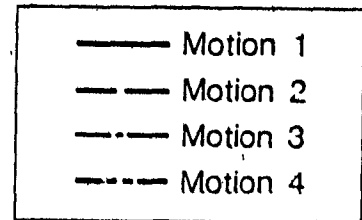
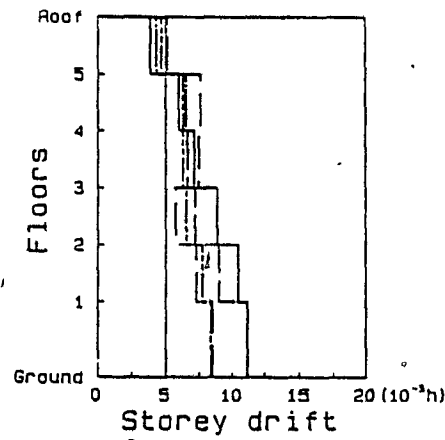


b) peak ground acceleration = 0.21g

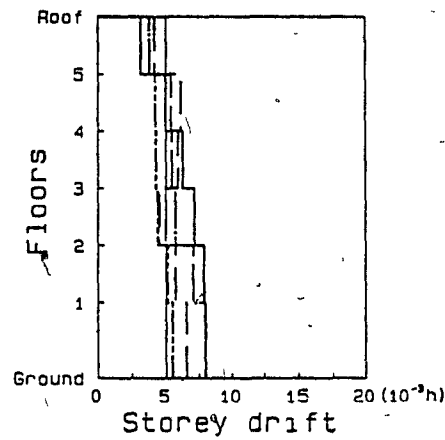


c) peak ground acceleration = 0.089g

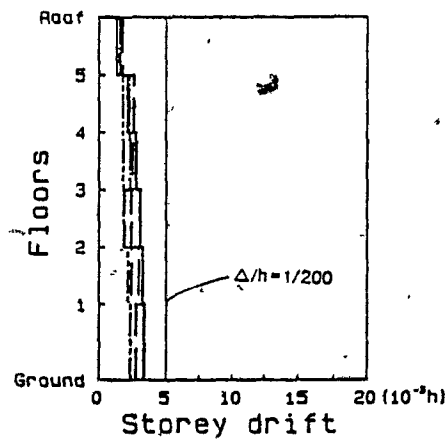
Fig. 7.20 Storey drift indices for $K=1.3$ structure in Vancouver



a) peak ground acceleration = 0.315g

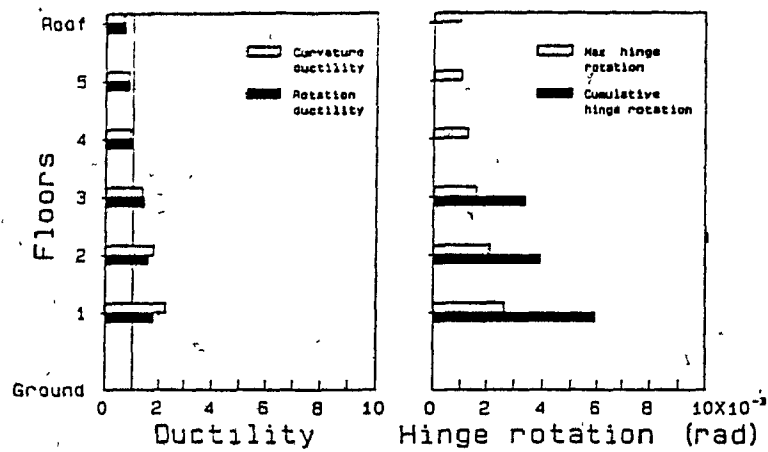


b) peak ground acceleration = 0.21g

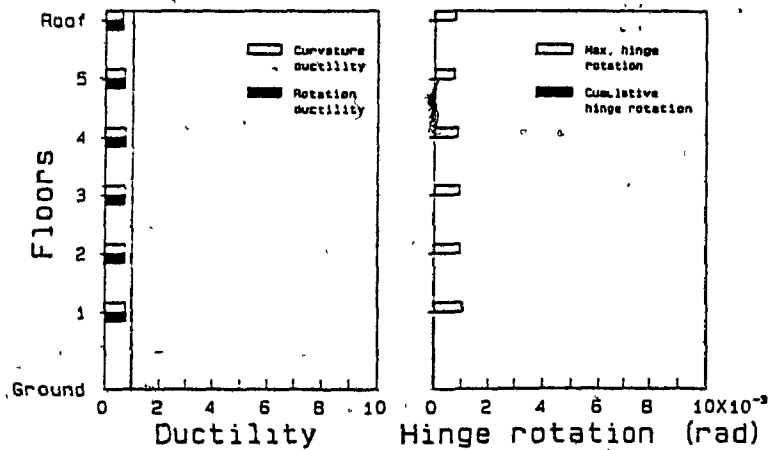


c) peak ground acceleration = 0.089g

Fig. 7.21. Storey drift indices for $K=0.7$ structure in Vancouver

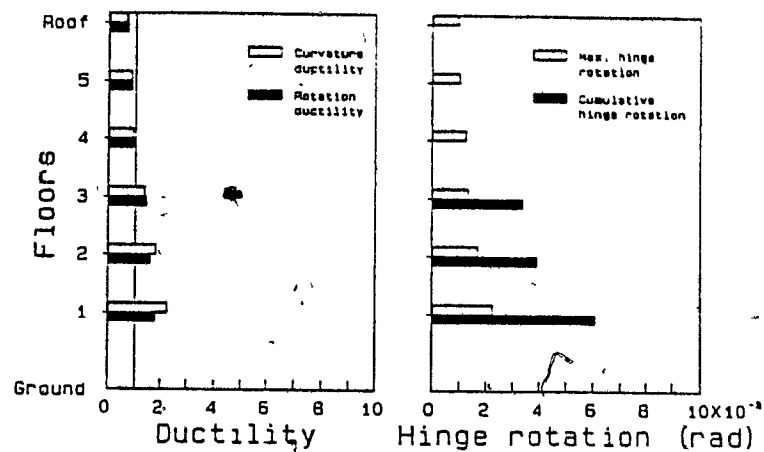


a) peak ground acceleration = 0.27g

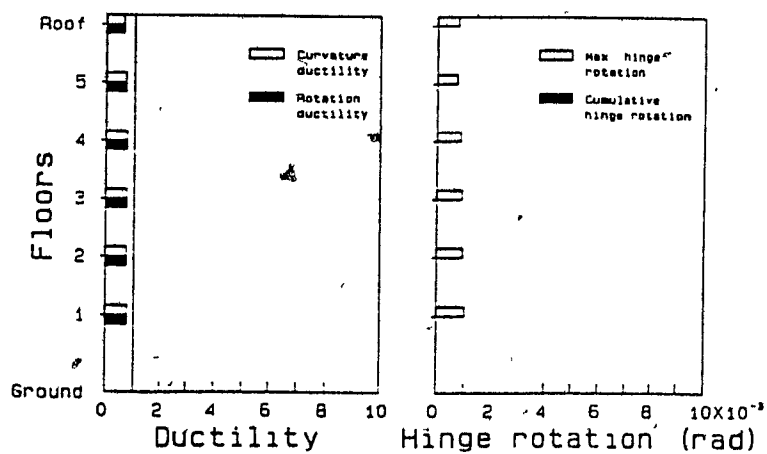


b) peak ground acceleration = 0.18g

Fig. 7.22 Estimated curvature ductilities and plastic hinge rotations for Old K=1.3 structure in Montreal

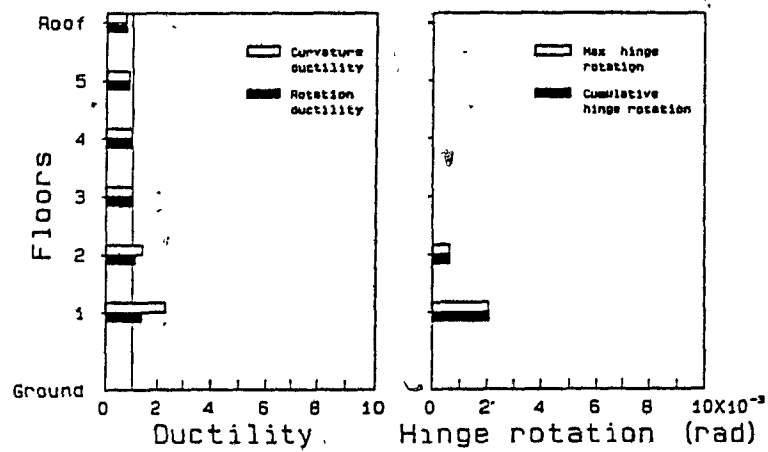


a) peak ground acceleration = 0.27g

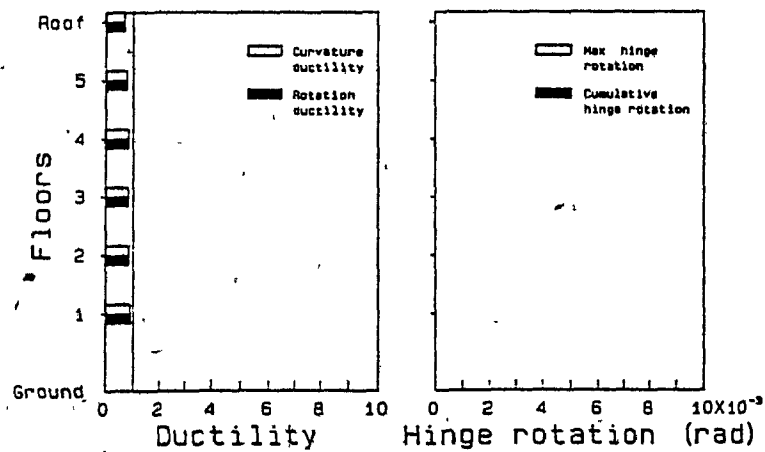


b) peak ground acceleration = 0.18g

Fig. 7.23 Estimated curvature ductilities and plastic hinge rotations for K=1.3 structure in Montreal

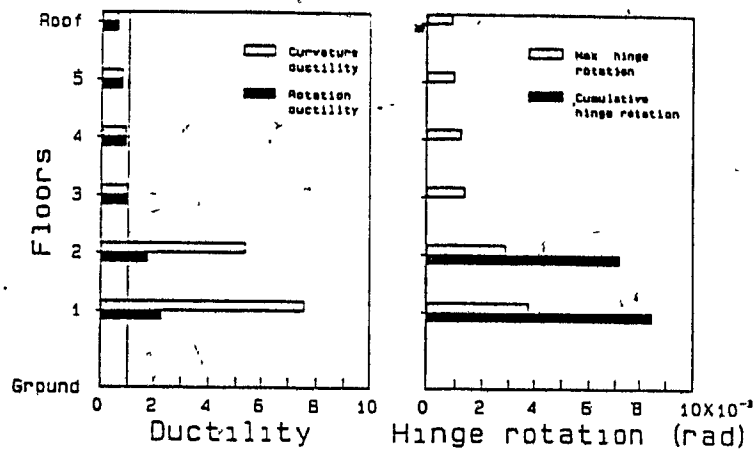


a) peak ground acceleration = 0.27g

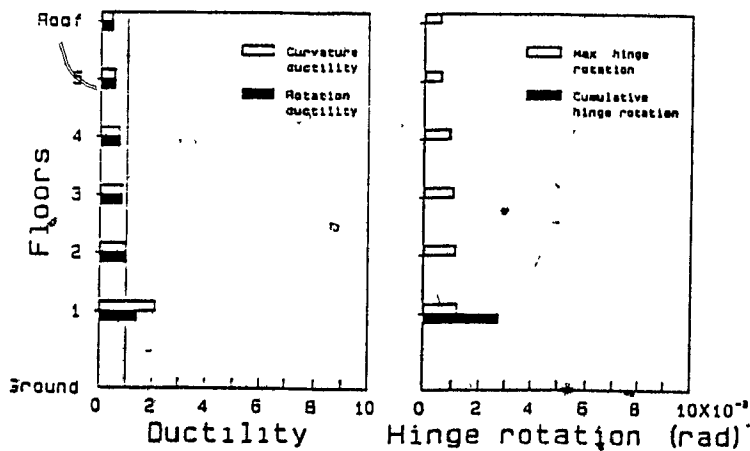


b) peak ground acceleration = 0.18g

Fig. 7.24 Estimated curvature ductilities and plastic hinge rotations for $K=0.7$ structure in Montreal

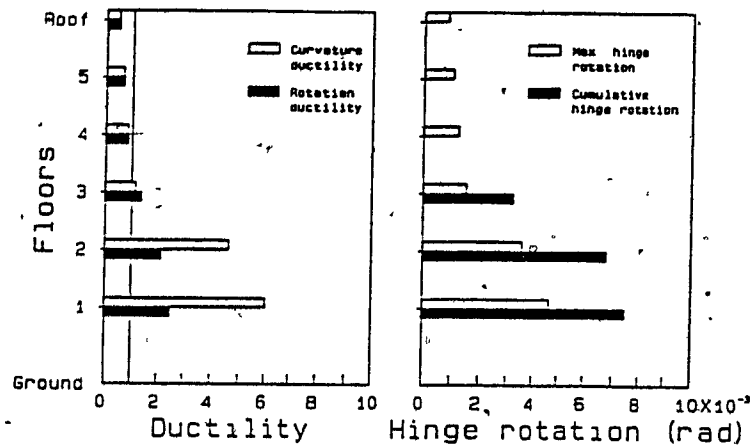


a) peak ground acceleration = 0.315g,

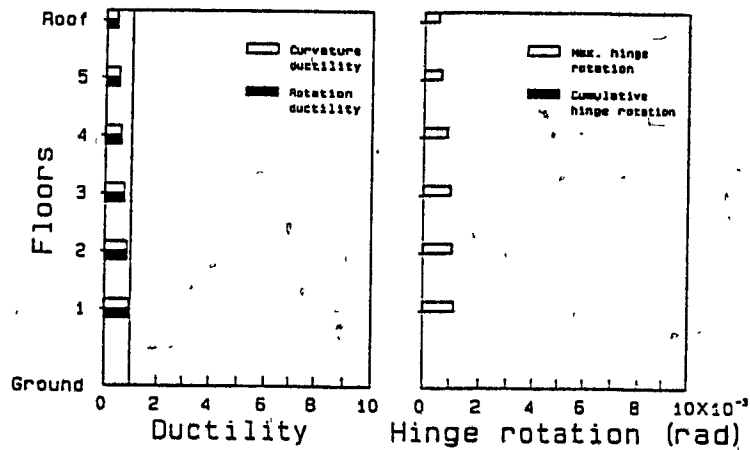


b) peak ground acceleration = 0.21g

Fig. 7.25 Estimated curvature ductilities and plastic hinge rotations for Old K=1.3 structure in Vancouver

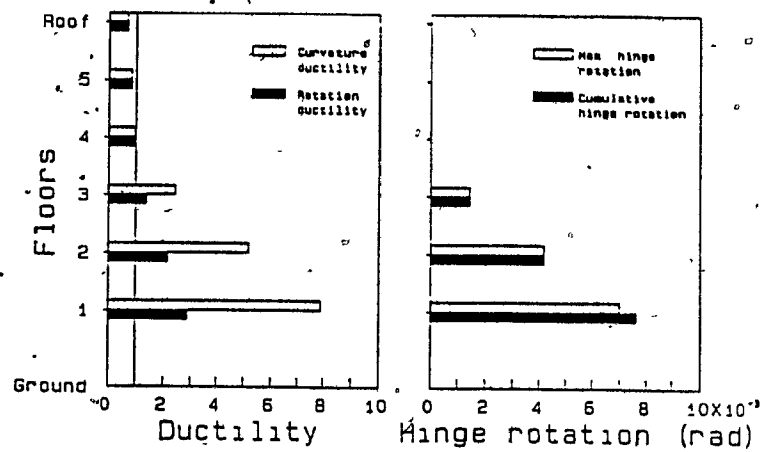


a) peak ground acceleration = 0.315g

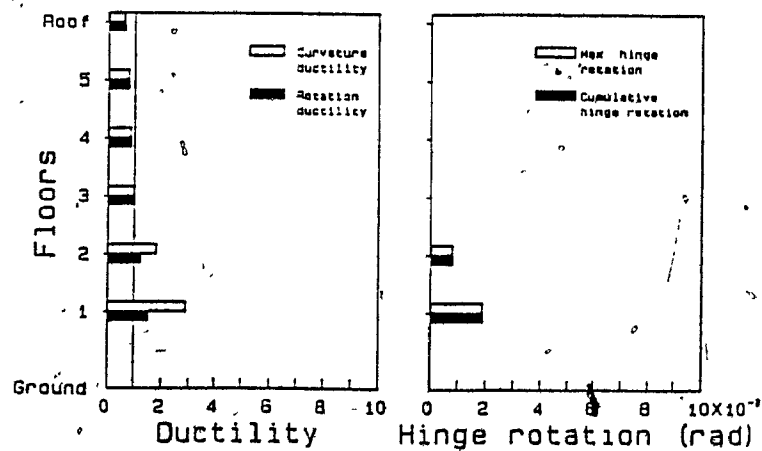


b) peak ground acceleration = 0.21g

Fig. 7.26 Estimated curvature ductilities and plastic hinge rotations for K=1.3 structure in Vancouver



a) peak ground acceleration = 0.315g



b) peak ground acceleration = 0.21g

Fig. 7.27 Estimated curvature ductilities and plastic hinge rotations for $K=0.7$ structure in Vancouver

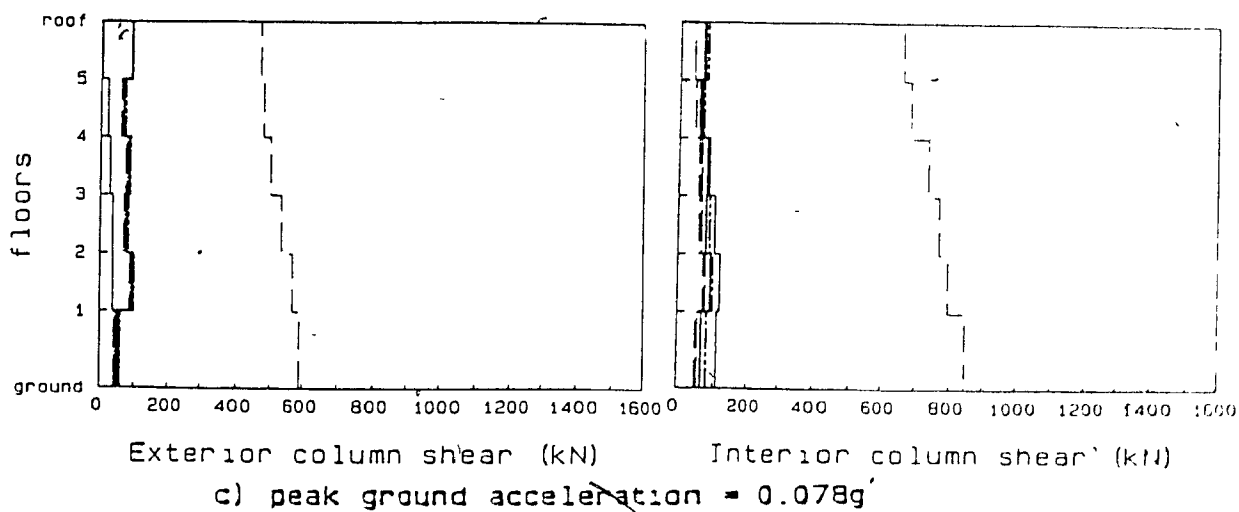
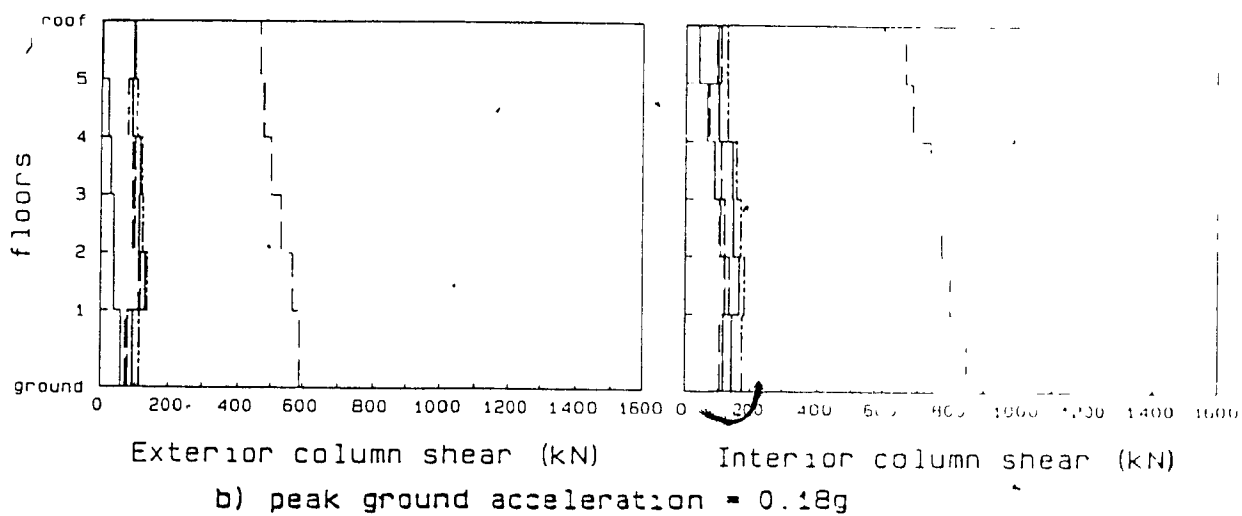
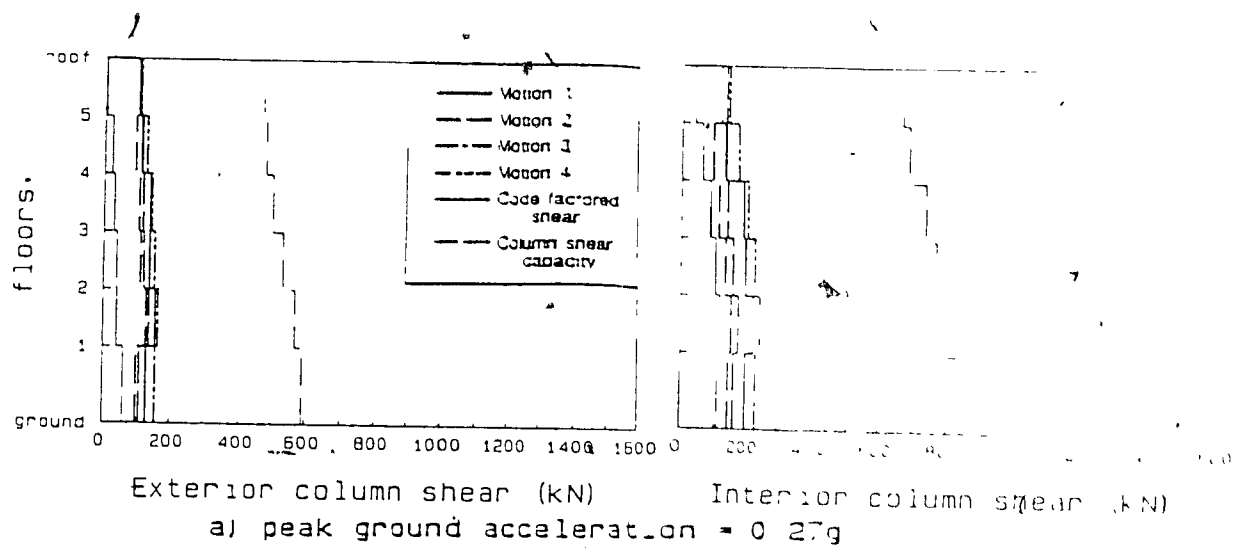
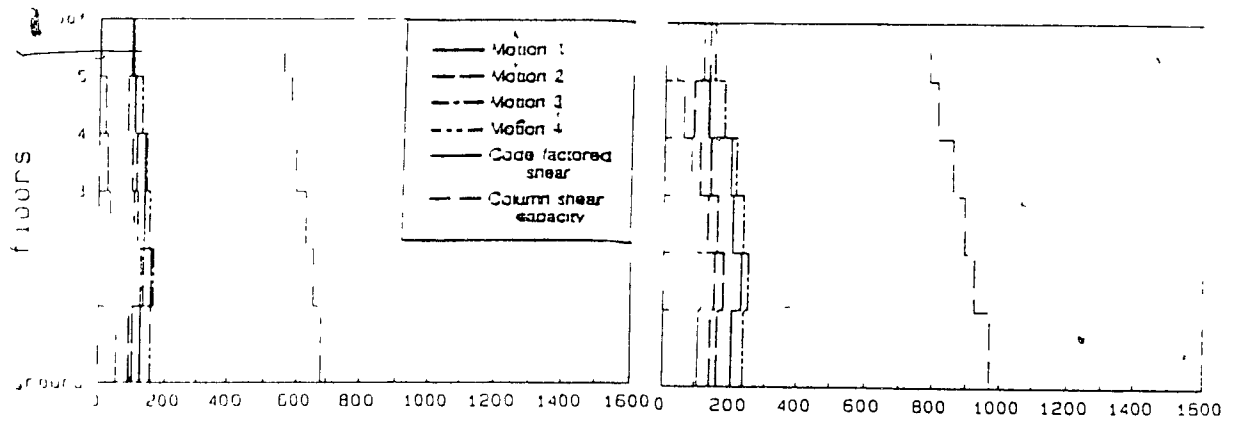
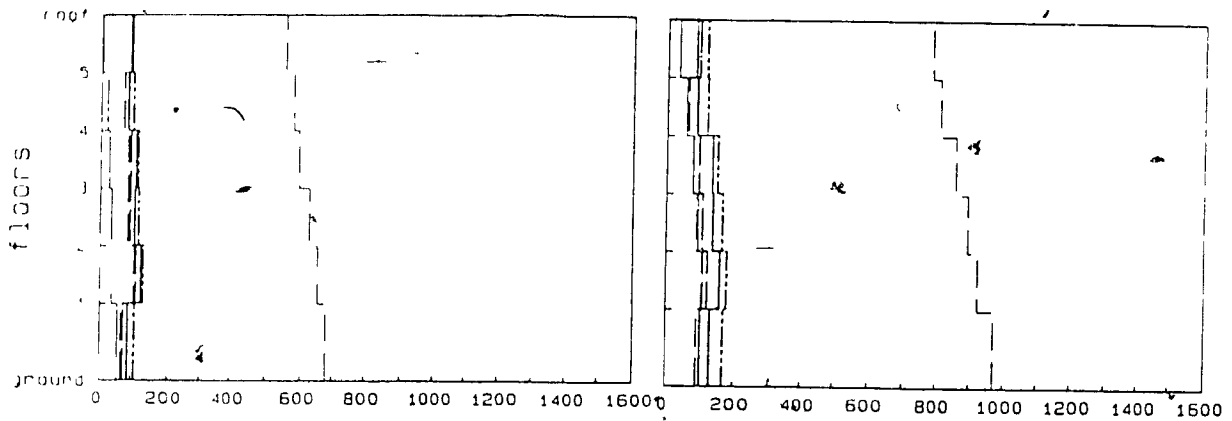


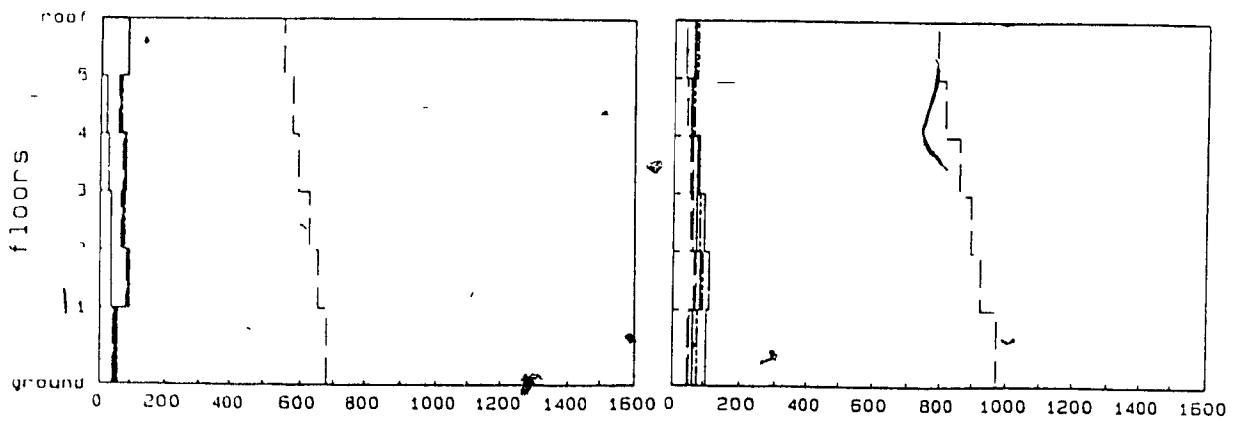
Fig. 7.28 Shear force envelopes for Old K=1.3 structure in Montreal



Exterior column shear (kN) Interior column shear (kN)
a) peak ground acceleration = 0.27g



Exterior column shear (kN) Interior column shear (kN)
b) peak ground acceleration = 0.18g



Exterior column shear (kN) Interior column shear (kN)
c) peak ground acceleration = 0.078g

Fig. 7.29 Shear force envelopes for K=1.3 structure in Montreal

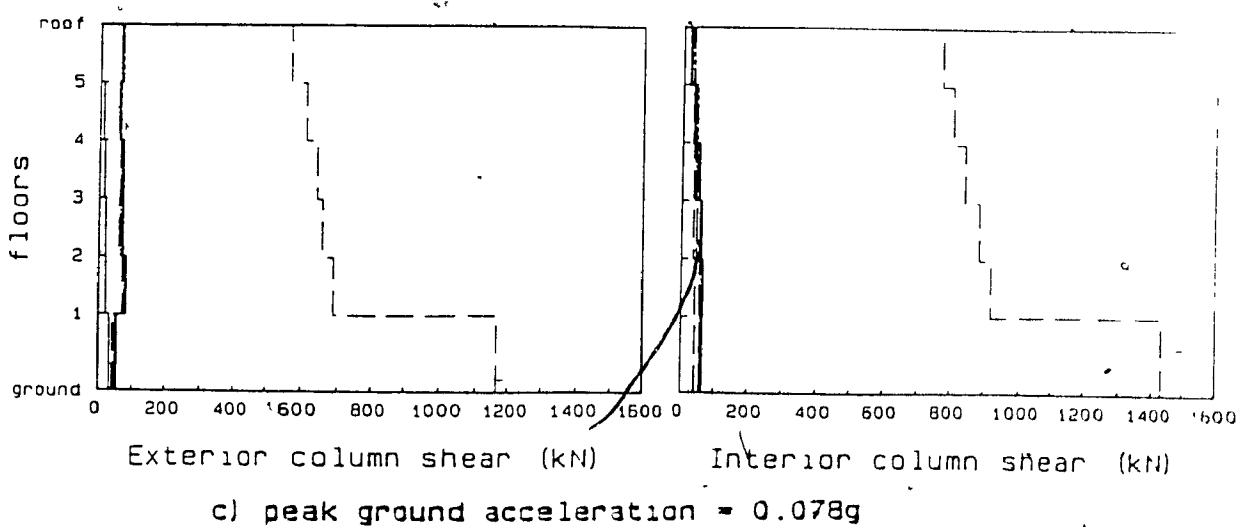
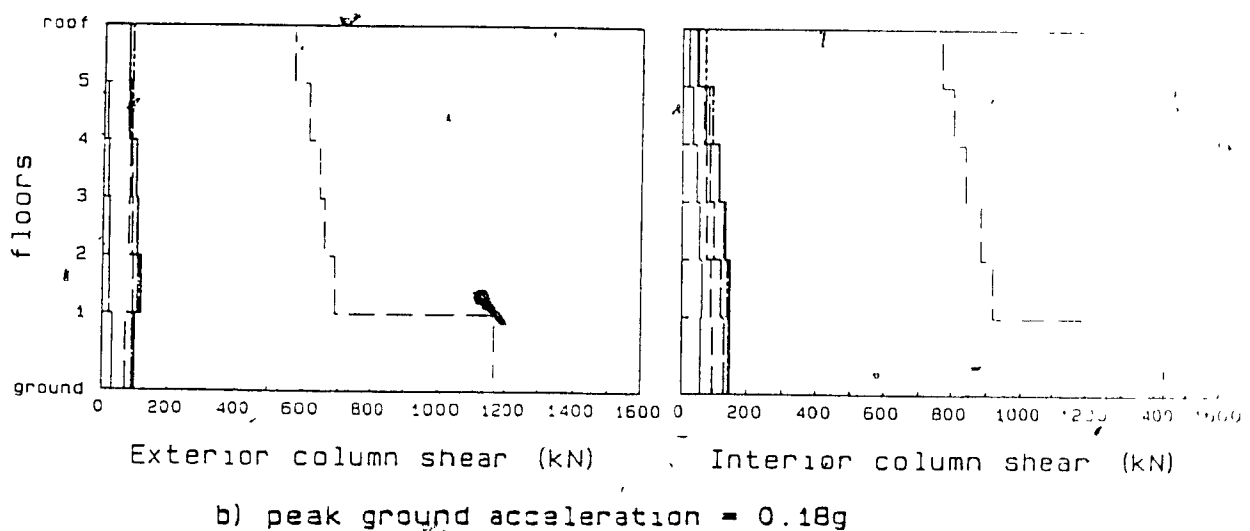
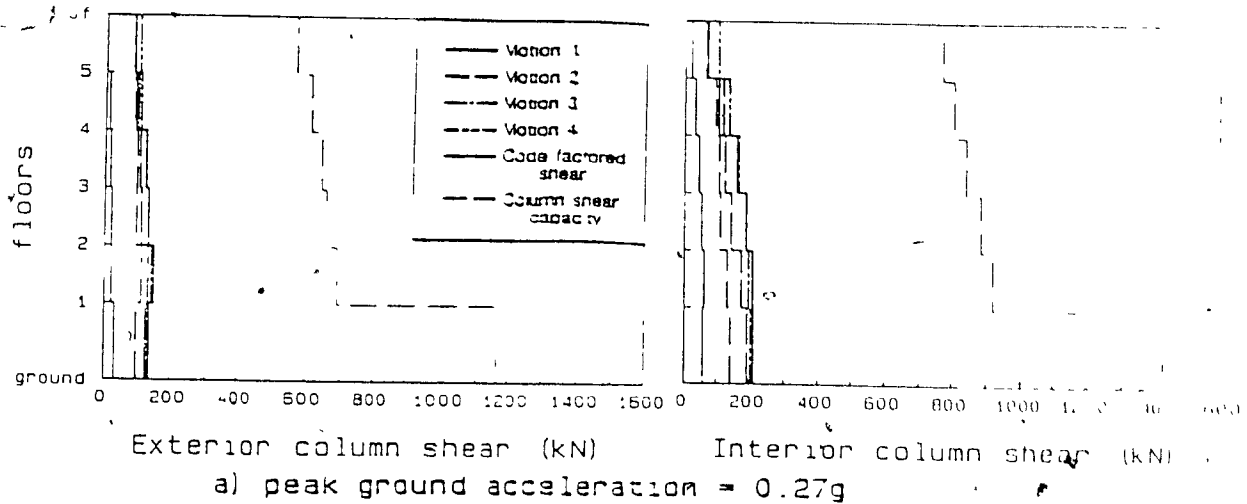


Fig. 7.30 Shear force envelopes for K=0.7 structure in Montreal

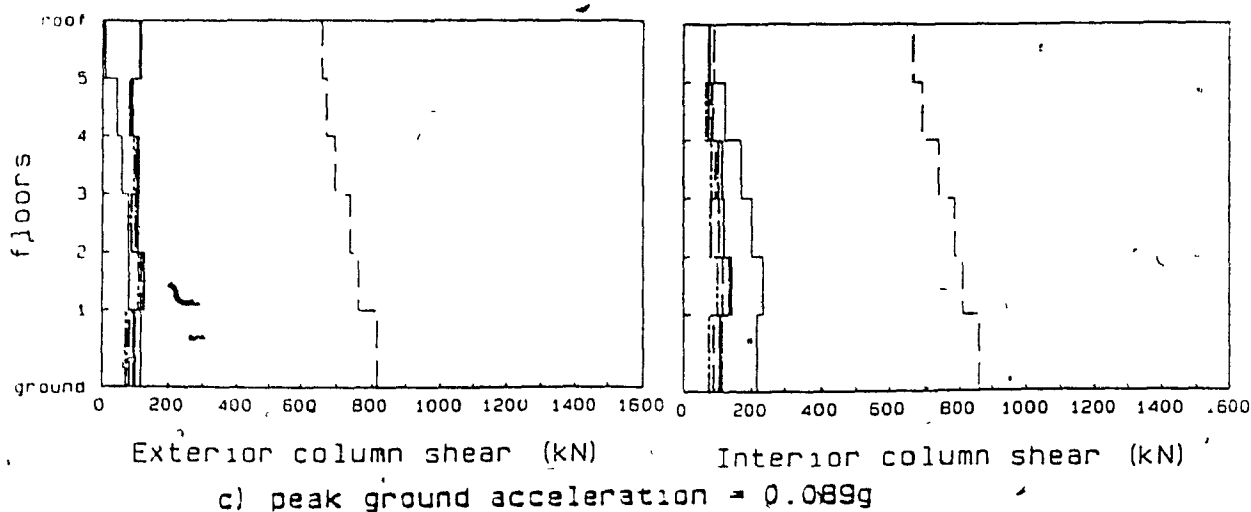
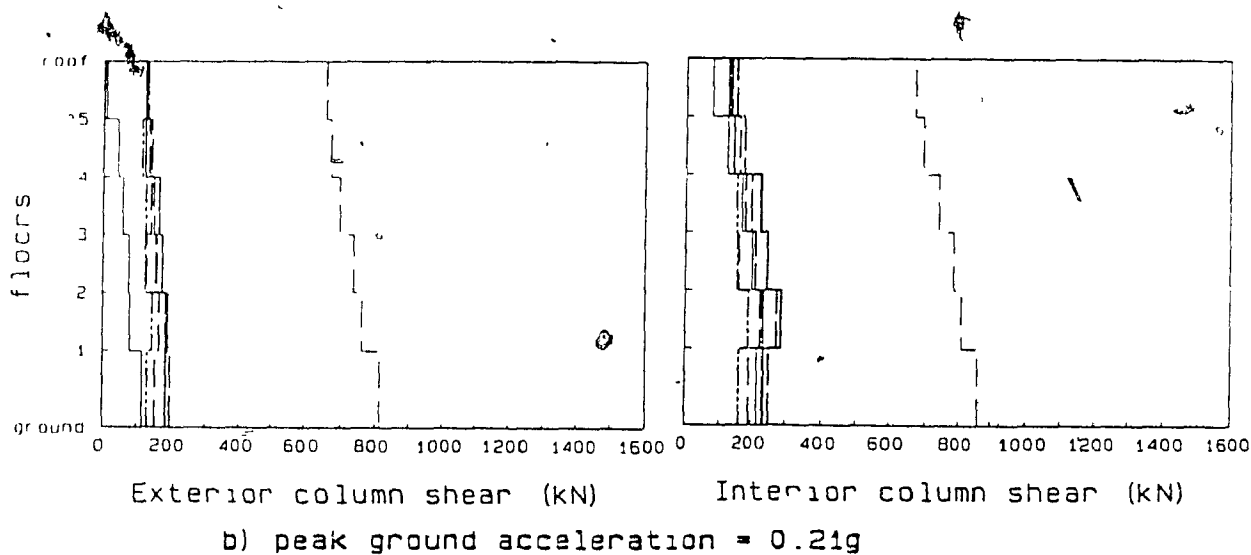
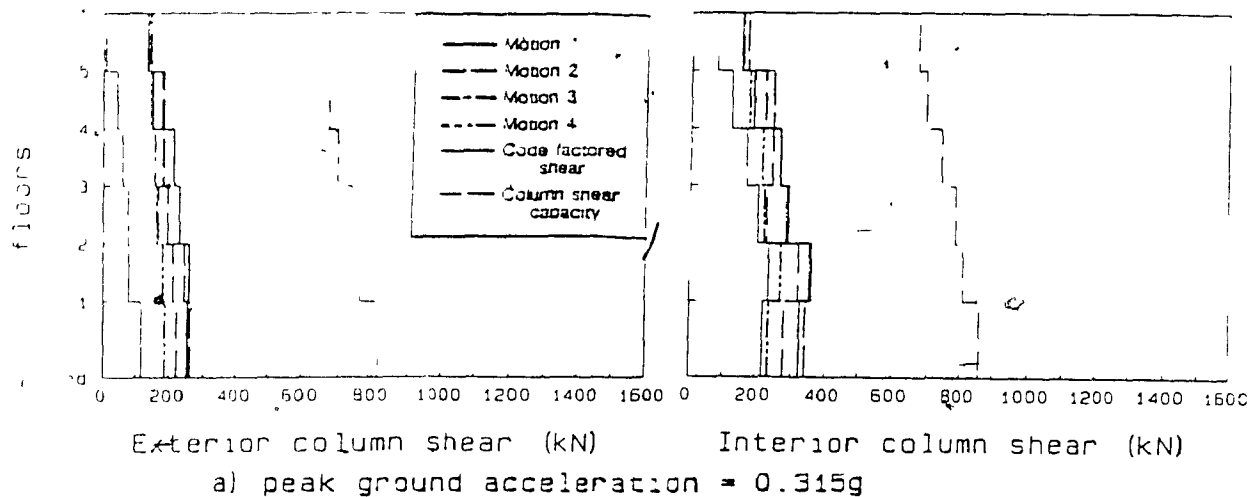
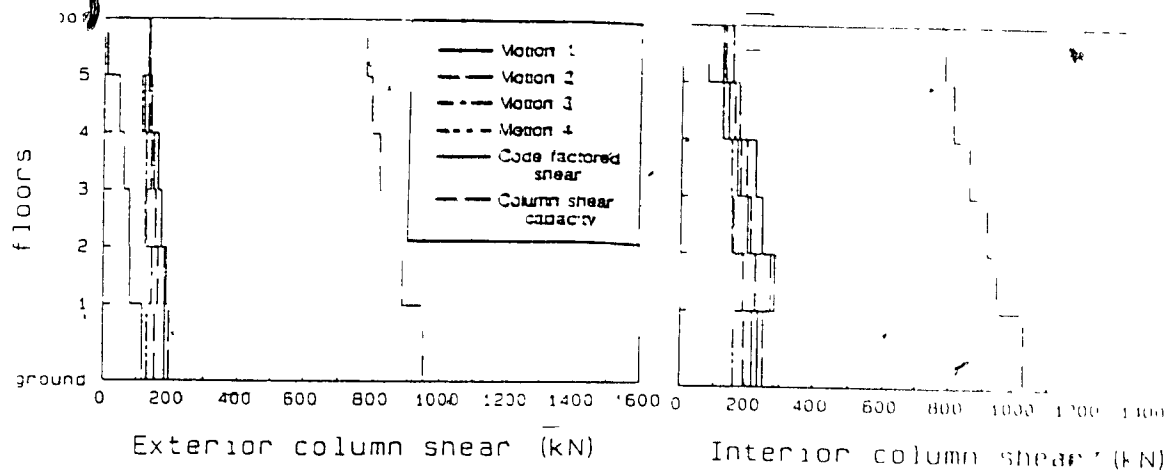
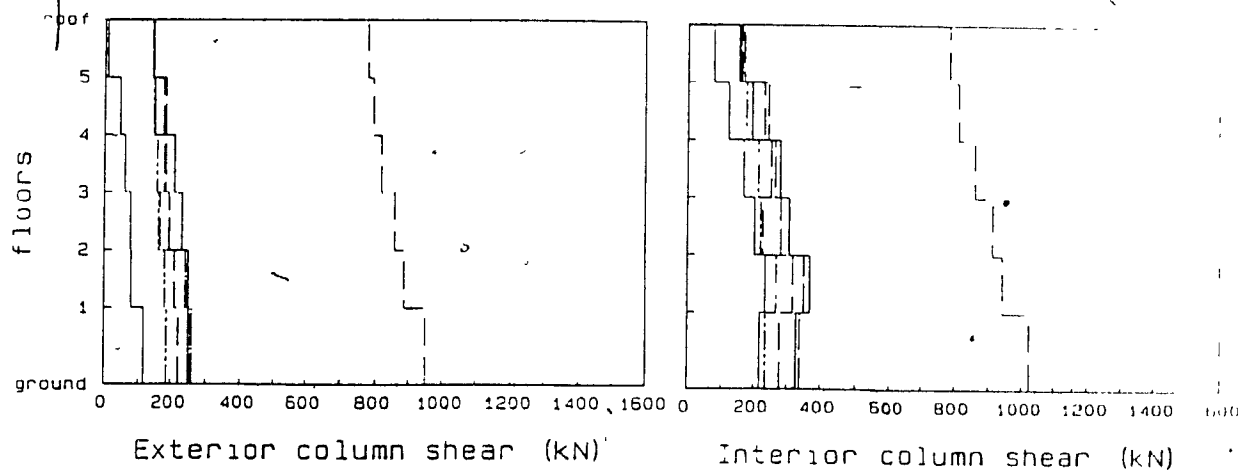


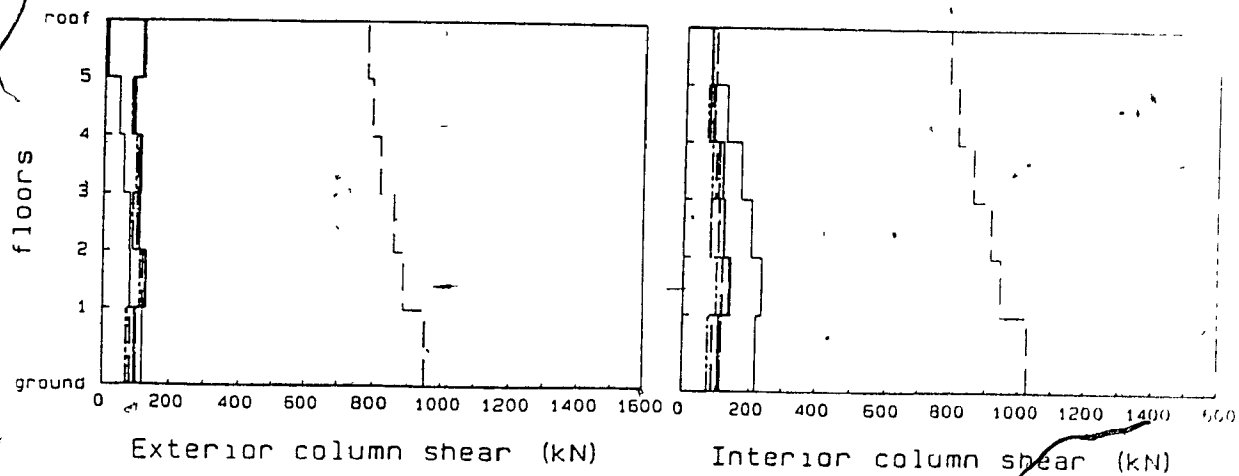
Fig. 7.31 Shear force envelopes for Old K=1.3 structure in Vancouver



a) peak ground acceleration = 0.315g



b) peak ground acceleration = 0.21g



c) peak ground acceleration = 0.089g

Fig. 7.32 Shear force envelopes for K=1.3 structure in Vancouver

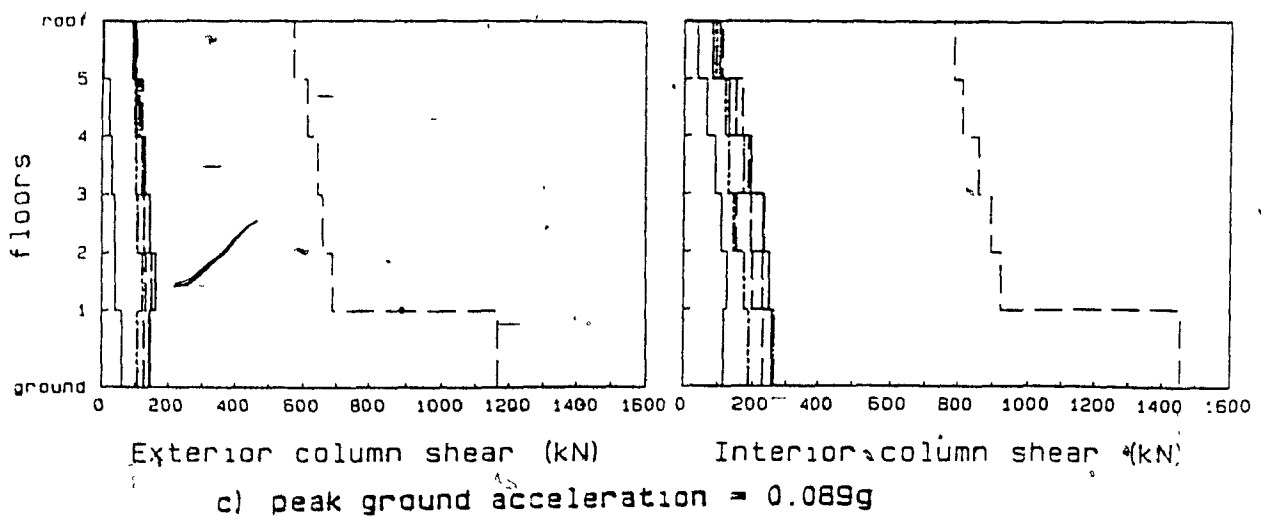
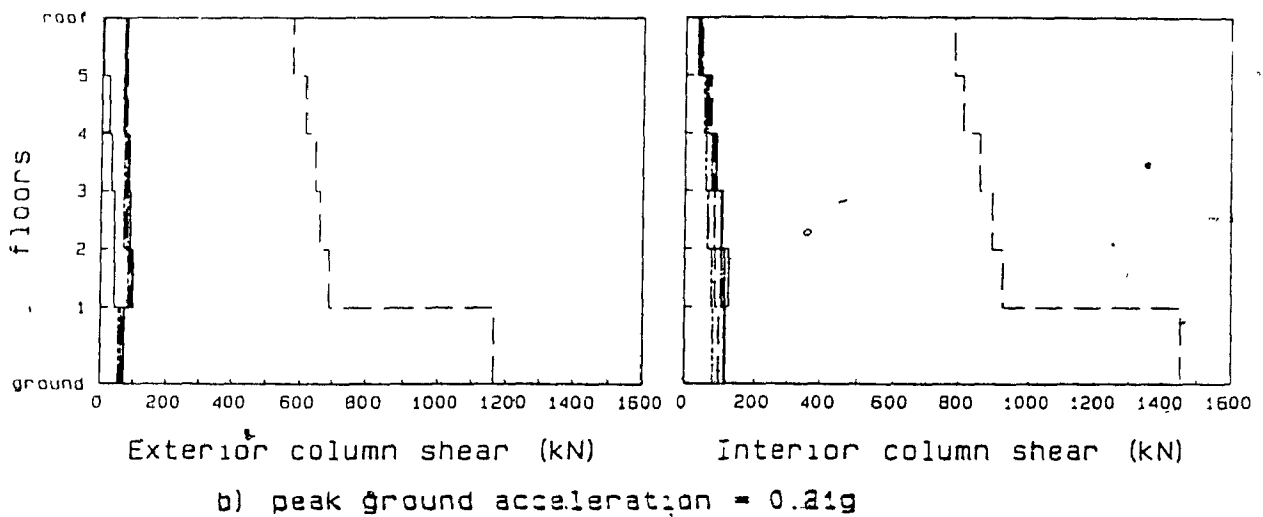
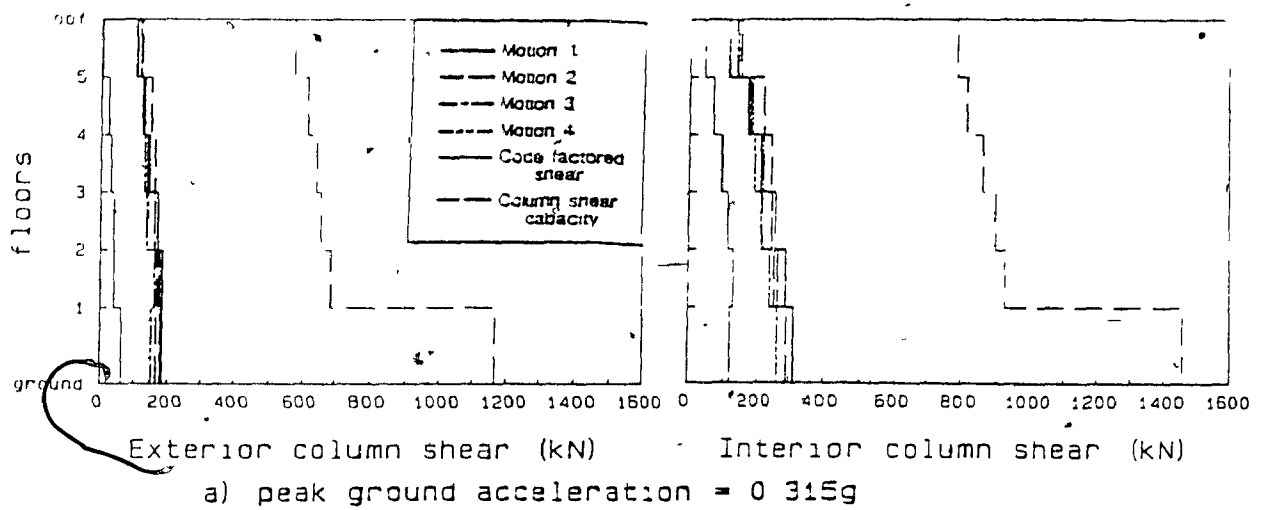
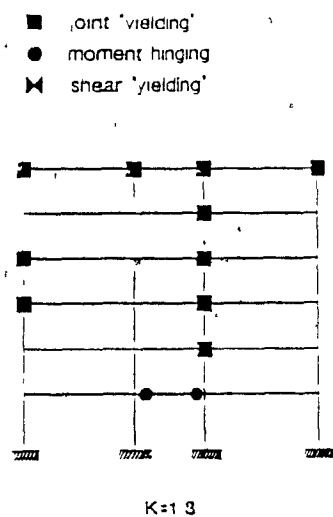
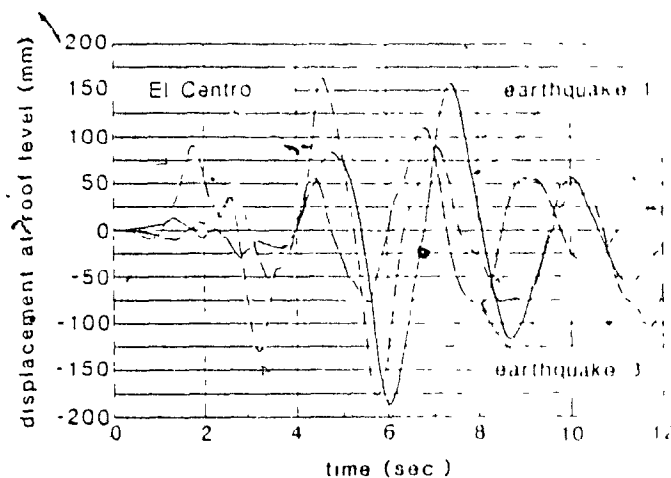


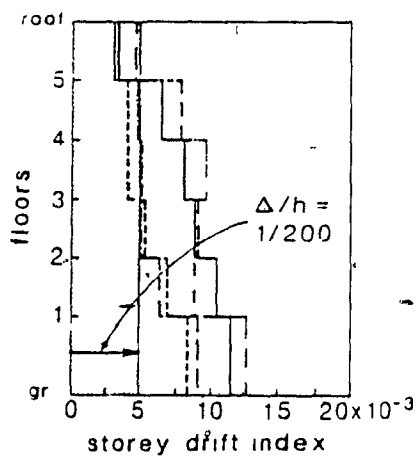
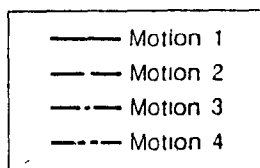
Fig. 7.33 Shear force envelopes for $K=0.7$ structure in Vancouver



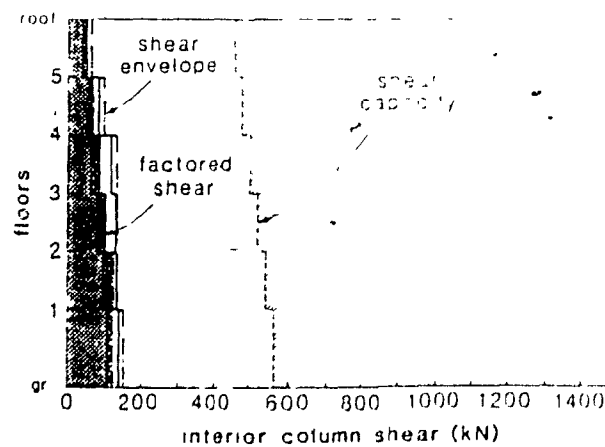
a) Hinge locations



b) Horizontal roof displacements



c) Interstorey drift envelopes



d) Shear force envelopes

Fig. 7.34 Summary of non-linear dynamic analyses for K=1.3 structure in Montreal with smaller columns

CHAPTER 8

DESIGN RECOMMENDATIONS AND CONCLUSIONS

The design recommendations and conclusions obtained from the test results and the non-linear dynamic analyses are given below:

- 1) The tests clearly indicated that the reinforcement in the slab contributes significantly to the response by increasing the beam strength and reducing the negative moment ductility of the beam. If this effect is not accounted for in the design process then the ratio of the column strength to the beam strength may be different than that assumed. This may lead to "weak-columns" and "strong-beams" which could alter the failure mode and significantly reduce the overall ductility of the structure.
- 2) A simple method of determining the "effective width" of the slab, which accounts for the role of the spandrel beam, is presented. The spandrel beam transmits eccentric tensile forces from the slab reinforcing bars by torsion in the spandrel beam to the column joint region. With increasing negative moment in the main beam, the torsions in the spandrel beams will also increase. Therefore when torsional yielding occurs the torsional stiffness drops, thus limiting the number of slab bars that are effective. The effective flange width predicted by this method agreed reasonably well with the test results. The resulting effective flange width can be significantly greater than 3 times the slab thickness, as suggested in the 1984 CSA Concrete Code [3].
- 3) A simple method of designing the shear reinforcement in the joint is proposed. This method accounts for the flow of the forces from the beam and slab reinforcement into the joint region. The forces from the beam reinforcement are transmitted,

in shear, directly into the joint while the forces from the slab reinforcement are transmitted by torsional shear flow into the side faces of the joint region. This method was verified by comparing the predictions with the test results of this experimental programme and with the test results of other researchers.

- 4) The CSA Concrete Code [3] should be more specific in requiring that all joints be designed to resist at least the factored shear. The test results indicate that joint yielding can occur prematurely in structures designed with $K=2.0$, $K=1.3$. The large number of joint failures observed in the 1985 Mexican earthquake [83] strongly emphasizes the need to address this problem.
- 5) The test specimen which was designed and detailed for $K=1.3$ according to the provisions of the 1977 [62] Canadian Concrete Code (i.e., corresponding to $K=2.0$ in the 1984 Code) displayed significant shear distress in the beam and severe buckling of the longitudinal beam bars. This test specimen exhibited a pinched hysteretic response and a severe drop in load carrying capacity after achieving a displacement ductility of about 2.8.
- 6) The test specimen which was designed and detailed with $K=1.3$ had a column which was stronger than the beam and contained shear reinforcement in the joint which was capable of transferring the shear resulting from yielding of the beam bars passing into the joint. It is noted that this amount of shear reinforcement was greater than that required in the current Canadian Concrete Code. The nominal detailing requirements of the Code resulted in excellent performance of the beam but the specimen failed by yielding of the reinforcement in the joint at a displacement ductility of 5.
- 7) The test specimen which was designed and detailed with $K=0.7$ performed very well and achieved a displacement ductility greater than 8. The additional hoops provided in the plastic hinge region were effective in preventing buckling of the bottom longitudinal beam bars and served to confine the concrete in the compression zone. The moments and shears in the columns were well below yielding.
- 8) The computer programs developed to analyze the response of reinforced concrete members subjected to axial-load, moment and shear were capable of accounting

for the combined loading effects, the complete stress-strain relationship for the reinforcement, the non-linear stress-strain relationship for the concrete including confinement, non-linear strain distribution in flanged sections, and spalling of the concrete cover. These programs enabled the axial-load-moment interaction diagrams, as well as moment-curvature responses to be predicted. In addition these programs enabled complete flexure-shear analysis of the beams in order to predict the shear and flexure deformations. The predictions of the responses agreed very well with the experimental observations.

- 9) As other researchers have found, the non-linear dynamic responses depend largely on the details of the ground motions, with ground motions having similar general characteristics giving different responses. Because of the large variation in the responses the results of the non-linear dynamic analyses are evaluated as a range of possible responses from the different earthquake motions.
- 10) As observed by other researchers it was found that the maximum roof displacements predicted for all six structures for the non-linear responses were approximately equal to the displacements predicted by the linear responses for the same motion.
- 11) The Montreal and Vancouver structures which were designed and detailed for $K=1.3$ according to the provisions of the 1973 Canadian Concrete Code (i.e., corresponding to $K=2.0$ in the 1984 Code) displayed large interstorey drifts. These large drifts were due mainly to the significant shear distortions of the joint regions in the lower storeys, yielding of the joint regions in the upper storeys and flexural yielding in some beams in the first two storeys. In the Vancouver structure the shorter interior beams also yielded in shear and would have also displayed significant buckling of the longitudinal beam bars. It is noted that the shear design for these beams was governed by minimum shear reinforcement requirements. Although many of the older designs may not have included shear reinforcement in the joints, the joints of these structures contained three sets of #3 ties (either three or four legs). The large predicted interstorey drifts together with the "poor" construction quality classification assigned to these buildings, resulted in very large

structural damage estimates for the most severe earthquakes investigated. It is emphasized that considerably more damage or even collapse of these structures would have been predicted if ties in the joints were not provided.

- 12) The Montreal and Vancouver structures which were designed and detailed for $K=1.3$ according to the 1984 Canadian Concrete Code [3] had columns which were stronger than the beams and contained joint reinforcement sufficient to permit yielding of the beam reinforcement. The reinforcement provided in the beams to achieve a level of "nominal ductility" as required by the Code prevented any shear problems in the beams. The responses of these structures were similar to the responses of the older structures described above. The large interstorey drifts were due mainly to large joint shear distortions and to flexural yielding of some beams in the first two storeys. Although the interstorey drifts were similar to those predicted for the older structures designed with $K=1.3$, the "average" construction quality classification due to the "nominal ductility" details resulted in significantly less structural damage than that predicted for the older structures.
- 13) The predicted responses of a Montreal structure designed with $K=1.3$ but with slightly smaller columns resulted in a significant increase in the number of joint hinges together with an increase in interstorey drifts. This study underlines the need to properly design the joints for shear and raises concern over the ability of older structures, with little or no shear reinforcement in the joints, to withstand moderate or large earthquakes.
- 14) The Montreal and Vancouver structures which were designed and detailed for $K=0.7$ according to the 1984 Canadian Concrete Code [3] satisfied the requirements corresponding to ductile moment resisting frames. These structures displayed smaller interstorey drifts than the $K=1.3$ structures due to the insignificant joint shear distortions, the absence of any shear problems in the beams and the ability to dissipate large amounts of energy. The small interstorey drifts together with the "good" construction quality, assigned to these well detailed structures, resulted in very light structural damage.
- 15) The test results and the non-linear dynamic analyses indicate the improved perfor-

mance of the structures designed according to the 1984 Canadian Concrete Code [3]. Structures designed with $K=1.3$ performed significantly better than structures designed with $K=1.3$ from previous codes. Further research is currently being carried out at McGill University to investigate the response of structures designed with $K=1.3$ having columns weaker than the beams and with only minimum shear reinforcement in the joints.

- 16) Further research is needed to study problems associated with existing buildings that do not satisfy the requirements of current codes and to study practical solutions for upgrading older concrete structures.

REFERENCES

- [1] Newmark, N. M. and Rosenblueth, E., *Fundamentals of Earthquake Engineering*, Prentice-Hall Inc., Englewood Cliffs, N.J., 1971, 640 p.
- [2] Associate Committee on the National Building Code, "National Building Code of Canada 1985" and "Supplement to the National Building Code of Canada 1985", National Research Council of Canada, Ottawa, 1985, 454 pp. and 278 pp.
- [3] Canadian Standards Association, "CSA Standard CAN3-A23.3-M84, Design of Concrete Structures for Buildings", Rexdale, December 1984, 282 pp.
- [4] Associate Committee on the National Building Code, "National Building Code of Canada 1953", National Research Council of Canada, Ottawa, 1953.
- [5] Associate Committee on the National Building Code, "National Building Code of Canada 1970", National Research Council of Canada, Ottawa, 1970.
- [6] Milne, W. G., and Davenport, A. G., "Distribution of Earthquake Risk in Canada", *Bulletin of the Seismological Society of America*, Vol. 59, 1969, pp. 729-754.
- [7] Cornell, C. A., "Engineering Seismic Risk Analysis", *Bulletin of the Seismological Society of America*, Vol. 65, No. 6, 1975, pp. 1583-1606.
- [8] Mahin, S. A., and Bertero, V. V., "Rate of loading effect on Uncracked and Repaired Reinforced Concrete Members" *EERC Report No. 72-9*, Earthquake Engineering Research Center, University of California, Berkeley, 1972, 315 p.
- [9] Blume, J. A., Newmark, N. M. and Corning, L. H., *Design of Multi-Story Reinforced Concrete Buildings for Earthquake Motions*, fourth edition, Portland Cement Association, Chicago, Illinois, 1961, 318 p.
- [10] Ma, S. M., Bertero, V. V., and Popov, E. P., "Experimental and Analytical Studies on the Hysteretic Behaviour of Reinforced Concrete Rectangular and T-Beams", *EERC Report No. 76-2*, Earthquake Engineering Research Center, University of California, Berkeley, May 1976, 241 p.
- [11] Bertero, V. V., and Popov, E. P., "Seismic Behaviour of Ductile Moment-Resisting Reinforced Concrete Frames", *Reinforced Concrete Structures in Seismic Zones*, Publication SP-53, American Concrete Institute, Detroit, 1977, pp. 247-291.
- [12] Paulay, T., "Capacity Design of Reinforced Concrete Ductile Frames", *Proceedings Workshop on Earthquake-Resistant Reinforced Concrete Building Construction*, University of California, Berkeley, July 11-15, 1977, Vol. III, pp. 1043-1075
- [13] Park, R., "Accomplishments and Research and Development Needs in New-Zealand", *Proceedings Workshop on Earthquake-Resistant Reinforced Concrete Building Construction*, University of California, Berkeley, July 11-15, 1977, Vol. II, pp. 255-295.
- [14] Kent, D. C., and Park, R., "Flexural Members with Confined Concrete", *Journal of the Structural Division, ASCE*, Vol. 97, ST7, July 1971, pp. 1969-1990.
- [15] Sheikh, S., and Uzumeri, S.M., "Strength and Ductility of Tied Concrete Columns", *Journal of the Structural Division, ASCE*, Vol. 106, ST5, May 1980, pp. 1079-1102.

- [16] Uzumeri, S. M., "Strength and Ductility of Cast-In-Place Beam-Column Joints", *Reinforced Concrete Structures in Seismic Zones*, Publication SP-53, American Concrete Institute, Detroit, 1977, pp 293-350.
- [17] Uzumeri, S. M., and Seckin, M., "Behaviour of Reinforced Concrete Beam-Column Joints Subjected to Slow Load Reversals", Publication No. 74-05, Department of Civil Engineering, University of Toronto, March 1974, 85 p.
- [18] Park R., and Paulay, T., *Reinforced Concrete Structures*, John Wiley & Sons, New York, 1975. 769 pp
- [19] Paulay, T., Park, R., and Priestly, M. J. N., "Reinforced Concrete Beam-Column Joints Under Seismic Actions", *ACI Journal, Proceedings* V 75, No. 11, Nov. 1978, pp. 585-593.
- [20] Zhu, S., and Jirsa, J. O., "A Study of Bond Deterioration in Reinforced Concrete Beam-Column Joints", *PMFSEL Report No. 83-1*, The University of Texas at Austin, July 1983, 69 p.
- [21] Charney, F. A., and Chowdhury, A. A., "Correlation of the Analytical and Experimental Responses of a 1/5-Scale Model Seven-Story R/C Frame-Wall Structure", *Proceedings of the Eighth World Conference on Earthquake Engineering*, San Francisco, California, U.S.A., July 21-28, 1984, Vol. VI, pp. 659-666
- [22] Ehsani, R. M., and Wight, J. K., "Behaviour of External Reinforced Concrete Beam to Column Connections Subjected to Earthquake Type Loading", *UMEE 82R5*, The University of Michigan, Department of Civil Engineering, July 1982, 243 p.
- [23] Ehsani, M. R., and Wight, J. K., "Effect of Transverse Beams and Slabs on Behaviour of Reinforced Concrete Beam-to-Column Connections", *ACI Journal, Proceedings*, V. 82, No. 17, March-April 1985, pp. 188-195.
- [24] Ehsani, M. R., and Wight, J. K., "Exterior Reinforced Concrete Beam to Column Connections Subjected to Earthquake-Type Loading", *ACI Journal, Proceedings*, V. 82, No. 43, July-August 1985, pp. 492-497.
- [25] Hawkins, N. M., and Lin, I. J., "Bond Characteristics of Reinforcing Bars for Seismic Loading", *Third Canadian Conference on Earthquake Engineering*, Montreal, Canada, June 1979, Vol. II, pp. 1225-1252.
- [26] Veletsos, A. S. and Newmark, N. M., "Effect of Inelastic Behaviour on the Response of Simple Systems to Earthquake Motions", *Proceedings 2nd World Conference on Earthquake Engineering*, Tokyo and Kyoto, 1960, Vol II, pp. 895-912.
- [27] Mahan, S. A., and Bertero, V. V., "An Evaluation of Some Methods for Predicting Seismic Behavior of Reinforced Concrete Buildings", *EERC Report No. 75-5*, Earthquake Engineering Research Center, University of California, Berkeley, 1975.
- [28] Clough, R. W., Benuska, K. L., and Wilson, E. L., "Inelastic Earthquake Response of Tall Buildings", and Discussions, *Proceedings of the Third World Conference on Earthquake Engineering*, Auckland and Wellington, New-Zealand, 1965, Vol. II, pp. 68-89.
- [29] Clough, R. W., and Benuska, K. L., "FHA Study of Seismic Design Criteria for High Rise Buildings", T.Y. Lin and Associates, Consulting Engineers, 1966, 368 p.

- [30] Paulay, T., "Capacity Design of Resisting Ductile Multistorey Reinforced Concrete Frames", *Third Canadian Conference on Earthquake Engineering*, Montreal, Canada, June 1979, Vol II, pp 917-947.
- [31] Clough, R. W. and Johnston, S. B., "Effect of Stiffness Degradation on Earthquake Ductility Requirements" *Proceedings of Japan Earthquake Engineering Symposium*, Tokyo, 1966, pp 227-232.
- [32] Clough, R. W., "Predicting the Earthquake Response of Reinforced Concrete Structures", *Reinforced Concrete Structures in Seismic Zones*, Publication SP-53, American Concrete Institute, Detroit, 1977, pp. 59-79
- [33] Hidalgo, P. and Clough, R. W., "Earthquake simulator study of a Reinforced Concrete Frame", *EERC Report No. 74-13*, Earthquake Engineering Research Center, University of California, Berkeley, 1972.
- [34] Takeda, T., Sozen, M. A. and Nielsen, N. N., "Reinforced Concrete Response to Simulated Earthquakes" *Journal of the Structural Division, ASCE*, Vol. 96, No. ST12, December 1970, pp 2557-2573.
- [35] Otani, S. and Sozen, M. A., "Behavior of Multistory Reinforced Concrete Frames During Earthquakes", *Structural Research Series No. 392*, University of Illinois, Urbana, Illinois, 1972, 551 p
- [36] Litton, R. W., "A Contribution to the Analysis of Concrete Structures under Cyclic Loading", Ph.D. Thesis, University of California, Berkeley, June 1975, 146 p
- [37] Kanaan, A. E., and Powell, G. H., "DRAIN-2D A General Purpose Computer Program for Dynamic Analysis of Inelastic Plane Structures", *EERC Report No. 73-22*, Earthquake Engineering Research Center, University of California, Berkeley, Aug. 1975, 138 p
- [38] Umemura, H. and Takizawa, H., "Dynamic Response of Reinforced Concrete Buildings", *Structural Engineering Documents 2*, International Association for Bridge and Structural Engineering, Zurich, Switzerland, 1982, 64 p
- [39] Otani, S., "Nonlinear Dynamic Analysis of Reinforced Concrete Building Structures", *Canadian Journal of Civil Engineering*, Vol. 7, No. 2, June 1980, pp. 333-344.
- [40] Takayanagi, T. and Schnobrich, W. C., "Computed Behavior of Reinforced Concrete Coupled Shear Walls", *Structural Research Series No. 434*, University of Illinois, Urbana, IL, 1976.
- [41] Aristizabal-Ochoa, J. D. and Sozen, M. A., "Behavior of Ten-Storey Reinforced Concrete Walls Subjected to Earthquake Motion", *Structural Research Series No. 431*, University of Illinois, Urbana, IL, 1976.
- [42] Saatcioglu, M., Derecho, A. T., and Corley, W. G., "Modelling Hysteretic Behavior of Coupled Walls for Dynamic Analysis", *Earthquake Engineering and Structural Dynamics*, Vol 11, 1983, pp. 711-726
- [43] Fintel, M., and Gosh, S. K., "Explicit Inelastic Dynamic Design Procedure for Aseismic Structures", *ACI Journal, Proceedings*, V.79, No. 2, March-April 1982, pp 110-118
- [44] Fintel, M., and Gosh, S. K., "Case Study of Aseismic Design of a 16 Story Coupled Wall Structure Using Inelastic Dynamic Analysis", *ACI Journal, Proceedings*, V 79, No. 3, May-June 1982, pp. 171-179.

- [45] "Inelastic Seismic Design Idea Simplifies Concrete High-Rise: Novel Technique Relieves Rebar Congestion", *Engineering News-Record*, V. 205, No. 9, Aug. 28, 1980, pp. 58-59.
- [46] Witham, K., Milne, W. G., and Smith, W. E. T., "The New Seismic Zoning Map of Canada, 1970 Edition", *Canadian Underwriter*, June 15, 1970.
- [47] Cornell, A. C., and Vanmarcke, E. H., "The Major Influences on Seismic Risk", *Proceedings of the Fourth World Conference on Earthquake Engineering*, Santiago, Chile, Vol. I, January 1969, pp. 69-83.
- [48] Merz, H. A., and Cornell, A. C., "Seismic Risk Analysis Based on a Quadratic Magnitude-Frequency Law", *Bulletin of the Seismological Society of America*, Vol. 63, No. 6, December 1973, pp. 1999-2006.
- [49] Basham, P. W., and Weichert, D. H., "Seismic Risk Mapping in Canada", *Third Canadian Conference on Earthquake Engineering*, Montreal, Canada, Vol. I, June 1979, pp. 23-47.
- [50] Powell, G. H., and Row, D. G., "Influence of Design and Analysis Assumptions on Computed Inelastic Response of Moderately Tall Frames", *EERC Report No. 76-11*, Earthquake Engineering Research Center, University of California, Berkeley, 1976.
- [51] Biggs, J. M., Hansen, R. J., and Höffley, M. J., "On Methods of Structural Analysis and Design for Earthquakes", In *Structural and Geotechnical Mechanics: A Volume Honoring Nathan M. Newmark*, Edited by W. J. Hall, Prentice Hall Inc., Englewood Cliffs, New-Jersey, 1977, pp. 91-101.
- [52] Tso, W. K., and Guru, B. P., "A Statistical Study on Artificially Generated Earthquake Records", *Canadian Journal of Civil Engineering*, Vol. 3, No. 1, March 1976, pp. 11-19.
- [53] Applied Technology Council Associated with the Structural Engineers Association of California, "Tentative Provisions for the Development of Seismic Regulations for Buildings", *ATC publication*, ATC 3-06, Washington, 1978, 505 p.
- [54] Newmark, N. M., and Hall, W. J., "Earthquake Spectra and Design", *Engineering Monographs on Earthquake Criteria, Structural Design, and Strong Motion Records*, Vol. 3, Earthquake Engineering Research Institute, Berkeley, California, 1982, 140 p.
- [55] Massachusetts Institute of Technology, "SIMQKE, A Program for Artificial Motion Generation. User's Manual and Documentation", Department of Civil Engineering, MIT, Nov. 1976, 32 p.
- [56] Gasparini, D. A., and Vanmarcke, E. H., "Simulated Earthquake Motions Compatible with Prescribed Response Spectra", *M.I.T. Publication No. R76-4*, 1976, 65 p.
- [57] Vanmarcke, E. H., "Structural Response to Earthquakes", in *Seismic Risk and Engineering Decisions*, C. Lomnitz and E. Rosenblueth editors, Elsevier, Amsterdam, 1976, pp. 287-337.
- [58] Housner, G. W., "Strong Ground Motion", In *Earthquake Engineering*, R. Wiegel editor, Prentice-Hall, Inc., Englewood Cliffs, NJ, 1970, pp. 75-91.
- [59] Cornell, A. C., and Merz, H. A., "Seismic Risk Analysis of Boston", *Journal of the Structural Division, ASCE*, Vol. 101, No. ST10, October 1975, pp. 2027-2043.
- [60] Associate Committee on the National Building Code, "National Building Code of Canada 1980" and "Supplement to the National Building Code of Canada 1980", National Research Council of Canada, Ottawa, 1980, 547 pp. and 293 pp.

- [61] Luyties, W. H., Anagnostopoulos, S. A., and Biggs, J. M., "Studies on the Inelastic Dynamic Analysis and Design of Multi-Story Frames", M.I.T. Report No. R76-29, 1976, 195 p.
- [62] Canadian Standards Association, "CSA Standard CAN3-A23.3-M77, Code for the Design of Concrete Structures for Buildings", Rexdale, December 1977, 131 p.
- [63] "Frame-2D, 2-D Plane Frame Analysis of Structural Systems", CMPT Software Inc., Montreal, 1985.
- [64] Rattray, S., "Reversed Cyclic Load Tests of Reinforced Concrete Frame Assemblages", M. Eng. Thesis, McGill University, May 1986, 143 p.
- [65] ACI Committee 318, "Building Code Requirements for Reinforced Concrete", ACI 318-83, American Concrete Institute, Detroit, 1983, 111 p.
- [66] "New Zealand Standard Code of Practice for the Design of Concrete Structures", NZS 3101 Part 1, and "Commentary", NZS 3101 Part 2, Standard Association of New Zealand, Wellington, New Zealand, 1982, 127 p. and 156 p.
- [67] Canadian Standards Association, "Weldable Low Allow Steel Deformed Bars for Concrete Reinforcement, G30.16-M 1977", CSA, Rexdale, Canada, 1977.
- [68] Canadian Standards Association, "Billet-Steel Bars for Concrete Reinforcement, G30.12-M 1977", CSA, Rexdale, Canada, 1977.
- [69] Corley, W. G., "Rotational Capacity of Reinforced Concrete Beams", *Journal of the Structural Division, ASCE*, Vol. 92, ST5, October 1966, pp. 121-146.
- [70] Mattock, A. H., Discussion of "Rotational Capacity of Reinforced Concrete Beams", by W. G. Corley, *Journal of the Structural Division, ASCE*, Vol. 93, ST2, April 1967, pp. 519-522.
- [71] Vecchio, F. J. and Collins, M. P., "The Modified Compression Field Theory for Reinforced Concrete Elements Subjected to Shear", *ACI Journal, Proceedings*, V. 83, No. 2, March-April 1986, pp. 219-231.
- [72] Ramberg, W. and Osgood, W. R., "Description of Stress-Strain Curves by Three Parameters", *Technical Note 902*, National Advisory Committee for Aeronautics, July 1943.
- [73] Mitchell, D., and Collins, M. P., "Diagonal Compression Field Theory - A Rational Model for Structural Concrete in Pure Torsion", *ACI Journal, Proceedings*, V. 71, August 1974, pp. 398-408.
- [74] Collins, M. P., "Towards a Rational Theory for RC Members in Shear", *Journal of the Structural Division, ASCE*, V. 104, April 1978, pp. 649-666.
- [75] Collins, M. P., and Mitchell, D., "Shear and Torsion Design of Prestressed and Non-Prestressed Concrete Beams", *PCI Journal* Vol. 25, No. 5, Sept.-Oct. 1980, pp. 32-100.
- [76] Collins, M. P., and Mitchell, D., "Evaluating Existing Bridge Structures Using the Modified Compression Field Theory", *Strength Evaluation of Existing Concrete Bridges*, Publication SP-88, American Concrete Institute, Detroit, October 1985, pp. 109-141.
- [77] Collins, M. P., and Mitchell, D., "Shear and Torsion", *Concrete Design Handbook*, Canadian Portland Cement Association, Ottawa, Ontario, December 1985, pp. 4-1-4-51.
- [78] Adeli, H., Gere, J.M., and Weaver, W., "Algorithms for Non-Linear Structural Dynamics", *Journal of the Structural Division, ASCE*, Vol. 104, ST2, February 1978, pp. 263-280.

- [79] Clough, R.W , and Penzien. J., *Dynamics of Structures*, McGraw Hill, Inc., New York, N.Y., 1975, 634 p.
- [80] Hasselman, T.K., and Wiggins, J.H., "Earthquake Damage to High-Rise Buildings as a Function of Interstory Drift", *Proceedings of the Third International Earthquake Microzonation Conference*, University of Washington, Seattle, June 28-July 1st, 1982, 12 p.
- [81] Hasselman, T K., Eguchi, R.T., and Wiggins, J.H., "Assessment of Damageability for Existing Buildings in a Natural Hazards Environment", *J.H. Wiggins Company Technical Report No. 80-1332*, prepared for the National Science Foundation, September 1980.
- [82] Paultre, P., and Mitchell, D., "Investigation of Canadian Seismic Code Requirements for Reinforced Concrete Frames", *Proceedings of the Fifth Canadian Conference on Earthquake Engineering*, Ottawa, A. A. Balkema Publishers, Rotterdam, July 6-8, 1987, 9 p.
- [83] Mitchell, D., "Structural Damage Due to the 1985 Mexican Earthquake", *Proceedings of the Fifth Canadian Conference on Earthquake Engineering*, Ottawa, A. A. Balkema Publishers, Rotterdam, July 6-8, 1987, 25 p.

STATEMENT OF ORIGINALITY

The original contributions described in this thesis include:

- 1) Three full-scale beam-column-slab subassemblages representing an exterior connection of the Montreal structures were built and tested under reversed cyclic loading. It is noted that two of the specimens were tested by S. Rattray as part of this research programme.
- 2) A method was developed to determine the effective width of the slab acting with the beam to resist flexure and to determine the shear reinforcement required in beam-column joints.
- 3) Computer programs were developed to predict the response of reinforced concrete components subjected to axial load, moment and shear. These programs compared well with the experimental results and were used to model the hysteretic responses in the non-linear dynamic analyses.
- 4) A multi-linear, reversed cyclic loading, hysteretic model was developed in order to include the effects of strength and stiffness degradation as well as pinching of the hysteretic response. This model was incorporated in the computer program DRAIN-2D for the non-linear dynamic analyses.
- 5) A total of twelve non-linear dynamic analyses were performed for each of the six structures. A study of these responses enabled the performance of these different structures to be compared.
- 6) Suggestions are given for code improvements and the poor performance of older structures is demonstrated.

APPENDIX A

ANALYSIS RESULTS USED FOR DESIGN

A1 SNOW LOAD

The snow load on the ground is prescribed to be 2.7 kPa for Montreal and 1.9 kPa for Vancouver. A 20% reduction as allowed by the Canadian Code [2], for a horizontal roof unexposed to wind, was used in calculating the snow load on the roof.

A2 DISTRIBUTION OF WIND LOADING

Horizontal wind pressure and suction was calculated according to the simplified method of the National Building of Canada [2]. The specified external pressure and suction due to wind were calculated from the following relationship:

$$p = q C_e C_g C_p \quad (A.1)$$

in which p is the specified external pressure acting statically in a direction normal to the surface, q is the reference velocity pressure, C_e is the exposure factor, C_g is the gust factor and C_p is the external pressure coefficient. Equivalent static lateral loads were calculated at each floor by multiplying p by the corresponding wall area exposed to wind.

A3 DISTRIBUTION OF EARTHQUAKE LOADING

The recommended static lateral load method of the National Building Code of Canada was used [2]. The lateral seismic force, V , was calculated from the following formula:

$$V = v S K I F W \quad (A.2)$$

in which v is the zonal velocity ratio, S is the seismic response factor, K is a constant that reflects the material and type of construction as well as ductility, I is the importance factor, F is the foundation factor, and W is the dead load plus 25 per cent of the snow load. In all the analyses I and F were taken as 1.0.

A4 ANALYSIS

The static analyses were carried out using the CMPT FRAME analysis package. The results of the analyses are presented in the following pages in tabular form.

Table A.1 Distribution of Wind Loading Over Height for Montreal Buildings

Floor	h , m	p , kN/m ²	F_x , kN†	$\frac{F_x}{8}$, kN ‡
Roof	23.10	1.03	79.0	9.9
6	19.45	1.03	157.9	19.7
5	15.80	1.03	157.9	19.7
4	12.15	1.03	157.9	19.7
3	8.50	0.95	145.6	18.2
2	4.85	0.95	169.6	21.2
1	0.00	—	—	—

† total force on building at floor level

‡ force at floor level taken by individual frame

Table A.2 Distribution of Wind Loading Over Height for Vancouver Buildings

Floor	h , m	p , kN/m ²	F_x , kN†	$\frac{F_x}{8}$, kN ‡
Roof	23.10	1.53	117.3	14.7
6	19.45	1.53	234.6	29.3
5	15.80	1.53	234.6	29.3
4	12.15	1.53	234.6	29.3
3	8.50	1.42	217.7	27.2
2	4.85	1.42	253.5	31.7
1	0.00	—	—	—

† total force on building at floor level

‡ force at floor level taken by individual frame

Table A.3 Distribution of Earthquake Loading Over Height for Montreal Buildings

Floor	h, m	W_x , kN	K=0.7		K=1.3	
			F_x , kN†	$\frac{F_x}{8}$, kN‡	F_x , kN†	$\frac{F_x}{8}$, kN‡
Roof	23.10	7756.2	261.3	32.7	485.3	60.7
6	19.45	7729.0	219.1	27.4	406.9	50.9
5	15.80	7729.0	178.0	22.3	330.6	41.4
4	12.15	8062.7	142.9	17.9	265.4	33.2
3	8.50	8062.7	99.9	12.5	185.5	23.2
2	4.85	8224.3	58.2	7.3	108.1	13.6
1	0.00	-	-	-	-	-
Sum		47563.9	959.4	120.1	1781.8	223.0

† total force on building at floor level

‡ force at floor level taken by individual frame

Table A.4 Distribution of Earthquake Loading Over Height for Vancouver Buildings

Floor	h, m	W_x , kN	K=0.7		K=1.3	
			F_x , kN†	$\frac{F_x}{8}$, kN‡	F_x , kN†	$\frac{F_x}{8}$, kN‡
Roof	23.10	7756.2	522.6	65.4	970.6	121.4
6	19.45	7729.0	438.2	54.8	813.8	101.8
5	15.80	7729.0	356.0	44.6	661.2	82.8
4	12.15	8062.7	285.8	35.8	530.8	66.4
3	8.50	8062.7	199.9	25.0	371.0	46.4
2	4.85	8224.3	116.4	14.6	216.2	27.2
1	0.00	-	-	-	-	-
Sum		47563.9	1918.8	240.2	3563.6	446.0

† total force on building at floor level

‡ force at floor level taken by individual frame

Table A.5 Beam Bending Moment (kN·m) at Joint A(B) Line 2 for Montreal K=1.3 Buildings. Results based on 0% Redistribution of Bending Moment due to dead and live loads

No.	Load Combination	Floors					
		Roof	6	5	4	3	2
1	1.25D	142	190	190	186	186	178
2	1.5L	81	103	103	101	101	98
3	1.5W	8	20	35	55	69	100
4	1.5Q	44	78	115	153	173	215
5	1.25D + 1.5L	222	293	293	287	287	276
6	1.25D + 1.5W	150	210	225	240	255	278
7	1.25D + 1.5Q	186	268	305	339	359	393
8	1.25D + 1.05L + 1.05W	204	276	287	295	305	316
9	1.25D + 1.05L + 1.05Q	229	317	342	363	378	397
10	0.85D + 1.5W	104	149	164	181	196	221
11	0.85D - 1.5W	89	109	94	72	57	22
12	0.85D + 1.5Q	141	207	244	279	299	336
13	0.85D - 1.5Q	52	51	14	27	46	93

Table A.6 Beam Bending Moment (kN·m) at Joint (A)B Line 2 for Montreal K=1.3 Buildings. Results based on 20% Redistribution of Bending Moment due to dead and live loads

No.	Load Combination	Floors					
		Roof	6	5	4	3	2
1	1.25D	177	189	189	189	189	189
2	1.5L	104	108	108	109	109	110
3	1.5W	7	18	31	48	62	83
4	1.5Q	36	70	103	135	155	181
5	1.25D + 1.5L	282	297	297	298	298	300
6	1.25D + 1.5W	184	207	221	237	252	272
7	1.25D + 1.5Q	213	259	292	324	344	370
8	1.25D + 1.05L + 1.05W	255	277	287	299	309	325
9	1.25D + 1.05L + 1.05Q	275	314	336	359	374	393
10	0.85D + 1.5W	128	146	160	176	191	212
11	0.85D - 1.5W	114	111	97	81	66	46
12	0.85D + 1.5Q	156	199	231	263	284	310
13	0.85D - 1.5Q	85	58	26	6	27	52

Table A.7 Beam Bending Moment (kN·m) at Joint B(C) Line 2 for Montreal K=1.3 Buildings. Results based on 0% Redistribution of Bending Moment due to dead and live loads

No.	Load Combination	Floors					
		Roof	6	5	4	3	2
1	1.25D	155	137	137	139	139	143
2	1.5L	106	122	122	123	123	125
3	1.5W	5	20	40	60	84	102
4	1.5Q	31	86	131	172	209	225
5	1.25D + 1.5L	261	259	259	262	262	268
6	1.25D + 1.5W	160	157	176	199	223	245
7	1.25D + 1.5Q	186	223	267	311	347	368
8	1.25D + 1.05L + 1.05W	233	236	250	268	284	302
9	1.25D + 1.05L + 1.05Q	251	283	314	345	371	388
1	0.85D + 1.5W	111	113	133	155	179	199
11	0.85D - 1.5W	100	73	53	34	10	5
12	0.85D + 1.5Q	136	179	224	266	303	322
13	0.85D - 1.5Q	75	7	38	77	114	128

Table A.8 Beam Shear Force (kN) at Joint A(B) Line 2 for Montreal K=1.3 Buildings. Results based on 0% Redistribution of Bending Moment due to dead and live loads

No.	Load Combination	Floors					
		Roof	6	5	4	3	2
1	1.25D	110	125	125	125	125	124
2	1.5L	60	66	66	66	66	66
3	1.5W	2	4	8	12	15	21
4	1.5Q	9	17	26	34	39	46
5	1.25D + 1.5L	170	192	192	191	191	190
6	1.25D + 1.5W	112	130	133	137	140	146
7	1.25D + 1.5Q	119	143	151	159	163	171
8	1.25D + 1.05L + 1.05W	153	175	177	180	182	185
9	1.25D + 1.05L + 1.05Q	158	184	190	195	198	203
1	0.85D + 1.5W	77	90	93	97	100	106
11	0.85D - 1.5W	73	81	78	73	70	63
12	0.85D + 1.5Q	84	103	111	119	123	131
13	0.85D - 1.5Q	65	68	60	51	47	38

Table A.9 Beam Shear Force (kN) at Joint (A)B Line 2 for Montreal K=1.3 Buildings. Results based on 20% Redistribution of Bending Moment due to dead and live loads

No.	Load Combination	Floors					
		Roof	6	5	4	3	2
1	1.25D	120	127	127	127	127	128
2	1.5L	64	67	67	67	67	68
3	1.5W	2	4	8	12	15	21
4	1.5Q	9	17	26	34	39	46
5	1.25D + 1.5L	184	194	194	195	194	196
6	1.25D + 1.5W	121	131	134	139	143	149
7	1.25D + 1.5Q	129	144	152	161	166	174
8	1.25D + 1.05L + 1.05W	166	177	179	183	185	191
9	1.25D + 1.05L + 1.05Q	171	186	191	198	201	208
1	0.85D + 1.5W	83	91	94	98	102	108
11	0.85D - 1.5W	80	82	78	74	71	66
12	0.85D + 1.5Q	91	104	112	120	125	133
13	0.85D - 1.5Q	72	69	61	53	48	41

Table A.10 Beam Shear Force (kN) at Joint B(C) Line 2 for Montreal K=1.3 Buildings. Results based on 0% Redistribution of Bending Moment due to dead and live loads

No.	Load Combination	Floors					
		Roof	6	5	4	3	2
1	1.25D	104	95	95	95	95	95
2	1.5L	79	96	96	96	96	97
3	1.5W	2	7	14	22	31	37
4	1.5Q	11	31	48	62	76	82
5	1.25D + 1.5L	184	191	191	192	192	193
6	1.25D + 1.5W	106	103	110	117	126	133
7	1.25D + 1.5Q	116	127	143	158	171	177
8	1.25D + 1.05L + 1.05W	161	168	173	178	184	189
9	1.25D + 1.05L + 1.05Q	168	184	196	207	216	221
1	0.85D + 1.5W	73	72	79	87	96	102
11	0.85D - 1.5W	69	58	51	43	34	28
12	0.85D + 1.5Q	82	96	112	127	141	147
13	0.85D - 1.5Q	60	34	17	2	11	17

Table A.11 Exterior Columns Bending Moments (kN·m) for Montreal K=1.3 Buildings

Load Combination	Storeys											
	1		2		3		4		5		6	
	top	bot	top	bot	top	bot	top	bot	top	bot	top	bot
1 1.25D	145	81	95	53	95	53	93	53	92	52	74	41
2 1.5L	4	46	52	29	52	29	51	29	50	28	40	22
3 1.5W	19	4	13	5	20	13	28	22	33	17	63	95
4 1.5Q	19	4	48	29	59	50	73	66	80	56	129	198
5 1.25D + 1.5L	150	127	147	82	147	82	144	81	142	80	114	63
6 1.25D + 1.5W	165	86	108	58	115	66	121	75	126	69	136	136
7 1.25D + 1.5Q	165	86	143	83	154	103	166	118	172	108	203	238
8 1.25D + 1.05L + 1.05W	162	116	140	77	145	83	148	88	151	84	146	122
9 1.25D + 1.05L + 1.05Q	162	116	165	94	172	108	180	119	183	111	192	195
10 0.85D + 1.5W	118	60	78	41	84	49	91	58	96	53	113	123
11 0.85D - 1.5W	80	51	52	31	45	23	36	14	29	18	12	68
12 0.85D + 1.5Q	118	60	113	66	124	86	137	102	142	92	179	226
13 0.85D - 1.5Q	80	51	17	7	6	13	10	30	17	21	78	171

Table A.12 Interior Columns Bending Moments (kN·m) for Montreal K=1.3 Buildings

Load Combination	Storeys											
	1		2		3		4		5		6	
	top	bot	top	bot	top	bot	top	bot	top	bot	top	bot
1 1.25D	63	35	48	27	48	27	47	26	46	26	37	20
2 1.5L	11	38	46	25	46	25	44	25	44	25	35	19
3 1.5W	62	46	27	22	43	40	59	53	80	76	95	113
4 1.5Q	62	46	97	85	129	124	154	146	184	181	194	234
5 1.25D + 1.5L	75	73	93	52	93	52	91	51	90	51	72	39
6 1.25D + 1.5W	125	81	75	49	91	66	105	79	126	102	132	133
7 1.25D + 1.5Q	125	81	145	112	177	151	201	172	230	207	232	255
8 1.25D + 1.05L + 1.05W	114	94	99	60	110	72	119	81	133	97	128	113
9 1.25D + 1.05L + 1.05Q	114	94	147	104	170	131	185	146	206	170	198	198
10 0.85D + 1.5W	105	70	60	40	76	58	90	71	111	94	120	127
11 0.85D - 1.5W	19	22	5	4	11	22	27	35	48	58	70	99
12 0.85D + 1.5Q	105	70	129	103	161	142	186	163	215	199	220	248
13 0.85D - 1.5Q	19	22	65	67	96	106	122	128	152	163	169	220

Table A.13 Exterior Columns Shear Forces (kN) for Montreal K=1.3 Buildings

Load Combination	Storeys											
	1		2		3		4		5		6	
	top	bot	top	bot	top	bot	top	bot	top	bot	top	bot
1 1.25D	73	73	48	48	48	48	48	48	47	47	27	27
2 1.5L	1	41	26	26	26	26	26	26	26	26	15	15
3 1.5W	7	7	6	6	10	10	15	15	15	15	35	35
4 1.5Q	7	7	24	24	33	33	43	43	41	41	72	72
5 1.25D + 1.5L	74	114	74	74	74	74	74	74	73	73	42	42
6 1.25D + 1.5W	81	81	54	54	58	58	63	63	62	62	62	62
7 1.25D + 1.5Q	81	81	72	72	81	81	91	91	88	88	99	99
8 1.25D + 1.05L + 1.05W	79	107	70	70	73	73	77	77	76	76	62	62
9 1.25D + 1.05L + 1.05Q	79	107	83	83	89	89	96	96	94	94	88	88
10 0.85D + 1.5W	57	57	38	38	43	43	48	48	47	47	53	53
11 0.85D - 1.5W	42	42	27	27	23	23	17	17	17	17	17	17
12 0.85D + 1.5Q	57	57	57	57	66	66	76	76	73	73	90	90
13 0.85D - 1.5Q	42	42	8	8	1	1	11	11	9	9	54	54

Table A.14 Interior Columns Shear Forces (kN) for Montreal K=1.3 Buildings

Load Combination	Storeys											
	1		2		3		4		5		6	
	top	bot	top	bot	top	bot	top	bot	top	bot	top	bot
1 1.25D	32	32	24	24	24	24	24	24	24	24	14	14
2 1.5L	6	34	23	23	23	23	23	23	23	23	13	13
3 1.5W	35	35	16	16	26	26	36	36	49	49	46	46
4 1.5Q	35	35	58	58	80	80	95	95	115	115	95	95
5 1.25D + 1.5L	38	66	47	47	47	47	47	47	46	46	26	26
6 1.25D + 1.5W	66	66	40	40	50	50	59	59	73	73	60	60
7 1.25D + 1.5Q	66	66	82	82	104	104	119	119	139	139	109	109
8 1.25D + 1.05L + 1.05W	60	80	51	51	58	58	65	65	74	74	55	55
9 1.25D + 1.05L + 1.05Q	60	80	80	80	96	96	106	106	120	120	89	89
10 0.85D + 1.5W	56	56	32	32	42	42	52	52	65	65	55	55
11 0.85D - 1.5W	13	13	1	1	10	10	19	19	33	33	37	37
12 0.85D + 1.5Q	56	56	74	74	96	96	111	111	131	131	104	104
13 0.85D - 1.5Q	13	13	41	41	63	63	79	79	99	99	86	86

Table A.15 Beam Bending Moment (kN·m) at Joint A(B) Line 2 for Montreal K=0.7 Building. Results based on 0% Redistribution of Bending Moment due to dead and live loads

No	Load Combination	Floors					
		Roof	6	5	4	3	2
1	1.25D	139	186	186	182	183	175
2	1.5L	78	100	100	98	98	94
3	1.5W	8	19	33	51	64	88
4	1.5Q	23	39	58	76	86	102
5	1.25D + 1.5L	217	286	286	280	281	269
6	1.25D + 1.5W	147	205	219	233	247	263
7	1.25D + 1.5Q	162	226	244	258	269	277
8	1.25D + 1.05L + 1.05W	199	269	279	286	296	302
9	1.25D + 1.05L + 1.05Q	209	284	297	304	311	312
10	0.85D + 1.5W	102	146	160	175	188	207
11	0.85D - 1.5W	87	108	94	73	60	31
12	0.85D + 1.5Q	117	166	184	200	210	221
13	0.85D - 1.5Q	72	87	69	48	38	17

Table A.16 Beam Bending Moment (kN·m) at Joint (A)B Line 2 for Montreal K=0.7 Building. Results based on 20% Redistribution of Bending Moment due to dead and live loads

No	Load Combination	Floors					
		Roof	6	5	4	3	2
1	1.25D	184	195	195	196	196	196
2	1.5L	104	108	108	109	109	110
3	1.5W	7	17	31	47	61	80
4	1.5Q	19	37	54	71	82	94
5	1.25D + 1.5L	288	303	303	304	304	306
6	1.25D + 1.5W	191	213	226	243	257	276
7	1.25D + 1.5Q	203	232	249	267	277	290
8	1.25D + 1.05L + 1.05W	261	283	292	305	314	329
9	1.25D + 1.05L + 1.05Q	270	297	309	322	329	339
10	0.85D + 1.5W	132	150	164	180	194	213
11	0.85D - 1.5W	118	115	102	86	72	54
12	0.85D + 1.5Q	144	170	187	204	215	227
13	0.85D - 1.5Q	106	96	79	62	51	40

Table A.17 Beam Bending Moment (kN·m) at Joint B(C) Line 2 for Montreal K=0.7 Building. Results based on 0% Redistribution of Bending Moment due to dead and live loads

No.	Load Combination	Floors.					
		Roof	6	5	4	3	2
1	1.25D	149	131	131	133	132	136
2	1.5L	104	119	119	120	120	122
3	1.5W	6	22	42	65	88	111
4	1.5Q	19	49	75	99	118	132
5	1.25D + 1.5L	252	249	249	252	252	257
6	1.25D + 1.5W	155	152	173	198	221	247
7	1.25D + 1.5Q	168	180	205	232	250	268
8	1.25D + 1.05L + 1.05W	225	229	243	262	278	299
9	1.25D + 1.05L + 1.05Q	234	248	266	286	299	313
10	0.85D + 1.5W	107	111	131	155	178	204
11	0.85D - 1.5W	95	68	47	25	2	19
12	0.85D + 1.5Q	120	138	164	189	208	224
13	0.85D - 1.5Q	82	40	14	9	28	40

Table A.18 Beam Shear Force (kN) at Joint A(B) Line 2 for Montreal K=0.7 Building. Results based on 0% Redistribution of Bending Moment due to dead and live loads

No.	Load Combination	Floors					
		Roof	6	5	4	3	2
1	1.25D	109	124	124	124	124	123
2	1.5L	59	65	65	65	65	65
3	1.5W	2	4	8	11	15	20
4	1.5Q	5	9	13	17	20	23
5	1.25D + 1.5L	167	190	190	189	189	188
6	1.25D + 1.5W	111	129	132	135	139	143
7	1.25D + 1.5Q	114	133	137	141	144	146
8	1.25D + 1.05L + 1.05W	151	173	175	177	180	182
9	1.25D + 1.05L + 1.05Q	153	176	179	181	183	184
10	0.85D + 1.5W	76	89	92	96	99	103
11	0.85D - 1.5W	72	80	77	73	70	64
12	0.85D + 1.5Q	79	94	98	101	104	107
13	0.85D - 1.5Q	69	76	71	67	65	61

Table A.19 Beam Shear Force (kN) at Joint (A)B Line 2 for Montreal K=0.7 Building. Results based on 20% Redistribution of Bending Moment due to dead and live loads

No	Load Combination	Floors					
		Roof	6	5	4	3	2
1	1.25D	121	128	128	128	128	129
2	1.5L	64	67	67	67	67	68
3	1.5W	2	4	8	11	15	20
4	1.5Q	5	9	13	17	20	23
5	1.25D + 1.5L	185	195	195	196	196	197
6	1.25D + 1.5W	122	132	135	140	143	149
7	1.25D + 1.5Q	126	137	141	146	148	152
8	1.25D + 1.05L + 1.05W	167	178	180	183	186	191
9	1.25D + 1.05L + 1.05Q	169	181	184	188	189	193
1	0.85D + 1.5W	84	91	94	99	102	108
11	0.85D - 1.5W	80	83	79	76	73	68
12	0.85D + 1.5Q	87	96	100	105	107	111
13	0.85D - 1.5Q	77	78	74	70	68	65

Table A.20 Beam Shear Force (kN) at Joint B(C) Line 2 for Montreal K=0.7 Building. Results based on 0% Redistribution of Bending Moment due to dead and live loads

No.	Load Combination	Floors					
		Roof	6	5	4	3	2
1	1.25D	104	95	95	95	95	95
2	1.5L	78	94	94	94	94	95
3	1.5W	2	8	15	24	32	41
4	1.5Q	7	18	27	36	43	48
5	1.25D + 1.5L	182	189	189	190	190	191
6	1.25D + 1.5W	107	103	111	119	128	136
7	1.25D + 1.5Q	111	113	123	131	138	143
8	1.25D + 1.05L + 1.05W	160	167	172	178	184	190
9	1.25D + 1.05L + 1.05Q	164	174	180	187	192	196
1	0.85D + 1.5W	73	73	80	89	97	105
11	0.85D - 1.5W	69	57	50	41	33	24
12	0.85D + 1.5Q	78	83	92	101	108	113
13	0.85D - 1.5Q	64	47	38	29	22	17

Table A.21 Exterior Column Bending Moment (kN·m) for Montreal K=0.7 Building

Load Combination	Storeys											
	1		2		3		4		5		6	
	top	bot	top	bot	top	bot	top	bot	top	bot	top	bot
1 1.25D	143	80	94	52	94	52	91	52	91	51	72	40
2 1.5L	4	44	50	28	50	28	49	28	49	27	39	21
3 1.5W	9	2	12	5	18	12	25	20	31	19	51	77
4 1.5Q	9	2	24	15	29	25	36	32	40	32	58	87
5 1.25D + 1.5L	146	124	144	80	144	80	140	79	139	79	111	61
6 1.25D + 1.5W	152	82	105	57	111	65	117	72	121	71	123	117
7 1.25D + 1.5Q	152	82	117	67	122	77	127	84	130	83	129	127
8 1.25D + 1.05L + 1.05W	152	112	137	75	141	80	143	85	146	84	135	109
9 1.25D + 1.05L + 1.05Q	152	112	145	82	149	89	151	94	153	93	139	116
10 0.85D + 1.5W	106	57	75	41	81	48	87	55	92	54	100	104
11 0.85D - 1.5W	88	52	52	31	46	23	37	15	31	16	1	50
12 0.85D + 1.5Q	106	57	87	50	93	60	98	67	101	67	106	114
13 0.85D - 1.5Q	88	52	40	21	35	11	26	3	22	3	7	60

Table A.22 Interior Column Bending Moment (kN·m) for Montreal K=0.7 Building

Load Combination	Storeys											
	1		2		3		4		5		6	
	top	bot	top	bot	top	bot	top	bot	top	bot	top	bot
1 1.25D	76	42	54	30	54	30	53	30	53	30	43	24
2 1.5L	13	46	51	29	51	29	50	28	50	28	40	22
3 1.5W	36	23	30	21	46	40	62	54	82	74	102	132
4 1.5Q	36	23	56	45	73	68	87	80	101	96	111	147
5 1.25D + 1.5L	89	88	105	59	105	59	103	58	103	58	83	46
6 1.25D + 1.5W	112	66	84	51	99	70	115	84	134	103	145	155
7 1.25D + 1.5Q	112	66	110	75	126	98	140	110	153	126	154	171
8 1.25D + 1.05L + 1.05W	110	91	111	65	122	78	132	87	145	101	142	131
9 1.25D + 1.05L + 1.05Q	110	91	129	82	141	98	149	106	158	117	149	142
10 0.85D + 1.5W	88	52	66	42	82	60	98	74	117	94	131	148
11 0.85D - 1.5W	16	6	7	1	9	19	26	33	46	53	73	116
12 0.85D + 1.5Q	88	52	92	66	109	88	123	101	136	116	141	163
13 0.85D - 1.5Q	16	6	19	25	36	47	51	60	65	76	82	131

Table A.23 Exterior Column Shear Force (kN) for Montreal K=0.7 Building

Load Combination	Storeys											
	1		2		3		4		5		6	
	top	bot	top	bot	top	bot	top	bot	top	bot	top	bot
1 1.25D	72	72	47	47	47	47	47	47	47	47	26	26
2 1.5L	1	40	25	25	25	25	25	25	25	25	14	14
3 1.5W	4	4	5	5	9	9	14	14	15	15	28	28
4 1.5Q	4	4	12	12	17	17	21	21	22	22	32	32
5 1.25D + 1.5L	72	112	72	72	72	72	72	72	71	71	41	41
6 1.25D + 1.5W	75	75	52	52	56	56	61	61	62	62	55	55
7 1.25D + 1.5Q	75	75	59	59	64	64	68	68	68	68	58	58
8 1.25D + 1.05L + 1.05W	75	102	68	68	71	71	74	74	75	75	56	56
9 1.25D + 1.05L + 1.05Q	75	102	73	73	76	76	79	79	79	79	59	59
10 0.85D + 1.5W	52	52	37	37	41	41	46	46	47	47	46	46
11 0.85D - 1.5W	45	45	27	27	23	23	18	18	17	17	10	10
12 0.85D + 1.5Q	52	52	44	44	49	49	53	53	53	53	50	50
13 0.85D - 1.5Q	45	45	20	20	16	16	11	11	10	10	14	14

Table A.24 Interior Column Shear Force (kN) for Montreal K=0.7 Building

Load Combination	Storeys											
	1		2		3		4		5		6	
	top	bot	top	bot	top	bot	top	bot	top	bot	top	bot
1 1.25D	38	38	27	27	27	27	27	27	27	27	16	16
2 1.5L	6	41	26	26	26	26	26	26	26	26	15	15
3 1.5W	19	19	16	16	27	27	37	37	49	49	53	53
4 1.5Q	19	19	32	32	44	44	53	53	62	62	58	58
5 1.25D + 1.5L	44	79	53	53	53	53	53	53	53	53	30	30
6 1.25D + 1.5W	57	57	43	43	54	54	64	64	76	76	68	68
7 1.25D + 1.5Q	57	57	59	59	71	71	81	81	89	89	74	74
8 1.25D + 1.05L + 1.05W	56	80	57	57	64	64	71	71	79	79	63	63
9 1.25D + 1.05L + 1.05Q	56	80	68	68	76	76	83	83	89	89	67	67
10 0.85D + 1.5W	45	45	35	35	45	45	56	56	68	68	63	63
11 0.85D - 1.5W	7	7	2	2	9	9	18	18	31	31	42	42
12 0.85D + 1.5Q	45	45	51	51	63	63	72	72	81	81	69	69
13 0.85D - 1.5Q	7	7	14	14	26	26	35	35	44	44	48	48

Table A.25 Beam Bending Moment (kN·m) at Joint A(B) Line 2 for Vancouver $K=1.3$ Buildings.
Results based on 20% Redistribution of Bending Moment due to dead and live loads

No.	Load Combination	Floors					
		Roof	6	5	4	3	2
1	1.25D	129	163	163	160	160	156
2	1.5L	72	87	87	86	86	84
3	1.5W	12	28	50	77	98	133
4	1.5Q	87	149	218	291	328	387
5	1.25D + 1.5L	200	250	250	246	247	240
6	1.25D + 1.5W	141	191	213	238	259	289
7	1.25D + 1.5Q	216	312	381	451	489	543
8	1.25D + 1.05L + 1.05W	187	243	259	275	289	308
9	1.25D + 1.05L + 1.05Q	240	328	377	424	451	486
10	0.85D + 1.5W	100	139	161	186	207	239
11	0.85D - 1.5W	75	82	61	32	11	27
12	0.85D + 1.5Q	175	260	329	400	438	493
13	0.85D - 1.5Q	1	39	108	182	219	281

Table A.26 Beam Bending Moment (kN·m) at Joint (A)B Line 2 for Vancouver $K=1.3$ Buildings.
Results based on 20% Redistribution of Bending Moment due to dead and live loads

No.	Load Combination	Floors					
		Roof	6	5	4	3	2
1	1.25D	176	189	189	189	189	189
2	1.5L	101	105	105	105	105	107
3	1.5W	11	26	46	70	91	116
4	1.5Q	73	139	201	265	305	341
5	1.25D + 1.5L	277	294	294	294	294	296
6	1.25D + 1.5W	187	215	235	259	280	305
7	1.25D + 1.5Q	250	328	390	454	494	530
8	1.25D + 1.05L + 1.05W	255	280	294	312	327	345
9	1.25D + 1.05L + 1.05Q	298	359	403	448	476	502
10	0.85D + 1.5W	131	155	174	199	220	244
11	0.85D - 1.5W	109	103	83	59	37	13
12	0.85D + 1.5Q	193	267	329	394	433	469
13	0.85D - 1.5Q	47	10	72	137	176	212

Table A.27 Beam Bending Moment (kN·m) at Joint (B)C Line 2 for Vancouver K=1.3 Buildings. Results based on 20% Redistribution of Bending Moment due to dead and live loads

No.	Load Combination	Floors					
		Roof	6	5	4	3	2
1	1.25D	117	104	104	105	105	107
2	1.5L	80	94	94	95	95	96
3	1.5W	10	32	61	94	129	153
4	1.5Q	71	179	269	356	428	453
5	1.25D + 1.5L	197	198	198	200	200	204
6	1.25D + 1.5W	127	136	165	199	234	260
7	1.25D + 1.5Q	188	283	372	461	533	560
8	1.25D + 1.05L + 1.05W	180	192	212	237	262	282
9	1.25D + 1.05L + 1.05Q	223	295	358	421	471	492
1	0.85D + 1.5W	89	102	132	165	200	226
11	0.85D - 1.5W	70	39	10	22	57	80
12	0.85D + 1.5Q	150	250	339	428	499	526
13	0.85D - 1.5Q	9	109	198	285	356	380

Table A.28 Beam Shear Force (kN) at Joint A(B) Line 2 for Vancouver K=1.3 Buildings. Results based on 20% Redistribution of Bending Moment due to dead and live loads

No.	Load Combination	Floors					
		Roof	6	5	4	3	2
1	1.25D	107	122	122	121	121	121
2	1.5L	58	64	64	64	64	64
3	1.5W	3	6	11	17	22	29
4	1.5Q	19	34	49	65	74	85
5	1.25D + 1.5L	166	186	186	186	186	185
6	1.25D + 1.5W	110	128	133	139	144	150
7	1.25D + 1.5Q	126	156	171	187	196	206
8	1.25D + 1.05L + 1.05W	150	171	175	178	182	186
9	1.25D + 1.05L + 1.05Q	161	190	201	212	218	225
1	0.85D + 1.5W	76	89	94	100	105	111
11	0.85D - 1.5W	70	76	72	65	60	53
12	0.85D + 1.5Q	92	117	132	148	157	168
13	0.85D - 1.5Q	54	49	34	17	8	3

Table A.29 Beam Shear Force (kN) at Joint (A)B Line 2 for Vancouver K=1.3 Buildings. Results based on 20% Redistribution of Bending Moment due to dead and live loads

No.	Load Combination	Floors					
		Roof	6	5	4	3	2
1	1.25D	122	130	130	131	131	131
2	1.5L	66	69	69	69	69	70
3	1.5W	3	6	11	17	22	29
4	1.5Q	19	34	49	65	74	85
5	1.25D + 1.5L	188	199	199	200	199	201
6	1.25D + 1.5W	125	137	142	148	153	160
7	1.25D + 1.5Q	141	164	179	196	205	217
8	1.25D + 1.05L + 1.05W	170	183	186	191	194	200
9	1.25D + 1.05L + 1.05Q	181	202	213	225	231	240
1	0.85D + 1.5W	86	95	100	106	111	118
11	0.85D - 1.5W	80	82	77	72	67	60
12	0.85D + 1.5Q	102	122	138	154	163	175
13	0.85D - 1.5Q	64	55	39	24	15	4

Table A.30 Beam Shear Force (kN) at Joint B(C) Line 2 for Vancouver K=1.3 Buildings. Results based on 20% Redistribution of Bending Moment due to dead and live loads

No.	Load Combination	Floors					
		Roof	6	5	4	3	2
1	1.25D	104	95	95	95	95	95
2	1.5L	77	94	94	94	94	95
3	1.5W	3	12	22	34	47	56
4	1.5Q	26	65	98	130	156	165
5	1.25D + 1.5L	181	189	189	190	190	190
6	1.25D + 1.5W	108	107	118	129	142	151
7	1.25D + 1.5Q	130	161	193	225	251	260
8	1.25D + 1.05L + 1.05W	161	169	176	185	194	201
9	1.25D + 1.05L + 1.05Q	176	207	229	252	270	277
1	0.85D + 1.5W	74	76	87	99	112	120
11	0.85D - 1.5W	68	53	43	31	18	9
12	0.85D + 1.5Q	97	130	163	194	220	230
13	0.85D - 1.5Q	45	0	33	65	91	100

Table A.31 Exterior Column Bending Moment (kN·m) for Vancouver K=1.3 Buildings

Load Combination	Storeys											
	1		2		3		4		5		6	
	top	bot	top	bot	top	bot	top	bot	top	bot	top	bot
1 1.25D	163	91	101	57	101	57	100	56	99	56	80	44
2 1.5L	7	50	54	30	54	30	53	30	53	30	43	24
3 1.5W	38	2	21	5	29	16	41	29	49	21	82	146
4 1.5Q	38	2	101	49	116	89	143	123	153	103	225	411
5 1.25D + 1.5L	169	141	156	87	156	87	153	86	152	86	123	67
6 1.25D + 1.5W	201	93	122	62	131	73	141	85	148	77	162	190
7 1.25D + 1.5Q	201	93	202	106	217	145	243	179	252	159	305	454
8 1.25D + 1.05L + 1.05W	194	128	154	81	160	89	166	98	170	92	167	163
9 1.25D + 1.05L + 1.05Q	194	128	210	112	220	140	237	163	243	149	267	348
10 0.85D + 1.5W	149	64	90	43	98	54	109	67	116	59	136	176
11 0.85D - 1.5W	72	60	48	34	40	23	26	9	18	17	28	116
12 0.85D + 1.5Q	149	64	170	88	185	127	211	161	220	141	279	440
13 0.85D - 1.5Q	72	60	32	11	47	50	76	84	86	66	170	381

Table A.32 Interior Column Bending Moment (kN·m) for Vancouver K=1.3 Buildings

Load Combination	Storeys											
	1		2		3		4		5		6	
	top	bot	top	bot	top	bot	top	bot	top	bot	top	bot
1 1.25D	69	39	51	28	51	28	50	28	49	28	40	22
2 1.5L	19	43	50	28	50	28	48	27	48	27	38	21
3 1.5W	135	89	43	31	67	58	90	78	121	113	133	174
4 1.5Q	135	89	202	165	265	248	325	290	371	365	364	487
5 1.25D + 1.5L	88	82	100	56	100	56	98	55	97	55	78	43
6 1.25D + 1.5W	204	127	94	59	117	87	140	106	171	141	173	196
7 1.25D + 1.5Q	204	127	253	193	315	277	365	318	421	392	404	509
8 1.25D + 1.05L + 1.05W	177	131	116	69	132	88	147	102	168	126	160	159
9 1.25D + 1.05L + 1.05Q	177	131	227	163	271	222	304	250	343	302	322	378
10 0.85D + 1.5W	182	115	78	50	101	78	124	97	155	132	160	189
11 0.85D - 1.5W	88	62	9	12	32	39	57	59	88	94	106	159
12 0.85D + 1.5Q	182	115	236	184	299	268	349	309	405	384	391	502
13 0.85D - 1.5Q	88	62	168	146	230	229	281	271	338	346	337	472

Table A.33 Exterior Column Shear Force (kN) for Vancouver K=1.3 Buildings

Load Combination	Storeys											
	1		2		3		4		5		6	
	top	bot	top	bot	top	bot	top	bot	top	bot	top	bot
1 1.25D	82	82	51	51	51	51	51	51	51	51	29	29
2 1.5L	0	45	27	27	27	27	27	27	27	27	16	16
3 1.5W	11	11	8	8	14	14	22	22	21	21	51	51
4 1.5Q	11	11	47	47	63	63	83	83	78	78	142	142
5 1.25D + 1.5L	82	127	78	78	78	78	78	78	78	78	45	45
6 1.25D + 1.5W	93	93	59	59	65	65	73	73	72	72	80	80
7 1.25D + 1.5Q	93	93	98	98	114	114	134	134	129	129	172	172
8 1.25D + 1.05L + 1.05W	90	121	76	76	80	80	86	86	84	84	76	76
9 1.25D + 1.05L + 1.05Q	90	121	103	103	114	114	128	128	124	124	140	140
10 0.85D + 1.5W	67	67	43	43	49	49	57	57	56	56	71	71
11 0.85D - 1.5W	44	44	27	27	21	21	13	13	13	13	31	31
12 0.85D + 1.5Q	67	67	82	82	98	98	118	118	113	113	162	162
13 0.85D - 1.5Q	44	44	13	13	29	29	48	48	44	44	123	123

Table A.34 Interior Column Shear Force (kN) for Vancouver K=1.3 Buildings

Load Combination	Storeys											
	1		2		3		4		5		6	
	top	bot	top	bot	top	bot	top	bot	top	bot	top	bot
1 1.25D	35	35	25	25	25	25	26	26	25	25	15	15
2 1.5L	9	39	25	25	25	25	25	25	25	25	14	14
3 1.5W	72	72	24	24	40	40	54	54	74	74	69	69
4 1.5Q	72	72	117	117	162	162	193	193	234	234	192	192
5 1.25D + 1.5L	44	74	50	50	50	50	50	50	50	50	29	29
6 1.25D + 1.5W	106	106	49	49	65	65	79	79	100	100	84	84
7 1.25D + 1.5Q	106	106	142	142	188	188	219	219	259	259	206	206
8 1.25D + 1.05L + 1.05W	91	112	59	59	71	71	80	80	95	95	73	73
9 1.25D + 1.05L + 1.05Q	91	112	125	125	156	156	178	178	206	206	159	159
10 0.85D + 1.5W	95	95	41	41	57	57	71	71	92	92	79	79
11 0.85D - 1.5W	48	48	6	6	22	22	36	36	57	57	59	59
12 0.85D + 1.5Q	95	95	134	134	180	180	211	211	251	251	202	202
13 0.85D - 1.5Q	48	48	99	99	145	145	176	176	217	217	182	182

Table A.35 Beam Bending Moment (kN·m) at Joint A(B) Line 2 for Vancouver K=0.7 Building. Results based on 0% Redistribution of Bending Moment due to dead and live loads

No.	Load Combination	Floors					
		Roof	6	5	4	3	2
1	1.25D	139	186	186	182	183	175
2	1.5L	78	100	100	98	98	94
3	1.5W	11	28	49	75	96	131
4	1.5Q	45	79	115	152	172	205
5	1.25D + 1.5L	217	286	286	280	281	269
6	1.25D + 1.5W	150	214	235	257	278	306
7	1.25D + 1.5Q	184	265	302	334	355	379
8	1.25D + 1.05L + 1.05W	201	276	291	303	318	333
9	1.25D + 1.05L + 1.05Q	225	311	337	357	372	384
10	0.85D + 1.5W	106	155	176	199	220	250
11	0.85D - 1.5W	83	99	78	49	29	12
12	0.85D + 1.5Q	140	206	242	276	296	323
13	0.85D - 1.5Q	49	48	12	28	48	36

Table A.36 Beam Bending Moment (kN·m) at Joint (A)B Line 2 for Vancouver K=0.7 Building. Results based on 20% Redistribution of Bending Moment due to dead and live loads

No.	Load Combination	Floors					
		Roof	6	5	4	3	2
1	1.25D	184	195	195	196	196	196
2	1.5L	104	108	108	109	109	110
3	1.5W	10	26	46	70	91	119
4	1.5Q	39	74	108	143	164	188
5	1.25D + 1.5L	288	303	303	304	304	306
6	1.25D + 1.5W	194	221	241	266	286	315
7	1.25D + 1.5Q	222	270	304	338	359	384
8	1.25D + 1.05L + 1.05W	264	289	303	321	335	357
9	1.25D + 1.05L + 1.05Q	283	323	347	371	386	405
10	0.85D + 1.5W	135	159	179	203	224	252
11	0.85D - 1.5W	115	107	87	63	42	15
12	0.85D + 1.5Q	164	207	241	276	297	321
13	0.85D - 1.5Q	86	58	24	10	31	54

Table A.37 Beam Bending Moment (kN-m) at Joint (B)C Line 2 for Vancouver K=0.7 Building. Results based on 0% Redistribution of Bending Moment due to dead and live loads

No.	Load Combination	Floors					
		Roof	6	5	4	3	2
1	1.25D	149	131	131	133	132	136
2	1.5L	104	119	119	120	120	122
3	1.5W	9	32	62	97	132	166
4	1.5Q	38	98	149	198	236	264
5	1.25D + 1.5L	252	249	249	252	252	257
6	1.25D + 1.5W	158	163	193	229	264	301
7	1.25D + 1.5Q	187	229	280	331	368	400
8	1.25D + 1.05L + 1.05W	228	236	258	284	308	337
9	1.25D + 1.05L + 1.05Q	248	283	318	355	381	406
10	0.85D + 1.5W	110	121	151	187	222	258
11	0.85D - 1.5W	92	57	27	6	41	73
12	0.85D + 1.5Q	139	187	238	289	326	356
13	0.85D - 1.5Q	63	9	60	108	146	172

Table A.38 Beam Shear Force (kN) at Joint A(B) Line 2 for Vancouver K=0.7 Building. Results based on 0% Redistribution of Bending Moment due to dead and live loads

No.	Load Combination	Floors					
		Roof	6	5	4	3	2
1	1.25D	109	124	124	124	124	123
2	1.5L	59	65	65	65	65	65
3	1.5W	3	6	11	17	22	29
4	1.5Q	10	18	26	35	39	46
5	1.25D + 1.5L	167	190	190	189	189	188
6	1.25D + 1.5W	111	131	135	141	146	152
7	1.25D + 1.5Q	119	142	151	158	163	169
8	1.25D + 1.05L + 1.05W	152	174	178	181	185	189
9	1.25D + 1.05L + 1.05Q	157	183	188	194	197	200
10	0.85D + 1.5W	77	91	96	101	106	113
11	0.85D - 1.5W	72	78	73	67	62	54
12	0.85D + 1.5Q	84	103	111	119	124	130
13	0.85D - 1.5Q	64	67	58	50	45	38

Table A.39 Beam Shear Force (kN) at Joint (A)B Line 2 for Vancouver K=0.7 Building. Results based on 20% Redistribution of Bending Moment due to dead and live loads

No.	Load Combination	Floors					
		Roof	6	5	4	3	2
1	1.25D	121	128	128	128	128	129
2	1.5L	64	67	67	67	67	68
3	1.5W	3	6	11	17	22	29
4	1.5Q	10	18	26	35	39	46
5	1.25D + 1.5L	185	195	195	196	196	197
6	1.25D + 1.5W	123	134	139	145	150	159
7	1.25D + 1.5Q	131	146	154	163	168	175
8	1.25D + 1.05L + 1.05W	167	179	182	187	191	197
9	1.25D + 1.05L + 1.05Q	172	187	193	200	203	209
1	0.85D + 1.5W	85	93	98	104	109	117
11	0.85D - 1.5W	80	81	76	70	65	59
12	0.85D + 1.5Q	92	105	113	122	127	134
13	0.85D - 1.5Q	72	69	61	53	48	42

Table A.40 Beam Shear Force (kN) at Joint B(C) Line 2 for Vancouver K=0.7 Building. Results based on 20% Redistribution of Bending Moment due to dead and live loads

No.	Load Combination	Floors					
		Roof	6	5	4	3	2
1	1.25D	104	95	95	95	95	95
2	1.5L	78	94	94	94	94	95
3	1.5W	3	12	23	35	48	60
4	1.5Q	14	36	54	72	86	96
5	1.25D + 1.5L	182	189	189	190	190	191
6	1.25D + 1.5W	108	107	118	131	143	156
7	1.25D + 1.5Q	118	131	150	168	181	191
8	1.25D + 1.05L + 1.05W	161	169	177	186	195	204
9	1.25D + 1.05L + 1.05Q	169	186	199	212	222	229
1	0.85D + 1.5W	74	77	88	100	113	125
11	0.85D - 1.5W	68	53	42	30	17	5
12	0.85D + 1.5Q	85	101	119	137	151	161
13	0.85D - 1.5Q	57	29	11	7	21	31

Table A.41 Exterior Column Bending Moment (kN·m) for Vancouver K=0.7 Building

Load Combination		Storeys											
		1		2		3		4		5		6	
		top	bot	top	bot	top	bot	top	bot	top	bot	top	bot
1	1.25D	143	80	94	52	94	52	91	52	91	51	72	40
2	1.5L	6	44	50	28	50	28	49	28	49	27	39	21
3	1.5W	19	5	17	7	26	18	37	30	46	29	75	115
4	1.5Q	19	5	47	30	58	49	72	65	80	63	113	174
5	1.25D + 1.5L	148	124	144	80	144	80	140	79	139	79	111	61
6	1.25D + 1.5W	161	84	111	60	120	71	129	81	136	80	148	155
7	1.25D + 1.5Q	161	84	141	82	151	102	163	116	170	115	185	214
8	1.25D + 1.05L + 1.05W	180	114	141	77	147	85	152	92	157	90	153	135
9	1.25D + 1.05L + 1.05Q	160	114	162	93	169	106	176	116	180	115	179	177
10	0.85D + 1.5W	116	59	81	43	90	54	100	65	107	64	125	142
11	0.85D - 1.5W	79	50	47	28	37	17	25	6	16	6	26	88
12	0.85D + 1.5Q	116	59	111	65	121	85	134	100	141	98	162	201
13	0.85D - 1.5Q	79	50	17	6	6	14	10	30	18	29	64	147

Table A.42 Interior Column Bending Moment (kN·m) for Vancouver K=0.7 Building

Load Combination		Storeys											
		1		2		3		4		5		6	
		top	bot	top	bot	top	bot	top	bot	top	bot	top	bot
1	1.25D	76	42	54	30	54	30	53	30	53	30	43	24
2	1.5L	19	46	51	29	51	29	50	28	50	28	40	22
3	1.5W	72	46	44	32	68	59	92	80	122	110	152	196
4	1.5Q	72	46	112	91	145	136	173	160	201	192	223	295
5	1.25D + 1.5L	95	88	105	59	105	59	103	58	103	58	83	46
6	1.25D + 1.5W	148	89	98	62	122	89	146	110	174	139	195	220
7	1.25D + 1.5Q	148	89	166	121	199	166	227	190	254	222	266	318
8	1.25D + 1.05L + 1.05W	140	107	121	72	137	91	153	106	173	126	177	176
9	1.25D + 1.05L + 1.05Q	140	107	168	114	191	145	210	162	228	184	227	245
10	0.85D + 1.5W	124	75	81	52	104	79	129	100	157	130	181	212
11	0.85D - 1.5W	21	18	8	11	31	38	56	59	86	89	123	180
12	0.85D + 1.5Q	124	75	148	111	182	156	210	181	237	212	252	311
13	0.85D - 1.5Q	21	18	75	70	108	115	137	140	165	172	194	270

Table A.43 Exterior Column Shear Force (kN) for Vancouver K=0.7 Building

Load Combination	Storeys											
	1		2		3		4		5		6	
	top	bot	top	bot	top	bot	top	bot	top	bot	top	bot
1 1.25D	72	72	47	47	47	47	47	47	47	47	26	26
2 1.5L	1	40	25	25	25	25	25	25	25	25	14	14
3 1.5W	7	7	8	8	14	14	21	21	22	22	42	42
4 1.5Q	7	7	24	24	33	33	42	42	44	44	63	63
5 1.25D + 1.5L	73	112	72	72	72	72	72	72	71	71	41	41
6 1.25D + 1.5W	79	79	55	55	61	61	68	68	69	69	69	69
7 1.25D + 1.5Q	79	79	71	71	80	80	89	89	90	90	90	90
8 1.25D + 1.05L + 1.05W	78	105	70	70	74	74	79	79	80	80	66	66
9 1.25D + 1.05L + 1.05Q	78	105	81	81	88	88	94	94	94	94	81	81
10 0.85D + 1.5W	56	56	40	40	46	46	53	53	54	54	60	60
11 0.85D - 1.5W	42	42	24	24	18	18	11	11	9	9	24	24
12 0.85D + 1.5Q	56	56	56	56	65	65	74	74	75	75	81	81
13 0.85D - 1.5Q	42	42	8	8	1	1	11	11	12	12	45	45

Table A.44 Interior Column Shear Force (kN) for Vancouver K=0.7 Building

Load Combination	Storeys											
	1		2		3		4		5		6	
	top	bot	top	bot	top	bot	top	bot	top	bot	top	bot
1 1.25D	38	38	27	27	27	27	27	27	27	27	16	16
2 1.5L	9	41	26	26	26	26	26	26	26	26	15	15
3 1.5W	38	38	24	24	40	40	55	55	73	73	79	79
4 1.5Q	38	38	64	64	89	89	107	107	125	125	117	117
5 1.25D + 1.5L	47	79	53	53	53	53	53	53	53	53	30	30
6 1.25D + 1.5W	76	76	51	51	67	67	82	82	100	100	94	94
7 1.25D + 1.5Q	76	76	91	91	116	116	134	134	152	152	132	132
8 1.25D + 1.05L + 1.05W	71	94	62	62	73	73	84	84	96	96	81	81
9 1.25D + 1.05L + 1.05Q	71	94	90	90	107	107	120	120	132	132	107	107
10 0.85D + 1.5W	64	64	43	43	58	58	73	73	92	92	89	89
11 0.85D - 1.5W	12	12	6	6	22	22	36	36	55	55	68	68
12 0.85D + 1.5Q	64	64	83	83	107	107	125	125	143	143	127	127
13 0.85D - 1.5Q	12	12	46	46	70	70	88	88	106	106	106	106

Table A.45 Lateral deflection envelope under specified earthquake and wind load , mm, Montreal Buildings

Floor	K=0.7	K=1.3
Roof	12.0	23.0
6	11.0	21.0
5	10.0	19.0
4	8.0	15.0
3	6.0	11.0
2	4.0	6.0
1	-	-

Table A.45 Lateral deflection envelope under specified earthquake and wind load , mm, Vancouver, Buildings

Floor	K=0.7	K=1.3
Roof	25.0	43.0
6	23.0	40.0
5	20.0	35.0
4	16.0	29.0
3	12.0	21.0
2	7.0	12.0
1	-	-